



University of HUDDERSFIELD

University of Huddersfield Repository

Al Thobiani, Faisal

The Non-intrusive Detection of Incipient Cavitation in Centrifugal Pumps

Original Citation

Al Thobiani, Faisal (2011) The Non-intrusive Detection of Incipient Cavitation in Centrifugal Pumps. Doctoral thesis, University of Huddersfield.

This version is available at <http://eprints.hud.ac.uk/14576/>

The University Repository is a digital collection of the research output of the University, available on Open Access. Copyright and Moral Rights for the items on this site are retained by the individual author and/or other copyright owners. Users may access full items free of charge; copies of full text items generally can be reproduced, displayed or performed and given to third parties in any format or medium for personal research or study, educational or not-for-profit purposes without prior permission or charge, provided:

- The authors, title and full bibliographic details is credited in any copy;
- A hyperlink and/or URL is included for the original metadata page; and
- The content is not changed in any way.

For more information, including our policy and submission procedure, please contact the Repository Team at: E.mailbox@hud.ac.uk.

<http://eprints.hud.ac.uk/>

The Non-intrusive Detection of Incipient Cavitation in Centrifugal Pumps

Faisal W H Al Thobiani

A thesis submitted to the University of Huddersfield in partial fulfilment of the requirements for the degree of Doctor of Philosophy

The University of Huddersfield

November 2011

TABLE OF CONTENTS

TABLE OF CONTENTS.....	2
FIGURES.....	7
TABLES	12
ABSTRACT.....	13
DECLARATION	14
DEDICATION.....	15
ACKNOWLEDGEMENTS.....	16
ABBREVIATIONS	17
NOTATIONS.....	18
COPYRIGHT.....	20
PUBLICATIONS ARISING FROM THIS RESEARCH.....	21
CHAPTER ONE.....	22
1. INTRODUCTION AND BACKGROUND	22
1.1 Applications of pumps and pump types.....	23
1.2 Development of the centrifugal pump	24
1.2.1 Radial flow centrifugal pumps.....	27
1.2.2 Mixed flow pumps	27
1.2.3 Axial flow pumps.....	28
1.2.4 The turbine pump	28
1.3 Research motivation.....	28
1.4 Research aim and objectives.....	30
1.5 Outline of the thesis	31
CHAPTER TWO	34
2. CENTRIFUGAL PUMPS AND CAVITATION	34
2.1 The centrifugal pump.....	35
2.2 Mechanical construction of centrifugal pumps	36
2.2.1 Pump impeller.....	36
2.2.2 Shaft and bearings.....	39
2.2.3 Pump casing (volute)	40
2.2.4 Wear rings and the auxiliary piping system.....	41
2.3 Characteristics of centrifugal pumps and pump systems	42

2.4 Cavitation.....	46
2.4.1 Types of cavitation.....	48
2.4.2 Cavitation number.....	49
2.4.3 Cavitation costs.....	50
2.4.4 Cavitation flow regimes.....	50
2.4.5 Cavitation as a system problem	53
2.4.6 Prevention of cavitation	53
2.5 Damage to centrifugal pumps caused by cavitation.....	54
CHAPTER THREE	58
3. METHODS USED FOR DETECTION OF CAVITATION AND STATISTICAL FEATURES..	58
3.1 Detection of cavitation using flow visualisation.....	59
3.2 Detection of cavitation using acoustic measurement.....	60
3.3 Detection of cavitation using vibration measurement.....	63
3.4 Detection of cavitation using acoustic emission methods.....	65
3.5 Recently developed methods for detection of cavitation	66
3.5.1 Angular speed of the pump shaft	66
3.5.2 Motor current signature analysis (MCSA).....	67
3.6 Possible novel method for detecting cavitation	69
3.7 Data analysis techniques	70
3.7.1 Signal processing for condition monitoring.....	70
3.7.2 Time domain	72
3.7.3 Frequency domain.....	76
CHAPTER FOUR.....	80
4. DESIGN AND CONSTRUCTION OF TEST-RIG.....	80
4.1 Introduction.....	81
4.2 General requirements	82
4.2.1 The test rig	83
4.3 Measurement system (instrumentation).....	86
4.3.1 The flow rate transducer	86
4.3.2 Pressure transducer	88
4.3.3 Vibration accelerometer.....	92
4.3.4 Acoustic microphone	93
4.3.5 Acoustic hydrophone	95
4.3.6 Shaft encoder	96

4.3.7 Speed controller	99
4.3.8 Data acquisition (Sinocera YE6230B).....	100
4.3.9 Data acquisition (CED 1401 1992).....	102
4.3.10 Centrifugal pump	103
4.4 Summary	107
CHAPTER FIVE	109
5. DESIGN OF A CAPACITANCE SENSOR FOR DETECTION OF CAVITATION	109
5.1 Introduction.....	110
5.2 Capacitance- sensor theory	110
5.3 Principles of design of capacitance sensor.....	113
5.4 Signal generator	115
5.5 Spectrum analyser.....	116
CHAPTER SIX.....	119
6. CAPACITANCE SIGNAL ANALYSIS FOR DETECTION OF CAVITATION	119
6.1 Introduction.....	120
6.2 Sensor equivalent circuit.....	121
6.3 Likely frequency shift	123
6.4 Acquisition of capacitance data	124
6.5 Summary	137
CHAPTER SEVEN	139
7. VIBRATION SIGNAL ANALYSIS FOR DETECTION OF CAVITATION	139
7.1 Advantages and disadvantages of vibration methods	140
7.2 Time domain analysis	140
7.3 Conventional statistical measures from the time domain	142
7.3.1 Probability density function.....	142
7.3.2 Peak value, RMS and Crest factor	144
7.3.3 Kurtosis	146
7.4 Spectrum analysis	147
7.4.1 Baseline spectral analysis.....	149
7.4.2 Spectral amplitude characteristics.....	153
7.5 Statistical measures from the frequency domain	155
7.5.1 Spectral crest factor.....	155
7.5.2 Spectral kurtosis.....	156

7.5.3 Spectral entropy	157
CHAPTER EIGHT	159
8. AIRBORNE ACOUSTIC SIGNAL ANALYSIS FOR DETECTION OF CAVITATION	159
8.1 Advantages and disadvantages of using airborne sound.....	160
8.2 Time domain analysis	160
8.3 Conventional statistical measures from the time domain	162
8.3.1 Probability density function	162
8.3.2 Peak value, RMS and Crest factor	164
8.3.3 Kurtosis	166
8.4 Spectrum analysis	167
8.4.1 Baseline spectral analysis.....	168
8.4.2 Spectral amplitude characteristics.....	171
8.5 Statistical measures from the frequency domain	174
8.5.1 Spectral crest factor.....	174
8.5.2 Spectral kurtosis.....	175
8.5.3 Spectral entropy	176
CHAPTER NINE.....	178
9. HYDROACOUSTIC SIGNAL ANALYSIS FOR DETECTION OF CAVITATION	178
9.1 Advantages and disadvantages of using hydrophone methods	179
9.2 Time domain analysis	179
9.3 Conventional statistical measures from the time domain	181
9.3.1 Probability density function	181
9.3.2 Peak value, RMS and Crest factor	183
9.2.3 Kurtosis	185
9.4 Spectrum analysis	186
9.4.1 Baseline spectrum analysis	188
9.4.2 Spectral amplitude characteristics.....	191
9.5 Statistical measures from the frequency domain	193
9.5.1 Spectral Crest factor.....	193
9.5.2 Spectral kurtosis.....	194
9.5.3 Spectral entropy	195
CHAPTER TEN.....	197
10.Conclusions and suggestions for further work.....	197

10.1 Review of aims and objectives.....	198
10.2 Conclusions on merits of the detection techniques	200
10.3 Conclusions regarding time domain features	201
10.3.1 Probability density function	201
10.3.2 Peak value	202
10.3.3 RMS value	203
10.4 Conclusions regarding frequency domain features	204
10.4.1 Spectral crest factor.....	204
10.4.2 Spectral kurtosis.....	205
10.4.3 Spectral entropy	206
10.5 Spectral amplitude characteristics.....	207
10.6 Progress with capacitive sensor	208
10.7 Contributions to knowledge	209
10.8 Suggestions for future work.....	210
APPENDIXS.....	213
REFERENCES	227

Total words: 45,787

Total pages: 237

FIGURES

Figure 1-1 Distribution of the new pump market (ISO/TC115, 2004)	23
Figure 1-2 World-wide distributions of sales of new pumps (ISO/TC115, 2004)	23
Figure 1-3 Hierarchy of the different types of pumps	25
Figure 1-4 Centrifugal pumps – basic construction (Girdhar, 2005).....	26
Figure 1-5 Radial flow pumps (Bachus and Custodio, 2003).....	27
Figure 1-6 Maintenance costs of rotating machines at a petrochemical plant (Wowk, 1991).29	
Figure 1-7 Centrifugal pump faults.....	29
Figure 2-1 Cross-section of a centrifugal pump	35
Figure 2-2 Closed impeller with impeller terminology	37
Figure 2-3 Semi-open impeller	38
Figure 2-4 Open impeller.....	38
Figure 2-5 Shaft and bearings	39
Figure 2-6 Shaft sleeve	39
Figure 2-7 Casing of centrifugal pump used on test rig.....	40
Figure 2-8 Pump mechanical seal	41
Figure 2-9 Simplified schematic of head versus pressure	43
Figure 2-10 Cavity flow on hydrofoil, (D'Agostino et al, 2008)	49
Figure 2-11 General characterisation of stable, unstable and transient regimes inlet pressure /time relationship (Grist, 1999)	51
Figure 2-12 Typical pitting damage locations in impeller.....	53
Figure 2-13 Location of likely cavitation sites on impeller used in tests	56
Figure 2-14 Cavitation damage on the blade of a closed impeller (Brennen, 1995)	56
Figure 2-15 Erosion to casing of pump used in the test rig	57
Figure 2-16 Seal damage	57
Figure 3-1 (A) - Centrifugal pump without cavitation (B) - Centrifugal pump with cavitation	59
Figure 3-2 Abrupt change in airborne sound level showing onset of cavitation, (adapted from McNulty, et al. 1982)	61
Figure 3-3 Standard deviation of the airborne acoustic signal from a centrifugal pump with the onset of cavitation (Alhasmi, 2005)	62
Figure 3-4 Positioning of vibration transducer(s) for cavitation detection (Cernetic 2009)....	63
Figure 3-5 Vibration signal from a centrifugal pump with and without cavitation (Cernetic, 2009)	64
Figure 3-6 Pump head and relative intensity of acoustic emission as functions of cavitation number, showing onset of cavitation (Courbiere, 1984).....	66
Figure 3-7 (a) Normalised IAS RMS with flow rate for the frequency band 100 to 2500 Hz	67
Figure 3-7(b) Normalised amplitude of 3rd harmonic of IAS with flow rate (Alhasmi,2005)67	
Figure 3-8 Power spectrum of the motor current of a motor driving a healthy centrifugal pump (Alhasmi, 2005)	68
Figure 3-9 RMS of one phase of the motor current of a motor driving a healthy centrifugal pump with increase in flow rate (Alhasmi, 2005).....	69
Figure 3-10 Signal processing techniques (Norton and Karczub, 2003)	70
Figure 3-11 Time-frequency domain	71
Figure 3-12 RMS amplitude of the vibration signal for centrifugal pump (Alhashmi, 2005).73	

Figure 3-13 PDF of the pump vibration (acceleration) spectrum with flow rate (Alhashmi, 2005)	75
Figure 3-14 Baseline vibration spectrum for centrifugal pump, 20 Hz to 1kHz (Alhashmi, 2005).....	77
Figure 3-15 Spectral entropy of vibration spectra for centrifugal pump with flow rate in the range 10 l/min to 370 l/min	79
Figure 4-1 Pump secured to floor	82
Figure 4-2 Three-phase mains supply via a D.O.L starter and a three-phase isolator.....	83
Figure 4-3 Photo of test rig	85
Figure 4-4 Schematic diagram of test rig system.....	85
Figure 4-5 Gems rotor flow type RFO (GEMS, 2011).....	87
Figure 4-6 Gems water flow meter in flow line (refer to Figure 4.4).....	87
Figure 4-7 Pressure transducer.....	89
Figure 4-8 Pressure transducer in suction line at the pump inlet.....	90
Figure 4-9 Pressure transducer in discharge line at the pump outlet	90
Figure 4-10 Typical online raw data measured by pressure transducer in suction line.....	91
Figure 4-11 Typical online raw data measured by pressure transducer in discharge line	91
Figure 4-12 Positions of the accelerometers (a)- At outlet of the pump (b) - Between pump casing and motor of the pump.....	92
Figure 4-13 Typical raw vibration signal from accelerometer on pump outlet.....	93
Figure 4-14 Microphone and position of microphone for airborne sound.....	94
Figure 4-15 Typical raw data for pump noise measured by the microphone	95
Figure 4-16 Hydrophone and position of hydrophone.....	96
Figure 4-17 Typical raw data for hydroacoustic signal measured by the hydrophone at pump outlet	96
Figure 4-18 Shaft encoder.....	97
Figure 4-19 Position of encoder shaft speed.....	97
Figure 4-20 Typical outlet signal of encoder	98
Figure 4-21 Omron speed controller.....	99
Figure 4-22 Sinocera YE6230B data acquisition system	101
Figure 4-23 Interface panel for YE6230B	101
Figure 4-24 CED 1401 Plus data acquisition system.....	102
Figure 4-25 Interface panel for CED 1401	103
Figure 4-26 Pedrollo F32/200AH centrifugal pump.....	104
Figure 4-27 Pump performance pump at 100% open valve	106
Figure 4-28 Head – Flow rate pump curve	106
Figure 4-29 Acquisition of e.g. accelerometer signals	107
Figure 4-30 Centrifugal pump test system.....	108
Figure 5-1 Examples of void fraction distribution along a steam Injector (Jaworek, et al., 2004)	110
Figure 5-2 Simple parallel plate capacitor with and without the addition of an insulating layer of thickness t , and relative dielectric constant ϵ_{in}	111
Figure 5-3 Capacitive sensors at inlet and outlet of the pump.....	114
Figure 5-4 Position of capacitance sensors at outlet of the pump.....	114
Figure 5-5 (a) CRYSTEK - CVCO55B Voltage Controlled Oscillator	115
Figure 5-5 (b) CRYSTEK - CVCO55B Voltage Controlled Oscillator	115
Figure 5-6 Advantest type R4131D spectrum analyser	117
Figure 5-7 Simplified schematic of capacitance sensor.....	118

Figure 6-1 Schematic diagram of capacitance sensor assembly	120
Figure 6-2 Schematic diagram of electrical equivalent circuit for capacitive sensor	121
Figure 6-3 Expected capacitance and frequency trends with cavitation	124
Figure 6-4 Schematic of test rig with addition of air inlet valve and air supply line.....	125
Figure 6-5 Air flow into pump circuit with air valve opening (0.43 bar pressure difference)	126
Figure 6-6 Water flow rate against air inlet valve opening	127
Figure 6-7 Images of bubbles in flow for pump speed 2900 rpm, suction line pressure 0.43 bar below ambient for different openings of the air valve in degrees.....	128
Figure 6-8 Output of spectrum analyser with 100% air and 100% water between capacitor plates for the three resonant frequencies 411MHz, 535MHz and 762MHz	130
Figure 6-9 Peak frequency shift behaviour with different air valve opening for the three resonant frequencies 411MHz, 535 MHz and 762 MHz	133
Figure 6-10 Variation of spectral peak with different air valve opening for the three resonant frequencies 411MHz, 535 MHz and 762 MHz.....	135
Figure 6-11 Variation of resonant frequency with different air valve opening for the three resonant frequencies 411MHz, 535 MHz and 762 MHz.....	136
Figure 6-12 Resonant frequency of signal against flow rate (controlled by throttle valve in discharge line, air inlet valve closed)	137
Figure 7-1 Raw time domain vibration signal (acceleration) for flow rate 249 l/min.....	141
Figure 7-2 Raw time domain vibration signals at different flow rates	142
Figure 7-3 (a) PDFs of time domain of vibration signal for different flow rates	143
Figure 7-3 (b) Amplitude of PDF curve of vibration signal against flow rate.....	146
Figure 7-4 Peak value of time domain of the vibration signal with flow rate	145
Figure 7-5 RMS of time domain of the vibration signal with flow rate	145
Figure 7-6 Crest factor of time domain of the vibration signal with flow rate.....	146
Figure 7-7 Kurtosis of time domain of the vibration signal with flow rate	147
Figure 7-8 (a) Spectra of the vibration signal from the pump for different flow rates.....	148
Figure 7-8 (b) Frequency spectra of the vibration signals at specified flow rates.....	159
Figure 7-9 Baseline vibration spectrum 20 Hz - 1 kHz for flow rate 249 l/min.....	151
Figure 7-10 Baseline vibration spectrum for 1 kHz - 2 kHz for flow rate 249 l/min.....	152
Figure 7-11 Baseline vibration spectrum for 2 kHz–10 kHz for flow rate 249 l/min	152
Figure 7-12 Waterfall for time-averaged Peak amplitude of vibration signal 20 Hz – 1 kHz	153
Figure 7-13 Waterfall for time-averaged Peak amplitude of vibration signal 1 kHz – 2 kHz	154
Figure 7-14 Waterfall for time averaged Peak amplitude of vibration signal 2 kHz – 10 kHz	155
Figure 7-15 Crest factor of vibration spectra (10 Hz to 10 kHz) for different flow rates	156
Figure 7-16 Kurtosis of vibration spectra (10 Hz to 10 kHz) for different flow rates.....	157
Figure 7-17 Spectral entropy of vibration spectra (10 Hz to 10 kHz) for different flow rates	158
Figure 8-1 Raw time domain airborne acoustic signal for flow rate 249 l/min.....	161
Figure 8-2 Raw time domain airborne acoustic signals at different flow rates	162
Figure 8-3 (a) PDF of time domain of airborne acoustics signal for different flow rates	163
Figure 8-3 (b) Amplitude of PDF curve for airborne acoustic signal against flow rates..	163
Figure 8-4 Peak value of time domain airborne acoustic signal with flow rate	164
Figure 8-5 RMS of time domain airborne acoustic signal with flow rate	165

Figure 8-6 Crest factor of time domain airborne acoustic signal with flow rate	166
Figure 8-7 Kurtosis of time domain airborne acoustic signal with flow rate	167
Figure 8-8 (a) Spectrum of the airborne acoustic signal from the pump for different flow rates	167
Figure 8-8 (b) Frequency spectra of acoustic signals at specified flow rates.....	178
Figure 8-9 Baseline airborne acoustic spectrum 20 Hz - 1 kHz for flow rate 249 l/min.....	169
Figure 8-10 Baseline airborne acoustic spectrum 1 kHz-2 kHz for flow rate 249 l/min.....	170
Figure 8-11 Baseline airborne acoustic spectrum for 2 kHz-20 kHz for flow rate 249 l/min.....	170
Figure 8-12 Waterfall time-averaged Peak amplitude of airborne acoustic signal 20 Hz- 1kHz	172
Figure 8-13 Waterfall of time-averaged Peak amplitude of airborne acoustics signal 1 kHz-2 kHz.....	173
Figure 8-14 Waterfall of time averaged Peak amplitude of airborne acoustics signal 2 kHz-20 kHz	174
Figure 8-15 Crest factor of airborne acoustic spectra for different flow rates: 20 Hz to 20 kHz	175
Figure 8-16 Kurtosis of airborne acoustics spectra for different flow rates: 20 Hz to 20 kHz	176
Figure 8-17 Spectral entropy of airborne acoustics spectrum with flow rate: 20 Hz to 20 kHz	177
Figure 9-1 Time domain of raw hydroacoustic signal for flow rate 249 l/min.....	180
Figure 9-2 Time domain of raw hydroacoustic signals at specified flow rates	181
Figure 9-3 (a) PDFs of hydroacoustic signal for different flow rates	182
Figure 9-3 (b) Amplitude of PDF curve of hydroacoustic signal against flow rate.....	183
Figure 9-4 Peak value of time domain of hydroacoustic signal with flow rate	184
Figure 9-5 RMS value of time domain of hydroacoustic signal with flow rate	184
Figure 9-6 Crest factor of time domain of hydroacoustic signal with flow rate.....	185
Figure 9-7 Kurtosis of time domain of the hydroacoustic signal with flow rate	186
Figure 9-8 (a) Spectra (20 Hz – 3 kHz) of the hydroacoustic signal from pump for different flow rates.....	187
Figure 9-8 (b) Spectra (20 Hz – 1.5 kHz) of the hydroacoustic signal from the pump for different flow rates.....	187
Figure 9-8 (c) Frequency spectra of the hydroacoustic signal at specific flow rates.....	188
Figure 9-9 Baseline hydroacoustic spectrum (20 Hz-1 kHz) for flow rate 249 l/min).....	189
Figure 9-10 Baseline spectrum of hydroacoustic signal (1 kHz-1.5 kHz) for flow rate 249 l/min	190
Figure 9-11 Baseline spectrum of hydroacoustic signal (1.5 kHz-3 kHz) for flow rate 249 l/min.....	190
Figure 9-12 Waterfall for time-averaged Peak amplitude of hydroacoustic signal 20 Hz – 1 kHz	191
Figure 9-13 Waterfall for time-averaged Peak amplitude of hydroacoustic signal 1 kHz – 1.5 kHz.....	192
Figure 9-14 Waterfall for time-averaged Peak amplitude of hydroacoustic signal 1.5 kHz – 3 kHz.....	193
Figure 9-15 Crest factor of hydroacoustic spectra (20 Hz to 1.5 kHz) for different flow rates	194
Figure 9-16 Kurtosis of hydroacoustic spectra (20 Hz to 1.5 kHz) for different flow rates..	195
Figure 9-17 Spectral entropy of hydroacoustic spectra (20 Hz to 1.5 kHz) for different flow rates.....	196

Figure 10-1 Normalised PDF for vibration, airborne acoustic and hydroacoustic time domain signals against flow rates in the range 10.5 l/min to 369 l/min	202
Figure 10-2 Normalised Peak values for vibration, airborne acoustic and hydroacoustic signals against flow rates in the range 10.5 l/min to 369 l/min	203
Figure 10-3 Normalised RMS values for vibration, airborne acoustic and hydroacoustic signals against flow rates in the range 10.5 l/min to 369 l/min	204
Figure 10-4 Normalised spectral Crest factor for vibration, airborne acoustic and hydroacoustic signals against flow rates in the range 10.5 l/min to 369 l/min ...	205
Figure 10-5 Normalised Spectral Kurtosis for vibration, airborne acoustic and hydroacoustic signals against flow rates in the range 10.5 l/min to 369 l/min	206
Figure 10-6 Normalised spectral entropy for vibration, airborne acoustic and hydroacoustic signals against flow rates in the range 10.5 l/min to 369 l/min	207
Figure 10-7 Resonant frequency of signal against flow rate	209

TABLES

Table 2-1 NPSH parameters	45
Table 2-2 Recommended impeller type according to specific speed (Lobanoff and Robert 1992)	46
Table 4-1 Details of piping system components, to be read with Figure 4.3	84
Table 4-2 Test-rig components, to be read with Figure 4.3	84
Table 4-3 Specifications of the Gems RFO flow rate sensor (GEMS, 2011)	88
Table 4-4 Specifications of pressure transducer in suction line (GST)	89
Table 4-5 Specifications of the pressure transducer in discharge line (Sinocera, 2009)	90
Table 4-6 Specifications of the accelerometers (Sinocera, 2009)	92
Table 4-7 Specifications of the microphone and preamplifier (Sinocera, 2009)	94
Table 4-8 Specifications of hydrophone (Sinocera, 2009)	95
Table 4-9 Specification of encoder (Hengstler, 2011)	98
Table 4-10 Technical specifications of the speed controller (Omron, 2009)	100
Table 4-11 Technical specifications of the Sinocera YE6230B	102
Table 4-12 Technical specifications of Pedrollo F32/200AH pump and motor (Pedrollo, 2008)	104
Table 5-1 Relative dielectric constant of air and water	112
Table 5-2 Specification of CRYSTEK CVCO55B Voltage Controlled Oscillator	116
Table 5-3 Specification of cable assembly, HF, SMA M/M, 0.25M	116
Table 5-4 Specification of the Advantest R4131D spectrum analyzer	117
Table 7-1 Pump flow rates used to evaluate system for detection of incipient cavitation.....	141
Table 7-2 The values of the variances for the five curves shown in Figure 7-3(a)	143
Table 8-1 The values of the variances for the five curves shown in Figure 8-3(a)	163
Table 9-1 The values of the variances for the five curves shown in Figure 9-3(a)	182

ABSTRACT

This thesis investigates methods for the detection of incipient cavitation in centrifugal pumps. The thesis begins by describing the working of the centrifugal pump which makes this type of pump particularly prone to cavitation. The basic mechanisms of cavitation are described, which explain why this phenomenon is so damaging.

The thesis reports the results of experiments to predict the onset cavitation using a range of statistical parameters derived from: the vibration signal obtained from an accelerometer on the pump casing, the airborne acoustic signal from a microphone close to the outlet of the pump and the waterborne acoustic signal from a hydrophone in the outlet pipe close to the pump. An assessment of the relative merits of the three methods for the detection of incipient cavitation is given based on a systematic investigation of a range of statistical parameters from time and frequency domain analysis of the signals.

It is shown that is the trends in the features extracted are more than their absolute values in detecting the onset of cavitation. A number of recommendations are made as to which features are most useful, and how future work incorporating these suggestions could give a powerful method for detecting incipient cavitation.

A major contribution of this research programme is the development of a novel capacitive method for the detection of cavitation. Some basic theory is presented to show the principles of the device and then the details of its construction and placement in the test rig built for the purpose. The data for the tests using the capacitive sensor are given and we can say definitely that it has been confirmed as a method of detecting cavitation in a pipe system, and that it is a promising method for the detection of the onset of cavitation.

DECLARATION

No portion of the work presented in this thesis has been submitted in support of an application for another degree or qualification of this or any other university or other institute of learning.

DEDICATION

Dedicated to my dear family for their unwavering support and especially my brothers, Mutabe and Fahad, for their unfaltering encouragement throughout my study

ACKNOWLEDGEMENTS

It is hard to begin to put into words how someone took me from a place I can only describe as being in the dark into a place of light. Professor Andrew Ball provided that ray of sunshine that enabled me to complete this study. I will be indebted to him always.

I would like to express my sincere gratitude to Dr Fengshou Gu for his support and guidance, above and beyond the merely technical during my research.

My special appreciation goes to Mr Chris Daykin for his kind help in this research.

I would like to express thanks to Dr Diane Coffey-Burke for her guidance and help in this research.

I would like to appreciate Dr Helen Perry for her assistance in this research.

My thanks to the technical team for their kind cooperation especially Mr Peter J Norman, Mr Steven Goldstein and Mr Philip Holdsworth for their interest, time, and patient guidance.

I would like to thank my friends Fahad and Abdullah Aladwani for their support throughout this study.

ABBREVIATIONS

ANN	An artificial neural network
AC	Alternating current
BEP	Best efficiency point
BPF	Blade passage frequency
CF	Cooling fan
CM	Condition monitoring
CWT	Continuous wavelet transform
DAQ	Data acquisition
dB	Decibels
DC	Direct current
DFFT	Discrete fast Fourier transform
DWT	Discrete wavelet transform
FFT	Fast Fourier transform
HOS	Higher order spectra
Hz	Hertz
IAS	Instantaneous angular speed
ISO	International Organization for Standardization
MCSA	Motor current signature analysis
NPSH	Net positive suction head
NPSHA	Net positive suction head available
NPSHR	Net positive suction head required
PD	Positive displacement
PDF	Probability density function
PVC	Polyvinyl chloride compound
Rf	Rotational frequency
RMS	Root mean square
SE	Spectral entropy
STFT	Short time Fourier transform
SVP	Saturated vapour pressure
UNEP	United Nations Environment Programme

NOTATIONS

A	Area of capacitor plates (m^2)
C	Capacitance of the capacitor (F)
C_T	The total capacitance (F)
C_f	Crest Factor
d	Distance between capacitor plates (m)
f	Resonant frequency (Hz)
$f(t)$	Random noise
RF	Oscillator (CVCO55BE)
g	Acceleration due to gravity ($9.81m/s^2$)
H_{at}	Atmospheric head (m)
H_i	Safety factor at throat of the pump (m)
H_f	Friction head (m)
H_s	Static suction head (m)
H_V	Velocity head (m)
H_{vp}	Vapour pressure head (m)
K	Kurtosis
m_d	The median value of the samples
N	The total number of samples
N_{sm}	Pump specific speed
P	Pressure produced by the pump (N/m^2)
P_g	Pressure gauge head attached to the pump suction(m)
P_r	A reference static head, dependent on the system (m)
Q	Pump capacity (m^3/s)
S_m	Specific speed
v	Velocity of the tip of the impeller (m/s)
V	Flow velocity (m/s)
σ	Cavitation Number
\bar{x}	The mean of the samples

x_i	The value of the i^{th} sample
$x(t)$	Time domain signal
ρ	Density of liquid (water = 1000kg/m ³)
ϵ_0	Dielectric constant of vacuum (pF/m)
ϵ_r	Relative dielectric constant of the fluid between the plates (pF/m)
α	Void fraction
σ	Standard deviation of the samples

COPYRIGHT

- i. The author of this thesis (including any appendices and/or schedules to this thesis) owns any copyright in it (the “Copyright”) and he has given The University of Huddersfield the right to use such Copyright for any administrative, promotional, educational and/or teaching purposes.
- ii. Copies of this thesis, either in full or in extracts, may be made only in accordance with the regulations of the University Library. Details of these regulations may be obtained from the Librarian. This page must form part of any such copies made.
- iii. The ownership of any patents, designs, trademarks and any and all other intellectual property rights except for the Copyright (the “Intellectual Property Rights”) and any reproductions of copyright works, for example graphs and (“Reproductions”), which may be described in this thesis, may not be owned by the author and may be owned by third parties. Such intellectual property rights and reproductions cannot and must not be made available for use without the prior written permission of the owner(s) of the relevant intellectual property rights and/or reproductions,

PUBLICATIONS ARISING FROM THIS RESEARCH

Al Thobiani, F., Gu, F., and Ball, A. (2010) The monitoring of cavitation in centrifugal pumps using spectral entropy of vibro-acoustic measurements, 7th Int. Conf. on Condition Monitoring and Machinery Failure Prevention Technologies, 22-24 June 2010, Stratford-upon-Avon, UK

Raharjo, P., Al Thobiani, F., Gu, F., and Ball, A. (2010) Early failure detection and diagnostics of a high speed self-aligning journal bearing, COMADEM 2010, June 28-July 2 2010, Nara, Japan

Al Thobiani, F., Gu, F., and Ball, A. (2011) Monitoring of cavitation in centrifugal pumps using a non-invasive capacitance sensor. Proc. 24th Int. Congress on Condition Monitoring and Diagnostics Engineering Management, Stavanger, Norway

Tesfa, Belachew, Fengshou, Gu, Arthur, Anyakwo, Faisal, Al Thobiani and Andrew, Ball (2011) Prediction of metal pm emission in rail tracks for condition monitoring application. In: RCM 2011: The 5th IET conference on Railway Condition Monitoring and Non-Destructive Testing, 29-30 Nov 2011, Derby, UK

Abdulrahman Albraik, Faisal Al Thobiani, Fengshou Gu and Andrew Ball. (2011) The Diagnosis of Centrifugal Pump Impeller Faults based on Vibration Analysis, In Proceedings of the 25th International Congress on Condition Monitoring and Diagnostics Engineering Management. COMADEM 2011, Huddersfield, UK

CHAPTER ONE

1. INTRODUCTION AND BACKGROUND

The chapter provides an overview of centrifugal pump types and their applications. It also gives an insight into the development of the centrifugal pump as a prime mover in modern industry, and presents the motivation for the research, its aims and objectives. The final part of the chapter outlines the content and structure of the thesis.

1.1 Applications of pumps and pump types

Nearly all industrial processes require the transfer of liquids from one place to another – so pumps are a fundamental component in industry (ISO/TC115, 2004; Mackay, 2004; Girdhar, 2005). Pumps are used in many different fields, including agriculture; mining; heavy-duty construction; electrical and nuclear power generation; petroleum, pharmaceutical and chemical plant; steel, pulp and paper mills, etc. There are too many applications of pumps for them all to be listed here, but a general idea of the new pump market can be seen in Figure 1-1.

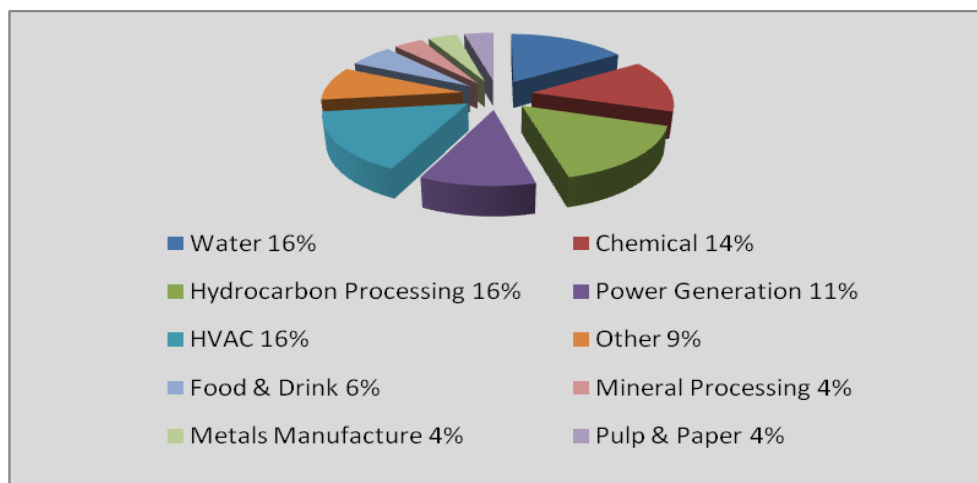


Figure 1-1 Distribution of the new pump market (ISO/TC115, 2004)

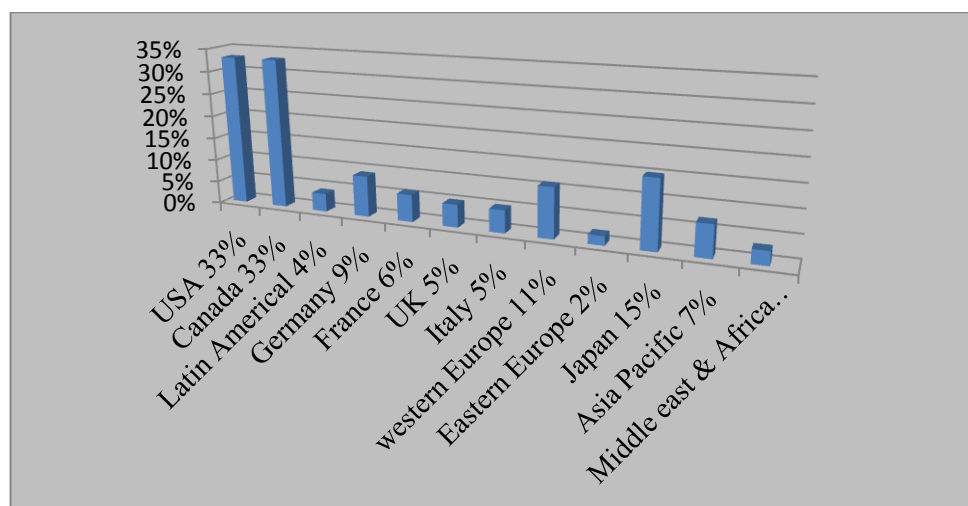


Figure 1-2 World-wide distributions of sales of new pumps (ISO/TC115, 2004)

In 2004 the International Organisation for Standardisation assessed the global market in pumps at \$18 billion, of which, approximately \$13 billion was spent on new pumps,

including after sales market service (ISO/TC115, 2004). In Europe more than 100, 000 people were working in the pump industry, so we can estimate that about 250, 000 to 300, 000 people world-wide are employed in the manufacturing, marketing and after sales servicing of pumps. Figure 1-2 presents the ISO data on the world-wide sales of new pumps.

All pumps transform mechanical energy into hydraulic energy, usually to increase the pressure in the liquid either to compress it or to move it from one place to another (Sahdev, 1987; Girdhar, 2005).

Centrifugal pumps generate pressure by accelerating and then decelerating the fluid through the pump (Mackay, 2004; Girdhar, 2005). The process is straightforward, and it has the capacity to create a moderately high-pressure ratio in a short axial distance. Centrifugal pumps account for about 64% of the new pump market. Figure 1-3 shows a hierarchy of centrifugal pumps classified according to their basic operating principles. In this thesis we are concerned with centrifugal pumps because they account for such a large proportion of the market.

Positive Displacement pumps increase pressure by expanding and then compressing a cavity or moveable boundary within the pump. Positive Displacement (PD) pumps account for 32% of the new pump market, of which about 11% are reciprocating, about 12%, rotary and about 9% diaphragm.

Other pumps include all other pumping mechanisms which, combined, account for about only 4% of new pumps (ISO/TC115, 2004).

1.2 Development of the centrifugal pump

The first design of the centrifugal impeller is attributed to French physicist and inventor, Denis Papin, in 1689. A centrifugal pump is a rotor-dynamic pump in which a rotating impeller converts kinetic energy into fluid pressure or the force needed to move the fluid. The first three-stage centrifugal pump was constructed by W.H. Johnson in 1846 and, in 1849 James Gwynne is reported to have begun the first systematic investigation of the multistage centrifugal pump. During the same period, experiments to determine the best shape of the impeller were carried out by John Appold, a British inventor, who showed that efficiency depended on blade curvature. In 1851 the use of a curved blade impeller with Appold's pump

improved its efficiency three-fold. These developments led to the modern centrifugal pump, see Figure 1-4.

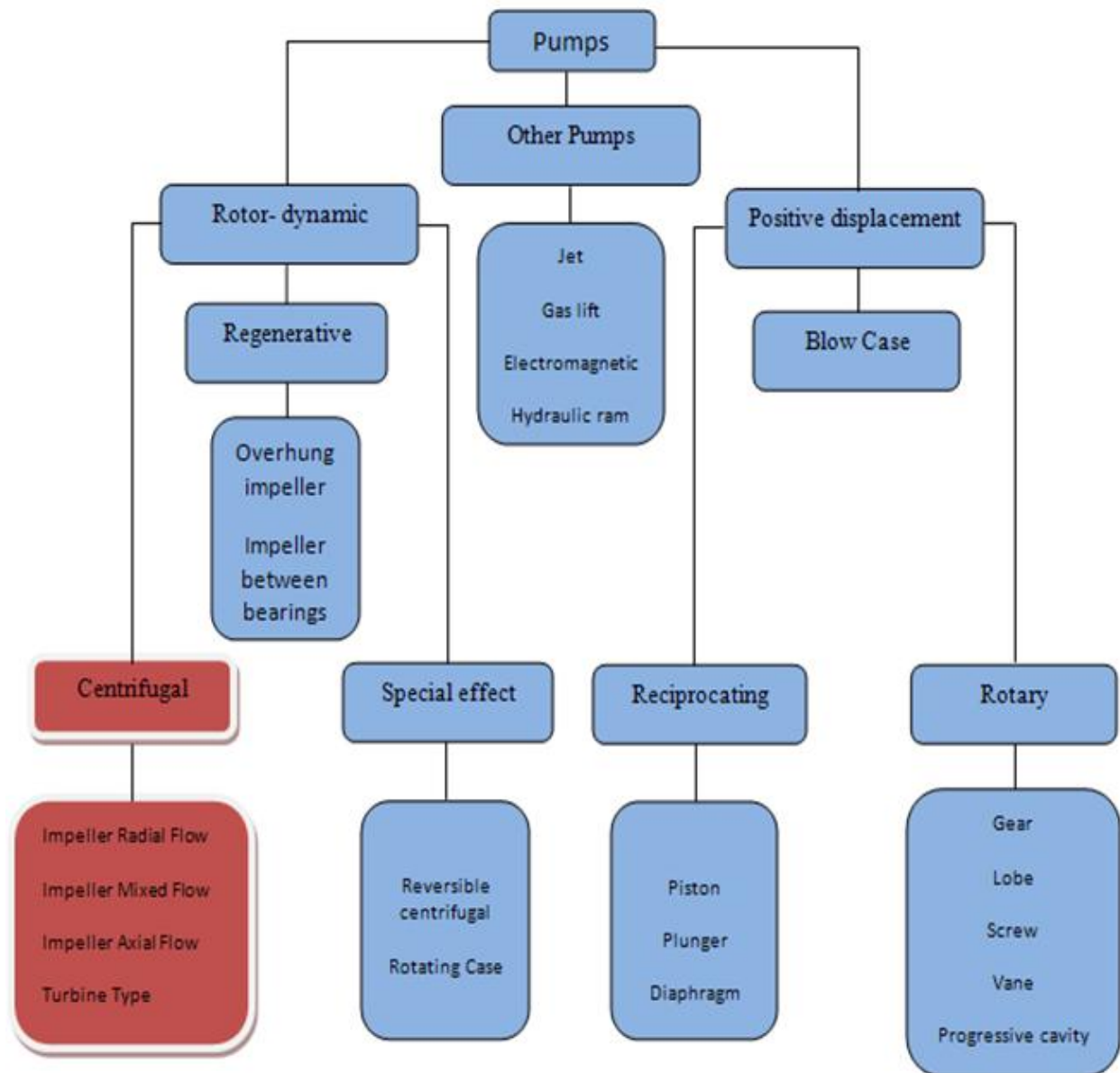


Figure 1-3 Hierarchy of the different types of pumps

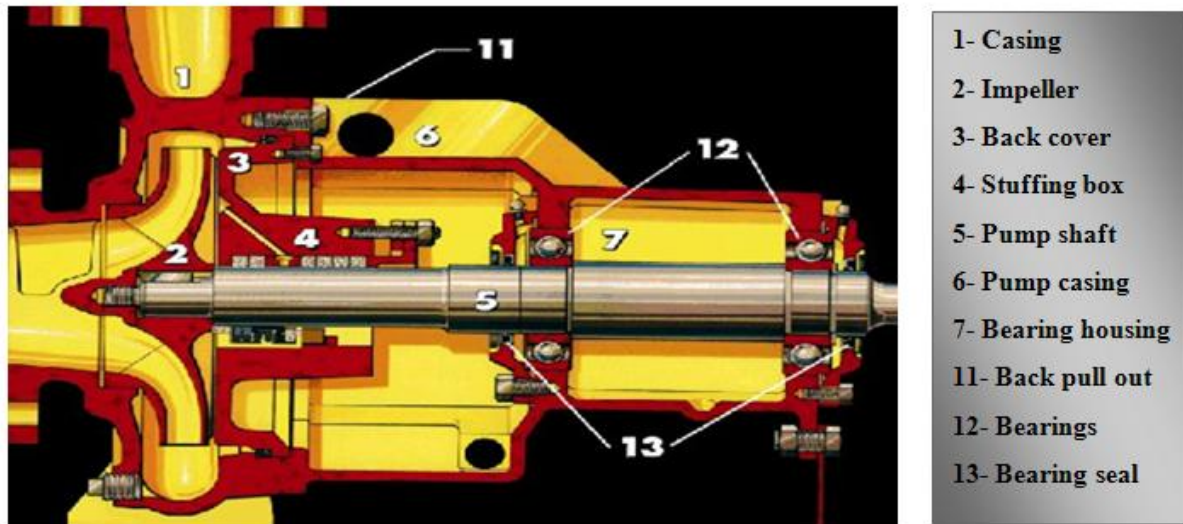


Figure 1-4 Centrifugal pumps – basic construction (Girdhar, 2005)

Centrifugal pumps are widely used because of their design simplicity, high efficiency, wide range of capacity, smooth flow rate, and ease of operation and maintenance (UNEP, 2004; Girdhar, 2005). Centrifugal pumps are relatively inexpensive, have fewer moving parts and tend to have greater onstream availability and lower maintenance costs than other pumps. They also tend to be relatively small with less weight and can be designed to handle liquids containing dirt, abrasives, solids, etc. (Arnold, 1999). Due to their operating principles centrifugal pumps are invariably supplied with the motor attached.

The pump itself has two main parts: the rotating element which consists of the shaft and the impeller, and the stationary element, which consists of the casing, casing box and bearing housing, see Figure 1-5, (Sahdev, 1987; Spectra Quest Inc., 2006). The fluid enters the pump impeller at or near to the rotating axis, and is accelerated by the impeller, flowing radially outward into a diffuser or volute chamber, from where it exits into the downstream piping system. As the fluid leaves the impeller, the fluid kinetic energy (velocity) is converted to (static) pressure due to the increase in area in the volute section, as described by Bernoulli's principle.

Centrifugal pumps are generally classified according to certain of their design features; the most common divisions, see Bachus and Custodio (2003), are between radial-flow pumps, axial-flow pumps, mixed flow pumps and turbines; However it is also common in the literature to find other classifications such as whether the pump is single-suction or double-

suction, single stage, double stage, or multi-stage, volute or diffuser. In this research attention is concentrated on the radial flow pump which is a high-volume, low-head pump having a steep head – capacity (H-C) curve. For industrial pumps of this type a typical flow capacity could range from about $0.5\text{m}^3\text{s}^{-1}$ to more than $500\text{m}^3\text{s}^{-1}$ but the discharge pressure will seldom exceed 3 bar gauge. Thus these pumps tend to be used in low-head, large-capacity applications (Wahren, 1997).

1.2.1 Radial flow centrifugal pumps

Radial flow centrifugal pumps are, probably the most common type of centrifugal pumps, the liquid enters at the centre of the impeller and is directed out along the impeller blades in a direction at right angles to the pump shaft. The radial flow pump is the pump of choice for pumping raw wastes because it can be designed so that the drive shaft does not extend into the suction passage. Thus, materials such as rags and trash that may be present in the flow do not clog the pump. Radial flow centrifugal pumps are available in high head and low flow and are suitable for either wet well or dry well applications see Figure 1-5 (Volk, 2005).

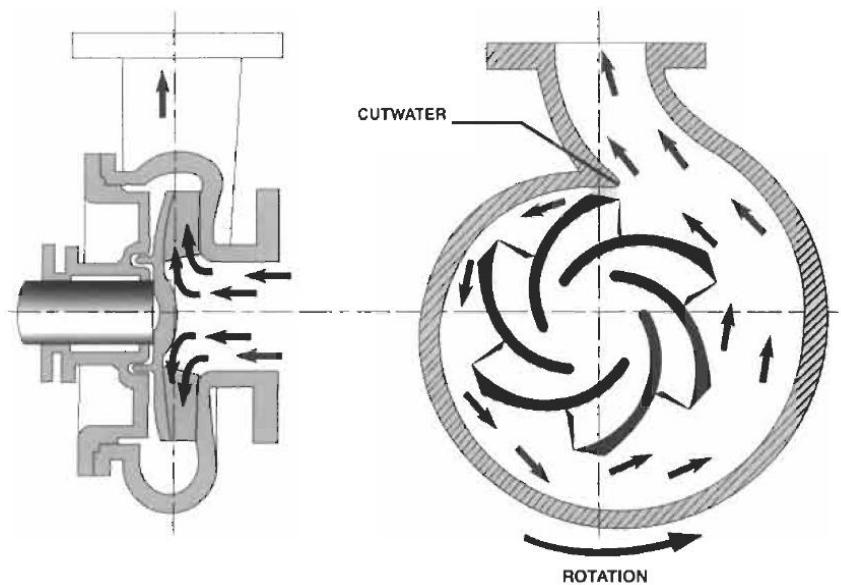


Figure 1-5 Radial flow pumps (Bachus and Custodio, 2003)

1.2.2 Mixed flow pumps

Mixed flow pumps are an intermediate design between radial flow and axial flow type pumps and the operating characteristic is a combination of both. The mixed flow pump generates the pressure head partly by centrifugal force and partly by the action of the impeller blades as they pass through the fluid increasing the velocity of the fluid, the fluid enters axially and can leave either axially or at the circumference of the impeller (Volk, 2005).

1.2.3 Axial flow pumps

Axial flow pumps are designed primarily for use with clear water services and for wet well installations. The axial flow pump is more usually known as a propeller pump and generates pressure due to the increased velocity given to the fluid as the propeller blades pass through the fluid, normally the fluid flows axially. These pumps are subject to being easily clogged by solids, rags, or trash (Volk, 2005).

1.2.4 The turbine pump

The turbine pump is a special form of the centrifugal pump. It resembles the turbine found on a modern jet engine, with many more individual blades than are usually found on centrifugal impellers. Turbine pumps are often used to pump surface waters from lakes and reservoirs, and are also employed extensively as deep-well pumps, which sometimes extend hundreds of meters below the ground surface. Turbine pumps have bearings lubricated with the pumped liquid. These pumps are popular in multi-stage construction (Karassik, et al, 2007).

1.3 Research motivation

Industrial organizations aspire to make profit from the use of equipment and employees. Generally profit is the difference between income from the end product and the total of the cost incurred in the operation process (Löfsten, 1999). Thus, proper maintenance procedures as a way to improve business profitability have developed tremendously over recent decades and are well understood in industry today (Söderholm, 2005).

However, the cost of maintaining pumps is high when compared with other machines. Figure 1-6 shows typical relative maintenance cost of rotating machinery at petrochemical plants. It can be seen that pumps accounted for some 70% of the total maintenance – over US \$70 million in 2011, (Wowk, 1991, amended for inflation). Therefore, any significant improvement in the maintenance of pumps will make significant savings to the cost of maintenance as well as improving productivity, and it is this thought that motivates this project.

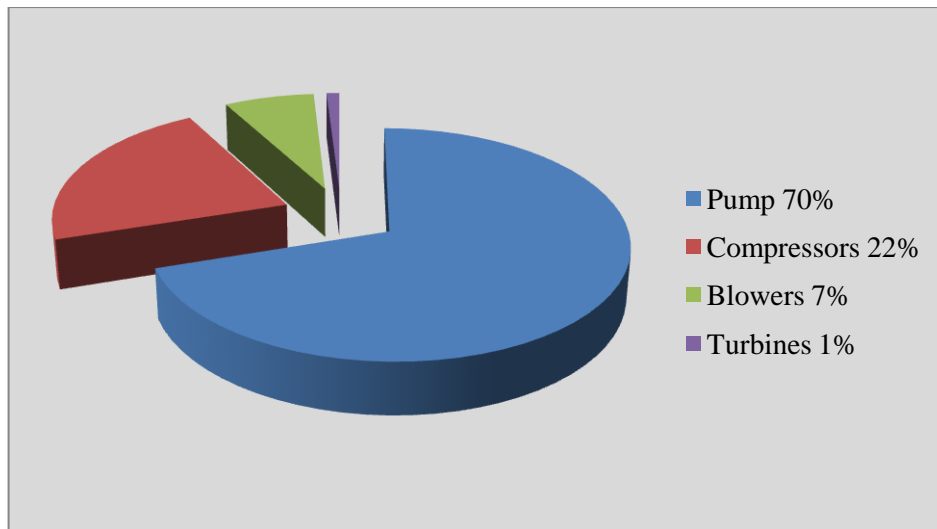


Figure 1-6 Maintenance costs of rotating machines at a petrochemical plant (Wowk, 1991)

In particular, this project will address cavitation which is a serious problem with larger centrifugal pumps, where the time from inception of the problem to catastrophic failure can be a very short time (Escaler, et al, 2006). Cavitation as a pump problem may represent only a small proportion of pump maintenance costs, (about 2% according to Hrivnak, 2003), see Figure 1-7. But that is not the point, cavitation can be hugely costly in downtime, as the between inception to pump destruction can be too short for remedial action. The other aspect is that to avoid cavitation, pumps operate at below full capacity which can be energy inefficient.

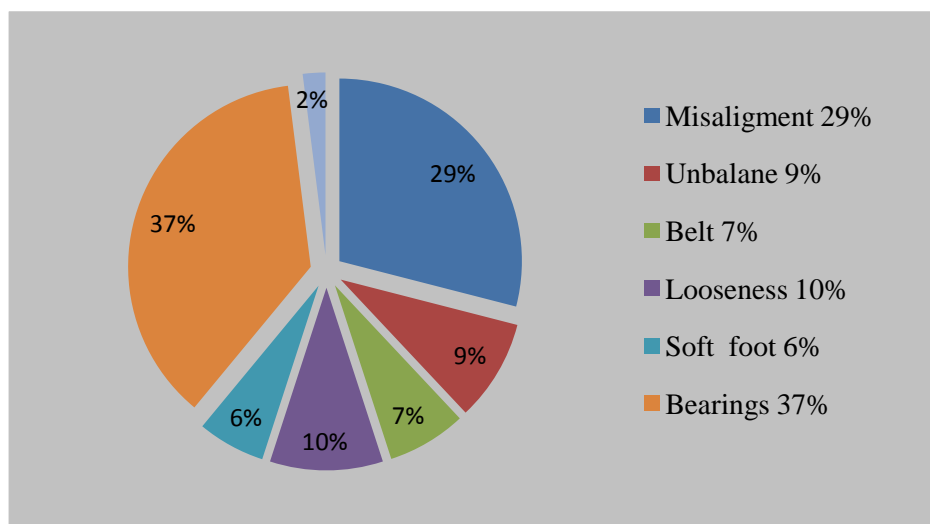


Figure 1-7 Centrifugal pump faults

The development of new technologies has allowed the automation of continuous condition monitoring (CM) which is just what is needed in the case of cavitation, and it is expected that their application to cavitation will lead to early diagnosis and possible remedial action before pump damage or failure occurs.

1.4 Research aim and objectives

Centrifugal pumps are by far the most commonly used pumps in industry and commerce and so have been chosen for this project. The research will investigate the phenomenon of cavitation in centrifugal pumps as it is a relatively common defect in these pumps that can produce high levels of vibration and noise, damage to the pump components and catastrophic failure.

The aim is to help develop an efficient system including a possible new method for reliable and accurate detection and diagnosis of cavitation in centrifugal pumps, with the aim of preventing the growth of cavitation, extending the life of the pump and protecting the system from emergency shutdown. The main objectives of this research are:

Objective one: To describe the dynamics of centrifugal pumps, and the processes by which cavitation is generated.

Objective two: To present and discuss the applications of machine health monitoring.

Objective three: To review conventional methods of monitoring pumps and detecting cavitation.

Objective four: To produce a new method for the detection of vapour bubbles in the flow that can be used alongside conventional methods. This novel sensing approach will be based on advances of sensor and material technologies and should be more sensitive and convenient than current methods.

Objective five: To design and build a test-rig that will allow the controlled onset of cavitation in a centrifugal pump, and allow the study of different pump parameters that may be used for cavitation detection and diagnosis. These parameters will include the signals

obtained from pump vibration, pump airborne and waterborne noise and the signal from any new method developed.

Objective six: To evaluate the pump system experimentally in terms of operational fault induction capability.

Objective seven: To process and analyse the data outputs from the accelerometers, microphone, hydrophone and the newly developed vapour bubble sensor. Analysis of the data will be performed in time and frequency domain.

Objective eight: To perform a relative evaluation of the different methods and statistical techniques to ascertain which is most promising for the detection of the onset of cavitation in the given system.

1.5 Outline of the thesis

The outline of this thesis is as follows:

Chapter One

The chapter describes applications where centrifugal pumps are used and pump types. It gives an overview of the background to the development of the centrifugal pump as a prime mover in modern industry. It also explains the motivation for the research, and its aims and objectives. The final part of the chapter outlines the content and structure of the thesis.

Chapter Two

This chapter reviews the mechanical construction of centrifugal pumps including the impeller, the pump casing and the auxiliary piping system. It then considers the characteristics of the centrifugal pump and its system, including the conditions for the onset of cavitation and cavitation as a system problem. The essential mechanism of the production of cavitation and its general effects are described and the chapter goes on to list the different types of cavitation likely to be met in centrifugal pumps and cavitation flow regimes. Finally, the chapter describes common methods used for the prevention of cavitation.

Chapter Three

This chapter discusses the most common methods of detecting cavitation: visual observation, vibration and airborne acoustic measurements, and waterborne sound using hydrophones. Two recently developed methods, measurement and analysis of the angular speed of the drive shaft of the pump and the current of the motor driving the pump, are briefly described. Introduced in this chapter is the novel idea of a capacitive method for detecting changes in flow conditions due to the inception of cavitation.

The second part of the chapter reviews statistical parameters to be extracted from the signals and their possible use as features to detect the onset of cavitation. Time averaged time domain, frequency domain analyses are presented: RMS, Crest factor, Kurtosis, time-frequency waterfalls and Spectral Entropy.

Chapter Four

This chapter reviews the design and construction of a test rig suitable for measurement of parameters associated with the onset of cavitation in a centrifugal pump. The parameters to be measured are discussed and details of the relevant transducers and data acquisition system given. There are details of measurement practice and data management, followed by a brief description of the use of Matlab for data processing. The manner in which cavitation is to be introduced into the centrifugal pumps is described.

Chapter Five

This chapter develops a new method suggested by the author: that of detecting changes in the capacitance between two electrodes through which pumped flow passes, as a technique for detecting the onset of cavitation. It is suggested that the appearance of vapour bubbles in the flow with the onset of cavitation will change the electrical parameters and this change can be detected and used to diagnose the early stages of cavitation in a pump circuit.

Chapter Six

This chapter describes the construction of the capacitance sensor assembly and presents an analysis of the sensor response based on an equivalent electrical circuit. The experimental response of the system to the introduction of varying air flow (varying void fraction) is given.

Chapter Seven

This chapter focuses on the analysis of the experimental vibration signal obtained from the test pump for the detection and diagnosis of cavitation. A number of statistical parameters are examined as possible indicators of the onset of cavitation.

Chapter Eight

This chapter reports the measurement and analysis of the experimental airborne acoustic signals obtained from the test pump. A number of statistical parameters are examined as possible useful indicators for detection and diagnosis of the onset of cavitation. For ease of cross-referencing, this chapter deliberately follows the structure of Chapter Seven.

Chapter Nine

This chapter reports the measurement and analysis of the experimental fluid pressure signal from the hydrophones. A number of statistical parameters are examined as possible useful indicators for detection and diagnosis of the onset of cavitation. For ease of cross-referencing, this chapter deliberately follows the structure of Chapters Seven and Eight.

Chapter Ten

The chapter is the conclusions and suggestions for future work. It compares and evaluates the different techniques and statistical parameters used in this thesis for the detection and diagnosis of the onset of cavitation in a centrifugal pump. It presents the author's conclusions on CM of a centrifugal pump using a capacitive method. It also reviews the aim and objectives, and describes the achievements one by one by comparing them to the objectives for this study presented in Chapter 1. Then, a summary of the novel features is given, followed by the contributions to knowledge made by this research. Finally the author makes recommendations for future work.

The next chapter introduces the centrifugal pump, and discusses its construction and characteristics. It also introduces flow behaviour and the onset of cavitation in systems powered by centrifugal pumps.

CHAPTER TWO

2. CENTRIFUGAL PUMPS AND CAVITATION

This chapter reviews the mechanical construction of centrifugal pumps including the impeller and pump casing, and the auxiliary piping system. It then considers the characteristics of the centrifugal pump and its system, including the conditions for the onset of cavitation and cavitation as a system problem. The essential mechanisms involved in the production of cavitation and its general effects are described, and the chapter lists the different types of cavitation likely to be met in centrifugal pumps and cavitation flow regimes. The chapter describes common methods used for the prevention of cavitation before describing possible damage caused by cavitation.

2.1 The centrifugal pump

A centrifugal pump is a machine which converts electrical energy into the rotational energy of an impeller, and hence increases the velocity of the fluid being pumped. Figure 2-1 shows the cross-section of a typical centrifugal pump and the direction of movement of the fluid. It is the presence of the stationary volute tongue (also known as diffuser) which converts the kinetic energy of the fluid into fluid pressure.

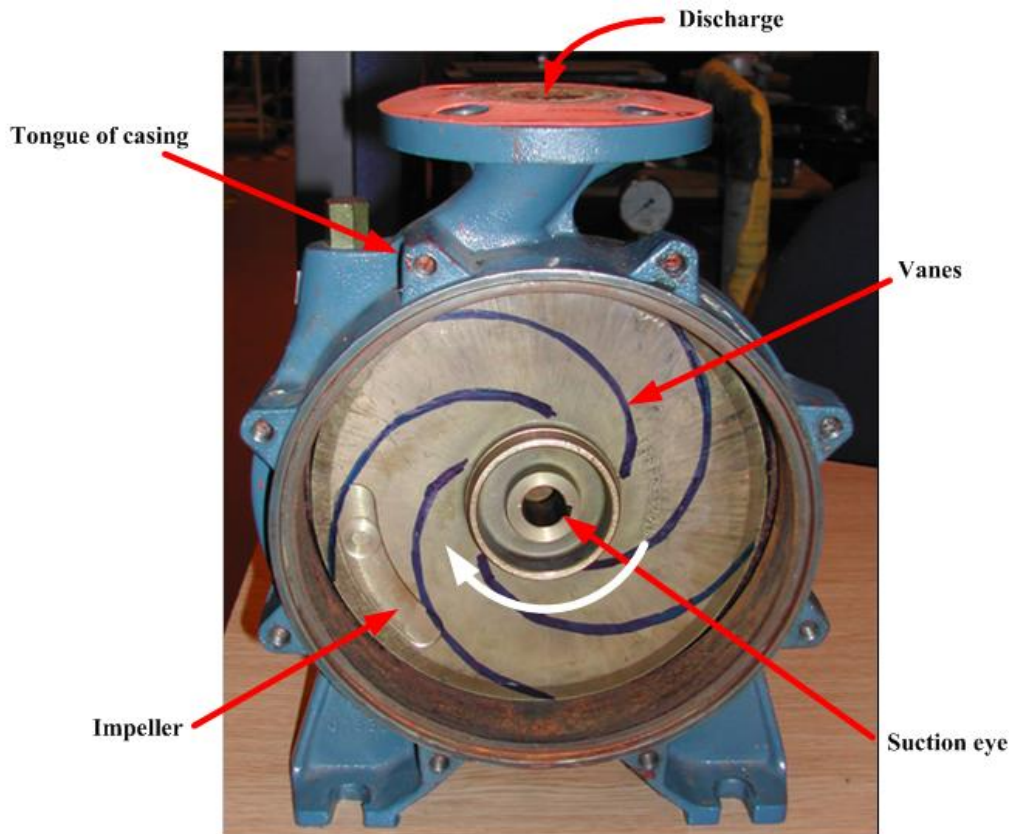


Figure 2-1 Cross-section of a centrifugal pump

The rotation of the impeller creates a centrifugal force which acts to push the fluid sitting between the vanes outwards. This outward movement of the fluid creates a low-pressure area at the suction eye, and liquid from inlet pipe is pushed into the suction nozzle. The curved shape of the impeller blades pushes the process fluid both radially outwards and tangentially.

The kinetic energy of the fluid at discharge will be directly proportional to the square of the speed of the tip of the impeller, and this will determine the pressure head developed by the pump. The volute/diffuser is a curved funnel of increasing area, see Figures 1-5 and 2-1, so that the speed of the liquid passing through it decreases and the pressure increases. The fluid decelerates further in the discharge nozzle, which again increases the pressure (Bachus and

Custodio, 2003; Tuzson, 2000). Because centrifugal pump design involves a large number of interdependent variables there are many possible pumps of different sizes and materials available for the same duty (Khin Cho Thin, et al, 2008).

2.2 Mechanical construction of centrifugal pumps

Because there is a multitude of pump designs that are available for any given task what follows is a general description of the mechanical components of centrifugal pumps. However, the aim of this thesis is to research the effects of cavitation on centrifugal pumps, thus this chapter emphasises damage to components that is caused or exacerbated by cavitation. Of course cavitation is not the only problem with centrifugal pumps. Fluctuating radial loads on the impeller are sometimes caused by unbalanced forces that can be due either to unevenness in the flow through the passages of the impeller, or mechanical imbalance superimposed on the steady radial load. The hydraulic loads are dependent on the type and size of impeller and casing, the pumps operations are conditional on pump speed, fluid suction pressure and the point of pump operation. The magnitude and direction of the hydraulic loads can change greatly with changes in these factors but, generally, the lowest hydraulic loads will exist when the pump is operating at maximum efficiency (Bloch and Budris, 2004). These fluctuating forces generated within the pump are considered only to the extent that they are a background and supplementary to cavitation.

2.2.1 Pump impeller

The rotation of the impeller converts the motor power into pressure and kinetic energy in the pumped fluid; and its shape, size and speed determine pump capacity. Pump impellers are usually made of brass, bronze, plastic or steel and any kind of impeller fault will cause a loss in efficiency and a decrease in pump performance (UNEP, 2004).

The central hub is the mechanism for attaching the impeller to the shaft of the pump. Extending outwards from the hub is a series of curved rigid arms called vanes, see Figure 2.2. The action of the vanes is to hurl the fluid outwards into the volute casing and the centrifugal forces involved transfer the mechanical energy of the motor to the fluid. The type of impeller vanes (thick, thin, long, short, straight or curved) determine the efficiency of a centrifugal pump which is invariably increased (and its structure strengthened) if the vanes are enclosed by sidewalls called shrouds (Spellman, et al., 2000; Grist, 1999).

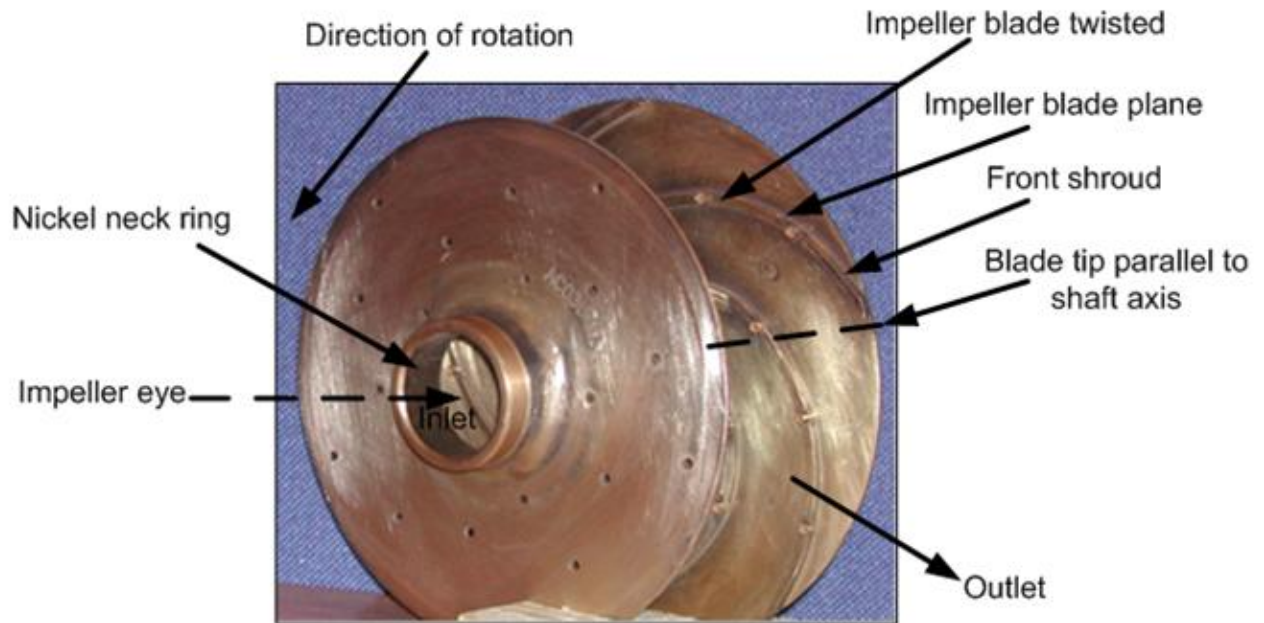


Figure 2-2 Closed impeller with impeller terminology

There are three common types of impeller:

Closed impellers are by far the most common type of impeller unless there are good reasons to choose an alternative. The shrouds extend from the impeller eye to the tips of the vanes, totally enclosing the impeller waterways. The total separation of the inlet and outlet chambers is achieved by the circular neck ring, shown in Figure 2-2, which forms a cylinder that extends from the shroud outwards to actually touch the casing. This has to be periodically renewed (Karassik et al, 2007).

Semi-open impellers have only a back shroud, see Figure 2-3. To prevent any foreign matter in the flow lodging at the rear of the shroud and possibly interfering with pump operation this shroud may have pump-out vanes located at its rear (Karassik, 2007).

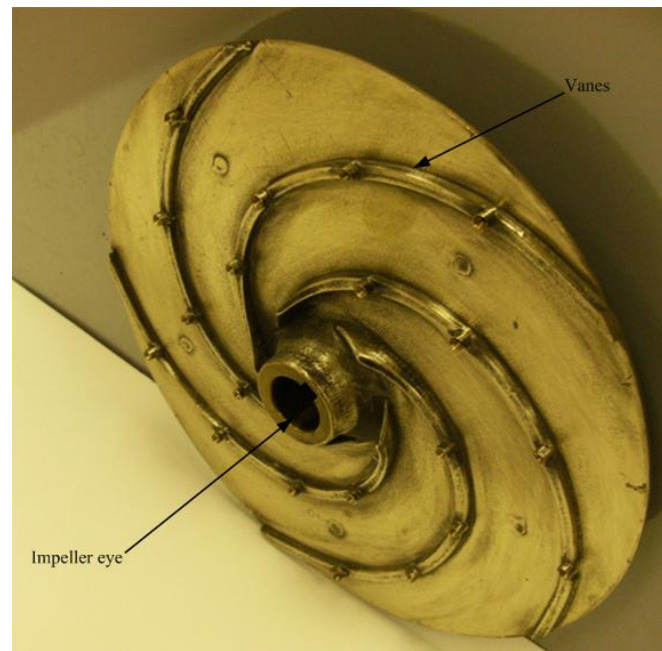


Figure 2-3 Semi-open impeller

Open impellers have no shrouds, see Figure 2-4. Such impellers are generally used only in small, low energy pumps. The vanes, which must be short, suffer from structural weakness and are more prone to wear than either enclosed or semi-enclosed impellers and so must be replaced much more frequently (Karassik, 2007). The greater running costs can usually be justified only in special applications where foreign matter in the liquid might clog a closed impeller pump.

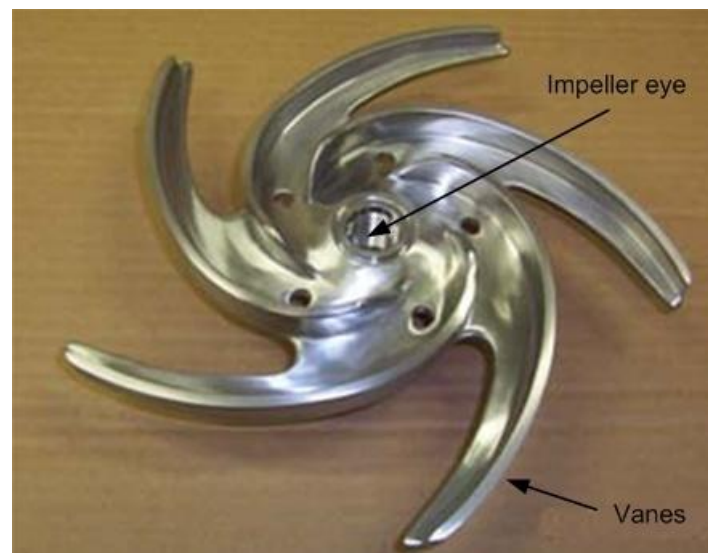


Figure 2-4 Open impeller

2.2.2 Shaft and bearings

The shaft of a centrifugal pump, see Figure 2-5, transmits the necessary torques for rotation of the impeller while supporting the impeller and other rotating parts. Shaft shape and materials will be such that deflection is kept to less than the clearance between the rotating and stationary parts (Choi, 2006). Pump shafts are usually protected from erosion, corrosion, and wear at the seal chambers, leakage joints, internal bearings, and in the waterways by renewable sleeves, see Figure 2-6, (Sahdev, 1987). The shaft sleeve assembly usually extends beyond the outer face of the seal gland plate. Leakage between the shaft and the sleeve should not be confused with leakage through the mechanical seal (Sahdev, 1987).

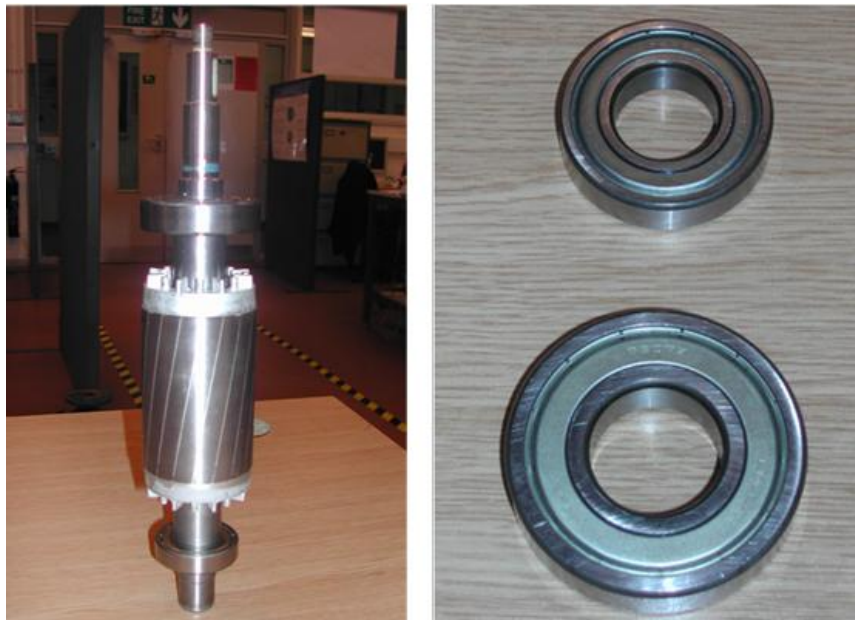


Figure 2-5 Shaft and bearings



Figure 2-6 Shaft sleeve

The bearing housing encloses the shaft bearings and keeps the shaft or rotor in correct alignment with stationary parts, despite radial and transverse loads. The bearing housing also includes an oil reservoir for lubrication, and jacket for cooling by circulating water (Choi, 2006).

2.2.3 Pump casing (volute)

The impeller in Figure 2-2 is not in the centre of the casing. This is a volute pump designed to create a pressure head. The inter-relation of impeller and casing is such that there should be a uniform distribution of velocity and pressure around the periphery of the impeller. This is pretty much achieved in a real volute except at the tongue, see Figures 1-5 and 2-1, which protrudes from the casing into the flow and cuts into the stream of water (hence the alternative name for tongue is cutwater), to deflect it into the discharge. The action of the tongue results in a net radial force on the impeller which is zero at no flow and close to its minimum value at the best efficiency point (BEP). With heavy duty pumps the use of a single volute can result in large unbalanced forces on the impeller, to overcome this a double volute casing can be used. This has two tongues placed to balance the load and significantly reduce the radial hydraulic load on the impeller (Bloch and Budris, 2004).

Smaller pumps usually have a single volute casing, see Figure 2-7, and, to provide more uniform velocity distributions with lower impeller loads, diffuser and circular volutes are commonly used.

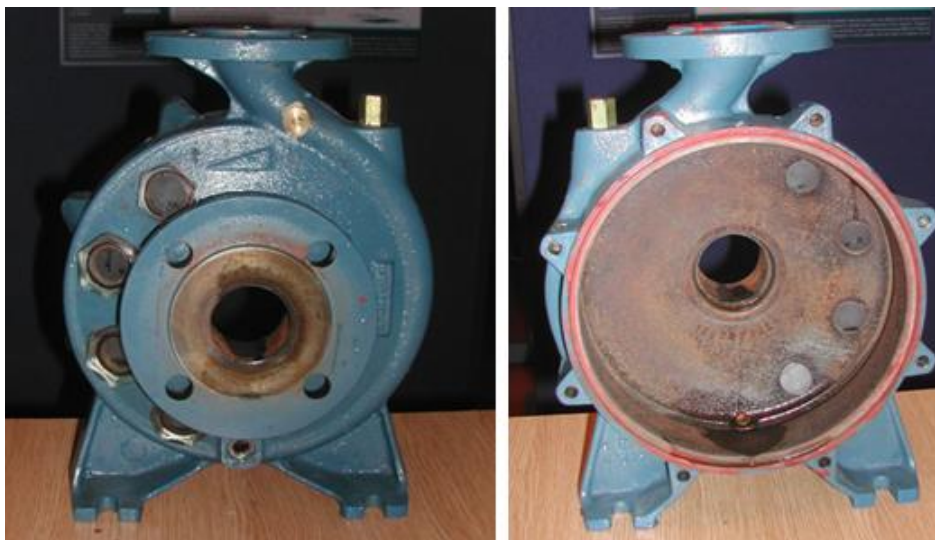


Figure 2-7 Casing of centrifugal pump used on test rig

2.2.4 Wear rings and the auxiliary piping system

As the impeller of a centrifugal pump spins, it creates a low-pressure zone on the suction side of the impeller at the impeller eye and a high-pressure zone inside the volute case. Wear rings are inserted to prevent water from the high-pressure zone being re-circulated and prevent permanent damage to the volute case and impeller. A major cause of pump breakdown is leaky seals, a failure which can be speeded up considerably if cavitation causes large amplitude vibration of the impeller.

Traditionally the most widely used materials for wear rings are bronze or brass alloys and are replaceable items. Bronze exhibits good resistance to corrosion and abrasion, with excellent casting and machining properties. Increasingly, however, O rings of plastic material are being used as these are more easily replaceable and do not cause wear of the metal (Spellman, 2003; Sticlaru and Davidescu, 2004), see Figure 2-8. For proper functioning, a fluid film is maintained between the faces which also act as a lubricant. Because face seals provide lower leakage, less maintenance and a longer life, they are now the first choice for sealing rotating shafts operating under high fluid pressures and at high speeds. A disadvantage of face seals is that when they fail, they do so completely (Sticlaru and Davidescu, 2004).



Figure 2-8 Pump mechanical seal

The auxiliary piping systems include lengths of piping, isolating valves, anti-vibration supports, control valves, relief valves, temperature gauges, thermocouples, pressure gauges, sight flow indicators, orifices for flow measurement, fluid reservoirs and tanks, etc., (Sahdev, 1987). Because the vibration set up by cavitation is wideband, it can excite resonances,

particularly in the pipe work, and can have serious adverse effects up to and including leaky joints and even the fracture of supply lines (Webb, 1976).

Descriptions of seal chambers and stuffing boxes are not included in this thesis even though they can be the cause of a significant proportion of centrifugal pump breakdowns (Barnard, 1991; Schöb, 2002) this is because, while vibration generated by cavitation will adversely affect seals, any resulting problems are not important when compared to the other consequences of cavitation.

2.3 Characteristics of centrifugal pumps and pump systems

The operation of the pump for maximum efficiency lies in the correct design of the pump circuit and the matching of the pump to the circuit. However, most real systems, designed to perform at minimum cost, will include compromises. Thus, in the design of pump systems a dynamic balance will be required, one important element of which is the avoidance of cavitation. This section introduces terms and relations necessary to understand the calculation of the Net Positive Suction Head Required (NPSHR) and the Net Positive Suction Head Available (NPSHA). The key performance parameters of centrifugal pumps are capacity, head, power, BEP and specific speed (Bachus and Custodio, 2003).

Pump Capacity (Q) is the flow rate at which the pump moves the liquid to the required point in the system. It is usually measured in either cubic meters per hour (m^3/hr) or litres per second (l/s). Capacity will usually change with change in operation of the process and depends on such factors as the process liquid, size of the pump and its inlet and outlet conditions, impeller size, impeller rotational speed, the geometry of the pump, and pump suction and discharge temperature and pressure conditions. As liquids are essentially incompressible, the pump capacity, Q , is given by:

$$Q = V \cdot A \quad m^3/s \quad \text{Equation 2.1}$$

Where: A is the cross-sectional area of the pipe into which the pump feeds, and V is the mean velocity of the liquid flow in the pipe.

Velocity Head (H_V) is the height to which the pump could shoot a jet of liquid (usually water) vertically upwards. The height of a liquid column is a measure of the kinetic energy that the pump imparts to the liquid. The main reason for using head to measure the energy of a

centrifugal pump is that the head remains constant with change of liquid so pump performance curves are mostly described in terms of head. Velocity head is also known as pump head (Rose, 2007). The velocity head, H_V , in metres of water is given by:

$$H_V = v^2 / 2g = P / \rho \cdot g \quad \text{Equation 2.2}$$

Where P is the pressure produced by the pump in N/m^2 , ρ is the density of liquid (water = 1000kg/m^3) g is 9.81 m/s^2 , and v is velocity of the tip of the impeller in m/s .

Friction Head (H_f) is the pump head required to overcome the resistance to flow offered by pipes and fittings (Gladstone, et al., 1996). H_f will vary with the diameters and lengths of pipe, the number and type of fittings, the liquid flow rate and nature of the liquid. Values of H_f for most common liquids, pipe materials and pipe sizes can be found in CIBSE Guide C: Reference Data.

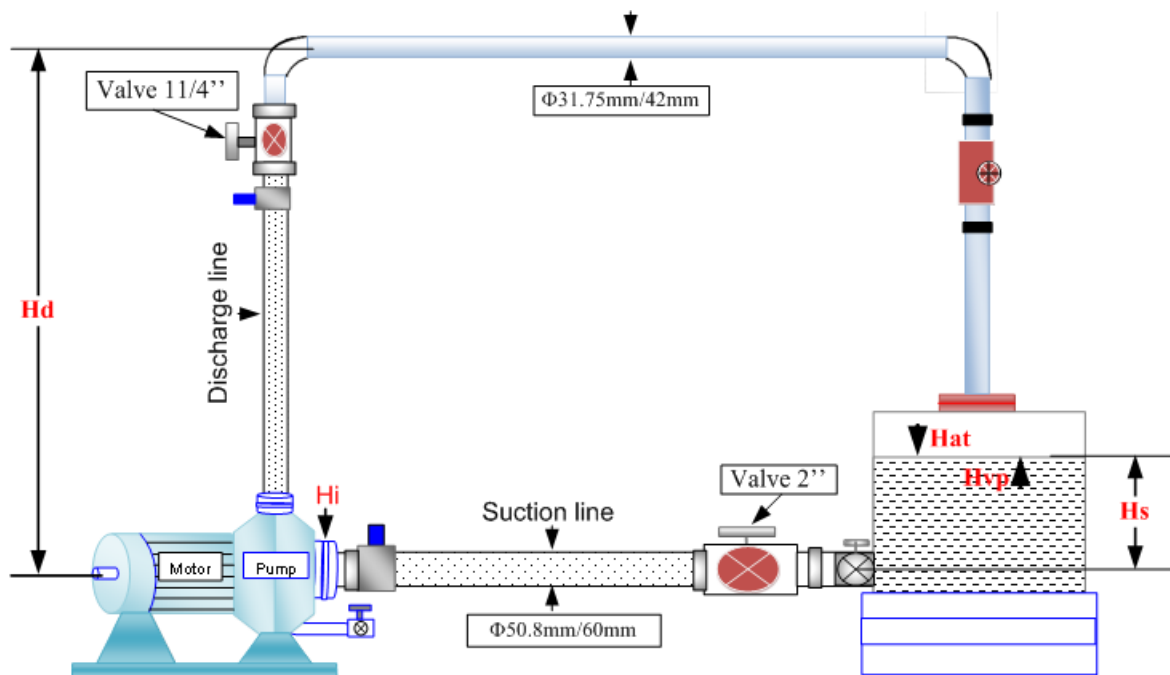


Figure 2-9 Simplified schematic of head versus pressure

Static Suction Head (H_s) is the vertical distance from the centre-line of the pump to the free water level of the source of supply of liquid, see Figure 2-9. When the source of supply is below the centre-line of the pump, it is known as static suction lift (Bachus and Custodio, 2003; Sahdev, 1987).

Vapour Pressure Head (H_{vp}) is the saturated vapour pressure (SVP) of the pumped liquid in terms of head. The SVP of water is readily available from websites such as Rose (2007), and $H_{vp} = [\text{SVP in m of water} / (9.81)]$.

Safety factor (H_i) is inlet head safety factor and usually has a value of between 500mm and 750mm. This is included in system evaluation because, while some pumps have insignificant H_i values, other pumps have inlet losses of this order. The inlet losses occur just prior to the fluid entering the impeller eye (Bachus and Custodio, 2003).

Net Positive Suction Head (NPSH) is equal to the pump static suction head, H_s , minus the vapour pressure, H_{vp} , of the fluid being pumped. For liquids at or near their boiling point the available NPSH is much lower than for cooler liquids.

$$NPSH = H_s - H_{vp} \quad \text{Equation 2.3}$$

Net Positive Suction Head Available (NPSHA) is the pressure head available at the pump inlet, allowing for the SVP of the liquid being pumped (Grist, 1999; Sinnott, et al., 2005). As a general rule the working NPSHA should be at least 10% above NPSH, though some practitioners suggest that NPSHA should be 50% greater than the NPSH to be sure of avoiding cavitation (Bachus and Custodio, 2003). If we assume an open tank then NPSHA will be given by:

$$NPSHA = H_{at} + H_s - H_f - H_{vp} - H_i \quad \text{Equation 2.4}$$

Where the pressure at the surface of the liquid in the feed tank is atmospheric, H_{at} , is 10.19m of water.

Net Positive Suction Head Required (NPSHR) is the minimum suction pressure necessary to ensure proper pump operation. It is currently defined as the suction pressure at which a particular pump's hydraulic performance is degraded by 3 percent (Grist, 1999; Bachus and Custodio, 2003). For a system where the supply tank is open to the atmosphere:

$$NPSHR = H_{at} + H_g + H_v - H_{vp} \quad \text{Equation 2.5}$$

Where: H_{at} , H_{vp} and H_v have their usual meaning as defined above. H_g is the pressure indicated on a gauge attached to the pump suction expressed in metres.

The reason why a centrifugal pump requires a positive suction head is because it is impossible to design a centrifugal pump with no pressure drop between the suction inlet and its minimum pressure point, which normally occurs at the entrance to the impeller vanes. If the pressure at this point drops below a certain level then cavitation will occur. (Cavitation, is discussed in some detail in Section 2.4, below.) Like NPSHA, NPSHR is a dynamic quantity and increases substantially with pump flow. It is accepted practice that $NPSHA > 1.1 NPSHR$ and often engineers work to $NPSHA \geq 1.5NPSHR$. However, once cavitation has started it may require a pressure of up to 2.5 times the NPSHA value to suppress it, or so claims the American Water Pump Industry (Budris, 2009).

The balance between the Net Positive Suction Head Required (NPSHR) and the Net Positive Suction Head Available (NPSHA) at pump impeller will determine the likelihood of cavitation. See Table 2-1

Table 2-1 NPSH parameters

Quantity	Symbol used	System Values (taken from test rig)
Local atmospheric pressure	H_{at}	10.19m (From table)
Static suction head	H_S	0.82m
Friction head	H_f	0.0425 x pipe length in m
Vapour pressure head	H_{vp}	0.255m
Pump pressure gauge reading	H_g	6.67m
Velocity head	H_v	0.708m
Safety factor at throat of the pump	H_i	0.5m – 0.75m

- Net Positive Suction Head Available (*NPSHA*)

$$\begin{aligned}
 NPSHA &= H_{at} + H_S - H_f - H_{vp} - H_i \\
 &= 10.19 + 0.82 - 0.0425 - 0.255 - 0.75 \\
 &= 9.9625\text{m}
 \end{aligned}$$

- Net Positive Suction Head Required (*NPSHR*)

$$\begin{aligned}
 NPSHR &= H_{at} + H_g - H_v - H_{vp} \\
 &= 10.19 + 0.0200 - 0.708 - 0.25 \\
 &= 9.24\text{m}
 \end{aligned}$$

Pump suction specific speed (N_{Sm}): practitioners use a number called the specific speed of a pump, N_S , whose value indicates which type of pump to use and is a way to compare the

efficiency of designs across a large range of pump models and types. Using historic data and laboratory and field tests, pumps have been compared against a number of criteria to help make the necessary decisions. Table 2-2 can be used to compare the efficiency of pumps with the same specific speed, or it can be used as the starting point for comparison or as a benchmark for improving the design and increasing system efficiency. Equation 2.6 gives the value for the pump specific speed, N_{Sm} ; H is the pump total head in metres, N the speed of the impeller in rpm and Q the flow rate in m^3s^{-1} (Chaurette, 2004). Chaurette (2004) gives no units for specific speed and, as can be seen from Equation 2.6, the units of “specific speed” are not rpm. In the literature no units are given.

$$N_{Sm} = \frac{N \cdot Q^{0.5}}{H^{0.75}} \quad \text{Equation 2.6}$$

Table 2-2 Recommended impeller type according to specific speed (Lobanoff and Robert 1992)

Impeller Type	Radial -Vane	Francis- Vane	Mixed Flow	Axial Flow
Specific speed	500-1500	1500-4500	4500-8000	8000-15000

Table 2-2 gives some ideas of the specific speeds associated with different types of pump. Pumps with a radial-flow impeller where the pressure generated is almost wholly by centrifugal force have N_s values between about 500 and 1,500. Pumps, where the pressure is developed partly by centrifugal force and partly by the lift of the vanes of the impeller on the liquid, have N_s values between about 1,500 and 8,000. Axial-flow impellers, where the fluid is moved by the action of the vanes pushing the liquid forward, have N_s values above 8,000 (Bachus and Custodio, 2003).

Also useful is the suction specific speed. The form of the equation is identical to that for the specific speed, but the value of the NSPHR is substituted for H.

$$S_m = \frac{N \cdot Q^{0.5}}{NSPHR^{0.75}} \quad \text{Equation 2.7}$$

The recommendation for avoiding cavitation is that S_m should not be greater than about 4 and Q should be within $\pm 10\%$ of the value for maximum efficiency of the pump.

2.4 Cavitation

The very nature of the centrifugal pump gives rise to a major defect. As explained above, as the fluid is flung outwards by the impeller a region of low pressure is created at the suction eye. If the pressure is lowered so much that it falls below the vapour pressure of the fluid at

local conditions, bubbles of vapour form and cavitation occurs. Experience has shown that severe cavitation can cause catastrophic collapse of the pump within short time (Escaler, et al., 2006). The problem is exacerbated by the fact that the impeller is enclosed and so, usually, the first noticeable sign of cavitation is the onset of severe noise and vibration.

Once generated, the cavitation bubble will travel with the liquid flow. As it does so, it will be subject to an increasing pressure (and possible drop in temperature) which will, eventually, cause its collapse. The collapse of an ideal cavitation bubble in an ideal liquid will follow the Rayleigh-Plesset equation (Ashok et al., 2002):

$$\ddot{R}R + \frac{3}{2}\dot{R}^2 = \frac{1}{\rho}(p_g - P_0 - P(t) - 4\mu\frac{\dot{R}}{R} - \frac{2\gamma}{R}) \quad \text{Equation 2.8}$$

Where R is the radius of the bubble, \dot{R} is the velocity of the surface of the bubble, and \ddot{R} is the acceleration of the surface of the bubble, γ is the surface tension of the liquid, μ is the liquid viscosity, P is the pressure inside the bubble, ρ is the density of the liquid and p_g is the hydrostatic pressure in the liquid. (After Equation 2.8)

The collapse of the cavitation bubble is rapid and results in a large acceleration and very intense local pressures which, even though acting for a very brief time over a small area, can lead to very serious erosion of boundary surfaces as well as high levels of noise and vibration and a drop in pump efficiency (Farhat et al., 2001; Cudina and Prezelj, 2003; Cudina and Prezelj, 2009). An ideal cavitation bubble contracts in size, then springs back, only to contract again, passing through a series of growths and collapses until it finally disappears. A real cavitation bubble, however, undergoes only a single cycle because the bubble breaks up into many smaller bubbles which constitute new nuclei in the liquid. The consequences of cavitation are, amongst other things, damage on solid-boundary surfaces by removing material from the surface. It has been found that cavitation can damage all types of solids, hard and soft, brittle or ductile, chemically active or chemically inert. The cavitation process often involves large fluctuating forces and if the frequency content of these fluctuations matches one of the natural frequencies of part of the machine or equipment, severe vibration may result.

Cavitation is a common fault in centrifugal pumps and, if a pump operates under cavitating conditions the following will always be observed (McNally Institute, 2009): Pump capacity reduced, pump head reduced, high noise level, and high levels of vibration.

If the pump runs for any length of time under cavitating conditions then the following are common (McNally Institute, 2009): Pitting of impeller blades and on the internal volute casing wall of the pump (usually), Mechanical failure of the impeller (often), Premature bearing failure, (severe cavitation) Premature mechanical seal failure (severe cavitation), and Shaft breakage and other fatigue failures in the pump, (very severe cavitation).

2.4.1 Types of cavitation

Incipient cavitation describes cavitation that is only just detectable. There is a certain hysteresis effect with the onset and disappearance of cavitation. The conditions at which cavitation becomes detectable are not the same conditions for cavitation to disappear. Usually an increase in pressure above that at which cavitation appears is required for it to disappear. Van der Meulen (1972) has suggested the term “desinent cavitation” for the latter condition. Cavitation is generally grouped as one of travelling cavitation, fixed cavitation, vortex cavitation, or vibratory cavitation.

Travelling cavitation is where individual transient bubbles appear in the liquid and move with the liquid until they collapse. Invariably such bubbles appear at low-pressure points at solid boundaries or within the body of liquid at points of low pressure generated in turbulent flow (Gorla and Khan, 2003).

Fixed cavitation is where an immersed rigid body is present in the flowing liquid and as the flow detaches from the body a pocket or cavity becomes attached to the boundary. Herbich, (2000) has defined such a fixed cavity as stable in a quasi-steady sense.

Vortex cavitation occurs when the cores of turbulence-generated vortices contain zones of high shear. Such cavities may appear as travelling or fixed (Gorla and Khan, 2003).

Vibratory cavitation is a special case and occurs when the flow velocity is so low that recirculation occurs in the pump and elements of the liquid experience many cavitation cycles. In all other types of cavitation any individual liquid element travels through the cavitation zone only once (Shah et al, 1999).

2.4.2 Cavitation number

The mathematics of cavitation is being investigated at a theoretical level (see, for example, Legarth and Tvergaard, 2010; Ashok et al., 2002) but in practice the situation is so complex that, presently, the universal approach to experimental laboratory and industrial investigations is empiric. For example, one of the most common current approaches developed by D'Agostino et al., (2008) characterises the degree of development of cavitation using a non-dimensional cavitation parameter, the cavitation number, σ , defined as:

$$\sigma = \frac{p_r - h_{vp}}{\frac{1}{2}\rho V^2} \quad \text{Equation 2.9}$$

Where:

p_r : A reference static head, dependent on the system (m)

ρ : Density of the pumped fluid (kg/m^3)

h_{vp} : Vapour pressure of the pumped liquid expressed as a head (m)

V : Velocity of flow (m/s)

It is easy to see why non-cavitating flow corresponds to large values of the cavitation number: large values of σ usually correspond to large values of the reference pressure. In which case, the pressure will everywhere be expected to be above the vapour pressure and the flow will remain free of cavitation. σ is of limited use and is relevant only for those flows for which it can be considered as a scaling parameter, and those parameters must be exactly specified for every situation. For example, consider a single aerofoil in a hydrodynamic tunnel. The flow is increased until cavitation occurs as shown in Figure 2-10. Here σ is usually defined by the pressure and velocity far from the foil, in the undisturbed liquid flow.

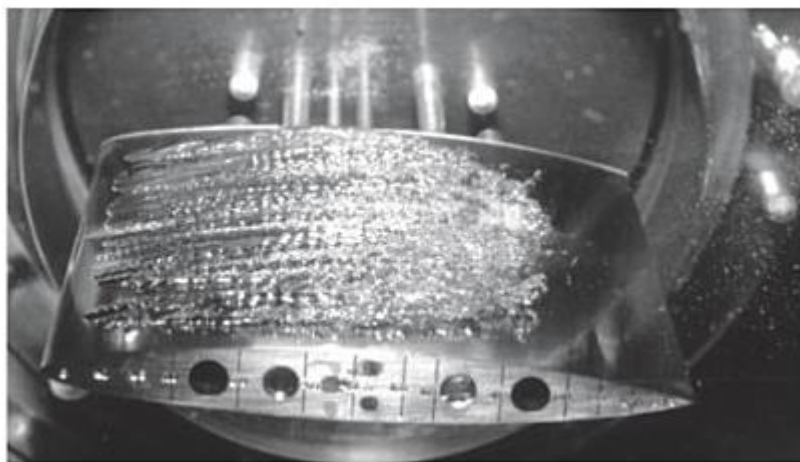


Figure 2-10 Cavity flow on hydrofoil, (D'Agostino et al, 2008)

2.4.3 Cavitation costs

In an industrial centre, in a developed country, when pump impellers fail the typical downtime during which production is lost is about 8 hours. In this situation, Bloch (1998) estimated the repair and replacement costs at that time as: use of maintenance crews about US\$100/hr, replacement impeller US\$3,000 with an additional US\$2,500 for replacement seals and incidental costs (including transporting the necessary items). In the case of severe failure, the downtime would be longer and the costs might also have to include pump housing (typically \$3,000), pump shaft (typically \$2,500), and couplings (typically \$400) (Bloch, 1998). However, in the oil and gas industry unexpected and sudden catastrophic failure of a large centrifugal pump could stop the local production process for a week while replacement parts are obtained and transported to a remote site. In these circumstances the loss of production is out of all proportion to the cost of the pump and its parts, so early detection of cavitation is important for the efficient functioning of the oil well or platform.

2.4.4 Cavitation flow regimes

For centrifugal pumps, when reducing the flow rate progressively from the BEP, three distinct flow cavitation regimes may be observed: stable, unstable, and transient. If either pump or plant is badly designed or mal-operated, it is possible to encounter these regimes (Grist, 1999).

The stable regime: here cavities beginning at the impeller eye develop progressively as they travel with the flow until they collapse somewhere along the vanes. Such flows - on a macro scale – are essentially stable and the inlet pressure of a pump is constant as shown in Figure 2-11.

The unstable regime: usually due to a combination of very low flow rates and inadequate NPSHA. Strong recirculation occurs within the pump and the adjacent inlet pipe work. The pump inlet pressure in the unstable regime will show periodic pulses, see Figure 2-11. Very severe pressure pulsations originate from this hydraulic instability and can be made much worse if the geometry of the impeller and inlet pipe act to assist recirculatory flow. The phenomenon is described as hydrodynamic induced cavitation surging and its onset is principally impeller induced.

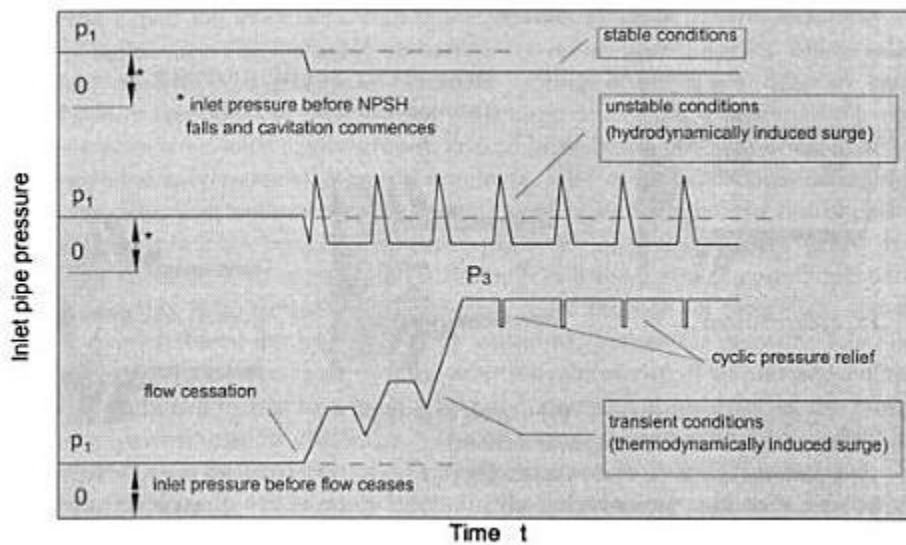


Figure 2-11 General characterisation of stable, unstable and transient regimes inlet pressure /time relationship (Grist, 1999)

The transient regime: here the flow rate has been reduced to such an extent that little or no flow actually passes through the pump. Practically all the energy put into the fluid by the impeller goes into hydraulic churning losses with a resulting temperature rise. The volume expansion associated with this temperature rise is constrained and the inlet pressure builds up, see Figure 2-11. However, the rise in temperature results in the processes associated with cavity growth and collapse to change considerably, and now thermodynamically induced changes dominate. The collapse of the cavitation bubbles associated with the migration of heated fluid from the impeller into the relatively cool liquid in the inlet pipe work gives this regime the appearance of a pressure pulsation which increases in magnitude with time. If a pressure relief valve is included in the system, surging will be observed, see Figure 2-11. Where no pressure relief is provided, the surge motion is suppressed after a cycle or two but the pressure within the pump continues to rise to a level where the mechanical integrity of the pump and inlet pipe work can be challenged.

However, the symptoms of cavitation can be generated by flow conditions other than those described above: high noise and high vibration levels may also be due suction or discharge recirculation or by air entrainment, which have little to do with cavitation.

Suction and discharge recirculation: occurs when the pump operates at a low flow rate, typically at flows lower than 30% of that at BEP, see Figure 2-12. Current evidence suggests

that pitting damage occurs at a point about halfway along the vane, see Figure 2-12, but this will vary with the impeller design and may be on either the trailing or the leading edge.

Discharge recirculation: is also the result of operating the pump at very low flow rates. It also causes pitting damage on the vanes, but at the tips, and sometimes at the volute tongue (especially if the clearance between the tip of the impeller vanes and the volute is incorrect).

Suction throttling valves: are sometimes placed in the pump suction line to better match pump flow to the system. Drieder (2000) has pointed out that this arrangement has a serious flaw – cavitation. The pressure drop across the valve represents an increase in H_f , and thus a reduction in NPSHA. If NPSHA falls too low, to below NPSHR, then cavitation will occur. As a general rule suction throttling should never be used to control pump flow.

Air entrainment: is where vapour bubbles are present in the fluid before it reaches the pump. The vapour bubbles reach the eye of the impeller and are pushed outwards along the vanes with the flow, to be subjected to increasing pressure and then implode. There is little difference in effect between these bubbles and bubbles generated at the pump eye. Vapour bubbles may be present in the system due to:

- Fermenting liquids or foaming agents.
- Liquids operating close to their boiling point.
- Turbulence in the suction line (this is a form of vortex cavitation mentioned above).

Air entrainment can appear very similar to cavitation. The same pitting damage is caused to the impeller in precisely the same location, and often the two problems can occur together. Mackay (2004) has suggested a quick review of the NPSHA will usually identify whether the cause of the symptoms is cavitation or air entrainment. This should be combined with a visual review of the piping to identify the cause of the air entrainment problem.

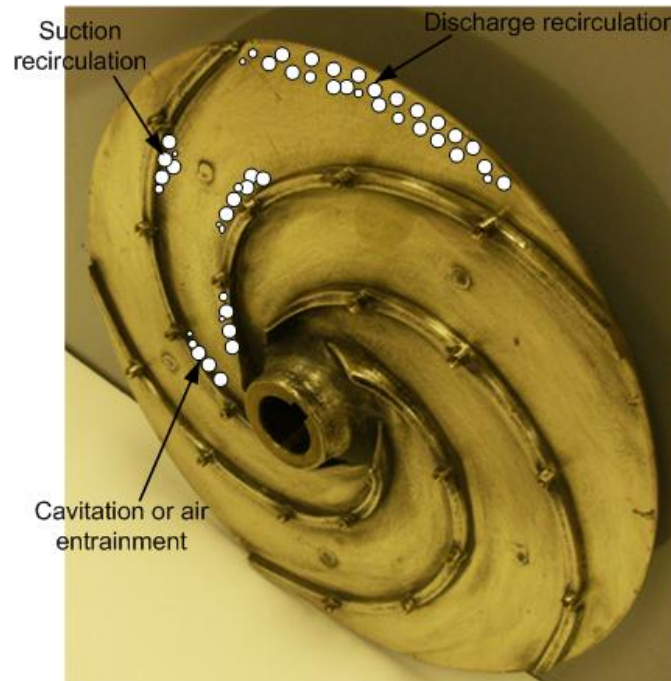


Figure 2-12 Typical pitting damage locations in impeller

2.4.5 Cavitation as a system problem

All pump manufacturers provide characteristic curves showing pump performance in terms of discharge flow rate and pump head. Usually details of pump power and operating efficiency will be included. The BEP is the ideal pump operating point, it is where pump capacity and pump head combine to give maximum pump efficiency. Away from the BEP the pump will be subject to increased wear and reduced operational life. Typically, NPSH data will be provided on the pump inlet pressure at which serious cavitation begins to occur. Cavitation often begins at about a 3% drop in head from BEP, but this value will vary with the physical properties of the liquid being pumped and the surface roughness of the particular hydraulic equipment (Alfayez et al., 2005). Increase in temperature (increase in SVP) will make the system more susceptible to cavitation, as will undesirable flow conditions caused by sharp elbows or obstructions in the suction line immediately before the pump.

2.4.6 Prevention of cavitation

It is usual to solve cavitation problems by a change of system design or operation to increase the NPSHA. If the NPSHA can be increased sufficiently above NPSHR, cavitation will cease. One method is to increase the pressure at the eye of the pump by raising the feed tank or the level of liquid in the feed tank (open to atmosphere) or artificially increasing the pressure in the space above the liquid (closed tank).

An alternative to increasing the NPSHA is to reduce the NPSHR, e.g. lower the temperature of the liquid being pumped so its SVP decreases. This can be an effective method provided the change in temperature is significant and the initial temperature of the fluid is relatively high with respect to its boiling point. An alternative method for decreasing NPSHR is to reduce friction head losses (H_f). Invariably the greatest contribution of H_f is made by the fittings such as valves, tees and elbows. Reducing these would be of prime importance. However, today it could also mean replacing iron pipe and fittings with plastic whose friction factor – all other things being equal – is likely to be lower by a factor of up to 100 (at least while new).

Bachus and Custudio (2003) have pointed out that the NPSHR is not a constant for a given pump under all conditions. They explained that, typically, reducing the flow rate through a pump will decrease NPSHR. However, a pump's flow rate is dictated by the needs of the system which it supplies, so only limited adjustments can be made.

2.5 Damage to centrifugal pumps caused by cavitation

There are no materials which are wholly resistant to cavitation damage. The vapour bubble collapse may produce shock waves of sufficient intensity that they plastically deform the metal locally and destroy any surface film protecting the metal from corrosion and so accelerate the local corrosion process. The tiny depressions so formed not only act as nuclei for the formation of new vapour bubbles which continue to form and collapse but produce pits by the combination of mechanical deformation and accelerated chemical corrosion (Grist, 1999). Cavitation may be reduced by appropriate detailed design changes of the pump such as smoothing the surfaces of the metal, coating the metal, using corrosion-resistant materials, minimizing pressure differences in the cycle, and using cathodic protection (Collins, 1993). There are of course substantial differences in resistance to cavitation between individual materials but in the end they are all attacked by the stresses it generates. The more brittle the material, such as cast iron, etc., the more they are damaged by cavitation because brittle materials fatigue more rapidly.

It is sometimes necessary to operate a pump close to the cavitation limit for reasons of design or price, in which case the parts subject to cavitation should be made of materials which withstand cavitation attack for as long as possible. These are mainly high grade steels;

laminar ferrite cast steel with high chrome content and various bronzes. It is also important that for impellers the cascade profiles have a good aerodynamic shape (Neumaier, 1997).

Cavitation can appear within the entire range of operating conditions, and all means should be taken to prevent it. However, to prevent cavitation in a pump, it is necessary to know how to detect its commencement and development. A smart device for determining the health of a centrifugal pump will continually measure the operating parameters of all key motor-pump-machine trains and present an analysis based on the fusion of current operating conditions. Such technology should be capable of more or less instantaneous in-situ assessments and warn plant personnel automatically whenever the possibility of cavitation exists. These automated diagnostics packages assist by transmitting the analysis directly to maintenance personnel in time for them to make appropriate corrections. Normally it would be expected that such information would be combined from several sources to present an accurate picture of the operating conditions of the pump and its potential for failure (Reeves, 2007).

Figure 2-13 shows where cavitation has occurred on a closed impeller at sites where the local pressure fell below the saturated vapour pressure of the fluid. These were probably the sites where the fluid velocity had a local maximum. The relative severity of the different forms of cavitation will depend on the geometrical parameters of impeller, inlet and collector, the pump flow and the prevailing suction pressure (Gulich, 2007).

Generally, pitting of the impeller surface caused by either cavitation or chemical reaction (corrosion or erosion) between the pumped liquid and the impeller material, can cause serious deterioration of the hydraulic performance which can give rise to damaging structural vibration with resulting high levels of noise. Figure 2-13 shows where cavitation can occur on a closed impeller. Figure 2-14 shows corrosion damage of pump impeller.

Cavitation can be a serious a problem for the pump casing because the forces involved could be so intense that any protective lining of the casing will be rapidly pitted or even stripped away, see Figure 2-15.

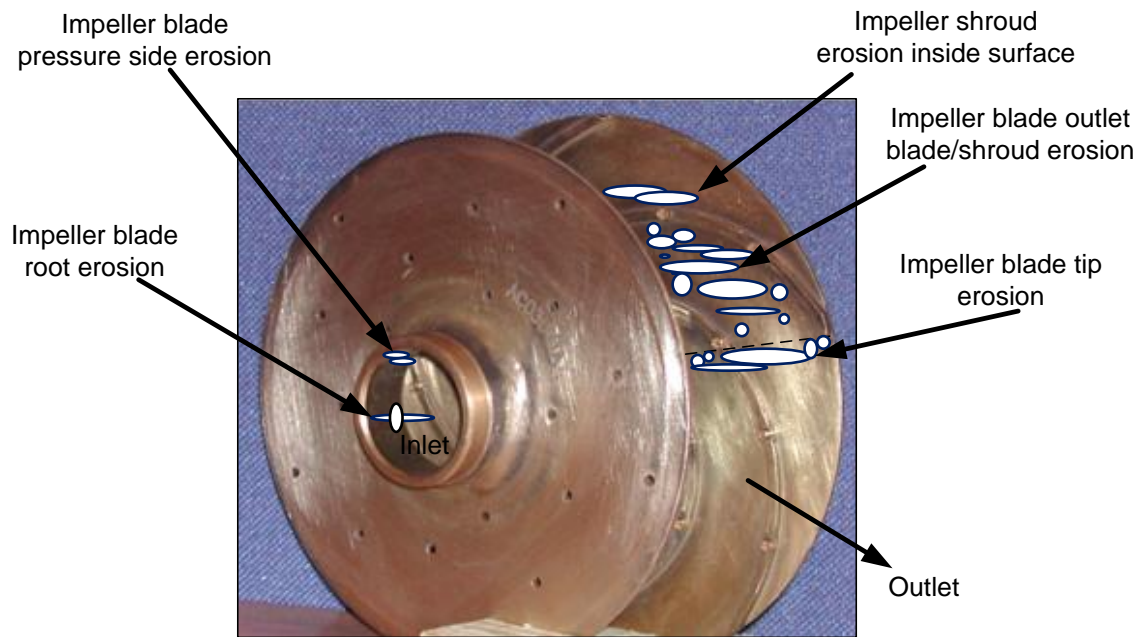


Figure 2-13 Location of likely cavitation sites on impeller used in tests



Figure 2-14 Cavitation damage on the blade of a closed impeller (Brennen, 1995)

A major cause of pump breakdown is leaky seals. The cause of such leaks will depend on operating problems, assembly errors, misalignment, poor selection of seal components and faults in the design of the lubrication circuit which can lead to overheating and degradation of the seal faces. However, failure can be speeded up considerably if cavitation causes large amplitude vibration at the impeller, see Figure 2-16.

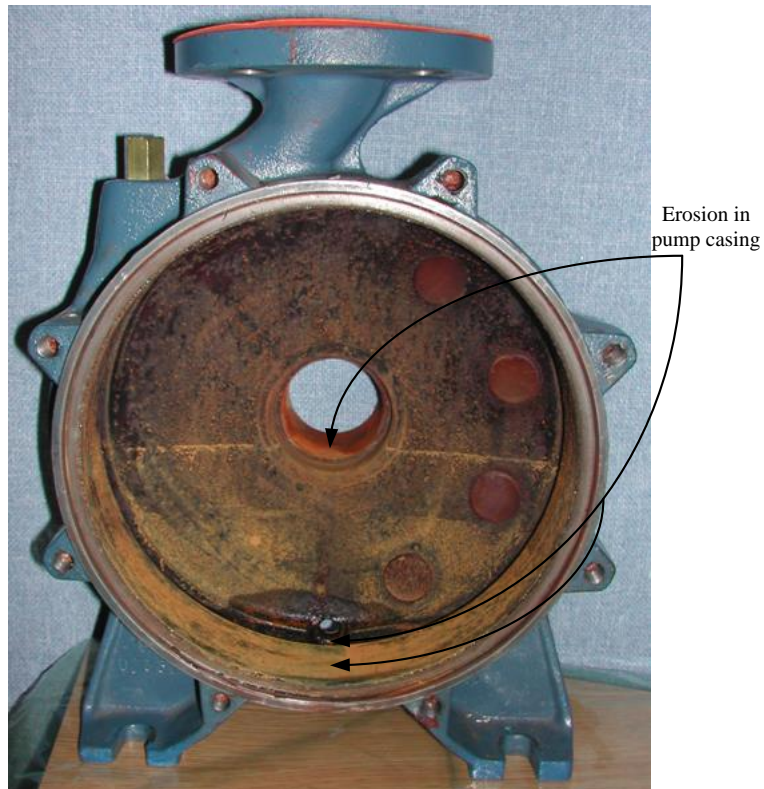


Figure 2-15 Erosion to casing of pump used in the test rig



Figure 2-16 Seal damage

The next chapter introduces current practical methods used for monitoring pumps and detecting cavitation. It then presents a description of statistical parameters that will be used in this research as features in determining the onset of cavitation.

CHAPTER THREE

3. METHODS USED FOR DETECTION OF CAVITATION AND STATISTICAL FEATURES

The first part of this chapter discusses the most common methods of detecting cavitation: visual observation, vibration and airborne acoustic measurements, and waterborne sound using hydrophones. Two recently developed methods, measurement and analysis of the angular speed of the drive shaft of the pump and the current of the motor driving the pump, are described. Introduced in this chapter is the novel idea of a capacitive method for detecting changes in flow conditions due to the inception of cavitation.

The second part of the chapter reviews statistical parameters to be extracted from the signals and their possible use as features to detect the onset of cavitation. Time averaged time-domain, frequency-domain and time-frequency-domain analyses are presented: RMS, Crest factor, Kurtosis, time-frequency waterfalls and Spectral Entropy.

3.1 Detection of cavitation using flow visualisation

Direct detection of cavitation is possible with flow visualisation. However, gas or vapour filled cavities can be seen only if the fluid is somewhat transparent (which, of course, water is) and visual devices can access the region of cavitating flow. Visual observation of cavities has been used with centrifugal pumps when clear pipes were mounted in the region of the cavitating flow, i.e. on the outlet of the pump (Koivula, 2000). Figure 3-1 shows a simple laboratory experiment to demonstrate water flow with and without cavitation, the difference is observable because the flow is seen through a transparent plastic tube. Figure 3-1(a) shows the flow without cavitation and the water is clear. Figure 3-1(b) shows the flow with cavitation and the water flow in the circuit is “cloudy” due to the presence of vapour bubbles.



Figure 3-1 (A) - Centrifugal pump without cavitation (B) - Centrifugal pump with cavitation

Flow visualisation can be a useful confirmation of cavitation, but is not widely used for three simple reasons, the pump and its associated pipe work may not be accessible to visual inspection, initially the cavitation bubbles may be too small to see with the naked eye, and for the bubbles to be “seen” cavitation must already be established. Some researchers have attempted to use light sources and photodiodes, or stroboscopes and computer aided cameras but no record was found of them being used industrially (Tropea, 2007). Čudina and Prezelj (2009) suggest that visualisation is suitable for high powered pumps and water turbines but cite no examples of its industrial use.

3.2 Detection of cavitation using acoustic measurement

A certain level of noise is to be expected from centrifugal pumps and their motors, which will be a minimum at the BEP. If the operating point is off-design, noise and vibration are increased due to instability and pressure pulsations, particularly at flow rates below about 65% of the BEP (Cernetic, 2009). However, high noise levels may be considered as an indication of the presence of cavitation. And it is this noise that is considered here. The bubbles generated by cavitation appear and collapse more or less randomly and produce a broadband acoustic spectrum. Mechanical noise sources within the pump will also contribute to the overall noise level and will contain discrete frequency components such as the blade passing frequency of the pump (generated as the vanes on the impeller pass the volute tongue). In this investigation the type of cavitation will be limited to that generated by low flow rate into the pump.

When cavitation within the pump occurs, noise is produced by the pressure pulses generated by the collapse of the vapour bubbles when they enter a region of high pressure. Because the diameters of the bubbles are so much smaller than the wavelength of the sound produced, they are considered monopole sources of sound. The bubbles are small so the frequency of the sound generated is high and cavitation noise has a characteristic hissing sound which is easily detected by the human ear. At the beginning of the cavitation process, bubbles are not only very small and but also very few and thus correspondingly hard to detect (Cernetic, 2009).

Airborne acoustic noise measurements on centrifugal pumps have been carried out by Alfayez and Mba (2005) and Cudina (1998). Microphones with a linear response over the audible spectrum were placed 0.5m and 1.0m from the test pump, this was considered the acoustical near field because the pump noise at those points was estimated to be substantially more than the background [however it is more usual to consider the near field as within a quarter of a wavelength of the source (Dowling and Ffowcs-Williams, 1983)]. Nevertheless, both these distances are too large to be of general use in industry due to the high levels of background noise that often exist. Both investigations found that cavitation noise was clearly discernable in any analysis of the measured sound pressure. Cavitation noise exceeded that of the pump, motor, and other fluid borne noises, by as much as 20dB, and the increase in the high frequency noise content was especially noticeable. Upstream and downstream pressures were varied as were solid and gaseous contaminant concentrations. For increasing amounts of

both solid and gaseous contaminants in the fluid being pumped, cavitation inception occurred sooner than with uncontaminated fluid.

McNulty and Pearsall (1982) showed that the noise measurements, when normalized to a reference level, had the same distinct shape confirming results reported by Knapp, et al., (1970), and Ball and Tullis (1973). Cavitation inception was defined as the first change in slope as indicated in Figure 3-2. As the downstream pressure decreased, noise emission increases strongly at inception of cavitation and continues to increase until fully developed cavitation occurs at roughly a 3% drop in pressure head.

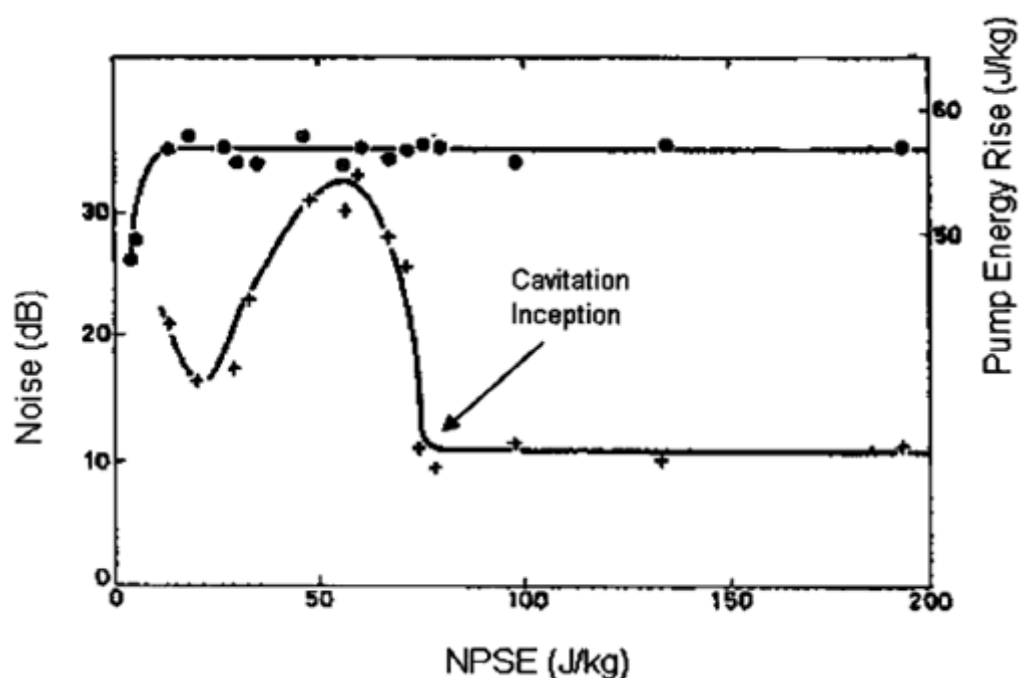


Figure 3-2 Abrupt change in airborne sound level showing onset of cavitation, (adapted from McNulty, et al. 1982)

This is still pretty much the present state of airborne acoustic detection of cavitation (Beebe, 2004). Recent developments by researchers such as Čudina and Prezelj (2009) have investigated the use of discrete frequencies. For example, they attempted to use multiples of the blade passing frequency, but their results appear to be pump specific (Cernetic, 2009).

Another and important development is the possibility of enhanced signal processing techniques extracting useful diagnostic information from contaminated acoustic signals (Cudina, 2003; Elhaj, et al., 2003; Albarbar, et al., 2004). While such techniques have proved valuable in fault detection in e.g. reciprocating compressors and electric motors, little has been achieved in the field of cavitation noise. Possibly the most useful indications for

future research have come from the work of Alhashmi, (2005) who analysed the near field sound radiated from a centrifugal pump. This researcher investigated the signal obtained in a number of ways; overall RMS noise level, frequency analysis (both fine frequency and frequency bands), probability density function, and standard deviation. The probability density function and overall RMS noise level showed nothing new, but did confirm the results of previous researchers, that the amplitude of the acoustic signal rose rapidly after the onset of cavitation. A normalised acoustic spectrum was presented – produced by dividing the RMS noise level measured over the range 2 kHz to 20 kHz by the RMS noise level measured over the range 20 Hz to 2 kHz – which produced a graph which showed an enhanced gradient with the onset of cavitation. However, this may be an anomalous result since the only set of readings for the 20 Hz to 20 kHz range shows an uncharacteristic dip in noise level at the onset of cavitation. More interesting was Alhashmi's finding that the standard deviation of the acoustic signal showed a drop just before a rapid rise due to the onset of cavitation see Figure 3-3.

Alhashmi placed the microphone 200 mm away from the discharge side of the pump and so was not in the near field for frequencies below about 6 kHz. This is unlikely to be important as long as it is recognised that the noise measurements before and after cavitation are only for comparison with each other.

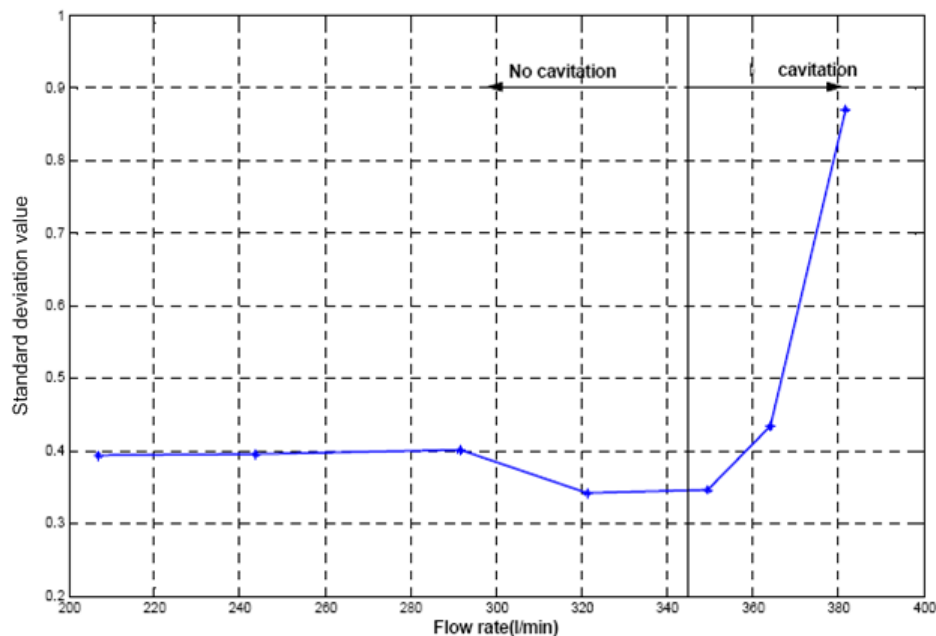


Figure 3-3 Standard deviation of the airborne acoustic signal from a centrifugal pump with the onset of cavitation (Alhashmi, 2005)

3.3 Detection of cavitation using vibration measurement

Vibration analysis has been proved a powerful tool for the early detection of faults in, and the potential failure of, many mechanical systems. Ideally, when considering a centrifugal pump the measurement locations should be sited so as to obtain a vertical, horizontal and axial vibration readings but this is not always possible or necessary in practical situations. For the detection of cavitation at least one of the transducers should be placed on the volute casing, as close to the source of the cavitation as possible (Beebe, 2004), see Figure 3-4.

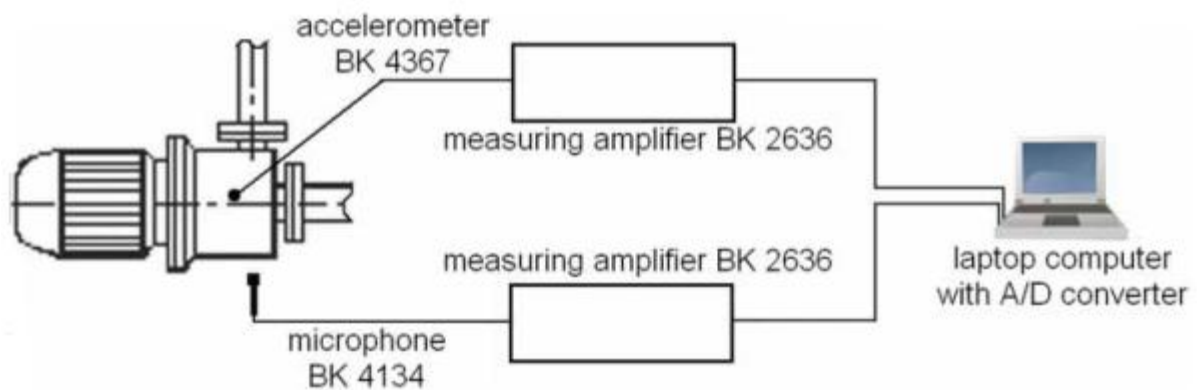


Figure 3-4 Positioning of vibration transducers for cavitation detection (Cernetic 2009)

The vibration signal is invariably measured on the outer casing of a pump and will be, essentially, a combination of the responses to two main types of vibration excitation: flow induced vibration such as occurs when fluid interacts with vanes or casing or other parts of the system to cause periodic oscillations in the flow; and vibration due to moving parts periodically passing each other (Scheffer, 2008). Traditionally, low-frequency vibration was best measured using displacement and, as the frequency increases, velocity and then acceleration became more suitable (Williams, et al., 1994). However, technological development has provided modern accelerometers with a wide frequency range, the limits of which are often determined by the manner in which they are mounted rather than the transducer itself. The preferred method for mounting accelerometers on machines such as pumps is stud mounting. A stud is rigidly attached, usually by drilling and tapping into the surface whose acceleration is to be measured. The accelerometer can then be screwed tightly onto the stud (not so tight as to generate a piezoelectric voltage in the device) and may be used for frequencies of interest up to at least 20 kHz (Bies and Hansen, 2003).

A number of authors Cernetic (2009), Cudina (2003), Dister (2003) and Escaler (2004) have investigated and discussed the main feature of the vibration signal of centrifugal pumps and

turbines under cavitation. They confirmed what had been previously reported, that the vibration signal from centrifugal pumps experiencing cavitation was broadband with a pronounced high frequency content and containing discrete frequency components. The upper limit to the frequency spectrum was determined more by the upper frequency limit of the transducer than the source. They also confirmed that, as with the airborne noise, the onset of the enhanced vibration due to cavitation was rapid. However, these authors tended to report increased levels of about 10 dB rather than the 20 dB found with airborne noise, this was due to the large levels of vibration already present in the system, see Figure 3-5.

Advances made in signal processing offer a possible advance in detecting the onset of cavitation. As yet this approach is not widely used, the signal processing being largely confined to spectral analysis and definition of defined peaks within the broadband vibration signal.

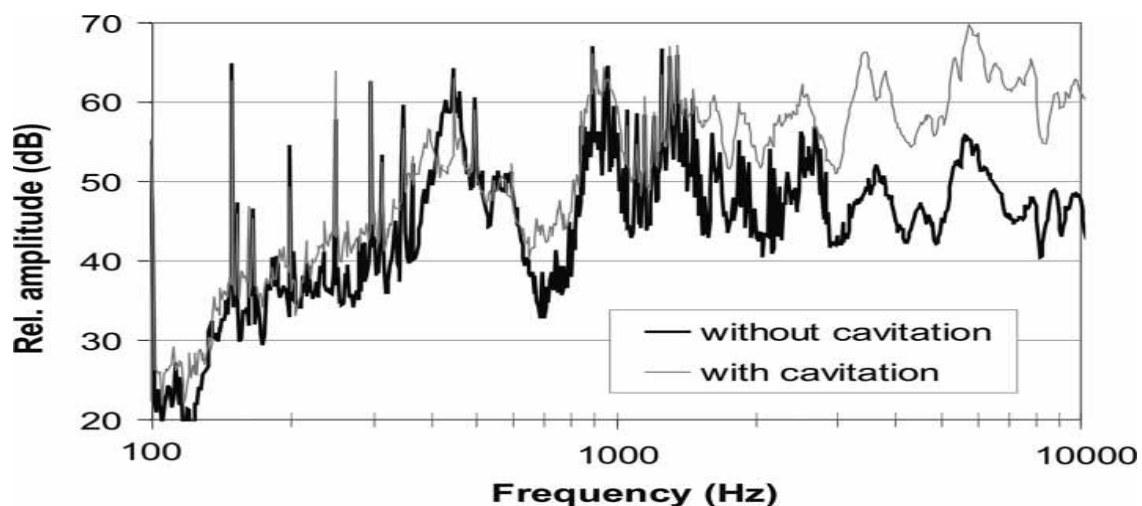


Figure 3-5 Vibration signal from a centrifugal pump with and without cavitation (Cernetic, 2009)

Alhasmi (2005) took the first steps in processing vibration signals from a centrifugal pump in an attempt to detect the onset of cavitation. He performed the standard time-domain analyses such as RMS and frequency spectrum but he also used probability density function and standard deviation for analysing the acquired data in the time-domain. It was Alhasmi's methods that were the useful step forward not his results, since for the vibration analysis his only suggestion was that the amplitude of the vibration signal in the lower part of the frequency range (<4 kHz) might be sufficient for the detection of cavitation. This latter point was also suggested by Cernetic (2009).

Čudina and Prezelj (2009) compared airborne, vibration and acoustic emission (AE) methods for the detection of cavitation and concluded, surprisingly, that the latter two offer fewer opportunities than airborne acoustic methods.

3.4 Detection of cavitation using acoustic emission methods

AE usually refers to transient elastic waves generated by the release of energy, or some other process, within a solid material and generally involves the detection of the waves within the range 40 kHz to 1 MHz. This frequency range is usually much higher than background and so has the useful consequence that a better signal to noise ratio can be achieved. Today, AE is predominantly used in the detection of microscopic changes in a material where deformation and cracking produces elastic waves which travel through the material and are detected by piezoelectric transducers. However, AE includes such phenomenon as cavitation because the collapsing vapour bubbles act as impulsive sources which generate acoustic noise (and vibration) with a frequency content which can range from less than 1 kHz to nearly 100 kHz (Sachse, 1991). The apparently continuous emission that occurs with cavitation results from rapidly occurring events and can be made up of a multitude of small discrete events that overlap so that the resolution of individual pulses is not possible.

It is a general rule in acoustics that high frequencies are attenuated more rapidly than low frequencies, and hence there is a relative decrease in amplitude of the high frequencies when measuring sound at any distance from the source. In addition, in industrial situations it is usual for several pumps to be in more than one circuit and to feed into a common header. Also the water flow in the pipe will itself generate noise particularly if it passes through valves and around bends. It is therefore practically important to place hydrophones as close to the source as possible because the AE features in the signal will change with sensor position with respect to the cavitation site. The further the sensor is from the site of cavitation the weaker and more contaminated the detected signal. Even 1m downstream much useful information can be lost. It is commonly recommended that hydrophones be placed immediately downstream of the discharge side of the pump (Chu et al., 1995; Neill et al., 1997; Rose, 2007). The signal from the hydrophone will also be contaminated by vibration of the surrounding structure and this is an additional reason for having the hydrophones as close to the source of cavitation as possible, though some researchers such as Čudina and Prezelj (2009) have used the A-weighting network as a filter to eliminate unwanted background noise.

AE has long been an accepted method for the detection of cavitation in pumps. Courbiere (1984) used piezoelectric pressure transducers as hydrophones installed at the suction and discharges of various sized pumps operating at different speeds. He was able to detect the onset of cavitation when the flow rate into the pump was decreased, see Figure 3-6.

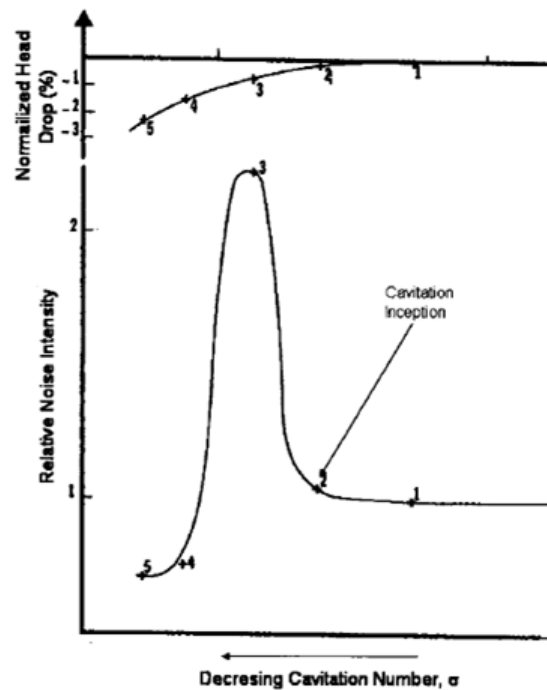


Figure 3-6 Pump head and relative intensity of acoustic emission as functions of cavitation number, showing onset of cavitation (Courbiere, 1984)

3.5 Recently developed methods for detection of cavitation

Alhasmi (2005) introduced two new possible methods for the detection of cavitation; the measurement of the instantaneous speed of rotation of the pump shaft and analysis of the electric current through the motor driving the pump.

3.5.1 Angular speed of the pump shaft

Pressure pulsations are unavoidable in a centrifugal pump due, e.g., to the action of the blades on the impeller as they pass the volute tongue, and this leads to fluctuations in the hydraulic load on the driving motor and a consequent change in the instantaneous speed of the pump shaft. There are standard methods for measuring the shaft speed using an encoder that will detect these fluctuations (see for example Elhaj, 2003).

The pressure pulsations within the pump will be a function of both pump design and operating conditions such as the delivery head and acoustic matching with the piping

systems. Of course, if a pump is cavitating that will cause a significant change in load on the motor which should affect the shaft speed and provide useful information on pump operation. Alhasmi (2005) analysed the spectrum of the angular speed and found that when plotting RMS of the amplitude of the IAS signal against flow rate there was a significant increase in shaft speed with the onset of cavitation for the frequency band 100 to 2500 Hz, see Figure 3-7a. Interesting was the much sharper increase in amplitude of the 3rd harmonic of the shaft speed which occurred with the onset of cavitation, Figure 3-7b.

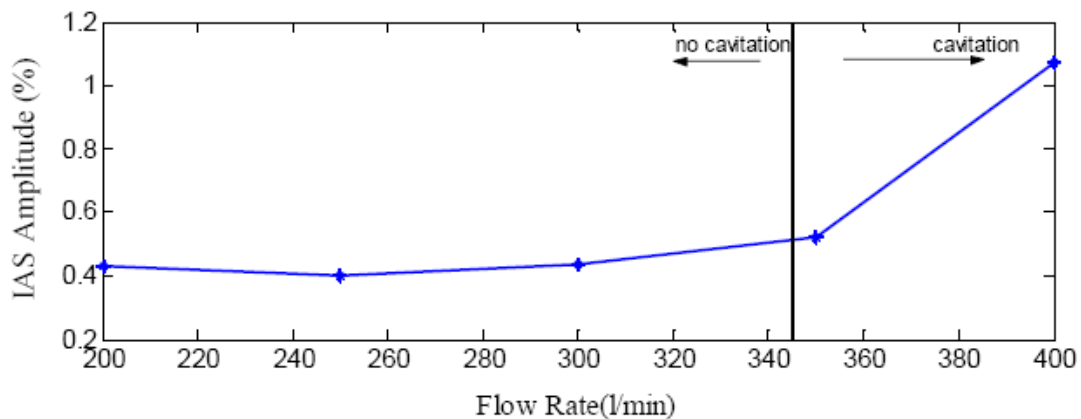


Figure 3-7 (a) Normalised IAS RMS with flow rate for the frequency band 100 to 2500 Hz (Alhasmi, 2005)

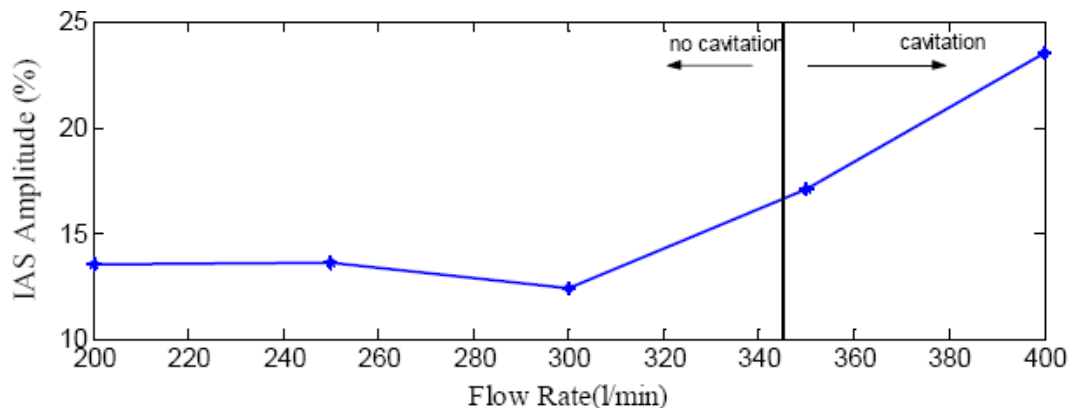


Figure 3-7 (b) Normalised amplitude of 3rd harmonic of IAS with flow rate (Alhasmi, 2005)

3.5.2 Motor current signature analysis (MCSA)

For over twenty years the stator current of an electric motor has been used widely to assess the health not only of the motor but also of the downstream equipment driven by that motor. It has been shown that downstream faults can result in rotor disturbances and these will be

translated into changes induced in the stator current which can be detected and analysed (Naid et al., 2009).

The spectrum of the motor current is complex even without adding a pump as a load. Alhasmi (2005) showed that, as expected, the 50Hz mains peak dominates the spectrum. However, also present are two sidebands due to the shaft frequency at 47.5Hz and 53Hz see Figure 3-8.

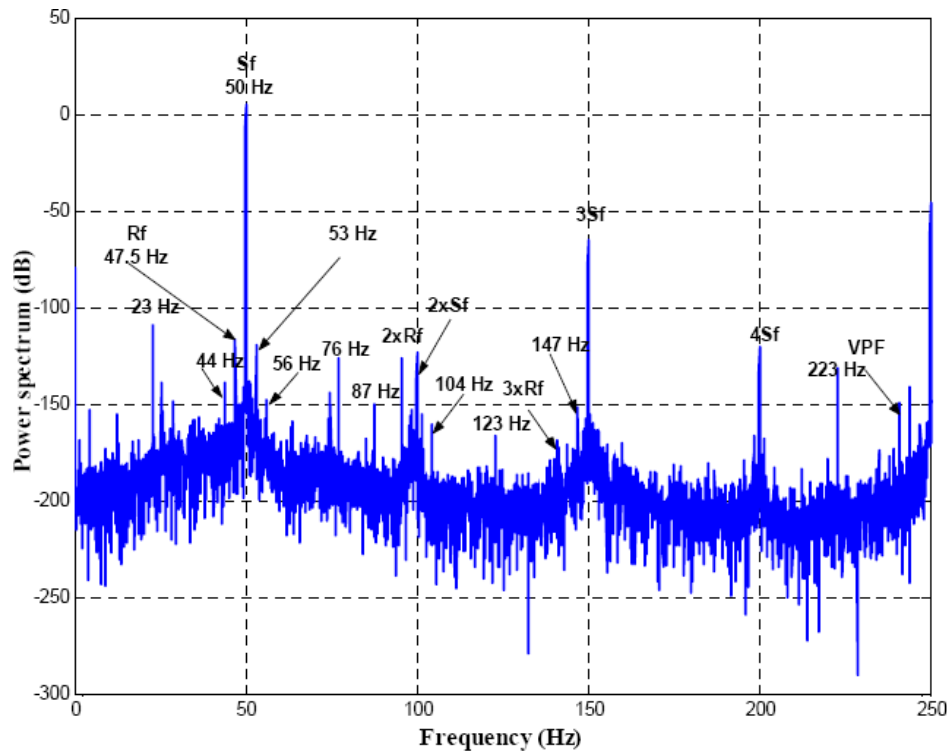


Figure 3-8 Power spectrum of the motor current of a motor driving a healthy centrifugal pump (Alhasmi, 2005)

It would be expected that as cavitation sets in, the load on the pump impeller would decrease since vapour is less dense than water, and the current drawn by the motor would also decrease. This is, indeed what Alhasmi (2005) found. The interesting thing here is that the RMS current increases with flow rate until the onset of cavitation and then decreases. This might suggest that the gradient of the curve would undergo a much greater change than for any of the previous parameters investigated, see Figure 3-9, but Alhasmi did not pursue that line of investigation.

Alhasmi (2005) also investigated the difference between the electrical mains frequency and the first sideband ($50\text{Hz} - \text{frequency of first sideband}$) and found that as the flow increased so did the difference. But with the onset of cavitation there was a sharp decline in the value of the difference so that the curve showed a shape very similar to that shown in Figure 3-9

above, and again suggests that the gradient of the curve might be a useful parameter for the detection of the onset of cavitation, but Alhasmi did not pursue that line of investigation.

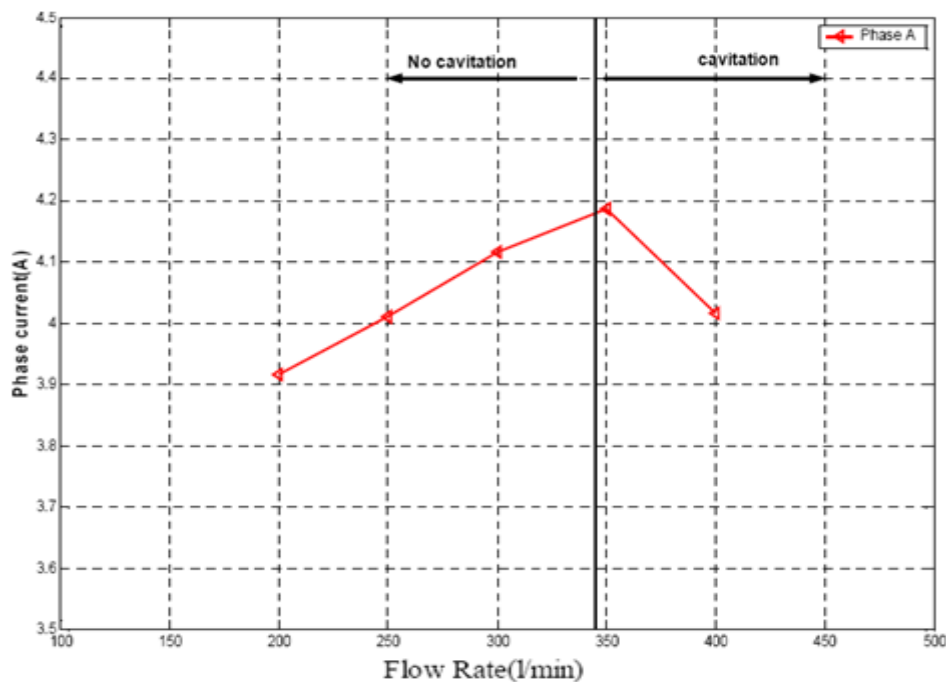


Figure 3-9 RMS of one phase of the motor current of a motor driving a healthy centrifugal pump with increase in flow rate (Alhasmi, 2005)

3.6 Possible novel method for detecting cavitation

The suggestion is that the capacitance between two plates placed on opposite sides of a non-conducting pipe through which pumped water flows can be used as a capacitive sensor to detect the onset of cavitation. This sensor will detect changes in the magnitude of the dielectric (water) as bubbles of vapour generated by cavitation begin to flow through the pipes and change the properties of the dielectric.

Capacitance-sensor techniques have been reviewed by Huanget, et al., (1988) who reported that this type of device had been used detection of liquid levels in natural gas–oil systems, oil storage tanks, breweries and waste water treatment; and measurement of concentration of solid particles in gas flows (Abouelwafa, 1980; Tollefsen and Hammer, 1998). Of course, as will be confirmed in this work, change in capacitance is not proportional just to the phase volume percentage; it also depended on the particular flow pattern. Nevertheless, capacitance sensors have recently been successfully used in capacitance tomography, a technique to assess flow patterns in gas–solid, gas–liquid or two-liquid mixture in real time (Loser, et al., 2001; White, 2002)

3.7 Data analysis techniques

3.7.1 Signal processing for condition monitoring

Useful machine condition monitoring (CM) and correct fault diagnosis often depends on using appropriate signal analysis methods. These methods are invariably divided into time domain, frequency domain, and time-frequency domain. Figure 3-10 taken from Norton and Karczub (2003) shows a schematic overview of commonly used signal processing techniques for CM.

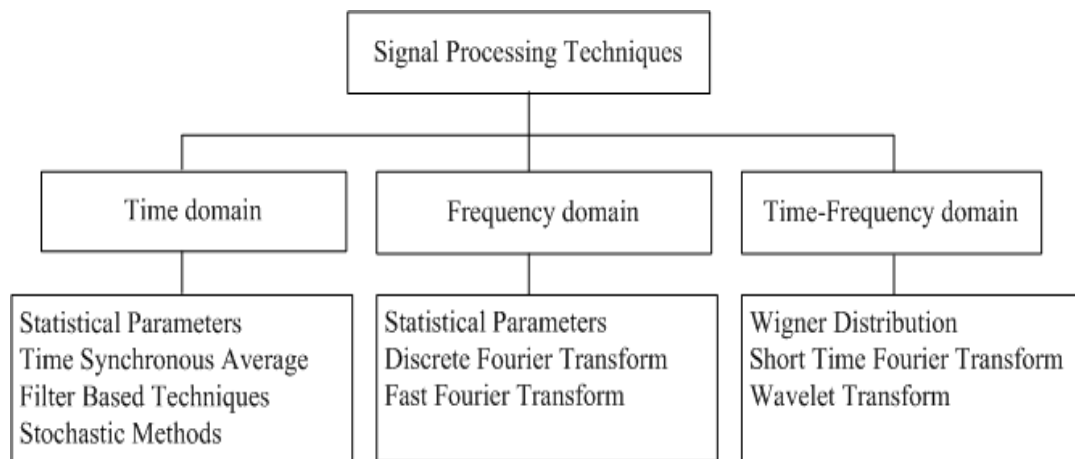


Figure 3-10 Signal processing techniques (Norton and Karczub, 2003)

The time domain of the signal is the record of the energy contained in the signal and so tends to be dominated by those elements which are the “noisiest”. The RMS level of the time domain signal can provide useful information of the presence of a fault, but generally the fault must have progressed sufficiently to be noticed against background noise. Periodicities can sometimes be detected by eye in the envelope of the time domain signal but this should be taken as an indication that frequency domain analysis is required. Time domain analysis usually requires only relatively unsophisticated and inexpensive instrumentation, with different sensors being used for the different frequency ranges and parameters of interest. The plot of the time domain signal will usually be RMS amplitude against time or, sometimes, instantaneous (also called peak) value against time.

Any signal whose amplitude varies with time will have a corresponding frequency domain signal. Usually it is assumed that the time domain signal is stationary, i.e. the time domain signal over one cycle will be exactly the same as the time-domain signal over any other cycle (all other things being constant). Of course, in reality this rarely happens so averaging is used to get mean values that help eliminate unwanted random variations. The Fourier transform is the preferred mechanism for transforming a time domain signal into its frequency domain

representation which describes the energy contained in the signal as a function of frequency. The great advantage of frequency domain analysis is that the signal generated by individual components can be seen. For example a fault in a roller bearing in its initial stages will be hidden in general bearing noise when using the time domain analysis, but after applying an FFT transform a peak in the spectrum at the characteristic fault frequency may be clearly seen. The plot of frequency domain signals will usually be amplitude against frequency and is called a spectrum.

However, both time domain and frequency domain signals are limited. The time domain contains little information on the frequency content of the signal while the frequency domain cannot trace the development of a fault, i.e. when the signal is time-varying. To overcome these limitations time frequency domain analysis is used. Put simply, the FFT is used to plot the spectrum of the signal at given time intervals and these plots are then combined into a three dimensional picture, see Figure 3-11. Here the plot has the amplitude as the z-axis, the time as the x-axis and the frequency as the y-axis. In the given plot, (i) the frequency of the peak amplitude first decreases with time, (ii) then there is a period where the amplitude of the signal decreases sharply then increases just as sharply, (iii) after which the frequency of the peak increases with time.

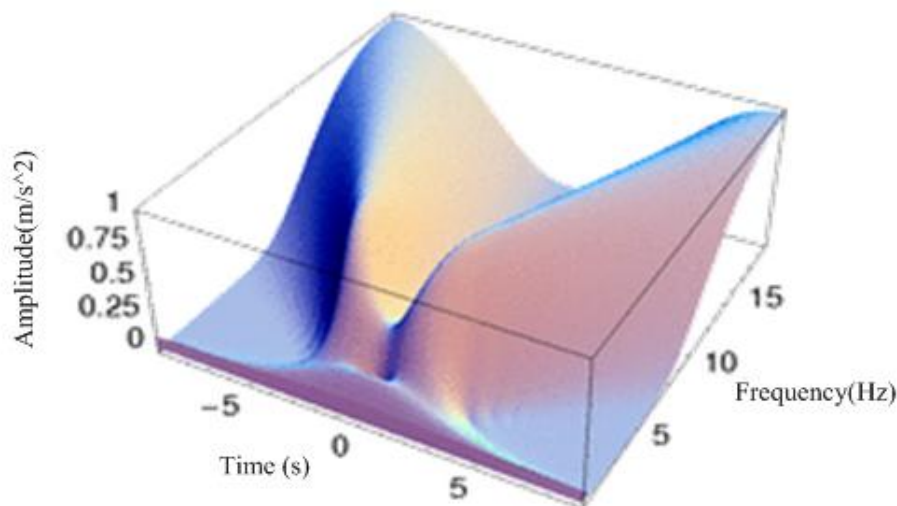


Figure 3-11 Time-frequency domain

A variation of the time-frequency domain is the waterfall plot, where instead of simply having a given time interval between consecutive spectra, each spectrum relates, for example, to a specific flow rate of the pump. In this way a 3-D picture is presented which shows the variation

of the spectrum of the pump with flow rate. It is this form of the time frequency domain which is used in Chapter 7, 8 and 9.

In a sense both time domain and frequency domain can be considered 2-D and time-frequency domain, 3-D. The analytical techniques associated with time-frequency domain are thus to be expected to be more sophisticated.

3.7.2 Time domain

The time domain is considered the most fundamental form of data collection for CM. The data collected and recorded from measurement sensors consists of values representing the amplitude of the signal at different instances. Traditionally, for analogue systems the time domain signal was considered continuous, but today with digital sampling the amplitude is collected at specific, separate instances. For an accurate picture of the signal, the rate of sampling should be at least twice the maximum frequency of interest.

The two most common parameters used to describe the time domain signal are the RMS value of the signal which describes the energy contained in the signal, and the peak value which describes the maximum value of the signal. For simple sinusoidal signals the peak value is $\sqrt{2}$ times the RMS value, $V_p = \sqrt{2}V_{RMS}$. No such simple relationship exists for real signals from, for example, centrifugal pumps. Indeed, without averaging to remove random effects it is unlikely that the same peak and RMS values will be returned for consecutive measurements, see following section.

Time domain averaging is a well-known and traditional technique for assisting the extraction of a periodic signal from a noisy time domain waveform (Braun, 1975). The averaging process is explained by assuming a signal $x(t)$ consists of the sum of a periodic signal $f(t)$ and random noise, $noise(t)$,

$$x(t) = f(t) + noise(t) \quad \text{Equation 3.1}$$

Suppose the instantaneous value is read many times. It is argued that the value of $f(t)$ remains constant but that random $noise(t)$ will very probably have both positive and negative values. When summing up for signal $x(t)$, the repeated signal $f(t)$ adds coherently, but the noise incoherently and to a degree will cancel itself out. In pump applications, time averaging requires a rotational reference signal to enable each reading to be made at the same angular

position. In its simplest form the reference signal could consist of a pulse train synchronised with the rotation of the pump.

Statistical parameters have been used by researchers in the CM of, e.g. gearboxes (Baydar, 2000), but they are not commonly used in industry. Industry tends to prefer the simple approach: single-value indicators obtained directly from the time domain signal which may be easily compared against accepted standards (e.g. allowable RMS vibration levels for electric motors in Entek IRD, 1993). Single-value measurements also have the great advantage that trends can be easily identified and remedial action taken when preset levels are reached. However, the setting of cost-effective action levels is usually not a simple task. By its very nature fault indication through trending comes at a late stage in the process (Ball, 1991; Starr, 1999).

However, the pressure for early detection and diagnosis of faults has meant a continuing search for more suitable measurements as a means of detecting small signals in a high level of background noise, and statistical analysis is one route to do this. Consider the case of fault development in a pump, changes in the time-domain of the vibration signal such as an increase in the RMS level or sharp peaks appearing are strongly suggestive of fault development and incipient damage. Extraction of useful information (“features”) from the time-domain can be achieved by calculating statistical parameters that can be related to changes in the signal induced by defects. The most obvious is the use of the peak or RMS value to indicate the severity of pump defects (Sun, et al., 1999). Figure 3-12 shows the RMS value of the vibration as a function of flow rate. It can be seen that, as would be expected, there is an increase in vibration with the onset of cavitation.

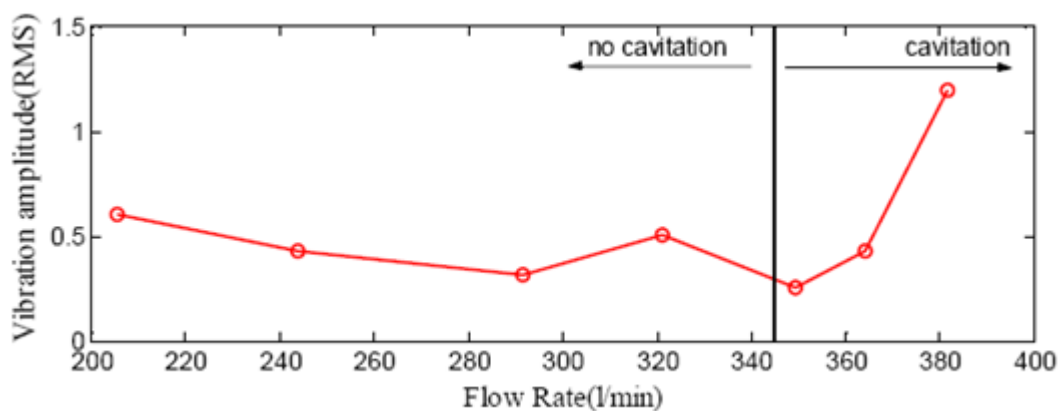


Figure 3-12 RMS amplitude of the vibration signal for centrifugal pump (Alhashmi, 2005)

Complex signals which are composed of a large number of sinusoids whose relative amplitudes and phases are not constant require additional descriptors. These have included Crest factor (C_f) and Kurtosis (K). Crest factor is given by: $C_f = V_p/V_{RMS}$, where V_p is the peak value of the signal and V_{RMS} its RMS value. Crest factor is a measure of the number and sharpness of the peaks in the signal and may be used to determine whether a signal contains repeated impulses. A high C_f value for the vibration signal from, say a roller bearing would be taken to be an indication of a bearing fault (Al Kazzaz, et al., 2002). Kurtosis is given by:

$$K = \frac{\sum_{i=1}^N (x_i - \bar{x})^4 / N}{(\sigma^2)^2} - 3 \quad \text{Equation 3.2}$$

Where σ is the standard deviation of the samples, N is the total number of samples, x_i is the value of the i^{th} sample, and \bar{x} is the mean of the samples. The “-3” is included to normalise the expression so that the Gaussian/Normal distribution has $K=0$. That is, the natural non-normalised kurtosis of a Gaussian distribution is 3. Where the peaks in the spectrum are sharper or more pointed than the Gaussian distribution the kurtosis is greater than 0. A high value for kurtosis usually means infrequent extreme deviations rather than frequent modestly sized deviations. If the value of K is negative it means the distribution is flatter than the Normal, if K is positive it means the distribution is more peaked than the Normal.

Kurtosis has been used successfully integrated into intelligent diagnostic systems and presents a useful way to detect and discriminate between different faults (Naid, 2009; Li, 2000), but it has an important weakness. If the defect is allowed to become severe enough, the signal will lose its peakedness, and then the value of K will fall and cease to be useful as a measure of the fault. Also kurtosis cannot be used, for example, to directly locate which bearing amongst several is defective.

The probability density function (PDF) for a continuous spectrum, is an expression that describes the probable value of the spectral energy between any two frequencies. The normalised Gaussian distribution curve is a probability density function where the PDF is equal to (Piersol and Paez, 2010):

$$PDF = \frac{1}{\sqrt{2\pi\sigma^2}} \exp^{-\frac{(x-\mu)^2}{2\sigma^2}} \quad \text{Equation 3.3}$$

The probability density of the vibration signal once cavitation is established is basically Gaussian (Li and Pickering, 1992). Figure 3-13 shows the normalised PDF of the pump vibration (acceleration) spectrum. It can be seen that the maximum value and standard

deviation (width) of the PDF curves change with flow rate. Equation 3.3 shows that the maximum of the PDF curve (its height) is inversely proportional to σ , where σ is the standard deviation and as such is a measure of the width of the curve. Thus peak value and width are inversely related, and only one – the peak value – needs to be considered when attempting to find a measure related to the onset of cavitation.

PDF curves obtained from the vibration signals of machines have been used for CM, and Li and Pickering (1992) have shown that the normalized PDF of the vibration signal from a pump broadens if the pump condition deteriorates, at least in the early stages of mechanical damage. Where the waveform is highly impulsive a high level of the PDF at the median frequency and a large spread at low probabilities are characteristics of the time-domain waveform (Mathew, 1989) and it is possible to quantify the variation in the skirt of the probability distribution by taking statistical moments. If the damage progresses sufficiently the PDF curve returns to a Gaussian shape.

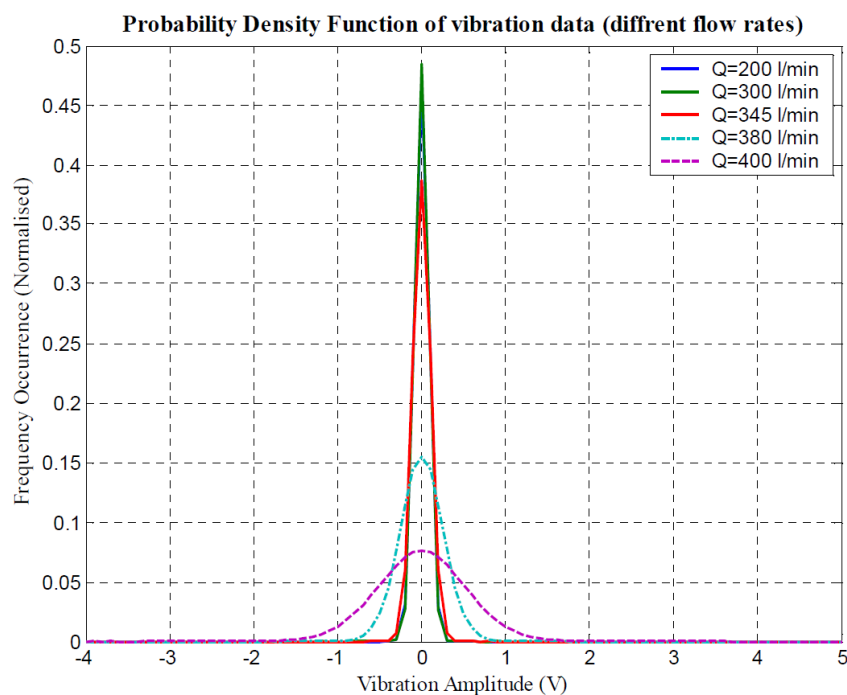


Figure 3-13 PDF of the pump vibration (acceleration) spectrum with flow rate (Alhashmi, 2005)

Alhashmi (2005) found that as the flow rate increased in his system the shape of the PDF curve changed in a regular manner. The width of the curve gradually increased and the amplitude correspondingly decreased, see Figure 3-13. Unfortunately Alhashmi labelled the ordinate axis incorrectly, this should read Probability Density.

3.7.3 Frequency domain

The Fourier transform is widely used to transform the time domain signal into the frequency domain on the assumption that the frequency components of the vibration signal are always directly related to the mechanical condition of the machine components. The Fourier transform produces a frequency spectrum which is the average of the input signal over the sampling period. It does not show how a signal spectrum changes with time (Ruqiang, 2007). The discrete Fourier transform obtained from a time-sampled signal is (Smith, 2007):

$$X(k) = \sum_{n=0}^{N-1} x(n) \exp(-j2\pi kn/N) \quad k = 1, 2, \dots (N-1) \quad \text{Equation 3.4}$$

Where $x(n)$ is the value of the n^{th} sample, N is the total number of samples and $X(k)$ is the discrete frequency transform of the signal.

Frequency domain analysis has serious advantages in machine CM and, today, the Discrete Fast Fourier Transform (DFFT) is the most popular method of deriving it (Mathew, 1989). However, care must be taken to ensure information isn't lost when the time domain signal is transformed into the frequency domain: the DFFT frequency spectrum is based on only a finite duration sample of a function so the assumption has to be made that the signal is stationary (Körner, 1996); the windowing function introduced to reduce consequential errors may itself be a source of leakage errors (Kaiser, 1994); and the sampling frequency must be at least twice the highest frequency of interest (Smith, 2007). However, despite these limitations the DFFT has been a hugely successful and useful investigative tool in many, many research programmes particularly in CM of rotating machinery such as compressors, motors, gears and pumps (Al Thobiani, et al., 2010).

The DFFT has proved particularly useful in CM because it is closely correlated with physical machine characteristics, and this section provides some brief information on its application (Payne, 2003). Frequency domain analysis is a widely used for examining signals emanating from rotating machines, and allows both detection and identification of faults from their frequency signatures. The DFFT frequency spectrum is interrogated for discrete frequencies demonstrating unusual amplitudes (Randall, 1977). The level and shape of the frequency domain spectrum will both reflect the mechanical condition of the machine and provide fault diagnosis (Bayder, 2000).

It is established that healthy rotating machines each produce a baseline frequency spectrum which can act as a template against which to compare the spectrum of a similar machine

operating under the same conditions. Because baseline spectra of healthy machines differ slightly from one machine to another, an average is taken of a number of machines, and the variations in the signals must be borne in mind when interpreting data. Significant increase over the baseline at any characteristic frequency is taken to indicate the presence of unwanted abnormalities.

Decades of practical application have confirmed frequency domain analysis can reliably identify frequency components within the signal indicative of a faulty condition of one or more components. In practice the frequency components identifying the presence of a fault may show themselves not as peaks in their own right but as sidebands to particular frequencies in the spectrum and it is the change in the amplitude of these sidebands that indicates the presence of mechanical problems in, say, a pump.

Figure 3-14 shows the spectra for a pump flow rate that does not generate cavitation. A clear change in the spectrum would be expected for different flow rates with an increase in amplitude as flow rate increases, and a clear and distinct increase in amplitude at the onset of cavitation. Also the shape of the spectrum would be expected to change as wide band cavitation noise increased in amplitude relative to the discrete components.

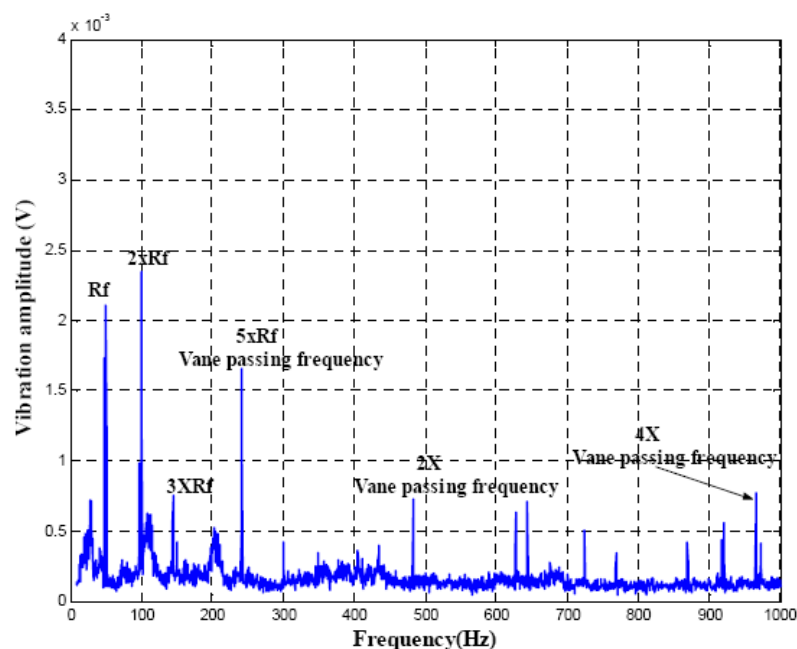


Figure 3-14 Baseline vibration spectrum for centrifugal pump, 20 Hz to 1kHz (Alhashmi, 2005)

Spectral entropy is described by Pan et al., (2009) as a generalized form of information entropy, a concept first proposed by Shannon (1948) as a measure of information uncertainty.

For a continuous random variable X having probability density function $f(x)$, Shannon defined the information entropy as

$$H(X) = - \int f(x) \log_2 (f(x)) dx \quad \text{Equation 3.5}$$

Pan et al., (2009) showed that for a discrete system the signal spectral entropy (SE) for a series of sampled values X_1, X_2, \dots, X_N is given by:

$$SE = - \sum_{i=1}^N p_i \cdot \log_2(p_i) \quad \text{Equation 3.6}$$

Where $p_i = \frac{x(i)}{\sum_{j=1}^N x(j)}$, $\sum_{i=1}^N p_i = 1$, N is the number of samples and $x(i)$ is the value of the i^{th} sample.

If the samples are from, say, the vibration spectrum of a machine component, then it follows that the value of p_i describes the i^{th} sample's contribution to the spectrum, so spectral entropy is capable of evaluating the spectral structure of the vibration signal.

Qiu and his colleagues (2003) have suggested that the spectral entropy be normalized to avoid effects due to data length. This simply means dividing by $\log_2(N)$.

$$SE = \frac{-\sum_{i=1}^N p_i \cdot \log_2(p_i)}{\log_2(N)} \quad \text{Equation 3.7}$$

Normalised spectral entropy has its largest value (=1) when the amplitude distribution is flat and each frequency component is equal (white noise), and low values when the distribution is a small number of large amplitude narrow peaks (pure tones). If the distribution is everywhere zero apart from a single narrow peak then the normalised spectral entropy has its smallest value which will be close to zero. Spectral entropy has been used to differentiate faults such as valve spring failure (Qiu et al., 2003; Tao et al., 2001; Liu et al., 1997).

Pan et al., (2009) have observed two significant limitations on spectral entropy analysis. The changes in SE that take place with the development of a fault are not always sufficiently consistent to be a measure of performance degradation, and SE lacks sensitivity to final failure. The researchers found that SE was better suited to fault detection in the initial stages when the peaks associated with the faults were relatively sharp, even though they were not of large amplitude. Figure 3-15 shows the vibration spectral entropy for the centrifugal pump used in this research programme for fourteen flow rates between 10 l/min and 370 l/min (that

is the entropy of the vibration spectrum at each of the fourteen flow rates is determined and plotted). No previous application of spectral entropy in this general area was found in the literature search so data from this project has had to be used to provide a suitable illustrative figure. The results appear promising as there is a marked change in SE at a flow rate where cavitation initiation would be expected.

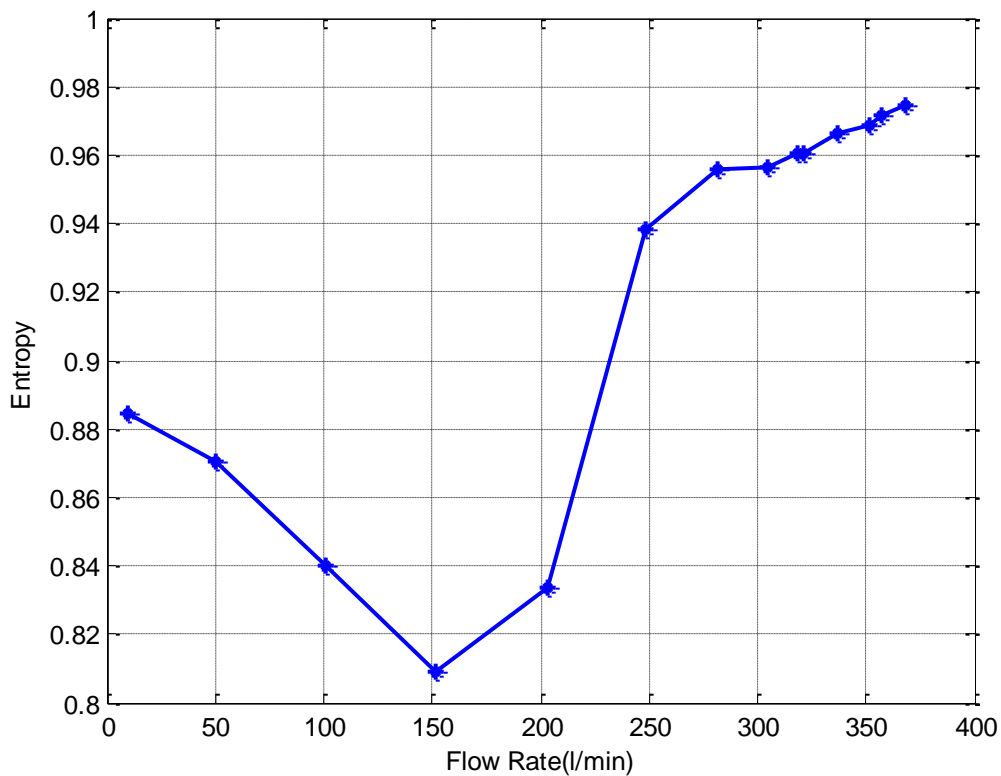


Figure 3-15 Spectral entropy of vibration spectra for centrifugal pump with flow rate in the range 10 l/min to 370 l/min

The next chapter describes the design and construction of the experimental test rig, items of equipment and procedures used for data acquisition.

CHAPTER FOUR

4. DESIGN AND CONSTRUCTION OF TEST-RIG

This chapter reviews the design and construction of a test rig suitable for measurement of parameters associated with incipient cavitation in a centrifugal pump. The parameters to be measured are discussed and details of the relevant transducers and data acquisition system given, as are details of measurement practice and data management. This is followed by a brief description of the use of Matlab for data processing. The manner in which cavitation is to be introduced into the centrifugal pumps is described.

4.1 Introduction

The aim of this study was to identify techniques for detecting and diagnosing incipient cavitation in a centrifugal pump. This was to be done by monitoring different parameters: visual observation of flow, vibration, airborne noise, hydroacoustic pressure and a new technique which measured change in capacitance with the onset of cavitation. In order to achieve this objective, it was necessary to design and construct a suitable test-rig. The essential features of the test rig were that it be as industrially relevant as possible, that it be as simple as possible, that the onset of cavitation could be achieved in a controlled manner and that the relevant parameters be measured to an acceptable level of accuracy.

An important aspect in the development of CM technologies is the seeding of faults in a controlled manner into a real system in the expectation that this will provide real data similar to that which might be recorded in an industrial scenario. The choice of a centrifugal pump is motivated by the awareness that this type of machine is in widespread use in a wide range of industries. The pump chosen for this experiment was a PedrolloF32/200AH which is typical (though on a smaller scale) of those used by industry. However, unlike in industry the test rig was designed so that cavitation could be introduced as desired. The system also had to include instrumentation for detecting cavitation using the well-tried and accepted techniques of vibration and acoustic measurement. The instrumentation and equipment used was selected on the basis that it was available within the Centre for Diagnostic Engineering at the University of Huddersfield and had been found accurate and reliable. New instrumentation was purchased from Sinocera on the basis that this was a company that produced quality products at competitive prices.

The design of a sensor suitable for the novel capacitive method for the detection and quantification of cavitation had to be done from first principles. From a survey of relevant literature it was obvious almost at once that the direct measurement of capacitance would not be as direct and as simple as measuring the change in frequency in a resonant circuit with change in capacitance. However, it was still necessary to design and construct the capacitor itself. The diameter of the pipes used on the test rig were the key factor in determining the size of the capacitor plates, since they had to fit on the surface of the pipe. Of the available metal sheets 2mm thick aluminium proved to be most sensitive for the purpose.

Thus the rig was constructed to provide a platform which would allow comparison of different methods and techniques for cavitation detection using the same user interface. However, the test rig had also to meet a number of other external requirements because it was desirable that it be designed in such a manner as to be applicable to as many industrial fields as possible, which reinforced the need for an essential simplicity.

4.2 General requirements

The test rig was located where there was sufficient access space for maintenance and inspection. The pump was secured to the floor via anti-vibration mounts and connected to the three-phase mains supply via a D.O.L starter and a three-phase isolator. The system was inspected and a pressure test carried out before use. In addition, an examination of the pump and its components was carried out by technicians with the required skills prior to the rig being assembled. Figure 4-1 shows the pump secured to the floor. Figure 4-2 shows the three-phase mains supply via the D.O.L starter and a three-phase isolator.

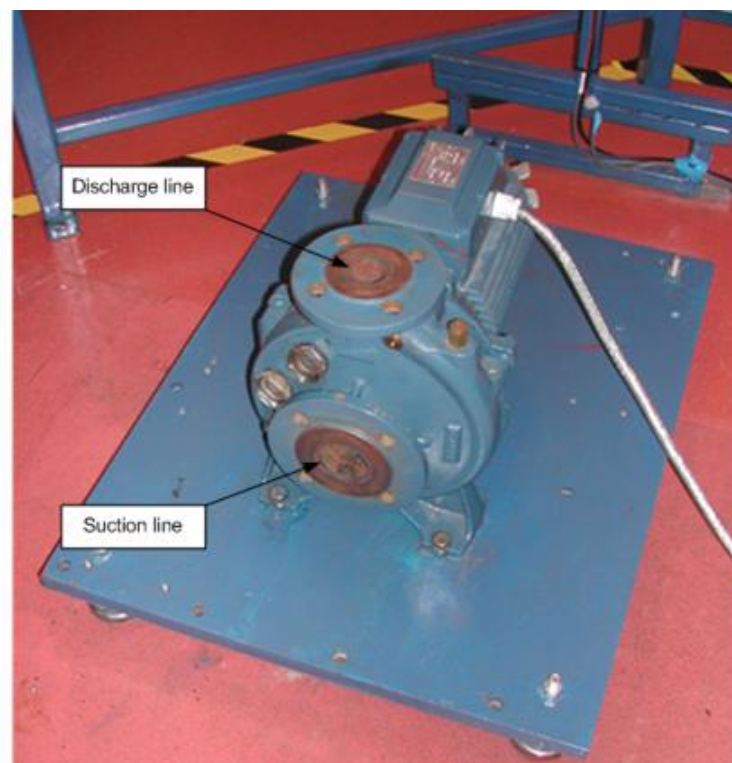


Figure 4-1 Pump secured to floor



Figure 4-2 Three-phase mains supply via a D.O.L starter and a three-phase isolator

4.2.1 The test rig

Figure 4-3 is a photo of the test rig, Figure 4-4 is a schematic diagram of the test rig and Table 4-1 details the system components. The centrifugal pump can supply water to the tank with a maximum pressure of about 10bar. The chosen system was re-circulatory and included a plastic water tank, PVC pipe and PVC components. The positions where the transducers were mounted on the test system are shown in Tables 4-1 and 4-2, and described in Section 4.3. The capacity of the tank was based on the maximum flow rate so that water temperature in the system could be maintained to within 1°C for more than one hour during which full measurements can be completed at different flow rates. The vertical discharge pipe on the outlet of the pump was 31.75 mm ID, thus a reducing coupling of 1¼” (31.75 mm) to 1” (25.4 mm) was used to connect the outlet of the pump to the discharge line. The horizontal suction line into the pump was a 50.8mm ID pipe. Each line has a transparent length of pipe to allow observation of cavitation bubbles.

Table 4-1 Details of piping system components, to be read with Figure 4.3

System Item	Specification	Quantity	Remark
Water tank (plastic)	Volume = 0.911 m ³ Dimensions 870*1080*970 mm	1	
PVC plastic valve 1½" BSP		1	Suction line
PVC plastic reducing bush 2" to 1½"		1	Suction line
PVC plastic valve 2" BSP		1	Suction line
PVC plastic transparent pipe 2"	ID = 50.8mm; OD = 60mm Length between the tank and pump 1690mm	1	Suction line
Equal tee 2" BSP		3	Suction line
PVC Plastic coupling 2" BSP		1	Suction line
PVC plastic socket 2" BSP		1	Suction line
PVC plastic reducing screwed socket 1½" -1¼" BSP		1	Suction line
PVC Plastic transparent pipe 1¼"	ID = 31.75mm OD = 42mm Height 1970mm; Length 1770mm Drop = 1070mm	1	Discharge line
Equal tee 1¼" BSP		2	Discharge line
PVC plastic valve 1¼" BSP		1	Discharge line
PVC plastic elbow 1¼" BSP		2	Discharge line
PVC Plastic coupling 1¼" BSP		1	Discharge line
PCV plastic reducing coupling 1¼" to 1"		2	Discharge line

Table 4-2 Test-rig components, to be read with Figure 4.3

Components	Type	Quantity	Remark
Centrifugal pump	Pedrollo F32 / 200AH	1	
Water flow rate	Gems Rotor flow RFO	1	In discharge line
High pressure transducer	Sinocera CY-YB-025-1 MPa	1	Discharge line 0-10 bar
Low pressure transducer	Sinocera CY-YB-025- 0.5 MPa	1	In suction line 0-5bar
Accelerometers	Sinocera YD3 8131	2	Inlet and outlet of pump
Shaft encoder	Hengstler R1 32	1	
Microphone	Sinocera type 4130	1	
Hydrophone	Sinocera precision hydrophone	1	In discharge line
Capacitor sensor		1	In discharge line
Capacitor sensor		1	In suction line
Speed controller	Omron 3G3MV	1	
Spectrum analyzer	Type R4131D	1	
Data acquisition	Sinocera, YE6230B	1	
Data acquisition	CED 1401 Plus	1	
Power supply	Farnell instruments L30/2	3	
Amplifier	Bruel & Kjaer type 2635	1	

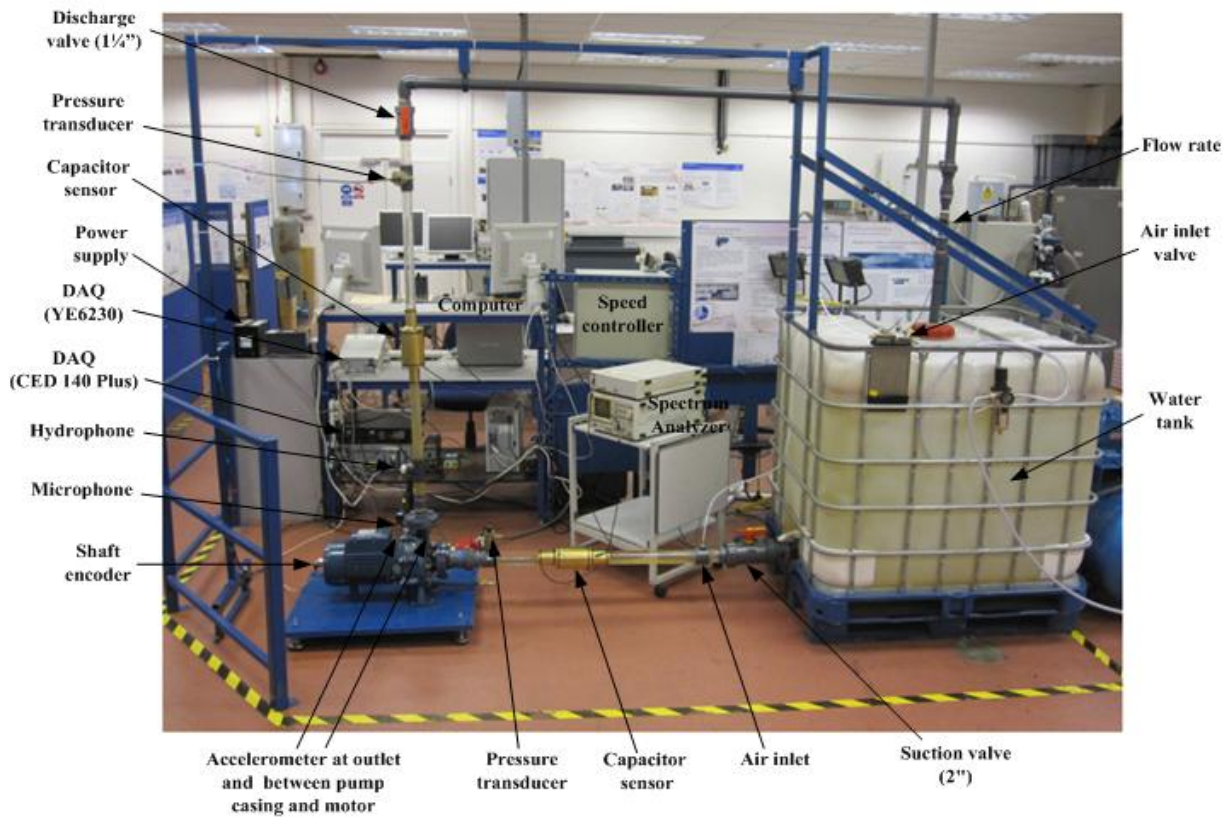


Figure 4-3 Photo of test rig

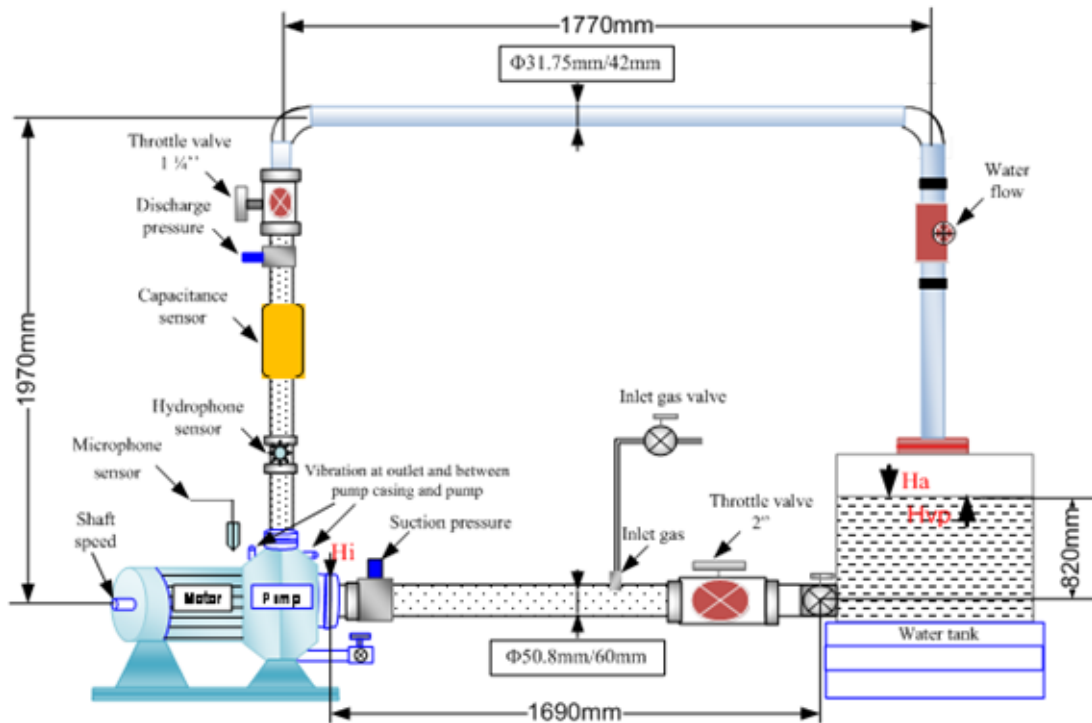


Figure 4-4 Schematic diagram of test rig system

4.3 Measurement system (instrumentation)

It was decided that it would be necessary to routinely measure the following system parameters:

- water flow rate using a paddle wheel type meter,
- water pressure using Sinocera general purpose industrial pressure transducers in the suction and discharge lines immediately adjacent to the pump,
- vibration of the pump using two Sinocera precision accelerometers placed at the outlet and between pump casing and motor of the pump ,
- airborne noise radiated from the pump using a Sinocera precision microphone placed 50mm from the outlet of the pump,
- hydroacoustic noise using a Sinocera type one inch precision hydrophone,
- speed of rotation of the pump shaft using a commercial encoder sensitive to 1° of rotation, and
- a capacitor sensor to detect changes in the value of the dielectric of the water as bubbles of vapour generated by cavitation begin to flow. The capacitor plates were placed on the outlet pipe of the pump,

The measured voltages from the transducers were routinely recorded, so that their relative potential usefulness in detecting the onset of cavitation could be investigated. In each case the transducers produced a voltage output corresponding to the amplitude of the measured parameter, and each was connected to a data acquisition system via coaxial BNC cables to avoid intrusive noise, and from the data acquisition system to a computer for signal conditioning and storage.

Each sensor (flow rate, pressure, encoder, accelerometer, hydrophone and microphone pre-amplifier), was connected to a Farnell Instruments Ltd L30/2 power supply and from that to the data acquisition system (CED 1401 Plus and YE6230B) and PC via a USB port.

4.3.1 The flow rate transducer

The flow rate transducer in the test-rig is a rotating vane device which is widely used for measurements in the gas and oil industries (Bolton, 2000), see Figure 4-5. The particular model was chosen to match the pump capacity. It consists of a cylindrical rotor with six vanes. The fluid flow causes the rotor to rotate and the number of revolutions of the rotor is a measure of the amount of fluid that has passed through the meter. Claimed accuracy is high,

about $\pm 0.1\%$. The flow meter was positioned on the outlet side of pump, in the down flow leading to the reservoir.

The flow meter contains a Hall Effect Sensor, producing a series of voltage pulses as the blades pass it. The frequency at which these on/off DC pulses occur is directly proportional to the flow rate. This particular meter has a frequency range from about 25Hz to about 225Hz, which represents a flow range of 100 to 400 l/min.

Figure 4-6 shows how the flow meter was installed in the pipe work. Specifications of the flow rate sensor are presented in Table 4-3.

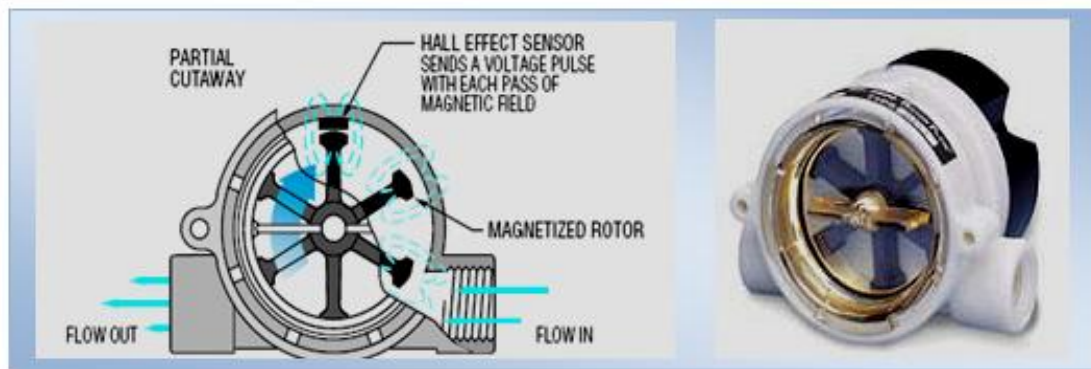


Figure 4-5 Gems rotor flow type RFO (GEMS, 2011)



Figure 4-6 Gems water flow meter in flow line (refer to Figure 4-4)

Table 4-3 Specifications of the Gems RFO flow rate sensor (GEMS, 2011)

Flow meter manufacturer	Gems
Type	Rotor flow RFO
Operating pressure, maximum Polypropylene body:	6.7 bar at 21°C, 2.8 bar max at 80°C
Max. operating temperature	80 °C
Electronics (both bodies)	65 °C Ambient
Max. viscosity	45 cSt
Input power	4.5 to 24 Vdc, (24Vdc regulated supply)
Output signal	4.5 to 24 Vdc pulse. Pulse rate dependent on flow rate, port size and range
RFO type	0-10VDC Analogy signal @ 1mA max.
Current consumption	8mA,no load
RFO Type	25mA max.
Max. current source output	70 mA
Frequency output range	15 Hz (low flow) to 225 Hz (high flow)

4.3.2 Pressure transducer

The pressure transducer installed was a Sinocera Type CY - YB - 025 general purpose industrial pressure transducer with an upper limit of about 10 bar gauge, see Figure 4-7. This transducer operates on the principle that the pressure to be measured acts on a diaphragm to which is bonded a strain gauge. The movement of the diaphragm induces a strain in the gauge which produces a change in electrical resistance proportional to the applied pressure. Claimed accuracy is high, better than $\pm 0.2\%$. Two such sensors were used on the test rig, the first was placed in the suction line at the inlet to the pump, see Figure 4-8, and the other was placed in the discharge flow, see Figure 4-9. The specifications for both pressure transducers are shown in Tables 4-4 and 4-5. Figures 4-10 and 4-11 show typical samples of the online raw data from both pressure transducers



Figure 4-7 Pressure transducer

Table 4-4 Specifications of pressure transducer in suction line (GST)

Pressure transducer manufacturer	Sinocera
Product	Strain gauge pressure transducer
Type	CY-YB-025-0.5MPa
Measurement range	0-0.5MPa
Operating voltage	12VDC
Output mode	0-5 \pm 0.2 VDC
Static precision	< 0.3%FS
Screw joint	1/ 4- NPT external
Operating temperature range	-10 ⁰ C to 50 ⁰ C

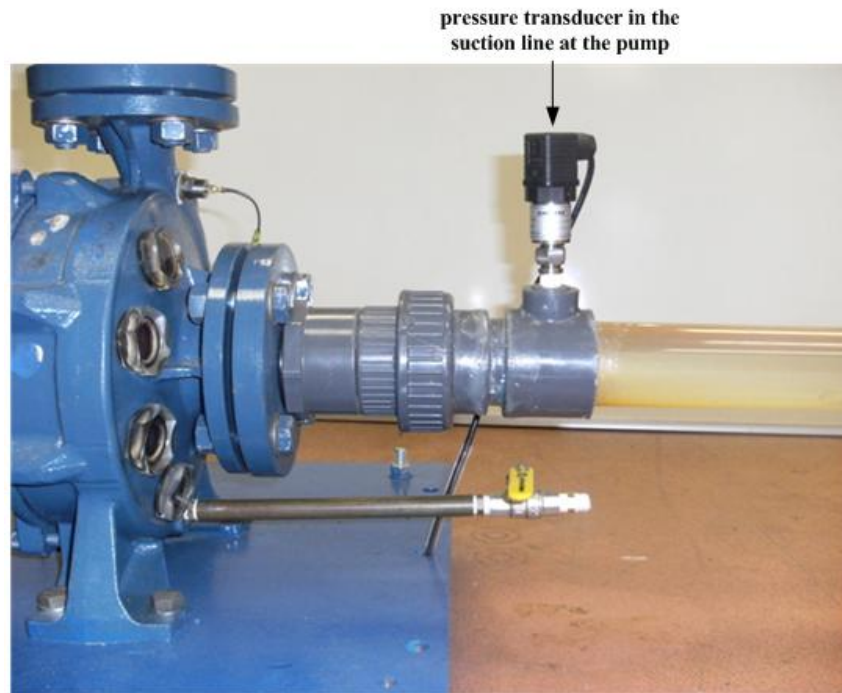


Figure 4-8 Pressure transducer in suction line at the pump inlet

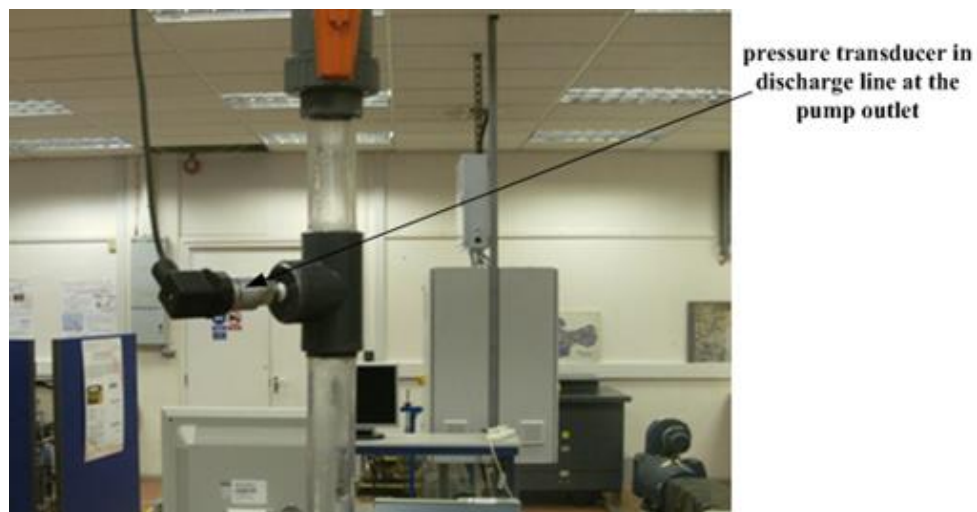


Figure 4-9 Pressure transducer in discharge line at the pump outlet

Table 4-5 Specifications of the pressure transducer in discharge line (Sinocera, 2009)

Pressure transducer manufacturer	Sinocera
Product	Strain gauge pressure transducer
Type	CY-YB-025- 1MPa
Measurement range	0-1MPa
Operating voltage	12VDC
Output mode	0-5 ± 0.2 VDC
Static precision	< 0.3% FS
Screw joint	1/ 4- NPT external
Operating temperature range	-10 ⁰ C to 50 ⁰ C

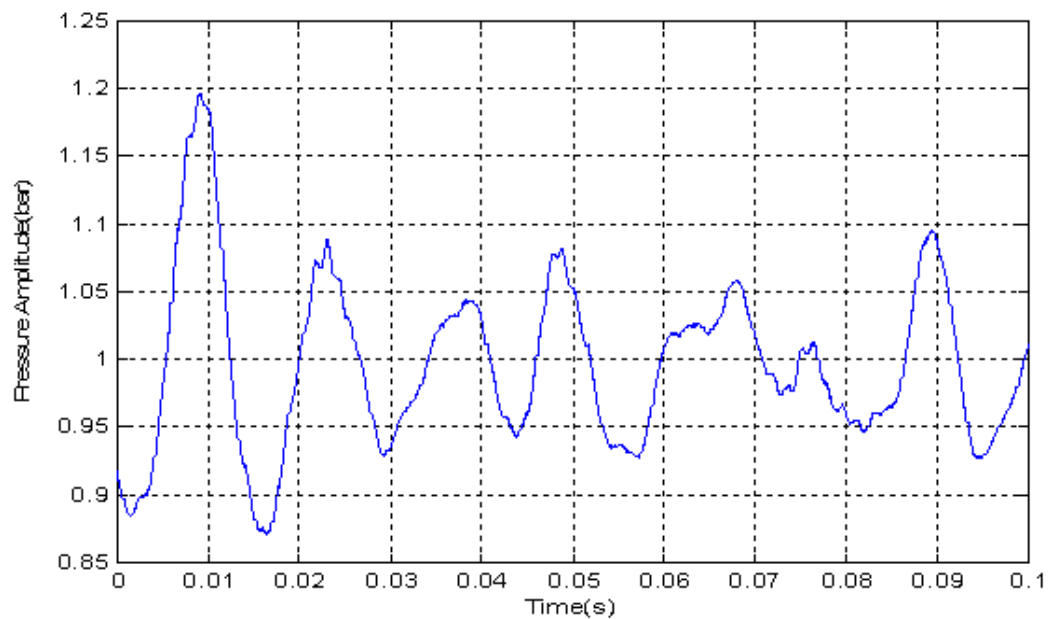


Figure 4-10 Typical online raw data measured by pressure transducer in suction line

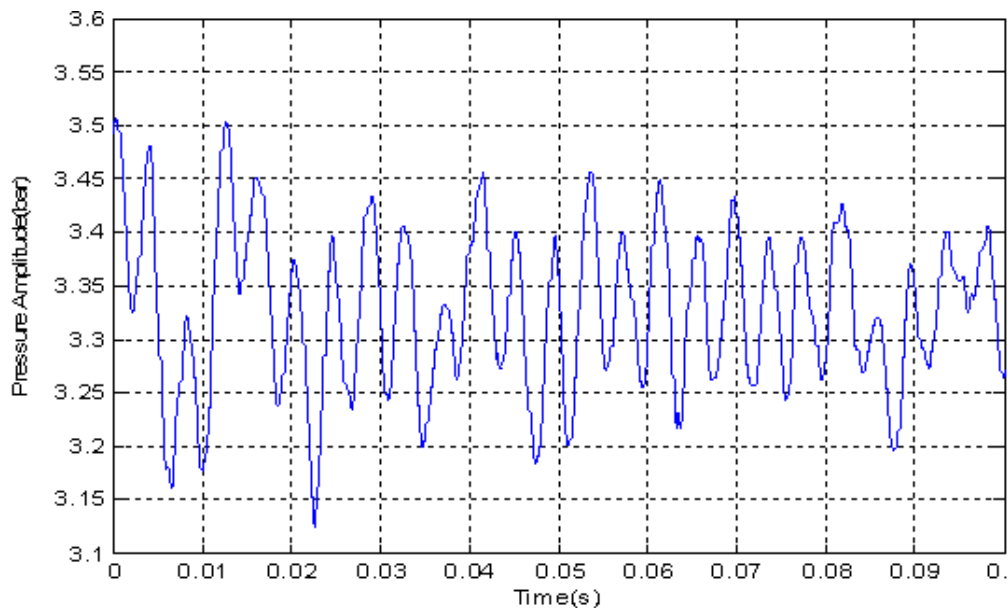


Figure 4-11 Typical online raw data measured by pressure transducer in discharge line

The sensors were selected based on estimates of the pressure expected in the test-rig: the water pressure in a pumping system normally ranges from 0–5 bars and, according to the manufacturer’s guidelines, the maximum pressure the sensor in the discharge can measure is 10 bars, and the maximum for the transducer in the inlet line is 5 bars. Because cavitation is related to the pressure on the suction side of the pump, monitoring of pressure at that point in

the system is an important element in the control cavitation. The pressure transducers were each connected to a Farnell Instruments Ltd L30/2 power supply, the data acquisition system and PC.

4.3.3 Vibration accelerometer

Accelerometers are the most commonly used sensors in CM of rotating machinery (Scannell and Colgrave, 2001). The accelerometers attached to the pump were Sinocera type YD3 8131 piezoelectric devices in which a piezoelectric material responds to a mechanical deformation by developing an electrical charge across its surfaces which is directly proportional to the applied mechanical stress (force). The specification of the accelerometers is shown in Table 4-6. Two accelerometers were used, one at the inlet and the other at the outlet of the pump, see Figure 4-12.

Table 4-6 Specifications of the accelerometers (Sinocera, 2009)

Maker	Sinocera
Type	Accelerometer (piezoelectric)
Model	YD3 8131
Frequency range	200Hz – 20KHz
Sensitive	1.51mv/m.s ⁻²
Range accretion	<2000ms ⁻²
Temperature range	To 250 ⁰ C

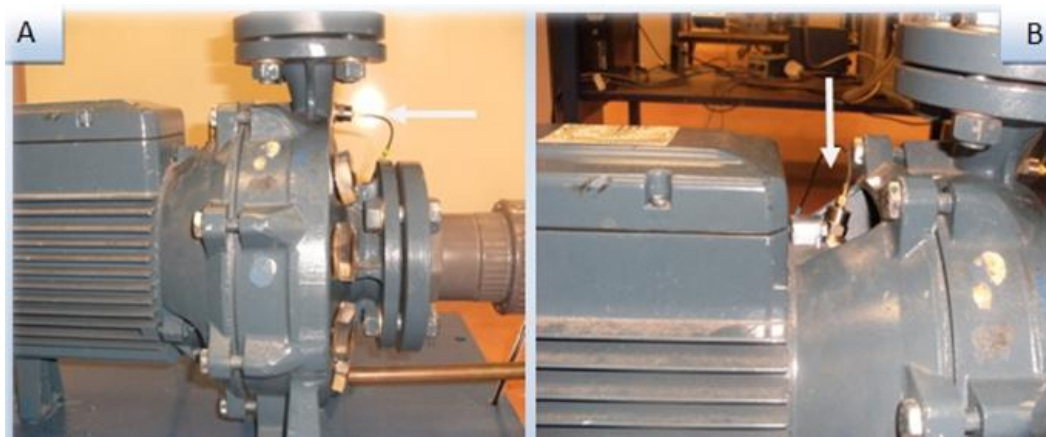


Figure 4-12 Positions of the accelerometers (a)- At outlet of the pump (b) - Between pump casing and motor of the pump

Piezoelectric accelerometers are the most widely used transducers for CM. They have no moving parts; are robust, easy to fit, have a wide frequency response and the benefit of low cost. Their output is directly proportional to acceleration and can be integrated to provide

measurement of velocity or displacement. These accelerometers are sufficiently robust to be suitable for most applications both in the laboratory and field, and have a dynamic range that will accommodate high shock levels, though the latter will not be required here. The accelerometers were attached to a screw-threaded brass stud which was attached to the casing by tapping and screwing. The vibration transducers were each connected to a charge amplifier (Sinocera YD3 131) and from the charge amplifier to the data acquisition system and then to the computer by USB. Figure 4-13 shows a typical sample of the online raw data from the accelerometer on the pump outlet.

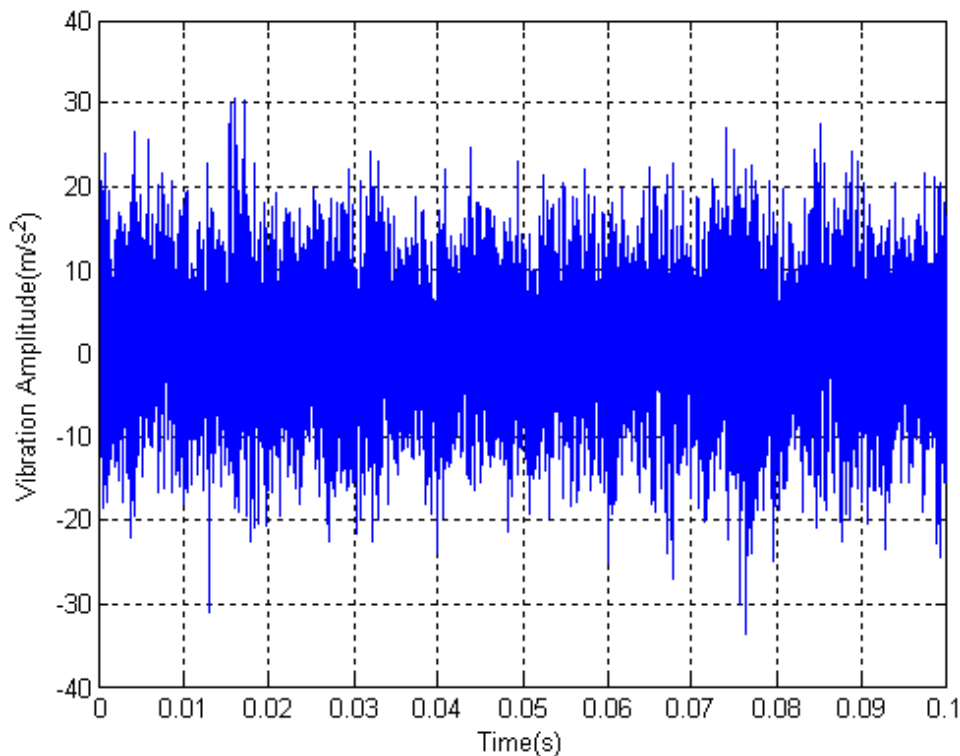


Figure 4-13 Typical raw vibration signal from accelerometer on pump outlet

4.3.4 Acoustic microphone

The microphone used to measure the noise radiated from the pump was a Sinocera type half inch free field precision microphone, see Figure 4-14. The microphone was placed 50mm away from the outlet of the pump. Table 4-7 shows brief specifications of the microphone and pre-amplifier. The microphone was connected to a preamplifier, the data acquisition and PC by USB. This sensor position was consistent with that of the vibration accelerometer and the results could be compared directly.

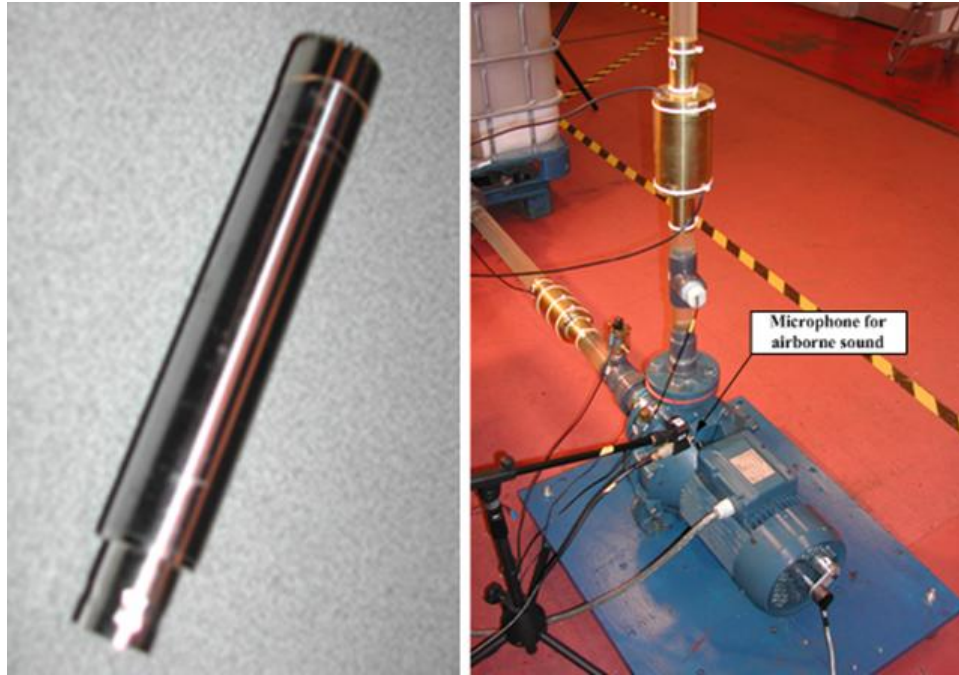


Figure 4-14 Microphone and position of microphone for airborne sound

Table 4-7 Specifications of the microphone and preamplifier (Sinocera, 2009)

Manufacturer	Sinocera
Microphone	Electret condenser microphone
Linear frequency range	20 Hz – 20kHz (free field)
Sensitivity	40mv/Pa
Microphone preamplifier	YG201
Linear frequency range	20Hz – 100 KHz ± 0.2 dB
Sensitivity	50 mV/Pa
Dimensions	\varnothing 12.7 mm x 70 mm (including connector)
Max output voltage	5.0 Vrms
Operating temperature range	-40 °C to +80 °C

Unlike accelerometers, microphones are not in contact with the source and are subject to high levels of background noise contamination in industrial use. Because of this, invariably, with cavitation detection, acoustic signals are used in support of the accelerometer measurements. The presence of high background noise levels from many different components, special conditioning techniques are often needed before the signals can be used for CM (Ramroop, et al. 2001). Figure 4-15 shows a typical sample of the online raw data from the microphone.

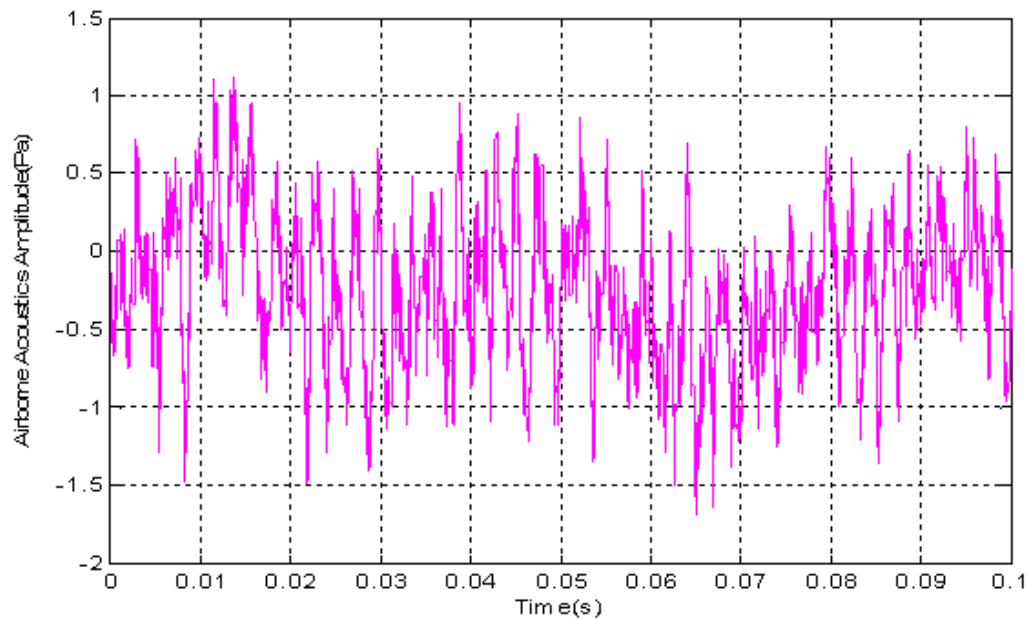


Figure 4-15 Typical raw data for pump noise measured by the microphone

4.3.5 Acoustic hydrophone

The hydrophone used to measure the hydroacoustic signal generated radiated by the pump was a Sinocera type one inch precision hydrophone, see Figure 4-16, placed in the discharge line at the outlet of the pump. Table 4-8 shows brief specifications of the hydrophone. The hydrophone was connected to a preamplifier, to the data acquisition system and then to computer by USB. This sensor position is thus consistent with that of the vibration accelerometer and the results can be compared directly. Figure 4-17 shows a typical sample of the online raw data from the hydrophone.

Table 4-8 Specifications of hydrophone (Sinocera, 2009)

Hydrophone manufacturer	Sinocera
Type	Precision hydrophone
Linear frequency range	5Hz – 20 KHz \pm 3dB
Dynamic range	13.5 – 142 dB
Hydrophone diameter	25mm

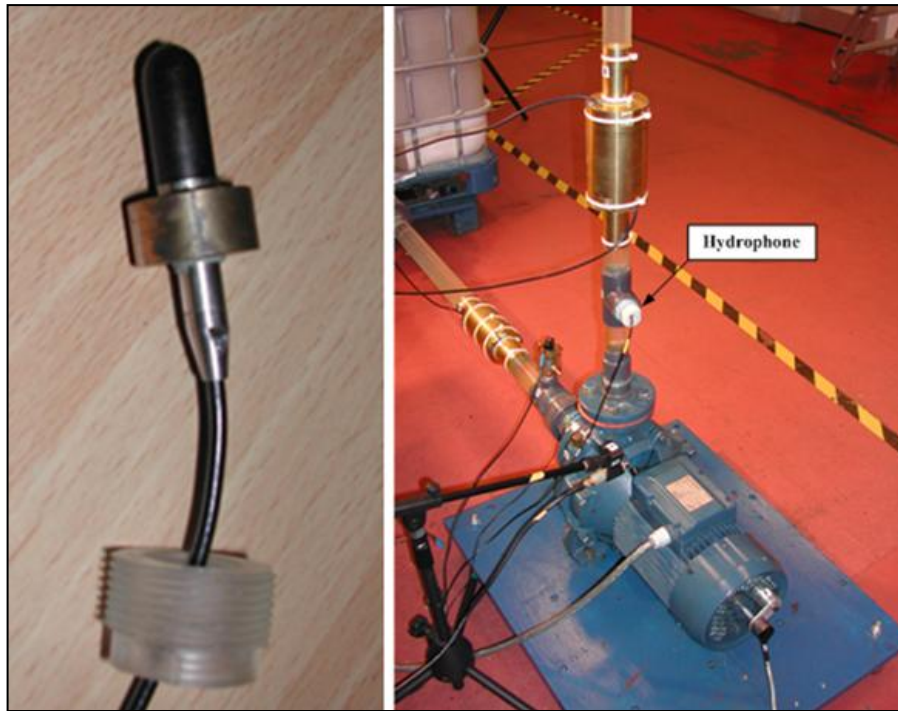


Figure 4-16 Hydrophone and position of hydrophone

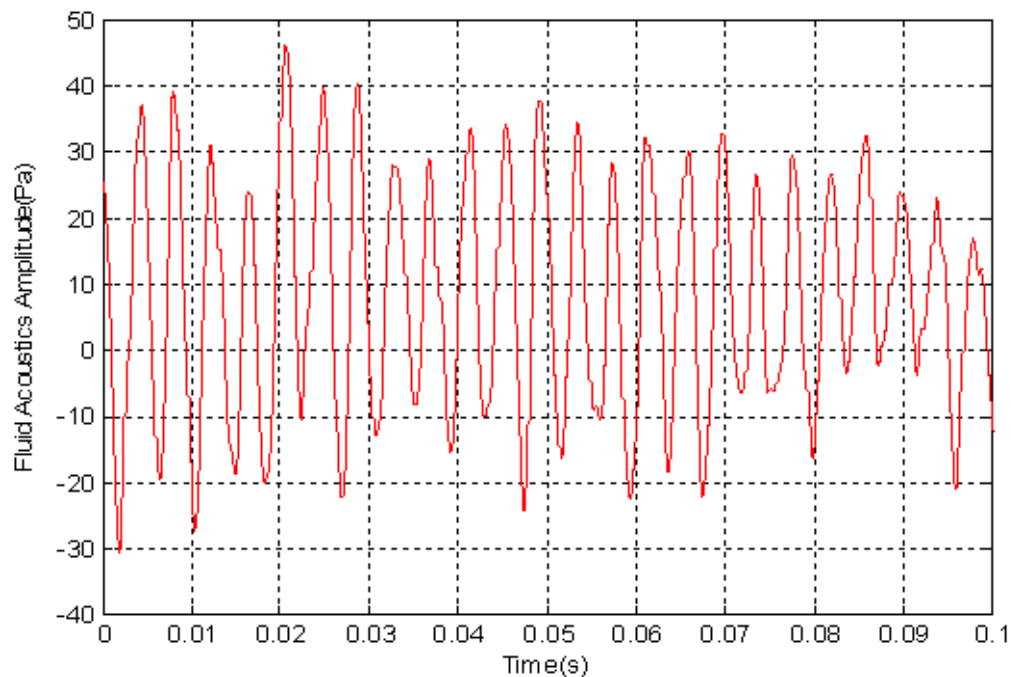


Figure 4-17 Typical raw data for hydroacoustic signal measured by the hydrophone at pump outlet

4.3.6 Shaft encoder

An incremental optical encoder was used to collect instantaneous angular speed data. Figure 4-18 shows the Hengstler R132 miniature shaft encoder. This was attached to the end of the

pump shaft, see Figure 4-19. Table 4-9 shows the specification of the encoder transducer. This is an optical encoder containing a disc made of glass with transparent and opaque areas. A light source and photo detector array reads an optical pattern that defines the position of the shaft at any one time. This code can be read by a controlling device, such as a microprocessor to determine the angle of the shaft and/or the shaft speed.



Figure 4-18 Shaft encoder



Figure 4-19 Position of encoder for shaft speed

No amplification of the measured encoder signal was required, and the encoder is directly connected to the data acquisition system and PC via the CED. The device produced a square pulse output for every angular degree (thus the term 360 line encoder) for every complete revolution and this enabled shaft speed to be determined. Figure 4-20 shows a typical sample of the online raw data from the encoder transducers

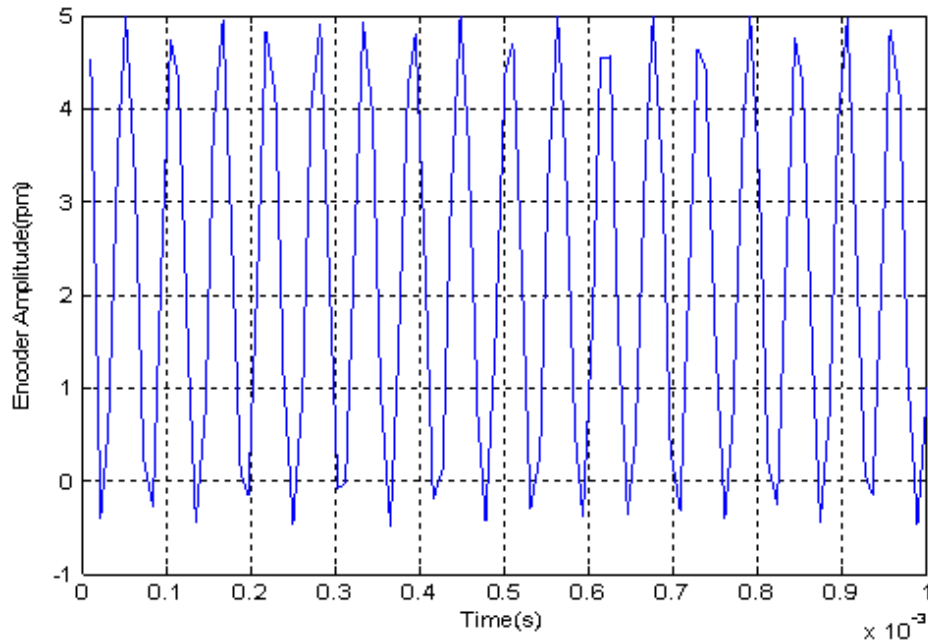


Figure 4-20 Typical outlet signal of encoder

Table 4-9 Specification of encoder (Hengstler, 2011)

Manufacturer of encoder	Hengstler
Type	R1 32
Out put	High 2.5V , low 0.5 V
Power supply	5V d.c
Max pulses per revolution	360
Mounting round	Flange
Shaft diameter	5 mm, 6 mm
Maximum speed	6,000 RPM
Torque	$\leq 0,05$ Ncm
Protection class housing/ball bearing	IP 50/40
Operating temperature	-10 ... +60 °C
Pulse shape	Rectangular
Vibration performance	(IEC 68-2-6) 100 m/s ² (10 ... 2000 Hz)
Shock resistance	(IEC 68-2-27) 1000 m/s ² (6 ms)
Connection	cable axial/radial
Material	flange: aluminium, cover: plastics
Weight	50 g approx
Bearing life	In excess of 10 ⁷ revolutions

4.3.7 Speed controller

Centrifugal pumps for any system are chosen so as to operate at their BEP, and the pump speed is determined by this condition. However, the flow through the pump is likely to vary and to maximise efficiency the speed of the pump should change to meet the new conditions. However, there are two severe limitations on this approach, the pump impeller is rigid and designed for a given flow rate and running speed, a change in speed could significantly reduce efficiency. Variable speed controllers are relatively expensive and for smaller systems the efficiency savings do not match the additional capital outlay. Having said that, with variable speed systems the design point no longer needs to be based on a fixed speed and any given pump has a better chance of operating at or near its BEP over a range of conditions (Casada, 1999). However, the range is limited and most pump companies want their pumps to operate within $\pm 5\%$ to 10% of the design BEP and careful selection is required for these applications to avoid operation below minimum allowable flow and possible deadheading (Stavle et al., 2000).

Incorporating a speed controller into the test rig was for a completely different reason, it meant that future students would be able to simulate a whole range of potential centrifugal pump faults at different speeds and even to study the effects of changing the pump speed on energy costs. Figure 4-21 shows the inverter-type speed controller that was used. This operates on the principle of rectifying the mains AC supply to DC and then converting it back to AC, providing the frequency required to match pump demand (Chapman, 1991; Say, 1982).



Figure 4-21 Omron speed controller

The Omron type 3G3MV speed controller proved easy to use and was able to deliver high-torque control at low speeds. The 3G3MV Inverter used was a three-phase model compatible with the given power supply. Table 4-10 shows the specifications of the speed controller (Omron, 2003). The maximum pump speed with the Omron speed controller was 3000rpm and this could be gradually reduced to zero. It is recognised that in an industrial situation anything lower than about 2900rpm would be unusual, but this is an experimental test rig.

Table 4-10 Technical specifications of the speed controller (Omron, 2009)

Speed controller manufacturer	Omron
Model	3G3MV
Allowable voltage fluctuation	±15% to 10%
Allowable frequency fluctuation	± 5%
Power supply	380 to 460 V AC at 50/60 Hz
Max output frequency	400 Hz
Heat radiation	20.1 W
Frequency control range	0.1 to 400 Hz
Output frequency resolution	0.01 Hz
Location	indoor
Control method	Sine wave PWM
Ambient temperatures	Operating ± 10 to 60 ⁰ C

4.3.8 Data acquisition (Sinocera YE6230B)

With this test rig it will be required to obtain the values of several variables simultaneously; flow rates, pressures, vibration levels, airborne noise, hydroacoustic noise, shaft speed, and impedance for the capacitive measurements. Here a Sinocera YE6230B, 8 channel, 16 bit, data acquisition (DAQ) system was used, see Figures 4-22.and 4-23.

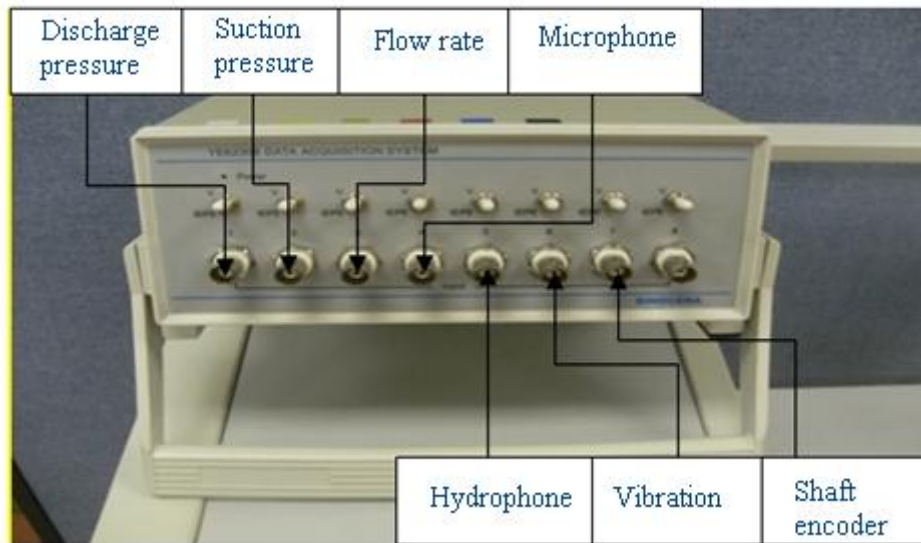


Figure 4-22 Sinocera YE6230B data acquisition system

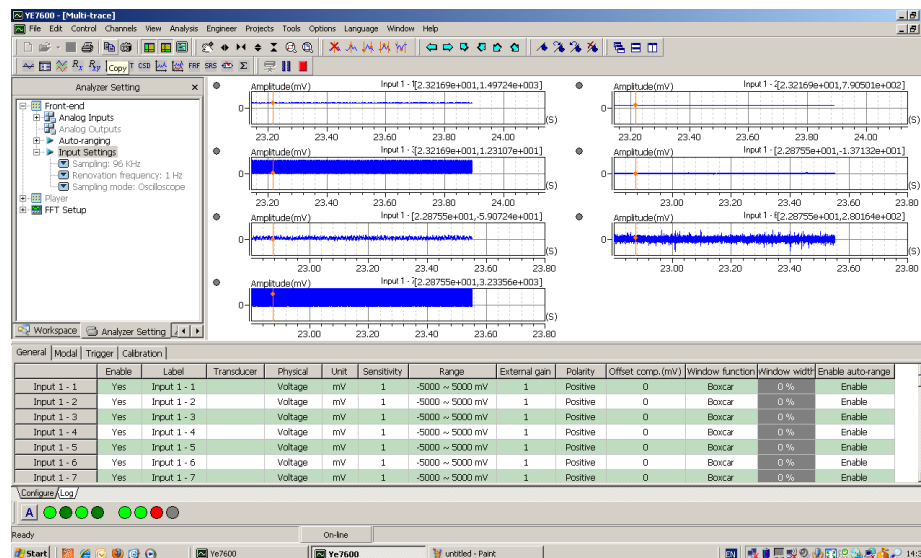


Figure 4-23 Interface panel for YE6230B

The outputs from each sensor are conditioned to convert them to a voltage and amplified to bring them to a common signal range, usually $\pm 5V$. The resulting voltage signals are then input to a multiplexer that is controlled by the microprocessor system. The microprocessor selects signals and passes them via a sample and hold unit to an A/D converter and so produces a parallel input to the PC where it can be processed before being displayed and stored.

The PC had a multiplexer and A/D converter mounted in one of the expansion slots within it. The unit included signal conditioning elements that could be used with the transducers and

sensors such as thermocouples. The card had 8 A/D input channels with 16 bit resolution and a conversion time of 25 μs (Bolton, 2000), see Table 4-11.

The gain coupled with the range, determines the smallest detectable change in input analogue voltage. If the gain is 10, say, and the range $\pm 5\text{V}$ for a 16-bit board, the smallest detectable change in input voltage is $5 \cdot (10 \cdot 2^{16}) \text{V} = 3.3 \mu\text{V}$.

Table 4-11 Technical specifications of the Sinocera YE6230B

DAQ system manufacturer	Sinocera
Type	YE6230B
Number of channels	8 channels selectable voltage/IPE input. multiplexing is Used to sample each channel in turn.
A/D conversion resolution	16 bit
Sampling rate (maximum)	100kHz per channel parallel sampling
Input range	$\pm 5\text{V}$
Gain	Selectable, either 1, 10 or 100
Filter	Anti-aliasing filter
Interface	USB 2.0

4.3.9 Data acquisition (CED 1401 1992)

Figures 4-24 and 4-25 show the CED 1401:1992. This is DAQ which can record and store digital (event) data and marker information for real-time, simultaneous, multi-tasking systems, under the control of the host PC. Here it was used to analyse the data obtained for water flow rate, pump inlet and outlet pressures and shaft speed. This DAQ has been used on many previous projects and is fully described in, for example, Elhaj, 2005.

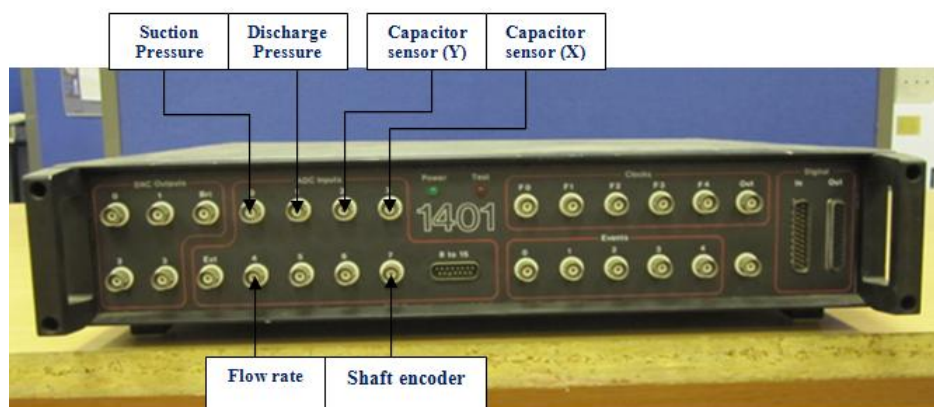


Figure 4-24 CED 1401 Plus data acquisition system

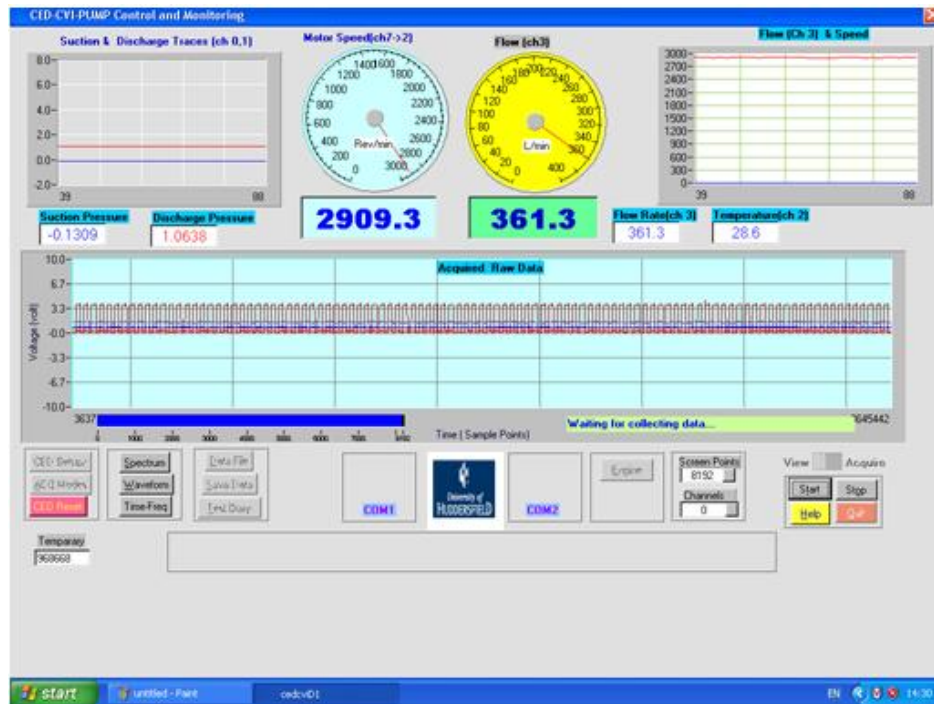


Figure 4-25 Interface panel for CED 1401

4.3.10 Centrifugal pump

Figure 4-26 shows a Pedrollo standard horizontal inlet, closed impeller, single stage general purpose centrifugal pump designed for civil, industrial and agricultural applications. This pump can deliver water at a rate of up to $30\text{m}^3\text{h}^{-1}$ (500l/min) at a head of up to 55m. It is driven by a three-phase electric motor running at 2900rpm on 9.5A at 380-400V (nominal 4kW/5.5hp). The details of the centrifugal pump are shown in Table 4-12. The speed controller, described below, allowed the speed of the pump – or any subsequent pump fitted in the circuit – to be varied in a controlled manner.



Figure 4-26 Pedrollo F32/200AH centrifugal pump

Table 4-12 Technical specifications of Pedrollo F32/200AH pump and motor (Pedrollo, 2008)

Pump Manufacturer	Pedrollo
Type	Centrifugal pump F32 / 200AH
Head	38 – 55 (m)
Capacity	10 – 30 (m ³ /h)
Speed	2900 (rpm)
Maximum pressure	10 (bar)
Impeller type	Closed, brass
Number of stages	Single
Power	4 kW
Frequency	50 Hz
Rated current	9.5 A
Rated voltage	400 V
Connection	Closed

The signals were measured for different flow rates but at a fixed pump speed of 2900 rpm. The flow rate was adjusted step by step by a throttling valve in the discharge line. Each test run had at least 14 data sets recorded which covered the necessary flow range. To obtain

reliable results, each test was repeated at least 3 times with a time interval between each test such that the water temperature for each test was the same. The data records from each test were processed in Matlab to analyse the signals and attempt to find a set of consistent parameters for cavitation diagnosis i.e. for determining the inception and progression of cavitation, at this stage based on vibro-acoustic measurements only.

According to ISO 3555, the predicted characteristics between the Net Positive Suction Head Available (NPSHA) and Net Positive Suction Head Required (NPSHR) for this system are obtained by throttling the valve in the discharge line progressively while the pump speed is at 2900rpm and the valve in the suction line is fully open (100%). Figure 4-27 shows that fully developed pump cavitation is expected to have occurred by about 345 l/min, when the head is 6.92m, where the NPSHR is higher than the NPSHA. It was found during the initial tests that at 344 l/min the cavitation was severe and so flow for rates higher than 345 l/min cavitation was considered fully developed, as suggested in ISO 3555.

However, during the initial study to test the system, it was found that both the vibration and acoustic signals had a noticeable change in amplitude and frequency content at a flow rate of 249 l/min, and so the flow 249 l/min was considered the point by which the onset of cavitation had definitely occurred. This is as would be expected, NPSHA and NPSHR are essentially average values, but inside the pump there will be local divergences from these mean values and it is at these points that cavitation will commence, and at flows less than 345 l/min. On Figure 4-27 there appear two vertical red lines, the first is at 249 l/min and this is taken as the flow rate at which cavitation is first definitely observed to be present in the flow (note that the inception flow rate will be less than this). The second red line is at 345 l/min and this is taken as the flow rate at which fully developed cavitation is present.

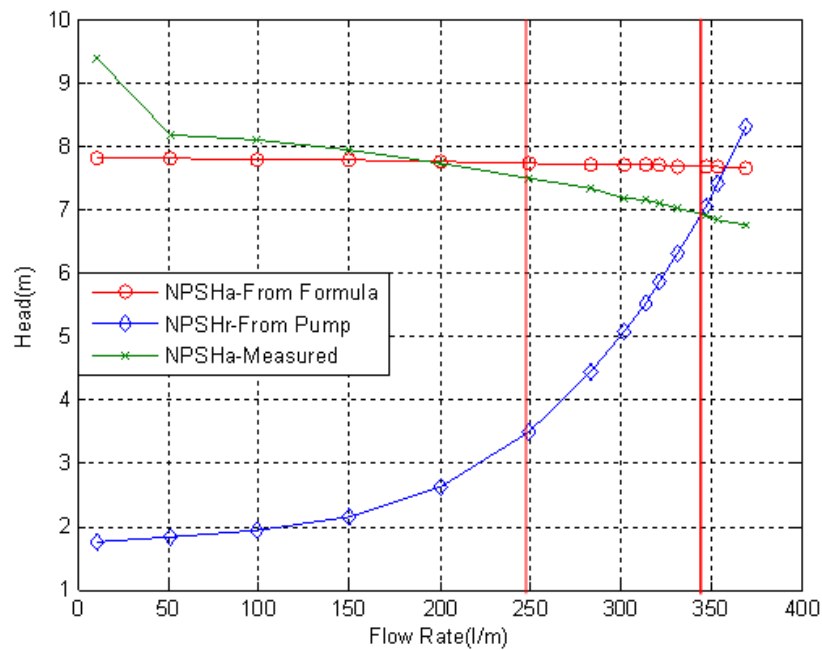


Figure 4-27 Pump performance pump at 100% open valve

Figure 4-28 is the pump flow rate curve, this shows the pump head and corresponding flow rates over the range from 10 l/min to 370 l/min. As the pump flow rate increases the developed head decreases. At flow rates above 344 l/min, lowering the resistance to flow (the developed head) will produce only a small increase in flow.

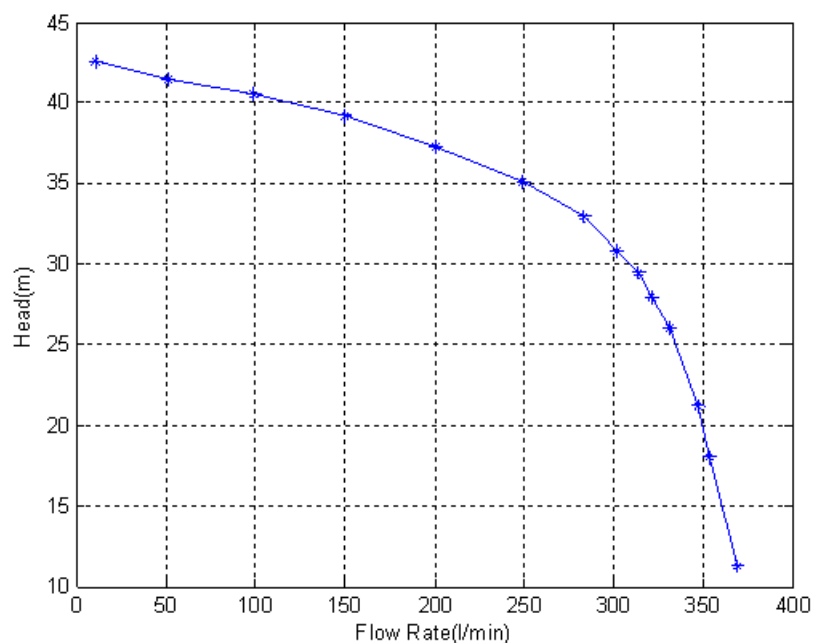


Figure 4-28 Head-Flow rate pump curve

4.4 Summary

The parameter of interest, e.g. vibration, was measured for different flow rates but at a fixed pump speed of 2900 rpm. The flow rate was adjusted by the throttling valve in the discharge line, step by step, visual observation of the flow through the transparent plastic pipe was maintained. A test run consisted of recording at least 14 sets of data which covered a flow rate range from 370 l/min to 10 l/min. Cavitation bubbles could be seen in the flow at a flow rate of about 249 l/min. To obtain more reliable results, each test was repeated 3 times. Care was taken so that the water temperature was the same for each test. The data records from each test were processed in Matlab.

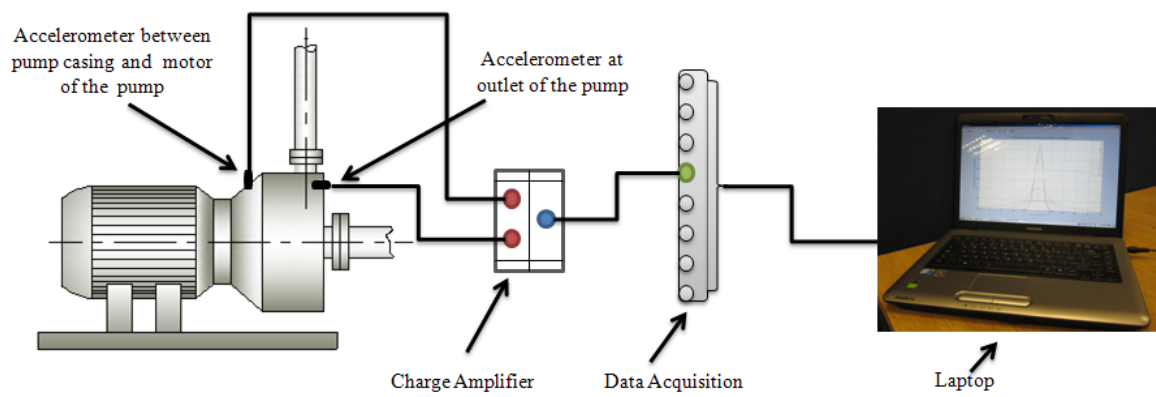


Figure 4-29 Acquisition of e.g. accelerometer signals

The collected data was sampled at 96kHz for 10 seconds. The acquired signals were averaged using a data segment averaging method. The FFT analysis gave a frequency resolution of 1Hz.

The measurement of the vibration, airborne acoustic and hydrophone signals was performed simultaneously, so the procedures for all three measurements are the same as described above and the instrumentation are shown in figures 4-29 and 4-30.

Time and frequency analyses were used to examine the signals. The time analysis provided raw waveforms, and such statistical parameters as PDF, peak value, crest factor, RMS and kurtosis. The frequency analysis provided a baseline spectrum, and the spectrum was also analysed to give spectral amplitudes, spectral, kurtosis and spectral entropy.

The next chapter will introduce the concept of using a capacitive method for the detection of cavitation in fluid flow.

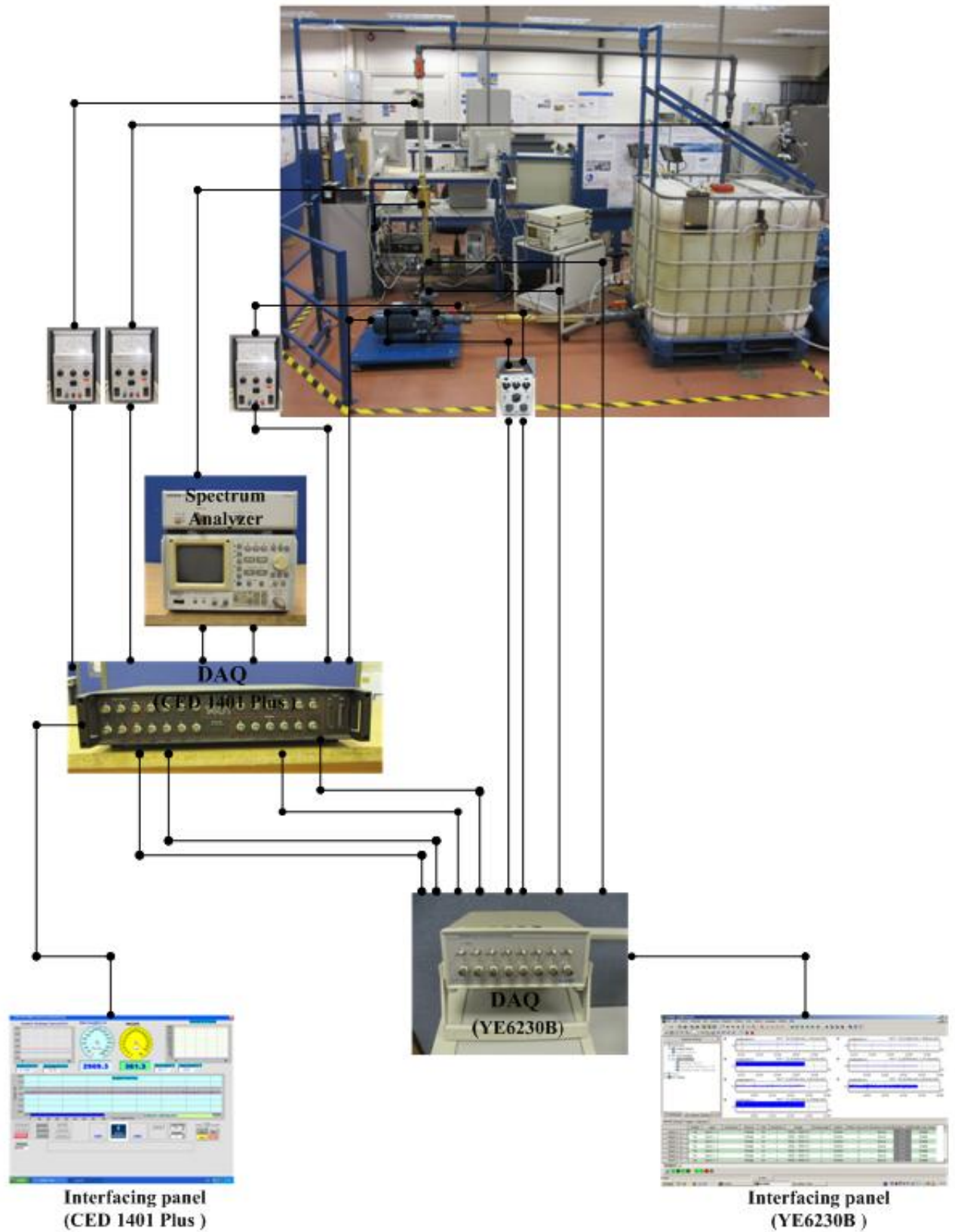


Figure 4-30 Centrifugal pump test system

CHAPTER FIVE

5. DESIGN OF A CAPACITANCE SENSOR FOR DETECTION OF CAVITATION

This chapter develops a new method suggested by the author as a technique for detecting incipient cavitation, that of detecting changes in the capacitance between two electrodes when pumped flow passes between them. It is suggested that the appearance of vapour bubbles in the flow with the onset of cavitation will change the electrical parameters and this change can be detected and used to diagnose the early stages of cavitation in a pump circuit.

5.1 Introduction

Section 3.3 introduced the idea that the capacitance between two plates on opposite sides of a non-conducting pipe can be used as a capacitance sensor to detect the onset of cavitation in water flowing through the pipe, see Figures 5-2 and 5-3. This presence of vapour bubbles in the flow will change the magnitude of the dielectric which will be detected.

A number of authors have used this technique to detect the presence of solid particles in fluid flows (Abouelwafa, 1980; Tollefsen and Hammer, 1998) and, more recently the relative phase proportions of oil-water mixes in real time (Loser, et al., 2001; White, 2002). An exciting development was the work of Jaworek, et al., (2004) who used capacitance methods to determine the phase conversion along a supercritical steam injector.

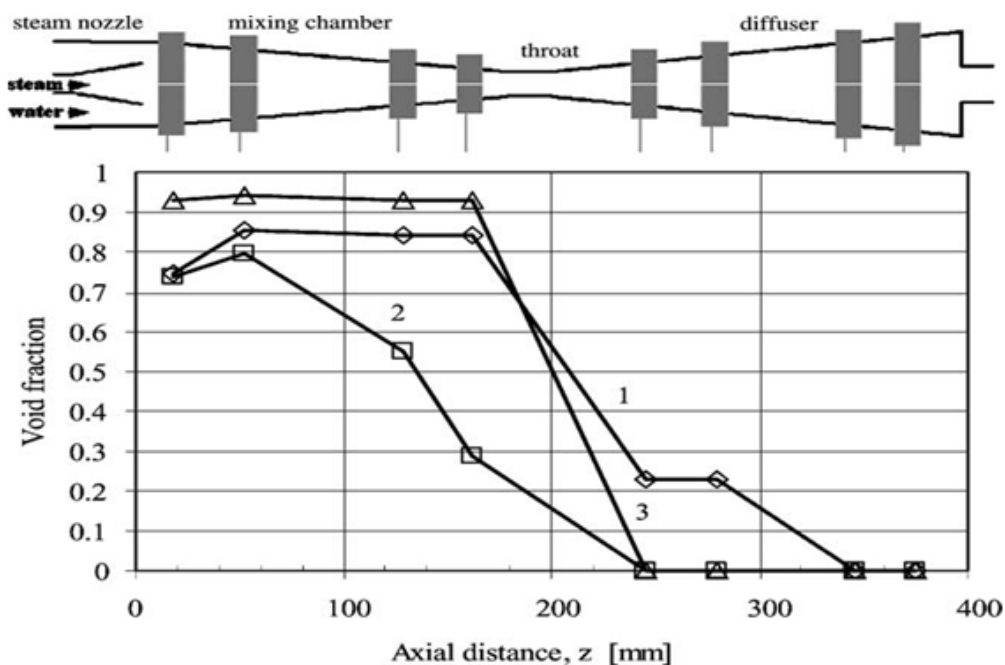


Figure 5-1 Examples of void fraction distribution along a steam Injector (Jaworek, et al., 2004)

If it is possible to measure the proportion of water in a steam/water mix moving at relatively high speed under highly turbulent conditions then it should be possible, in principle, to detect the presence of vapour in water flow.

5.2 Capacitance- sensor theory

As far as the author is aware no-one has previously used a capacitance based method for detecting cavitation in pumped water systems. A simple capacitor consisting of two parallel conducting plates, isolated from each other by a dielectric can store an electric charge when

the plates are at different potentials. Figure 5-2 (a) shows a parallel plate capacitor with plates of area A , separated by a gap d filled with a liquid of relative dielectric constant ϵ_r . The capacitance (C) of a capacitor is calculated from the physical dimensions and relevant dielectric constant, see Equation 5.1. Thus if the space between the electrodes is filled with either water or air, its measured capacitance will change by a factor of up to about 80, see Table 5-1. However, the dielectric constant of a liquid will vary with temperature.

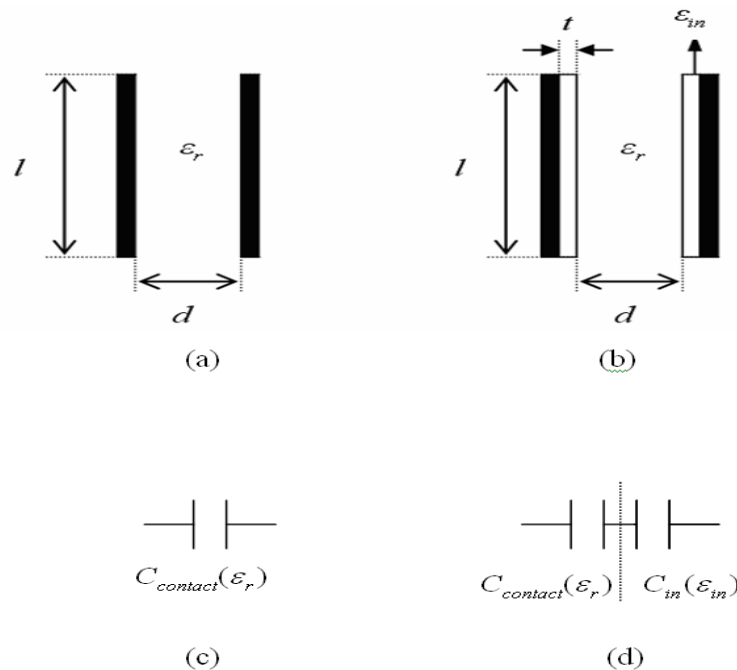


Figure 5-2 Simple parallel plate capacitor with and without the addition of an insulating layer of thickness t , and relative dielectric constant ϵ_{in}

$$C_{contact} = \epsilon_0 \epsilon_r A/d \quad \text{Equation 5.1}$$

Where $C_{contact}$ is the capacitance of the capacitor, A and d are area of the plates and distance between the plates respectively, dielectric constant of vacuum is $\epsilon_0 = 8.8542 \times 10^{-12}$ pF/m and ϵ_r is the relative dielectric constant of the fluid between the plates.

If A and d remain constant, the capacitance will vary only as a function of the liquid filling the gap between the plates, see Table 5-1 for typical values. If a change in the liquid causes a change in the value of dielectric of the capacitance system because, for example air bubbles have been introduced into the flow the measured capacitance will change, possibly in a manner that could be used to detect the onset of cavitation.

Table 5-1 Relative dielectric constant of air and water

Material	Temp °C	Dielectric Constant
Air	21	1.00
Water	0	88.0
Water	20	80.0
Water	100	48.0

For a capacitor where the electrodes are insulated from the liquid being investigated, for example where the plates are placed on the outside of a plastic pipe (considered an insulating layer) of thickness t , as shown in Figure 5-2 (b), the resulting capacitance can be calculated by assuming the arrangement acts as simple capacitances in series:

$$\frac{1}{C_{non-contact}} = \frac{1}{C_{in}} + \frac{1}{C_{contact}} \quad \text{Equation 5.2}$$

Where C_{in} is the total capacitance of the two layers of insulating material (one on each plate), each of thickness t and of permittivity ϵ_{in} , and can be written as:

$$C_{in} = 0.5 \epsilon_0 \epsilon_{in} A/t \quad \text{Equation 5.3}$$

From Equation 5.1, 5.2 and 5.3 it follows

$$C_{non-contact} = \epsilon_0 \epsilon_r \epsilon_{in} A / (2t\epsilon_r + d\epsilon_{in}) \quad \text{Equation 5.4}$$

Of course, the capacitor plates may not be plane. If they are to fit on a pipe they would have to be curved, and the smaller the pipe diameter the greater the curvature of the plates and the greater the digression from Equation 5.4. The essence here is not whether the precise value of the capacitance is known – though subroutines within the general Matlab package will calculate the capacitance for non-uniform, non-plane geometry electrodes – but the change in capacitance. A precisely correct formula or predicted value for the capacitance it not required at this stage, but could be required for commercial development of such a device.

An experiment using capacitance to detect incipient cavitation would be looking for a change in the value of the capacitance. In much the same way that vibro-acoustic techniques to detect the onset of cavitation look for a sudden change in either vibration levels or in airborne sound. Here a sudden detectable drop in the capacitance would indicate the possible presence of voids in the water flow.

5.3 Principles of design of capacitance sensor

The sensor will be used to detect changes in capacitance as the dielectric constant of the water changes as bubbles of vapour generated by cavitation begin to flow. The sensors were placed close to the pump inlet and outlet; see Figure 5-3, because it is at these two positions that the presence of cavitation bubbles will be most obvious. The plates of the capacitor forming the sensor placed on the outside of the plastic outlet pipe of the pump are shown in Figure 5-4. The sensor was shielded to minimise errors due to stray electromagnetic fields. The shield was grounded and the capacitor plates made as large as reasonably possible to minimise end effects and any resultant variations in capacitances, see Appendix D for dimensions and materials used.

As the measurements are to be of changes in the value of the capacitance, and it is not yet clear what the magnitude might be, direct measurement of the capacitance is unlikely to be a successful approach. It is much more common to use a resonant circuit technique whereby change in the capacitance cause a change in the resonant frequency, which is relatively easy to measure (Jaworski, et al., 1999; Schüller, et al., 2004; Jaworek, et al., 2004).

The measurement of capacitance of a capacitor filled with a fluid is difficult if the fluid has a low resistivity. Pure water does not conduct (resistivity about $20 \times 10^6 \Omega.m$), but the kind of water likely to be found in a pumped system could have a resistivity as low as that of tap water, $20\Omega.m$. Unfortunately at low frequencies this resistance acts as a short-circuit, (electrical impedance of a capacitor is inversely proportional to the frequency of the applied signal, while resistance is more or less constant). For the capacitance effect to dominate the applied frequency has to be high.

Jaworek, et. al. (2004) successfully used a frequency of 80 MHz to excite a capacitance sensor in their void fraction measurements. It was argued that at this frequency the characteristic time of the electrical processes of the water was defined by the product of the liquid's resistivity and absolute permittivity. The former has units of $m^{-1}.kg.s^{-3}.A^{-2}$ the latter has units of $m.kg^{-1}.s^4.A^2$, so their product has units of s^{-1} . Jaworek's general reasoning appears correct and the frequency he used was acceptable. The likely resonant frequency of the circuit used in this work was not known in advance so it was found, essentially, by trial and error. There were just too many unknowns to calculate it in advance. Thus, beginning at 10MHz a series of frequency bands were used until a resonant frequency at about 411 MHz

was located. Subsequently two other resonant frequencies were found, one about 534 MHz and the other at about 762 MHz.



Figure 5-3 Capacitive sensors at inlet and outlet of the pump

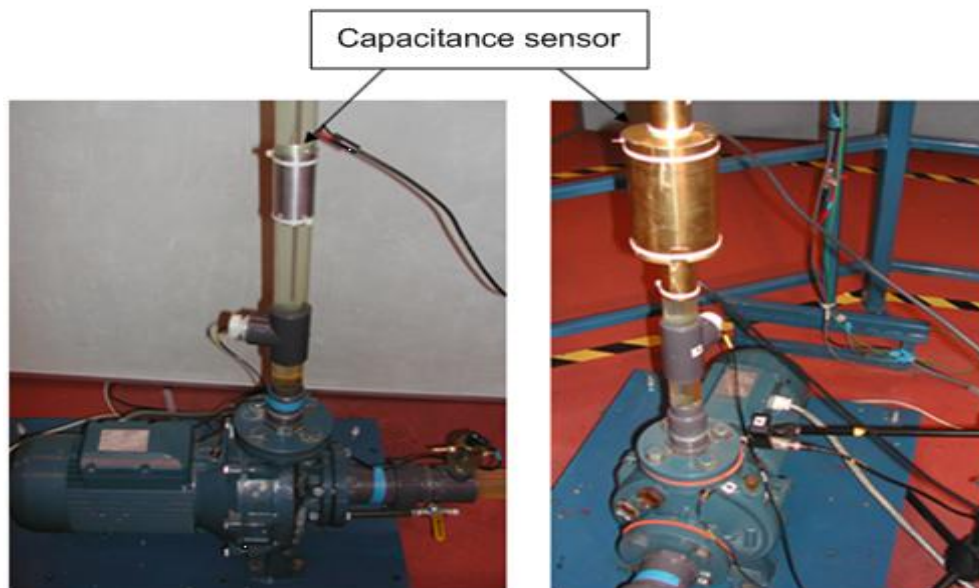


Figure 5-4 Position of capacitance sensors at outlet of the pump

5.4 Signal generator

The signal generator was a Crystek type CVCO55BE voltage controlled oscillator which produces a signal in the range 400MHz to 800Mz. Figures 5-5 (a) and 5-5 (b) shows the oscillator and the board to which it is attached. The supply voltage of 5V is attached to VCC and the tuning voltage (0 – 12V) was attached to Vt. The signal was taken from the connection marked RF. Details of the oscillator are provided in Tables 5-2 and Appendix E.

The oscillator and reference generator were on a printed circuit board placed close to the capacitor to minimise stray capacitance and reduce any distortion. Minimum dimensions for this device were achieved by using surface mounted devices.

The input of the capacitor sensor was connected to RF, and the output of capacitor sensor connected to the spectrum analyser. RADIALL high frequency cables with male connectors at each end and 0.25 m long (HF, M/M, 0.25M) were used with Sub Miniature version A (SMA) coaxial RF connections.

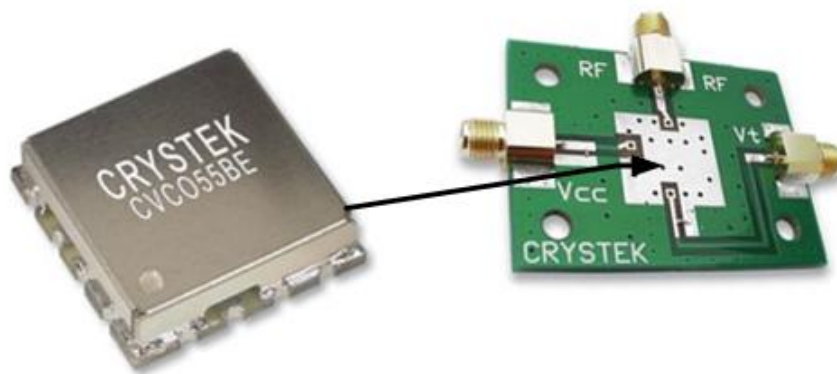


Figure 5-5 (a) CRYSTEK - CVCO55B Voltage Controlled Oscillator



Figure 5-5 (b) CRYSTEK - CVCO55B Voltage Controlled Oscillator

This was not sufficient to fully screen the measuring capacitors from stray affects and in the end they were completely enclosed within a brass container, see Figure 5-3. The output of the spectrum analyser was connected to the data acquisition system and then to the PC via a USB port, see Figure 5-7.

Table 5-2 Specification of CRYSTEK CVCO55B Voltage Controlled Oscillator

CRYSTEK CVCO55B	Voltage controlled oscillator
Frequency range:	400MHz to 800MHz
Harmonic suppression(2nd Harmonic)	5dBc
Tuning voltage	0-12V
Supply voltage	5V
Operating temperature range	-10°C to +70°C
Oscillator / resonator case style	SMD
No. of Pins	16
Tuning sensitivity	47MHz/V
Type phase noise (dBc / Hz)	-129dBc/Hz
Crystal case type	12.7 x 12.7mm x 3.81 mm
Center frequency	600MHz
ICC Max	17mA
KVCO(MHz/V)	47
Power (dB)	7 ±5
Phase noise type (dB/Hz)	-105

Table 5-3 Specification of cable assembly, HF, SMA M/M, 0.25M

RADIALL	Cable assembly, HF, SMA, M/M, 0.25M
Type	Audio/Video
Cable length	0.50m
Cable type	HF Coax
Connector type A	SAM plug
Connector type B	SAM plug
Max operating temperature	125C ⁰
Min operating temperature	55C ⁰
Outer insulation colour	Green
Impedance	50ohm

5.5 Spectrum analyser

The Advantest type R4131D spectrum analyser has a measurement-condition memory function which includes waveforms, an auto-recall function which recalls measurement conditions when power is switched on and other features to simplify operation. It also provides automatic frequency control, enabling highly stable spectrum analysis giving frequency characteristic measurements with a wide dynamic range. The R4131D has a save

/recall function not only for measurement condition settings but allows up to three waveforms to be stored and recalled, enabling a stored waveform to be used as a reference in comparison measurements. Figure 5-6 and Table 5-4 show the spectrum analyser and its specifications (ER4131 Operation Manual).

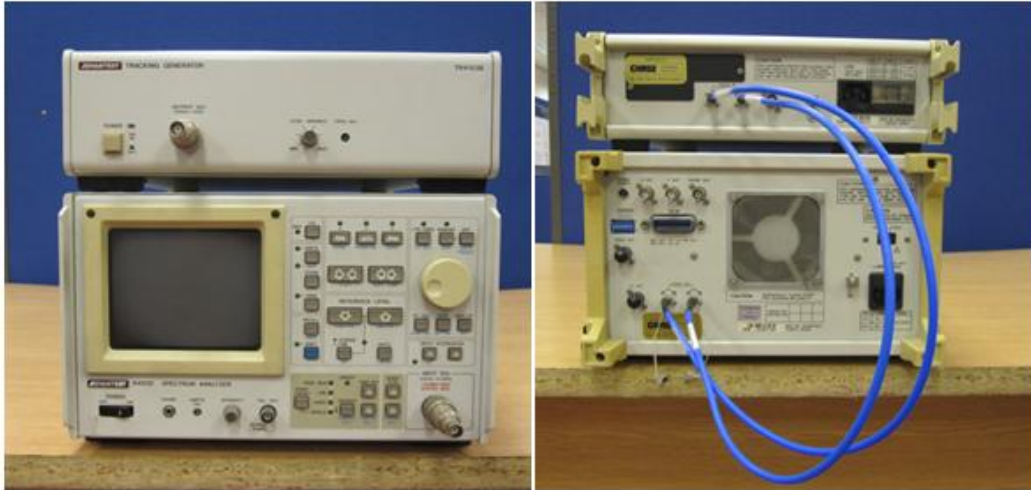


Figure 5-6 Advantest type R4131D spectrum analyser

Table 5-4 Specification of the Advantest R4131D spectrum analyzer

Spectrum analyzer	Advantest
Type	R4131D
Input impedance	50-75 Ω
Frequency span	4GHz-50KHz
Resolution	1MHz-1kHz
QP valve automatic operation. Antenna factor automatic operation. GPIB control.	Standard mounting
Save/Recall function	Storing three setting conditions in its non-volatile memory. Storing three display waveforms in its non-volatile memory. Possible to set automatically at power on.
Displaying function	Write and view screen display POST/NEG display
Occupied band-width	Standard configuration
Ambient condition	0 ⁰ C to 50 ⁰ C and 85% RH

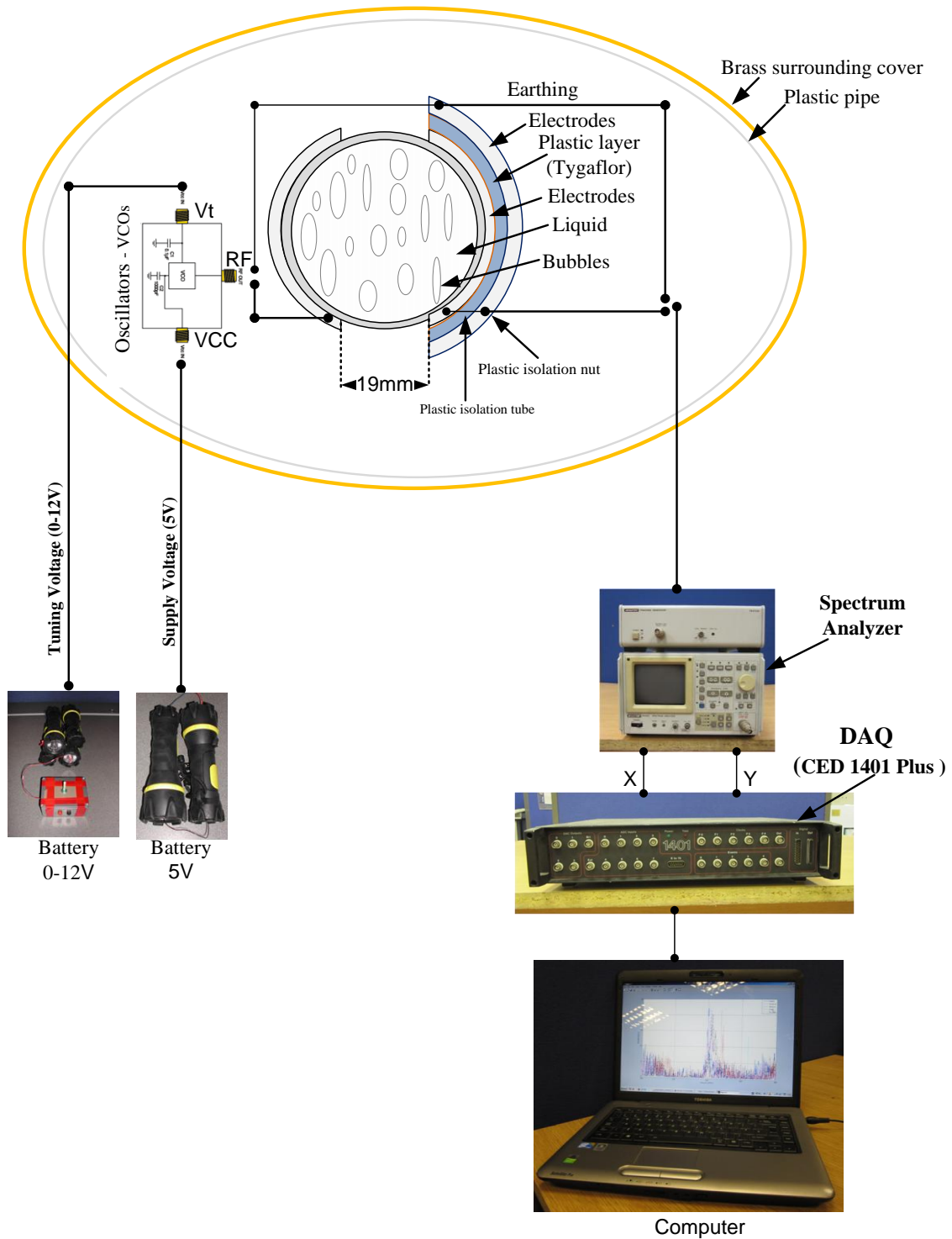


Figure 5-7 Simplified schematic of capacitance sensor

CHAPTER SIX

6. CAPACITANCE SIGNAL ANALYSIS FOR DETECTION OF CAVITATION

This chapter focuses on the experimental results obtained from the use of change in capacitance to detect and diagnose cavitation. It begins with a description of the equivalent LCR resonance circuit used to model the sensor, then describes the acquisition of data as a function of air flow in the pump circuit and finally examines the experimental data obtained as possible indicators of the onset of cavitation.

6.1 Introduction

A considerable part of this chapter has been published in the Proceedings of the 24th International Congress on Condition Monitoring and Diagnostics Engineering Management, (Al Thobiani et al, 2011).

As has been described in Chapter Five an electrical capacitance sensor has been suggested for the non-invasive detection of the presence of vapour bubbles in water flowing in a pipe. The sensor was used to detect changes in the measured resonant frequency as the capacitance changed due changes in the value of the dielectric as bubbles of vapour generated by cavitation at the pump began to flow. The device was found to be extremely sensitive to electrical interference and complete screening was necessary, see Figure 6-1 before useful readings were obtained. To minimize the influence of end effects and any resultant capacitances and stray electromagnetic fields the sensor assembly was as large as feasible and shielded by completely enclosing in a brass container. The change in capacitance was very small but, with the correct screening the consequent change in resonant frequency could be detected. Initially attempts were made to measure the capacitance directly with the help of Mr. Chris Daykin, and the degree of shielding was determined by this procedure which was abandoned in favour of measuring the resonant frequency.

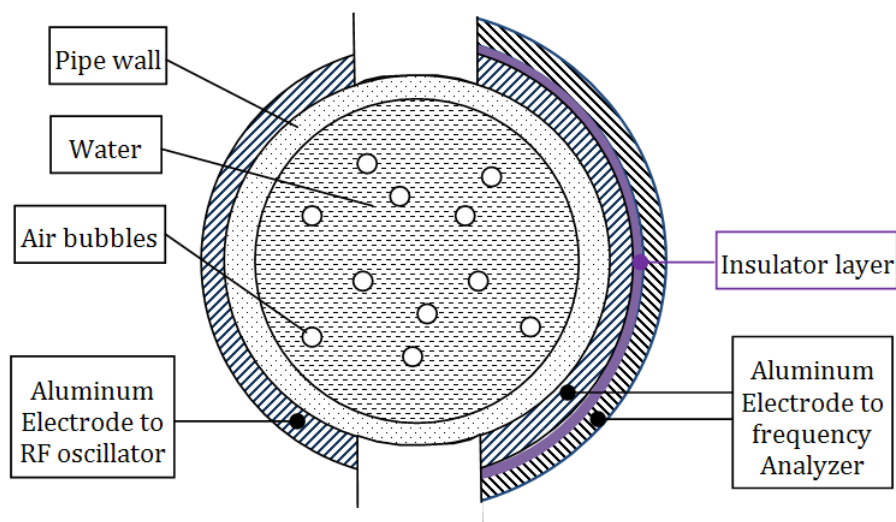


Figure 6-1 Schematic diagram of capacitance sensor assembly

6.2 Sensor equivalent circuit

The two plates forming the capacitor were placed on the outside of the plastic pipe carrying the water flow. The first part of capacitor sensor was connected to the oscillator (CVCO55BE) and the second part was connected to spectrum analyzer, to the DAS and then to the computer via the USB port. The sensor assembly consists of a pair of aluminium alloy electrodes in the form of semi-cylindrical plates. As shown in Figure 6-1, the electrodes are placed directly facing each other on the external wall of the discharge line which is constructed from nonconductive transparent PVC material (see Section 4.2.1). One of the electrode plates is smaller than other to reduce capacitance edge effects: the size of the smaller plates is $97 \times 34 \times 2$ mm and the larger plate is $97 \times 43 \times 2$ mm.

Based on work of Jaworek, et al., (2004 and 2010) and Huang, et al., (1998), one plate of the capacitance sensor was connected to an RF oscillator and the other was connected to a spectrum analyzer, so the sensor system can be modelled electrically as shown in Figure 6-2. Rather than using a demodulation approach to measuring the frequency changes, a direct frequency measurement method was used to gain a better understanding of frequency shift behaviour with the presence of bubbles in the flow, and to reduce possible adverse influences caused by the modulation circuits.

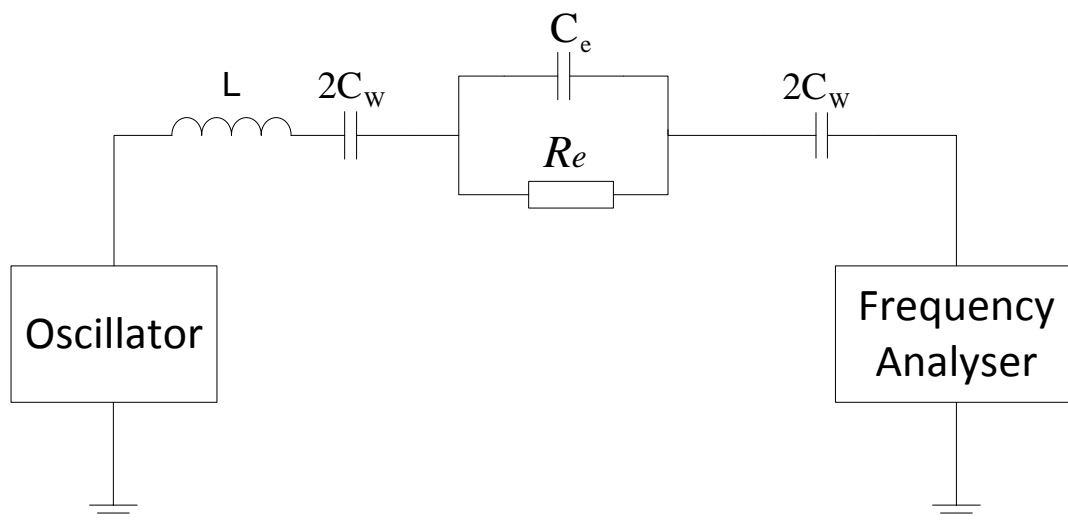


Figure 6-2 Schematic diagram of electrical equivalent circuit for capacitive sensor

It is assumed that the heterogeneous water/bubble flow inside the pipe can be represented by a single lumped capacitance C_e with unknown relative permittivity, ϵ_r . The pipe wall between the flowing water and the electrode forms an equivalent capacitance $2C_w$ in series with the water/bubble flow capacitance (the value $2C_w$ is used simply to remove an unwanted half that

would otherwise appear in subsequent equations). Therefore, the effective or total capacitance of the sensor assembly, three capacitors in series, will be

$$C_T = \frac{C_e C_w}{C_e + C_w} \quad \text{Equation 6.1}$$

A parallel resistance R_e represents the resistance of the mixture of vapour bubbles and water within the pipe and the self-inductance L represents the inductance in the sensor circuit. As can be seen in Equation 6.2 below the value of R_e has no effect on the frequency of resonance but, of course, the greater the resistance the lower the magnitude of the resonance peak. A high frequency band from 400MHz to 800MHz was used to operate the sensor, to reduce resistance effects and improve the performance of measuring micro-bubbles in cavitation flow.

As shown in Figure 6-2 the output of the RF oscillator passes through the capacitance circuit and can be measured and analysed using a frequency analyser. In such circuits there will be a resonant frequency which depends on the value of the capacitance and can be sensitive to the changes of capacitance. Here it is assumed that only C_e will vary with introduction of bubbles into the water flow.

For an LC circuit such as in Figure 6-2, the resonant frequency is:

$$f = \frac{1}{2\pi} \sqrt{\frac{1}{LC_T}} \quad \text{Equation 6.2}$$

Thus the change of frequency due to the change of capacitance can be found by simple differentiation:

$$df = -\frac{1}{2} \frac{f}{C_T} dC_T \quad \text{Equation 6.3}$$

The “-“ sign that appears in Equation 6.3 is the mathematical representation of the fact that the resonant frequency decreases as the capacitance increases.

Differentiating Equation 6.1:

$$dC_T = \left(\frac{C_w}{C_e + C_w} - \frac{C_e C_w}{(C_e + C_w)^2} \right) dC_e$$

$$dC_T = \left(\frac{C_w}{C_e + C_w} \right)^2 dC_e \quad \text{Equation 6.4}$$

Substituting Equation 6.4 into Equation 6.3 and dividing both sides by f to find relative changes:

$$\frac{df}{f} = -\frac{1}{2} \frac{dC_T}{C_T} = -\frac{1}{2} \left(\frac{C_w}{C_e + C_w} \right)^2 \frac{dC_e}{C_T}$$

$$\frac{df}{f} = -\frac{1}{2} \frac{C_w}{(C_e + C_w)} \frac{dC_e}{C_e} \quad \text{Equation 6.5}$$

Perusal of Equation 6.5 shows that dC_e/C_e , which may be taken as a measure of the sensitivity of the capacitance to change in the void fraction is multiplied by a quantity which is less than unity for all values of the void fraction. That means the relative change in frequency due to change in void fraction will be less than the relative change in C_e . The reason why resonant frequency is used here is because it is so much easier to measure than capacitance, see Section 5.3.

6.3 Likely frequency shift

C_e will vary according to the ratio of bubbles/water. Once the size and materials of the sensor assembly are fixed, C_e is mainly determined by the relative permittivity, ϵ_r , which will decrease with void fraction (but not linearly) as confirmed by Jaworek, et al., (2010). From first principles, see Equation 5.4, the total capacitance, C_T , will vary approximately as $(A + B/\epsilon_r)^{-1}$. Therefore, with increase in the void fraction, we would expect an increase in the value of ϵ_r , a corresponding decrease in value of C_T and an increase of the resonant frequency.

However, for the onset of cavitation in flows, the void fraction will be very small and the associated change in capacitance can be approximated as a linear decrease as void fraction increases (as cavitation increases), as:

$$C_e = C_{e,0} [\alpha + \epsilon_L (1 - \alpha)] \quad \text{Equation 6.6}$$

Where α is the void fraction ($\alpha \leq 1$), ϵ_L is the relative permittivity of the liquid (water in this case), the relative permittivity of air is taken to be unity. For 100% water between the plates ($\alpha = 0$ and $\epsilon_L = 80$), and Figure 6-3 (a) shows the expected behaviour of the relative capacitance ($C_e/C_{e,0}$) with change in void fraction. Jaworek, et al., (2004) used a sensor of similar construction with $C_{e,0} \approx 0.5$ pF and $C_w \approx 5$ pF, so the expected change in resonant frequency with void fraction should be as shown in Figure 6-3 (b).

The capacitance will decrease linearly over the range of void fraction for which Equation 6.6 is valid. In parallel, the frequency increases nonlinearly.

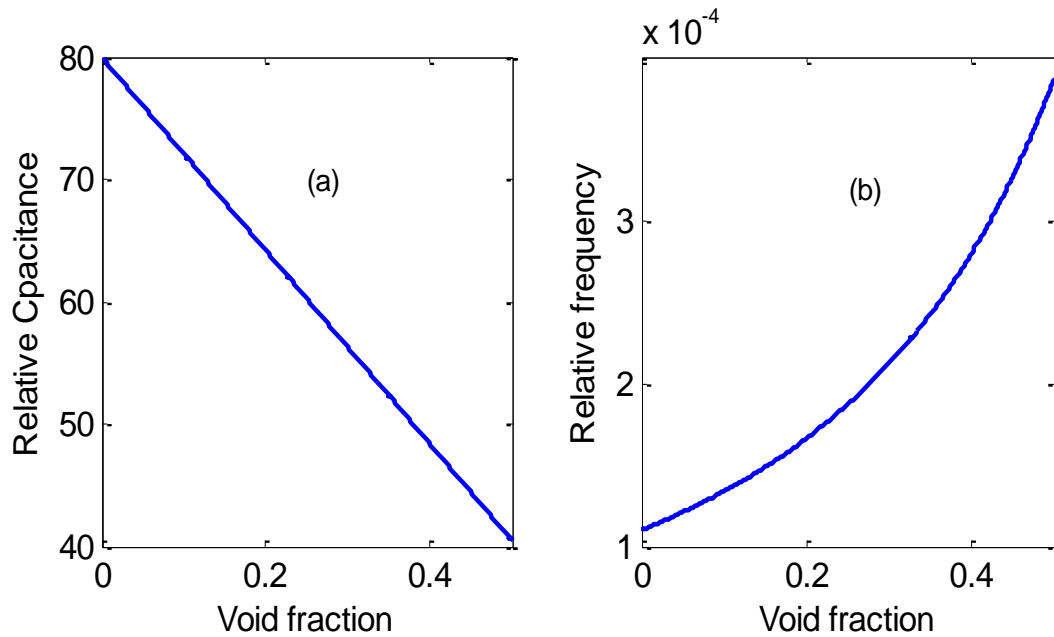


Figure 6-3 Expected capacitance and frequency trends with cavitation

It is recognised that the measured signal depends not only on the phase volume percentage but also on the flow pattern.

6.4 Acquisition of capacitance data

The pump test rig shown in Figure 4-4 was used to simulate different degrees of pump cavitation, that figure is shown again here as Figure 6-4 with more detail of the gas injection into the pump supply line. To simulate different levels of cavitation flows under more controlled conditions an air-inlet valve was installed in the suction line. This allowed air to enter the pump in quantities controlled by the valve and the pressure in the supply line. Visual observation of the mixed flow was possible through the sections of transparent pipe in the pump circuit.

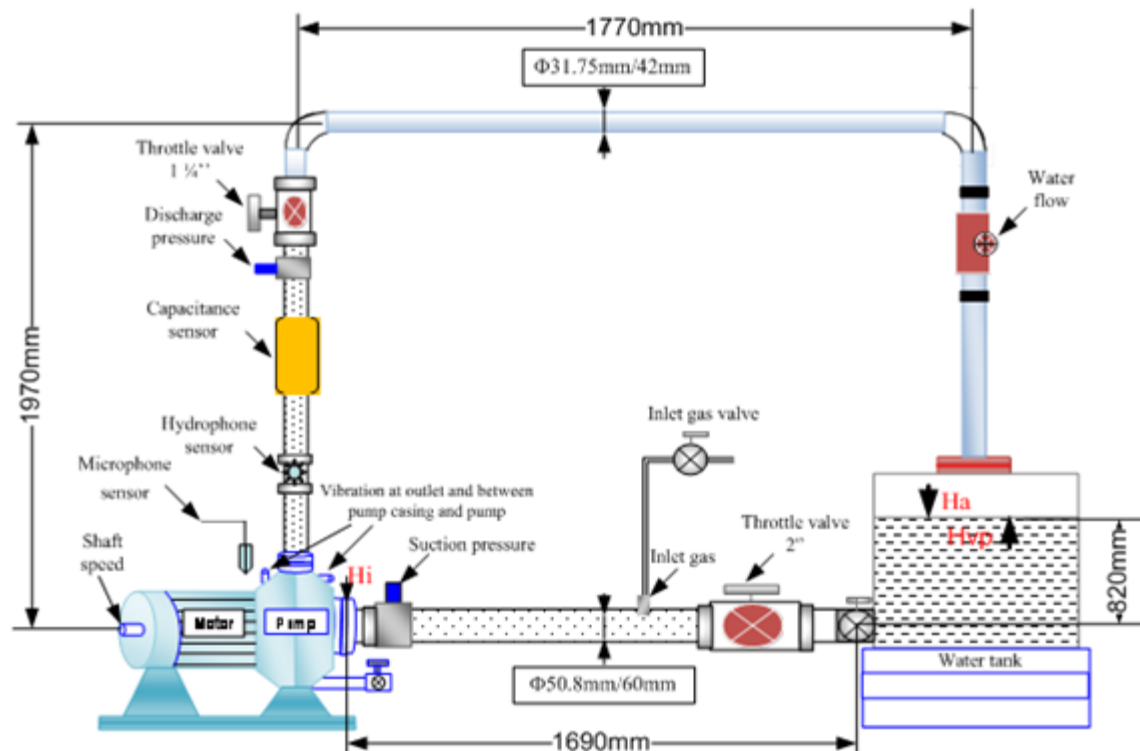


Figure 6-4 Schematic of test rig with addition of air inlet valve and air supply line

Capacitance based cavitation measurement was first done at full flow rate with pump speed of 2900rpm. At this speed the pressure in the suction line is below ambient. Opening the air-inlet valve in the suction will allow air to enter and mimic cavitation inside the pump.

Figure 6-5 shows the air flow through the air valve when a pressure difference of 0.43 bar was applied, but with the open end of the valve venting to atmosphere, i.e. into the open air. It was found that the flow rate is approximately proportional to the angle of opening. It is suggested that much the same air flow rate will take place when the open end of the valve is inserted into the supply line to the pump, since for the supply line pressure is 0.43 bar below ambient.

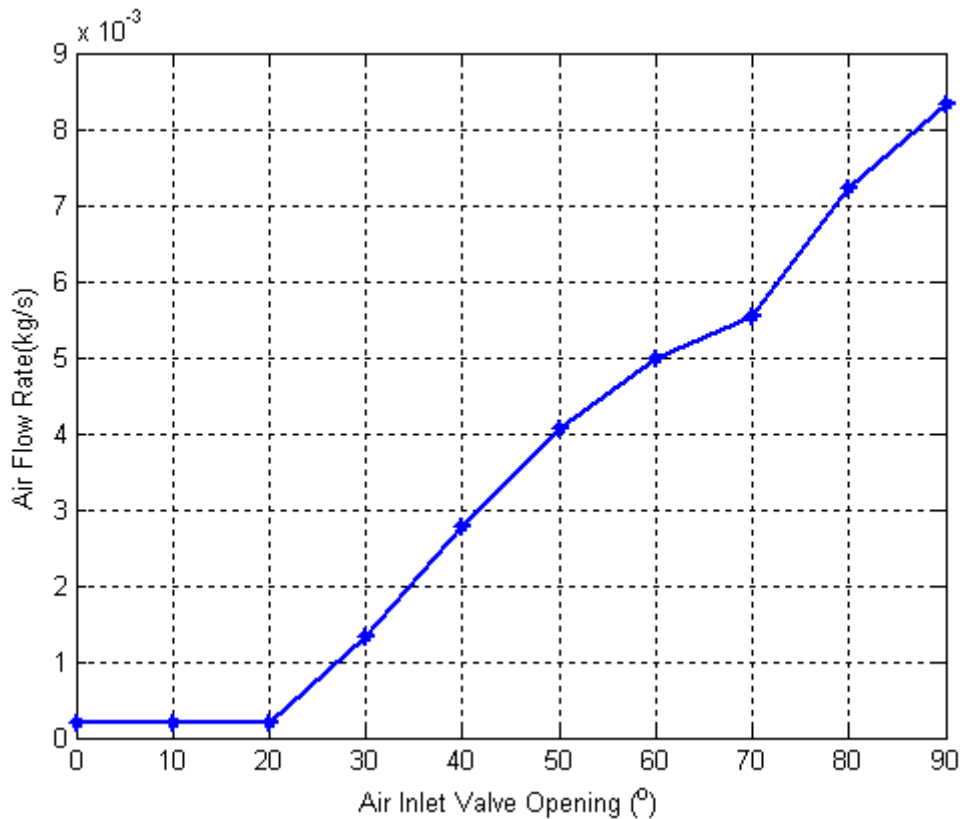


Figure 6-5 Air flow into pump circuit with air valve opening (0.43 bar pressure difference)

Figure 6-6 shows the measured water flow rates for the given pump speed (2900 rpm) with increasing air valve opening. Based on this, the air to water ratio in the flow can be estimated at different valve openings. For example with the valve open 80° the air flow rate was about 0.72×10^{-3} kg/s and the water flow rate was about 328 kg/min (= 5.47 kg/s) thus the air to water mass ratio was about $(0.72 \times 10^{-3})/5.47 = 1.32 \times 10^{-4}$. Assuming the air and water temperatures in the experiment to be 20°C the volume flow rate of the air into the water was 0.60×10^{-3} m³/s. The simple volume ratio ignores pressure differences and other effects such as viscous and surface tension forces would be about 0.11, which appears to be of the right order from the photographs shown in Figure 6-7.

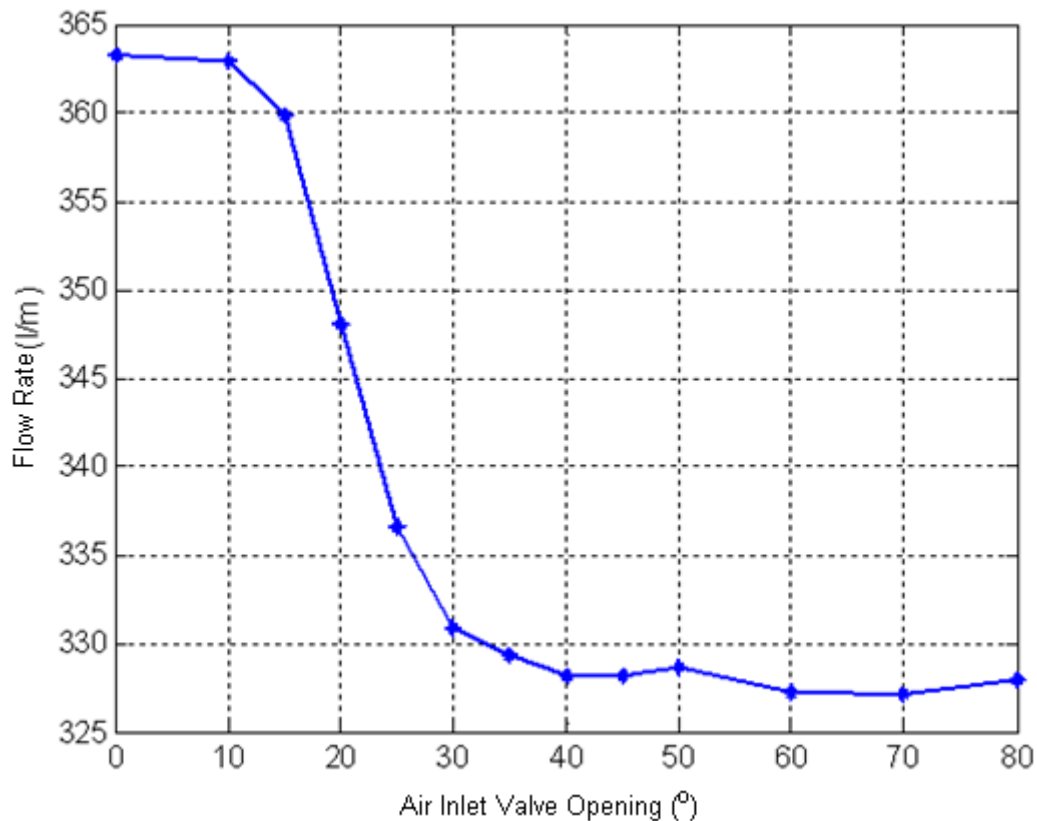


Figure 6-6 Water flow rate against air inlet valve opening

Figure 6-7 shows photos of the air bubbles inside the pump suction line for different valve openings. Even bearing in mind that the flow pattern is three-dimensional the bubble densities seen in Figure 6-7 show little change at higher valve openings. However, because liquid is present the out of line testing may not be an accurate estimation of air ingestion due to the influence of the water flow and of viscous and surface tension effects. Bubble density observed from Figure 6-7 also shows little change at high degrees of valve opening.

The capacitance was measured at full flow rate at pump speed of 2900 rpm. The valve was first fully closed – no air in the water flow – and was then opened 10^0 at a time until it was fully open (90^0). This test was repeated three times. The data records from each test were processed using Matlab, as with e.g. the vibration measurement; the signal was sampled at 96 kHz for 10 seconds.

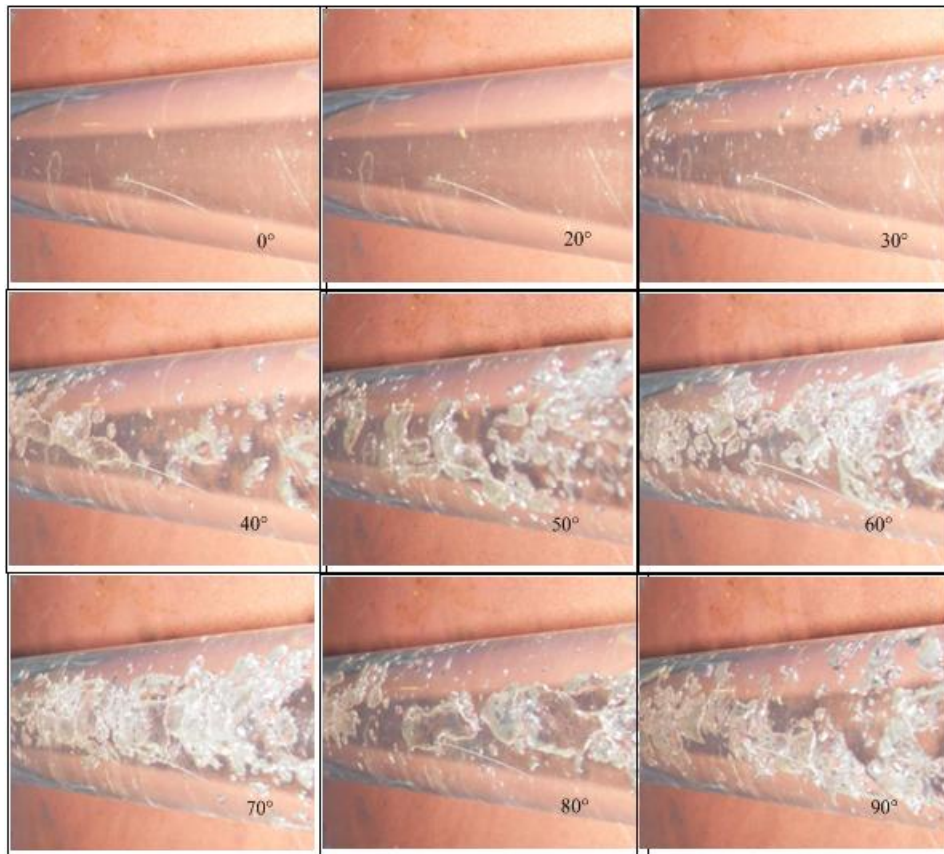


Figure 6-7 Images of bubbles in flow for pump speed 2900 rpm, suction line pressure 0.43 bar below ambient for different openings of the air valve in degrees

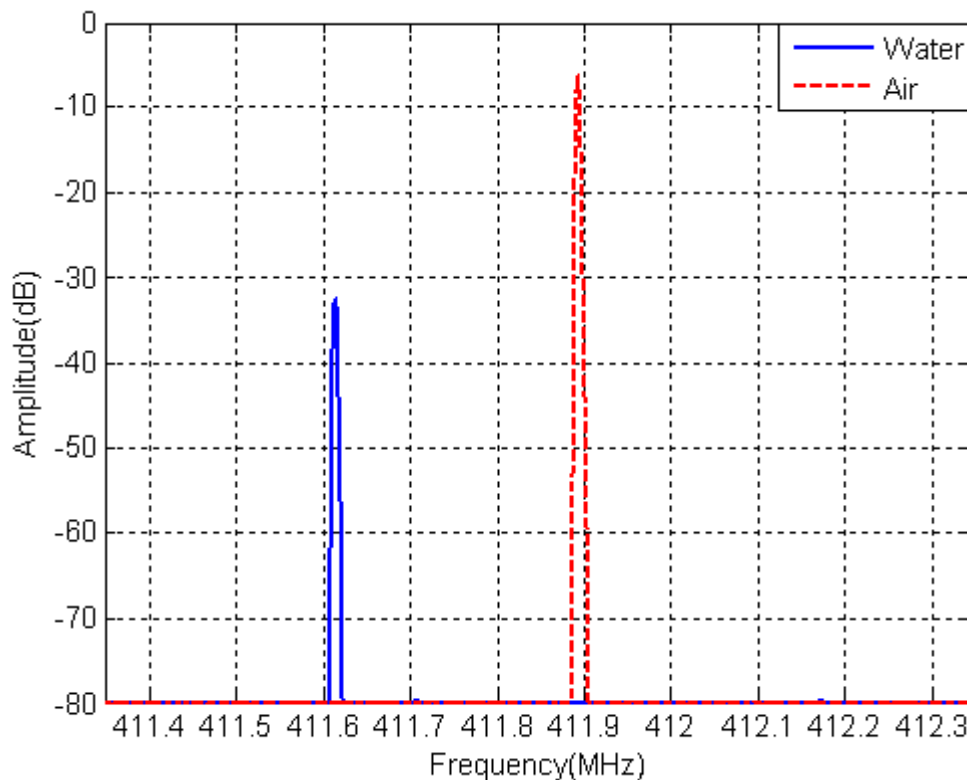
The measurement system is shown in Figure 6-1. The sensor assembly was conveniently mounted on the outside wall of the discharge line. The excitation source of the sensor assembly was the sinusoidal oscillation output from the RF oscillator described previously, in the frequency range 400 MHz to 800 MHz. The output of the sensor assembly was connected to a high frequency spectrum analyzer to detect and measure the frequency at circuit resonance. Simultaneously, the spectrum from the analyser was recorded by a host PC for further analysis.

The frequency of the oscillator was adjusted by varying the tuning voltage. However the mains based voltage supply was found not steady enough and the peaks moved due to small fluctuations in the mains voltage. Nevertheless, using such a device with 100% water in the system it was possible to locate three peaks in the output of the capacitor system; at about 411 MHz, 535 MHz and 762 MHz. For stability of output it was decided to power the oscillator using alkaline batteries. With a tuning voltage of 1.521 V and 100% water in the pipes there was a sharp peak at 411.411 MHz, the bandwidth of the supply was 1 MHz. When the battery voltage was increased to 3.06 V (by doubling the number of batteries or using

3.06 V batteries instead of 1.5 V batteries) the peak moved to 535.009 MHz. Similarly when the supply battery voltage was further increased to 7.80 V a single steady peak was found at 762.467 MHz. Cavitation should be detected though shifts in the frequency of these peaks. The measuring system for the outputs from the spectrum analyser, accelerometer, microphone and hydrophone are all as shown in Figure 4-30.

Before commencing measurements the capacitor system was tested to ascertain its likely sensitivity to the presence of air in water. With no flow the vertical arm (the pipe exiting the pump) was filled with water until the level was just equal to the bottom of the capacitor plates and the resonant frequency measured. Then the water level in the pipe was raised until it was higher than the top of the capacitor plates and the resonant frequency measured. The output of the R4131D spectrum analyzer was as shown in Figure 6-8.

Three separate sets of tests were performed, one for an applied tuning voltage of 1.521 V and resonant frequency about 411 MHz, one for a tuning voltage of 3.06 V and 535 MHz, and one for 7.80 V and 762 MHz. Distinct frequency shifts and changes in peak level were observed. It is clear from this figure that the resonance at 535 MHz is the most sensitive both in terms of frequency shift and change in magnitude.



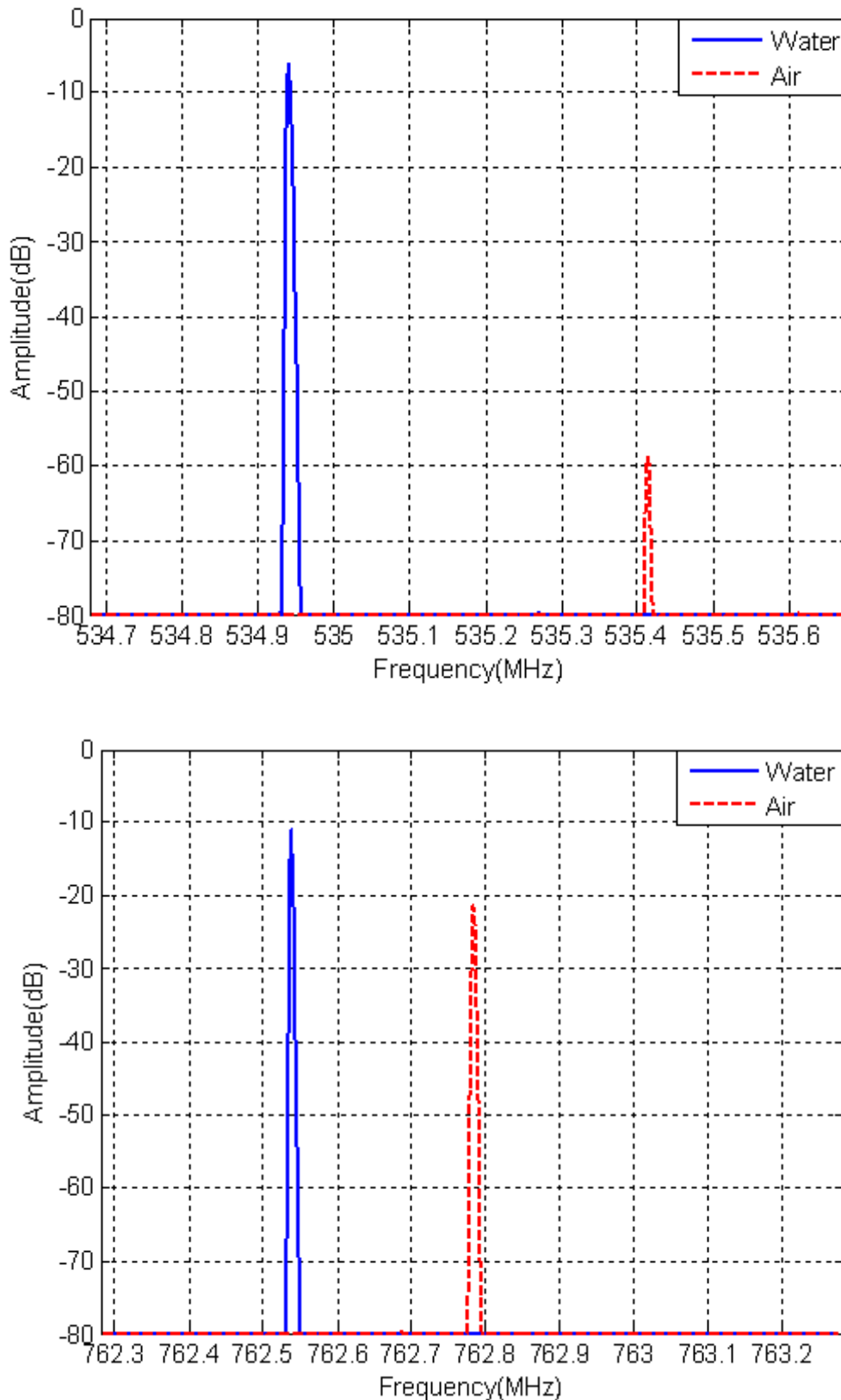


Figure 6-8 Output of spectrum analyser with 100% air and 100% water between capacitor plates for the three resonant frequencies 411MHz, 535MHz and 762MHz

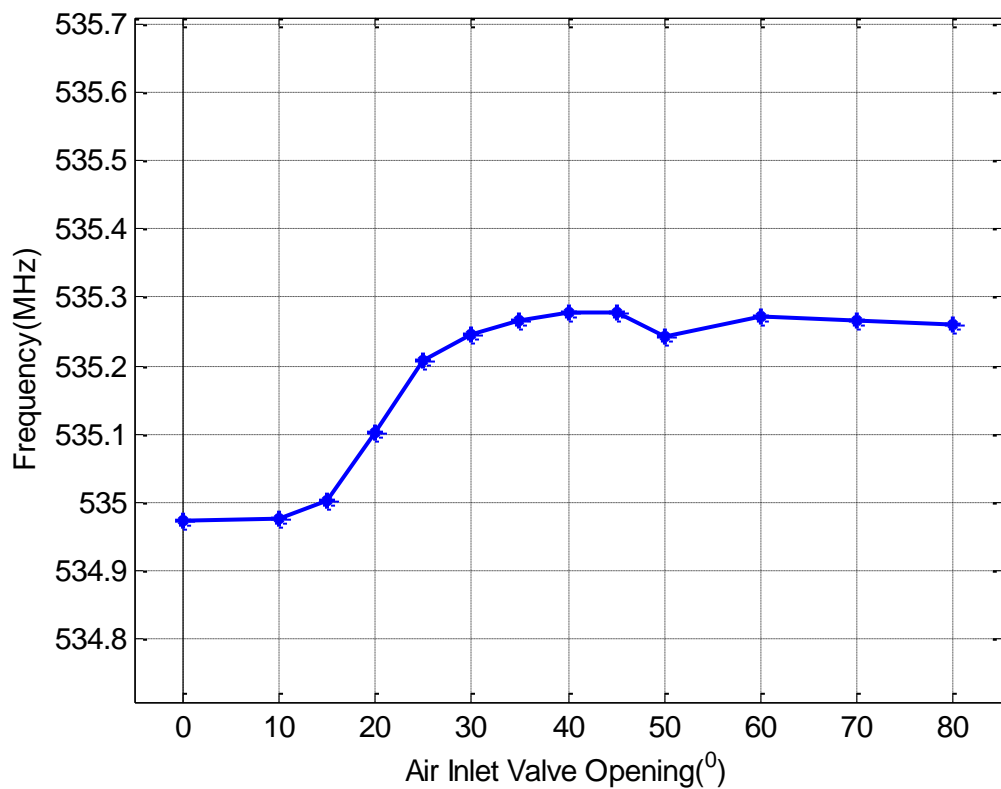
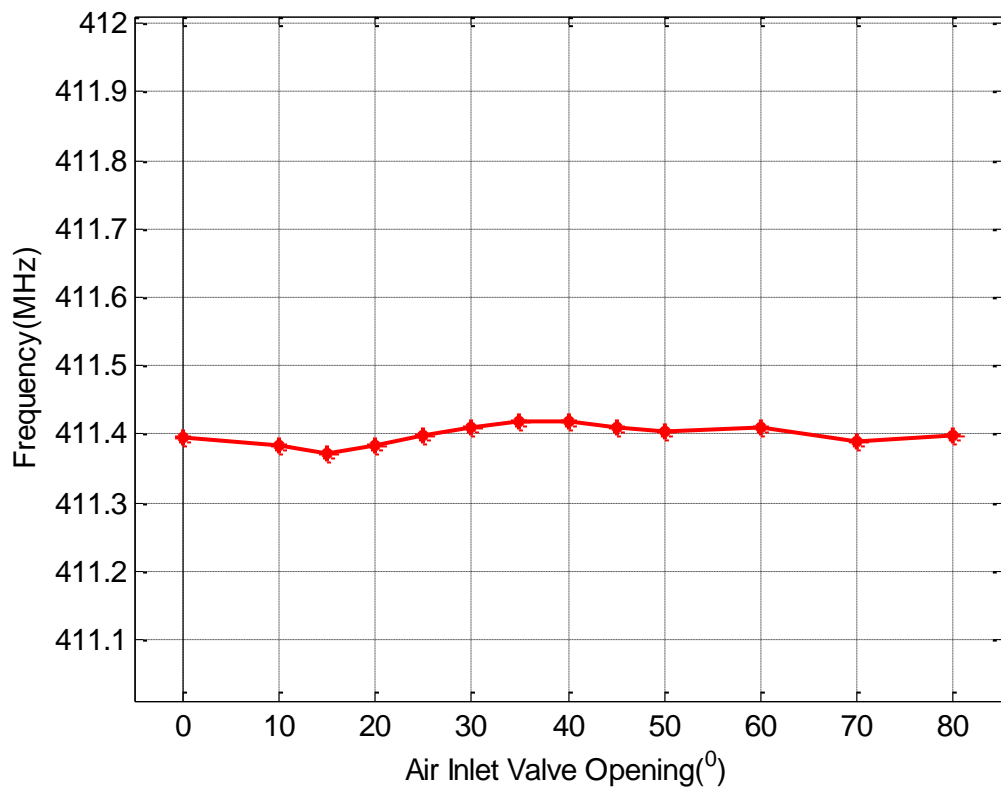
The results obtained were consistent with prediction that a water filled pipe will result in a lower frequency due to its higher capacitance.

Figure 6-9 shows results of three tests and it can be seen that the measurements have good repeatability. Figure 6-8 shows the output of the analyser with water flowing in the pipe and different degrees of opening of the air inlet valve. For 100% water in the pipe and a tuning voltage of 0.521V a clear and distinct peak in the spectrum is seen at about 411MHz. The air inlet valve was then opened in steps of 10^0 , allowing larger amounts of air to be “drawn” into the pipe, as expected and as can be seen in Figure 6-8 the greater the proportion of air in the two-phase flow the higher the frequency at which the peak occurred. I.e. as the valve was opened and air flowed into the pipe the resonant frequency increased, which is consistent with the findings shown in Figure 6-8.

Figure 6-9 shows that with a tuning voltage of 3.06V and 100% water flowing in the pipe a clear and distinct peak in the spectrum is seen at 533.352 MHz. It should be pointed out that this is not the same value as that obtained when there was no flow, see Figure 6-8. The air inlet valve was then opened in steps of 10^0 , allowing larger amounts of air to be “drawn” into the pipe and, as expected the greater the proportion of air in the two-phase flow the higher the frequency at which the peak occurred.

Figure 6-9 also shows that with a tuning voltage of 7.80V and 100% water flowing in the pipe a distinct peak in the spectrum is seen at 672.74MHz. Again it should be pointed out that this is not the same value as that obtained when there was no flow, see Figure 6-8. As the air inlet valve was opened and larger amounts of air were “drawn” into the pipe there was an increase in the resonance frequency.

It can be seen that the maximum frequency shift differs with resonant frequency being greatest for the 533 MHz peak (about 225 kHz), and this mainly occurs for lower valve opening positions (20^0 to 30^0). This is the range which is important for a good estimation of the onset of cavitation and the frequency shift for small air-inlet openings could be the basis for estimation of cavitation inception and severity.



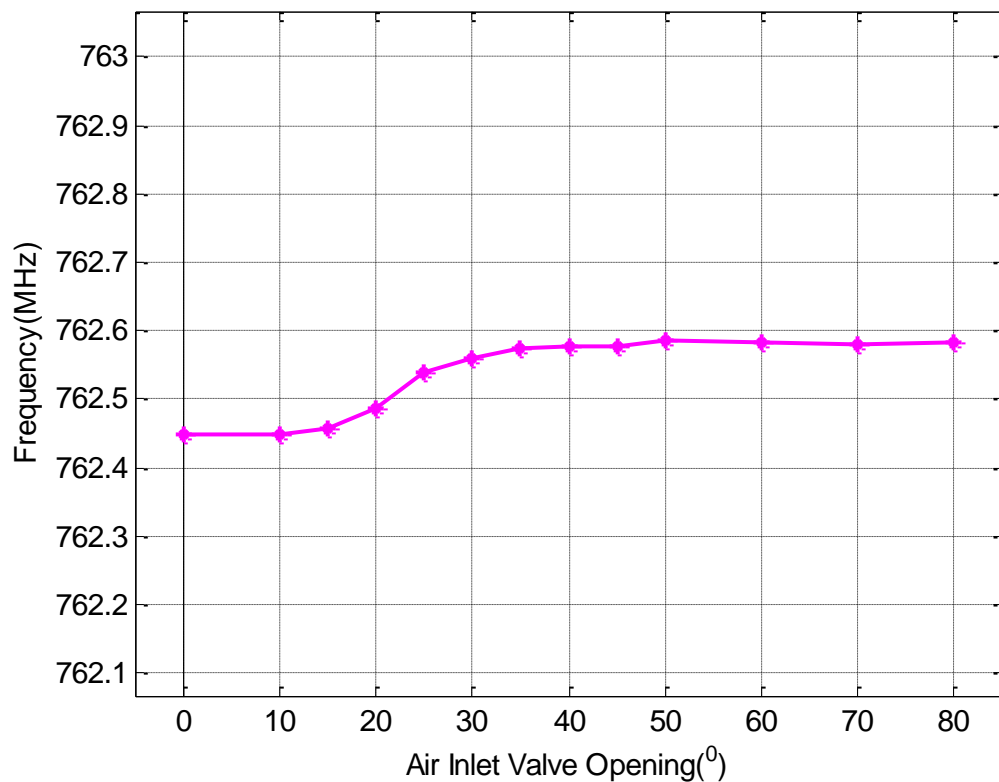
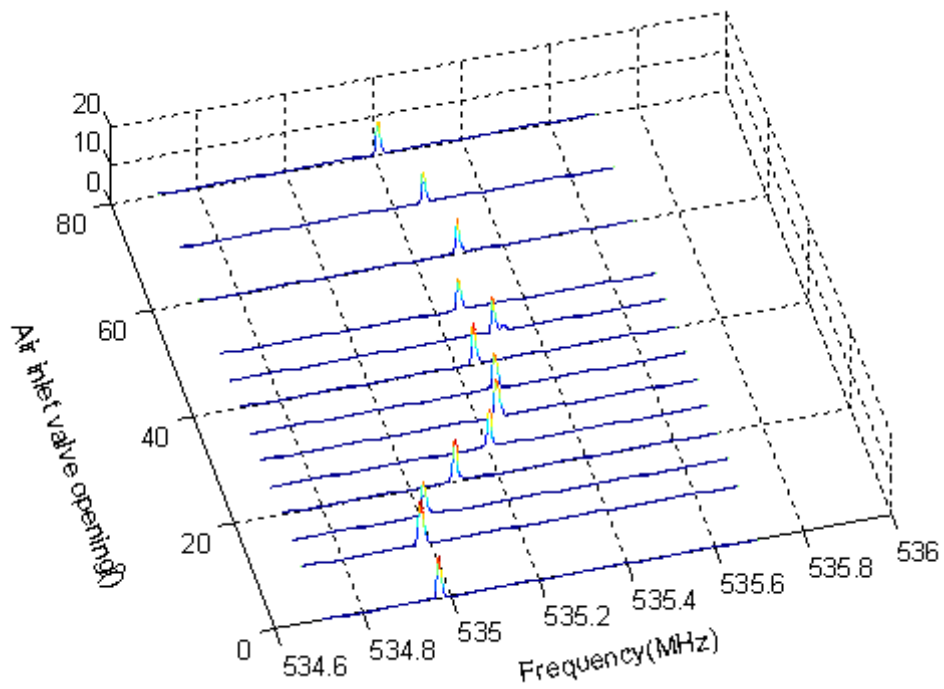
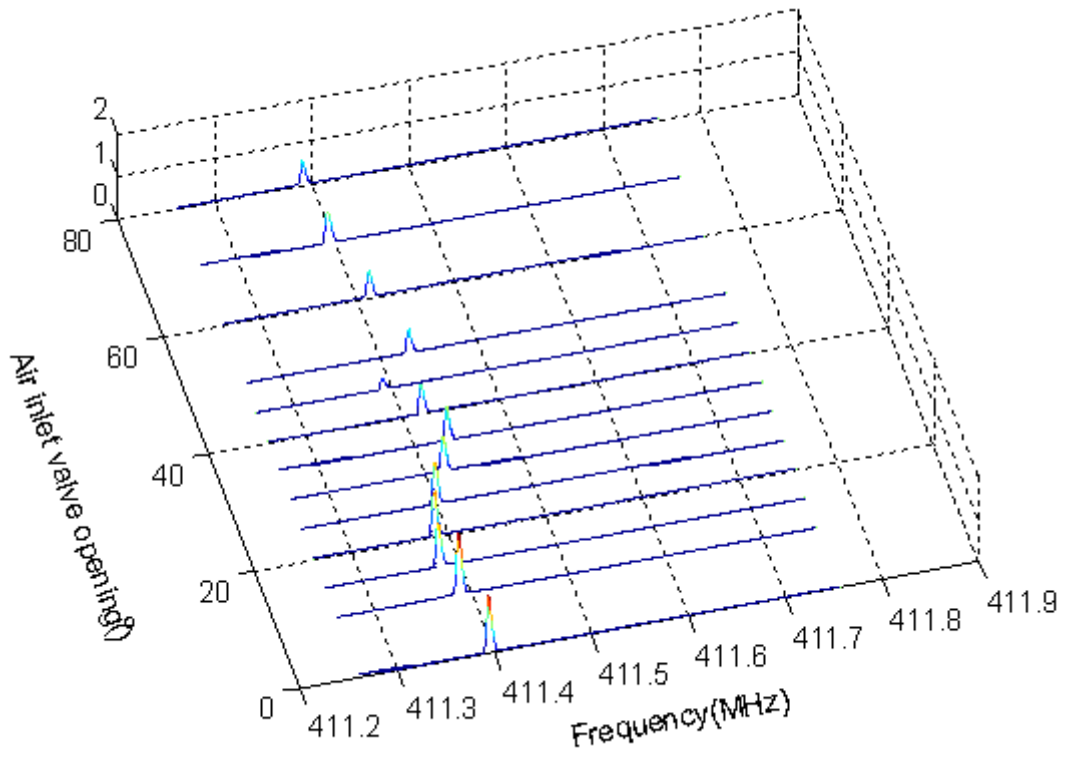


Figure 6-9 Peak frequency shift behaviour with different air valve opening for the three resonant frequencies 411MHz, 535 MHz and 762 MHz

Figure 6-10 shows the output of the spectrum analyser for the same three sets of conditions as for Figure 6-9, with the addition of the amplitude of the peaks. The author is grateful to Dr Gu [second supervisor] for suggesting the inclusion of this figure.



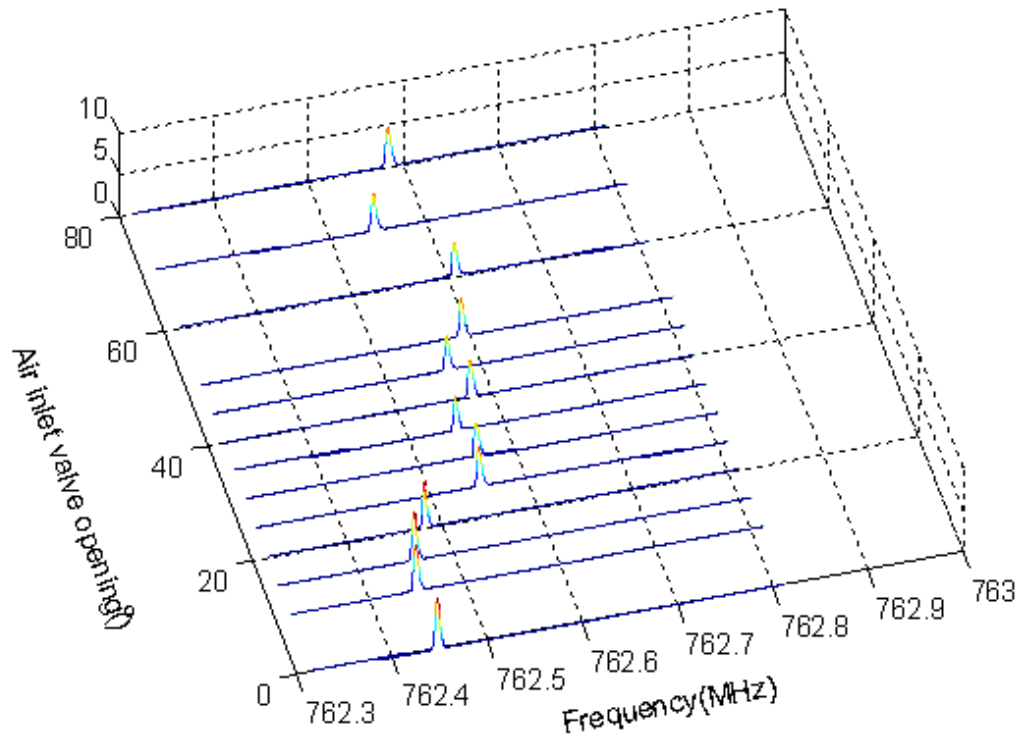


Figure 6-10 Variation of spectral peak with different air valve opening for the three resonant frequencies 411MHz, 535 MHz and 762 MHz

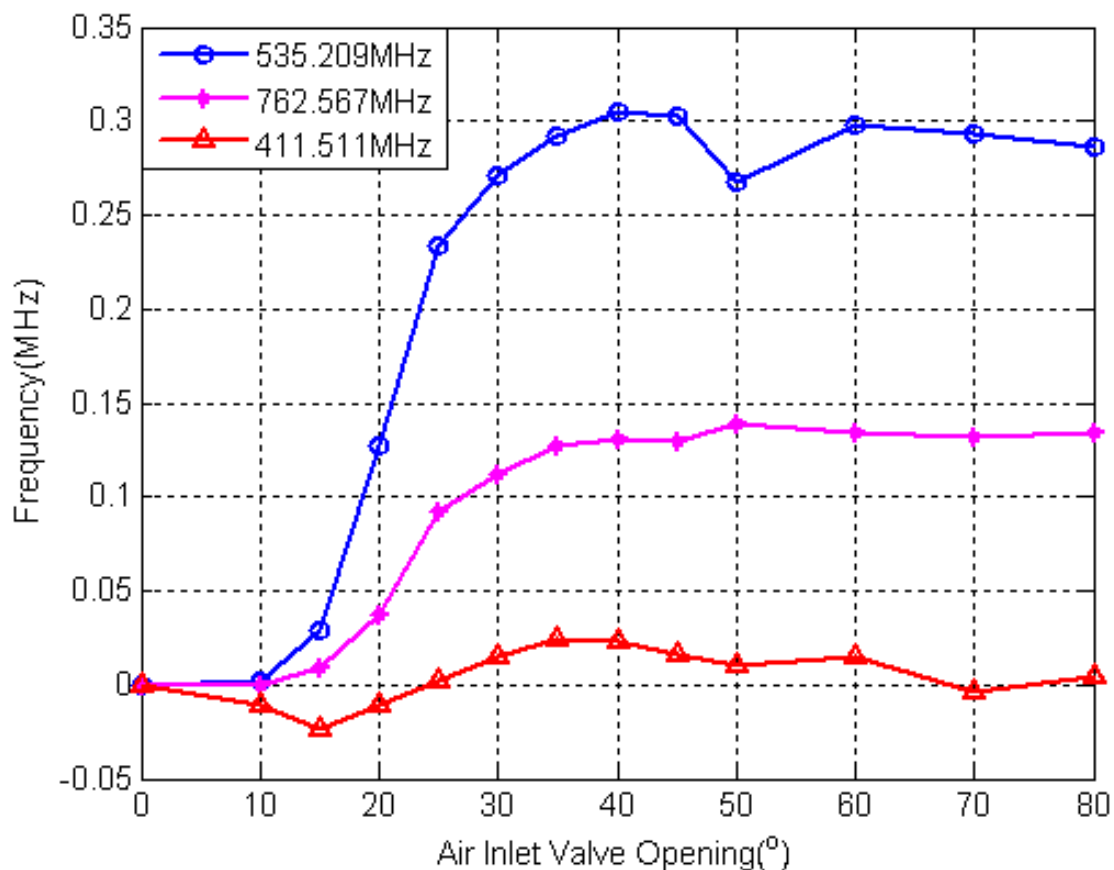


Figure 6-11 Variation of resonant frequency with different air valve opening for the three resonant frequencies 411MHz, 535 MHz and 762 MHz

Figure 6-11 shows the relative changes in peak frequency for each of the applied tuning voltages with increase in air valve opening. Clearly the maximum rate of change is achieved with resonant frequency 533 MHz (tuning voltage of 3.06V) and it was this frequency that was used to investigate change in resonant frequency with increase in water flow rate in the system with the air valve closed.

Figure 6-12 shows how the 533 MHz resonant frequency changed with increase in flow rate. As flow rate increased there was a gradual but clear increase in the value of the resonant frequency. As explained in Section 4.3.10 (Centrifugal pump) some cavitation bubbles were clearly observable in the flow at 250 l/min, so it is reasonable to expect that some bubbles will be present at lower flow rates.

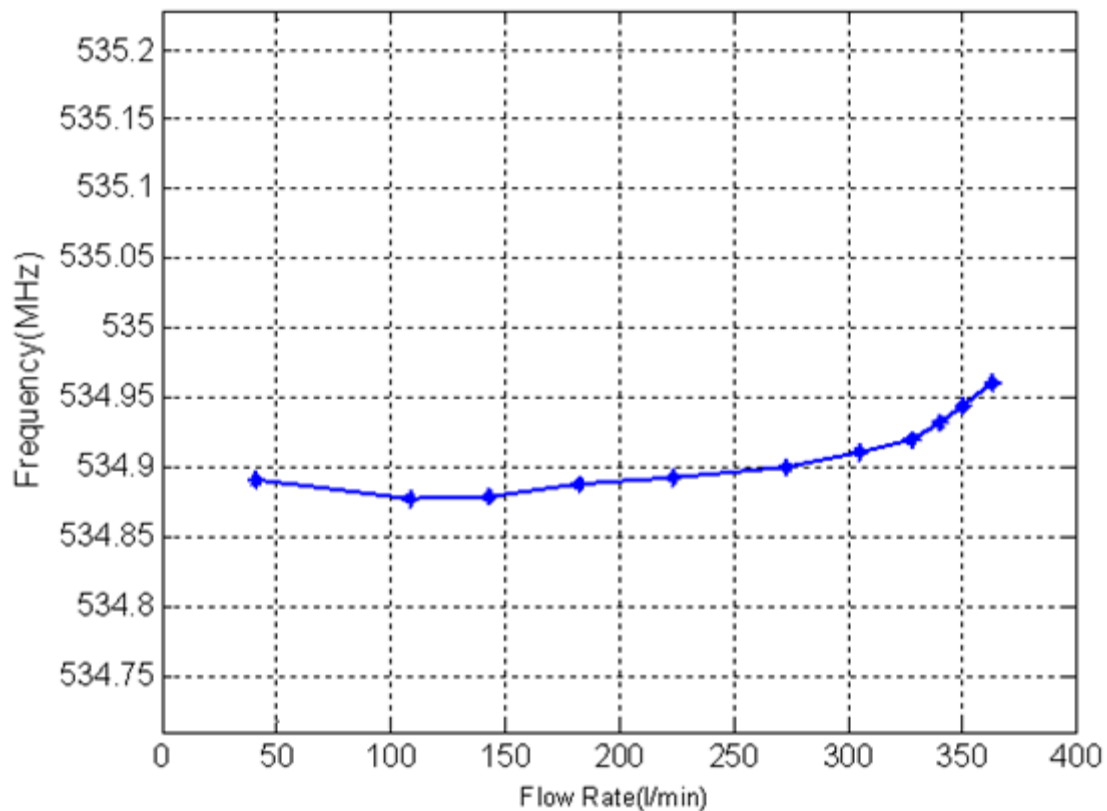


Figure 6-12 Resonant frequency of signal against flow rate (controlled by throttle valve in discharge line, air inlet valve closed)

The curve shown in Figure 6-12 shows a small but distinct change in gradient of the curve after the flow reaches about 150 l/min. This could be the first production of vapour bubbles in very first stage of cavitation. As the flow rate increases and cavitation becomes more established the gradient remains more or less constant until as cavitation becomes well established and the gradient increases rapidly. It would thus appear that the measurement of the resonant frequency of the LCR circuit is a method of detecting cavitation in a pipe system.

6.5 Summary

The electrode plates, pipe wall and dielectric have been modelled electrically using an RLC circuit. Air bubbles in the water flow give the flowing medium (water/vapour mix) a lower dielectric value than for water alone, this decreases the capacitance which, in turn causes an increase in the resonant frequency of the circuit. Initial results have shown that the frequency shifts can be as high as 250 kHz with a relatively small proportion of bubbles present in the pump flow.

The capacitive sensor has demonstrated, in principle and in practice that it will detect the presence of air bubbles in water flows, and the work reported here provides a basis for further investigation towards developing this method as a non-invasive and possibly cost effective tool for the monitoring of cavitation.

The next three chapters report the results obtained using vibration and airborne and waterborne sound measurements to detect the onset of cavitation. This work was performed earlier in the project than the design and testing of the capacitive sensor but the perceived relative importance of the latter means it has been placed earlier in the thesis.

CHAPTER SEVEN

7. VIBRATION SIGNAL ANALYSIS FOR DETECTION OF CAVITATION

This chapter describes the analysis of the experimental vibration signal obtained from the test pump for detection of incipient cavitation. A number of statistical parameters (features) are examined as possible indicators of the onset of cavitation.

7.1 Advantages and disadvantages of vibration methods

The vibration sensors (accelerometers) available today have the necessary frequency and dynamic ranges, sensitivities, temperature ranges, etc., to be useful in the detection of cavitation of most if not all centrifugal pumps. Generally, accelerometers are easy to install on the pump casing and can usually be placed close to the position of any expected fault. The different sizes and types of commercial accelerometers available mean that it should always be possible to select one for easy positioning. Both time domain and frequency domain analysis of the vibration signal are shown to provide useful information about severity of cavitation in centrifugal pumps, especially once cavitation is established.

However, in industrial application it is sometimes difficult to control the vibration arising from other parts of the same machine, or other machines, and this intrusive background vibration may contaminate the signal and make cavitation diagnosis more difficult, hence the need for statistical analysis.

7.2 Time domain analysis

Figures 7-1 and 7-2 show the raw vibration acceleration signals for the pump operating at 249 l/min, the flow rate at which cavitation was first definitely noticed, and at other flow rates. These flow rates are samples from the total number of flow rates shown in Table 7-1 and in Appendix C, and were chosen simply for convenience to demonstrate the change in vibration signal with flow rate. It can be seen that the raw amplitude of the vibration acceleration changes with change in flow rate, and the question is whether there is sufficient change over a suitable flow range to confidently detect the onset of cavitation. As stated in Chapter 4, both time and frequency domain analyses are used to look for features which will indicate incipient cavitation.

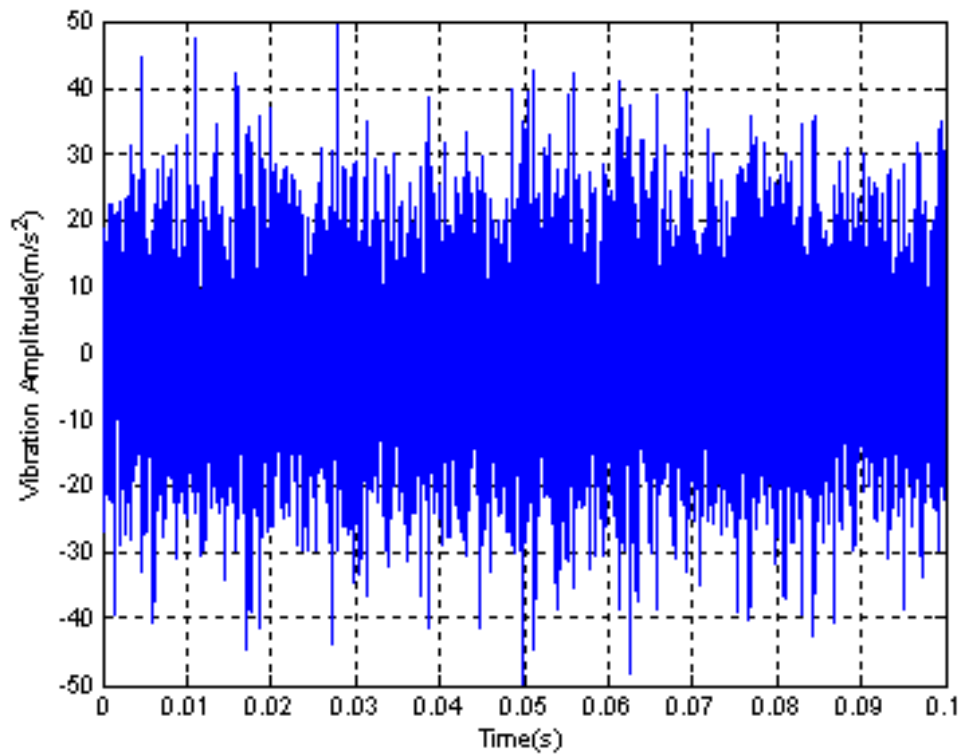


Figure 7-1 Raw time domain vibration signal for flow rate 249 l/min

Table 7-1 Pump flow rates used to evaluate system for detection of incipient cavitation

Flow rate (l/min)	369	354	347	332	322	313	302	283	249	200	150	99.4	51.2	10.2
-------------------	-----	-----	-----	-----	-----	-----	-----	-----	-----	-----	-----	------	------	------

The common statistical parameters PDF, Peak and RMS values, Crest factor and Kurtosis were used to analyse the time domain vibration signals to determine whether they could be used to identify trends in the signal. The spectral analysis used Kurtosis, Crest factor and Spectral entropy.

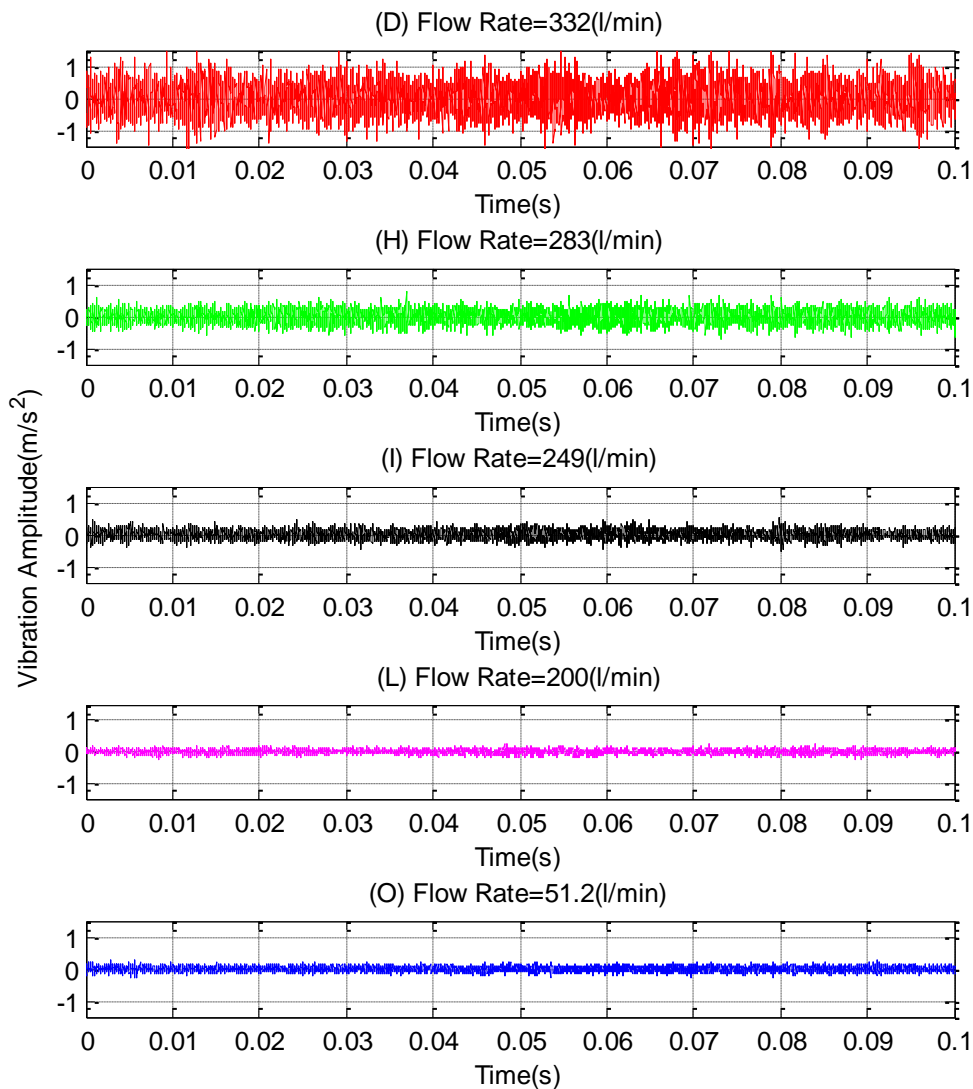


Figure 7-2 Raw time domain vibration signals at different flow rates

7.3 Conventional statistical measures from the time domain

7.3.1 Probability density function

Pump cavitation is just discernible to the eye and to touch at a flow rate of about 249 l/min and is fully developed at about 344 l/min, see Figure 4-5. Figure 7-3 (a) shows the PDFs of the time domain of the vibration signal at different flow rates. From first principles it can be seen that the PDF of such signals will be approximately Gaussian, with the specific shape depending upon the details of the signal (De Silva, 2005). As the flow rate increases and approaches the onset of cavitation, the vibration signal will change and so, obviously, the

shape of the PDF curve will also change. The question is whether these changes are sufficient to identify the onset of cavitation.

Figure 7-2 shows a clear change in the time domain of the vibration signal as the flow increased, with a particularly rapid rate of change close to the onset of cavitation. It was found that the vibration signal undergoes a clear change in amplitude and frequency content at about 250 l/min. The trend of the PDF is to broaden and for the peak to get smaller, as pump flow rate increases.

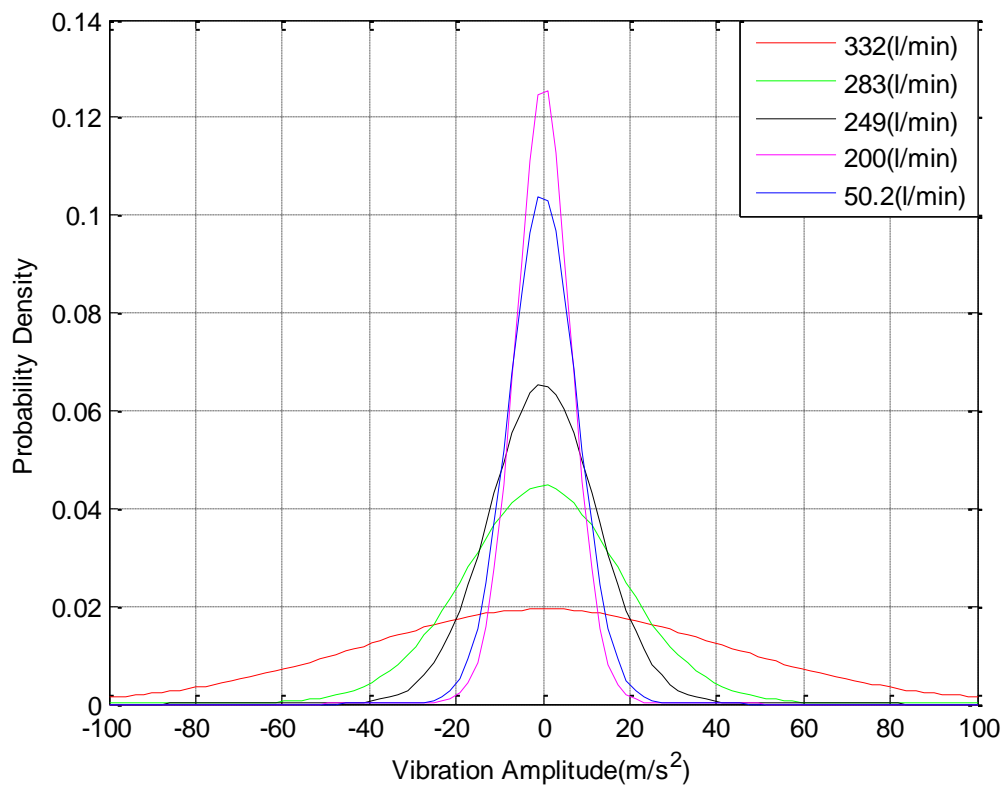


Figure 7-3 (a) Probability Densities of time domain of vibration signal for different flow rates

Table 7-2 The values of the variances for the five curves shown in Figure 7-3(a) are:

PDF (Flow rate, l/min)	50.2	200	249	283	332
Variance	30.0	212.8	363.9	641.1	791.3
Standard deviation (m/s ²)	5.48	14.6	19.1	25.3	28.1

The shape, or pattern, of the PDF curves changes with flow rate. This is because the distribution of frequencies in the vibration signal changes with flow rate. As the flow approaches cavitation the spectral content of the vibration signal changes, see especially

Figure 7-14, where at low flow rates the spectrum contains a few isolated low level structural resonances at flow rates approaching established cavitation there are a number of distinct large amplitude peaks (PDF has its sharpest peak), but at established resonance there is a large number of peaks across the spectrum (PDF curve flattens out).

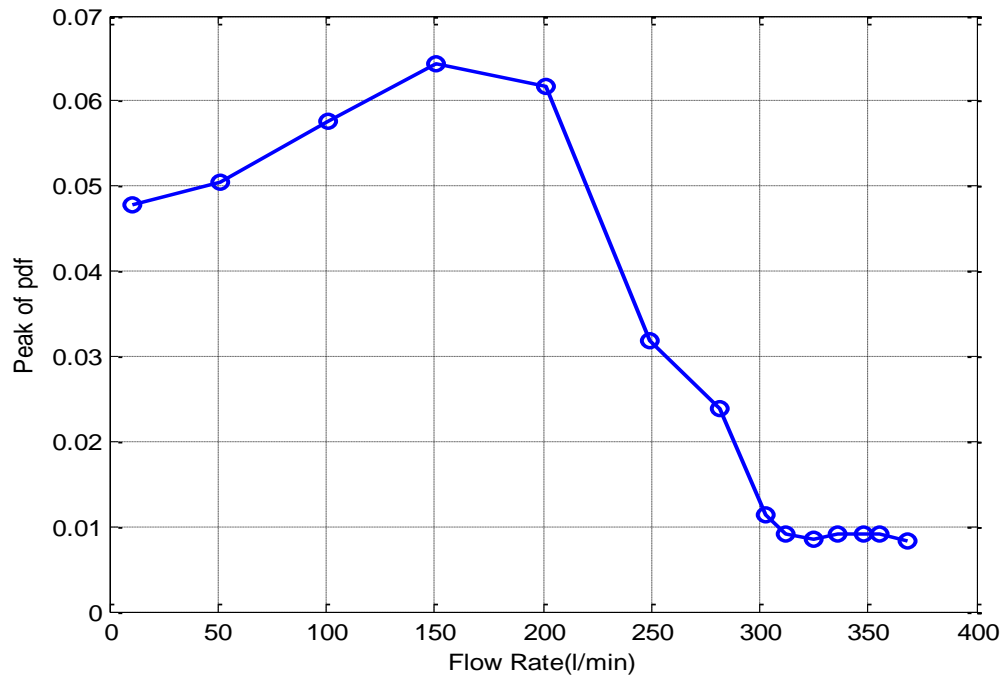


Figure 7-3 (b) Amplitude of PDF curve of vibration signal against flow rate

Figure 7-3 (b) clearly shows that there is a broad maximum value of the PDF centred at a flow rate of about 150 – 200 l/min. After this maximum there is a definite decline in the PDF value which accelerates as the flow approaches 249 l/min. If this is confirmed as a general phenomenon then the turning point in the peak PDF curve can be taken as a definite indication of the likely onset of cavitation and can be used as such.

7.3.2 Peak value, RMS and Crest factor

Figures 7-4, 7-5 and 7-6 show the three statistical parameters: Peak value, RMS and Crest factor for pump flow rates between 10.5 l/min and 370 l/min. Given the clear increase in vibration amplitude with flow rate shown in Figure 7-2, the increase in Peak and RMS values for the vibration signal are to be expected. At less than about 200 l/min there is a nearly constant vibration level, at about 200 l/min the peak and RMS values have begun to increase, and for flow rates greater than about 270 l/min the Peak and RMS values rise rapidly to a maximum value indicating that cavitation has been established. Clearly the increase in both Peak and RMS values that starts at about 200 l/min can be taken as an indication of incipient

cavitation, and the very rapid increase just before 300 l/min definite confirmation of established cavitation.

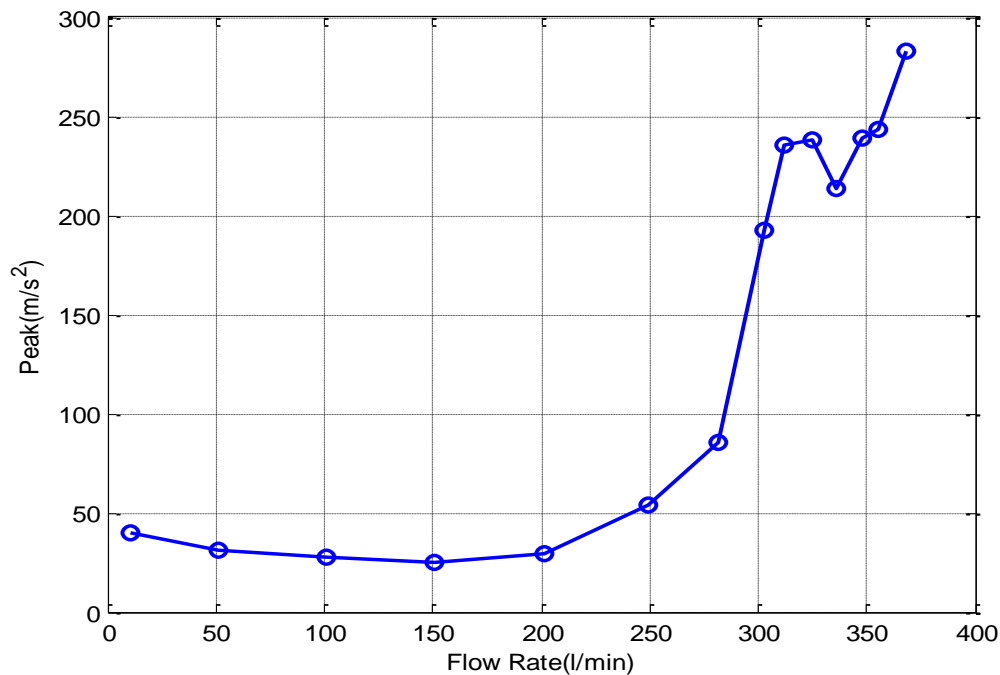


Figure 7-4 Peak value of time domain of the vibration signal with flow rate

Crest factor is defined as the Peak factor divided by the corresponding RMS value, thus Figure 7-6 adds nothing qualitatively new to the discussion.

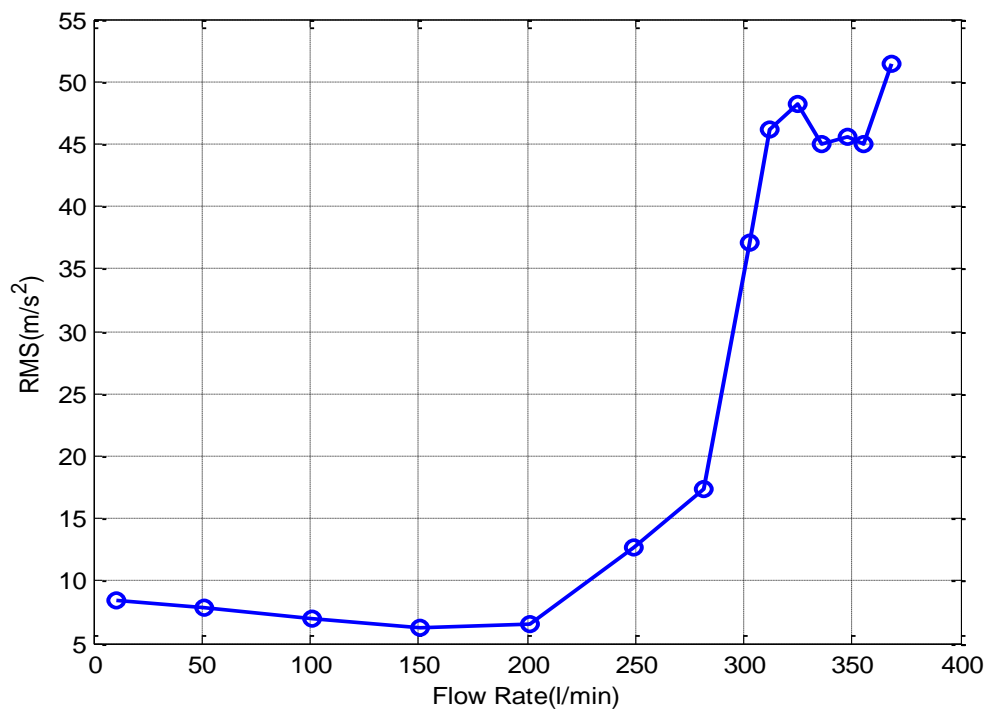


Figure 7-5 RMS of time domain of the vibration signal with flow rate

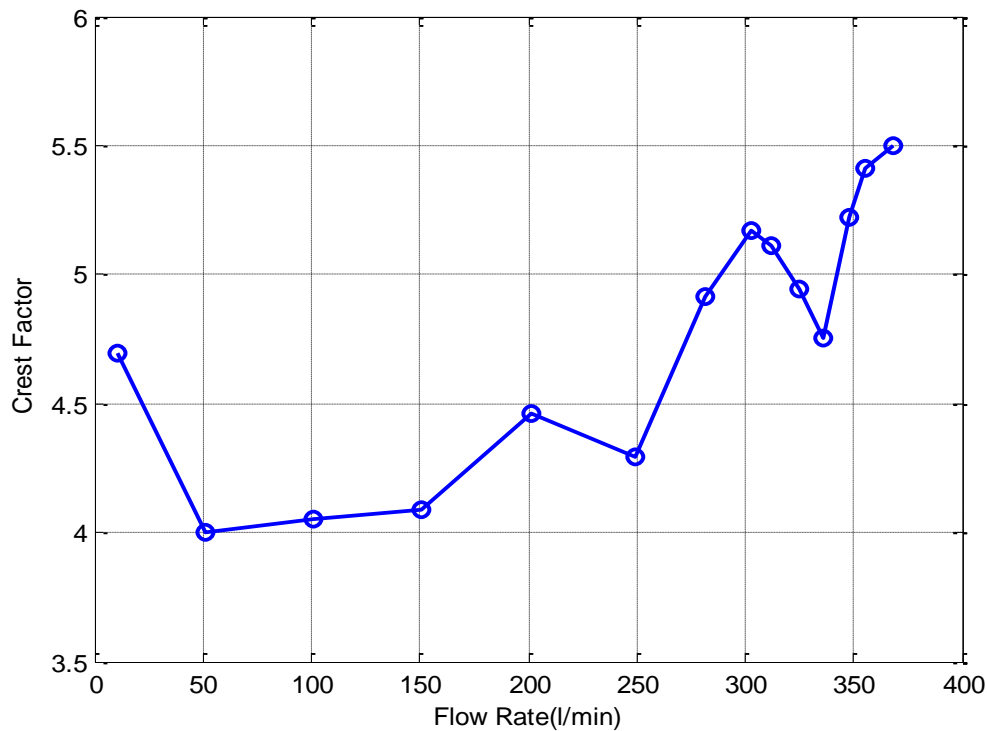


Figure 7-6 Crest factor of time domain of the vibration signal with flow rate

7.3.3 Kurtosis

Kurtosis is invariably normalised so that the Kurtosis of a Gaussian distribution is 0, see Equation 3.2. Where the peaks in a particular spectrum are sharper or more pointed than the Gaussian distribution the Kurtosis is greater than 0. In Figure 7-7 the Kurtosis has a value close to zero up to a flow rate of about 250 l/min which suggests few extreme deviations in the amplitude of the time domain signal. The very sharp rise in Kurtosis at about 10 l/min is most surprising and is likely to be a measurement anomaly.

Figure 7-7 suggests that the temporal pattern of the vibration signal, as expected, exhibits sharper peaks as the flow rate increases; there is a definite increase in the Kurtosis after the flow rate of about 250 l/min. This apparent anomaly was checked by repeated measurements, but was definitely present for this pump system. However, the conclusion here is limited to saying that the increase in Kurtosis with cavitation can be used as confirmation of the presence of cavitation, but not its onset.

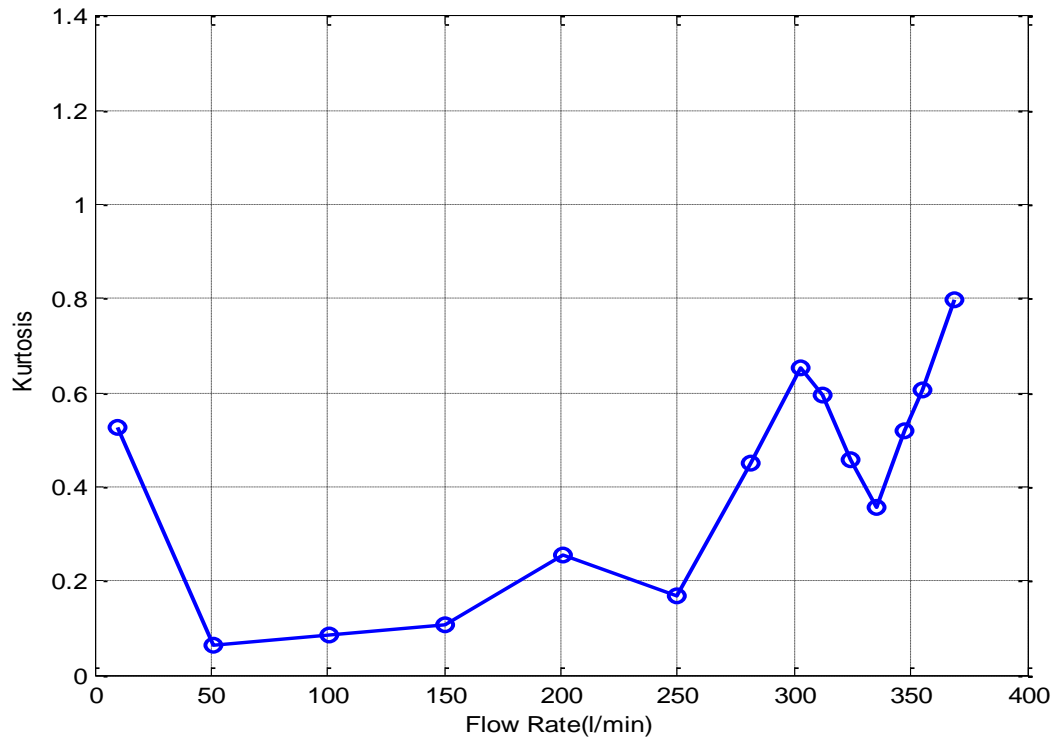


Figure 7-7 Kurtosis of time domain of the vibration signal with flow rate

The most likely explanation for the increase in Kurtosis as the flow rate increases from 250 l/min to 370 l/min is that this is the flow region in which the cavitation, first noticeable at 249 l/min, becomes established. It would be expected that over this flow region the vibration acceleration signal would become increasingly more “spiky” as shown in Figure 7-2.

7.4 Spectrum analysis

For a better understanding of the vibration signals associated with pump dynamics and cavitation formation, the time domain vibration signals were transformed to the frequency domain using a FFT. Figure 7-8 shows the spectrum of the vibration signal from the pump, it consisted of two distinctive parts: discrete components superimposed on a broadband background.

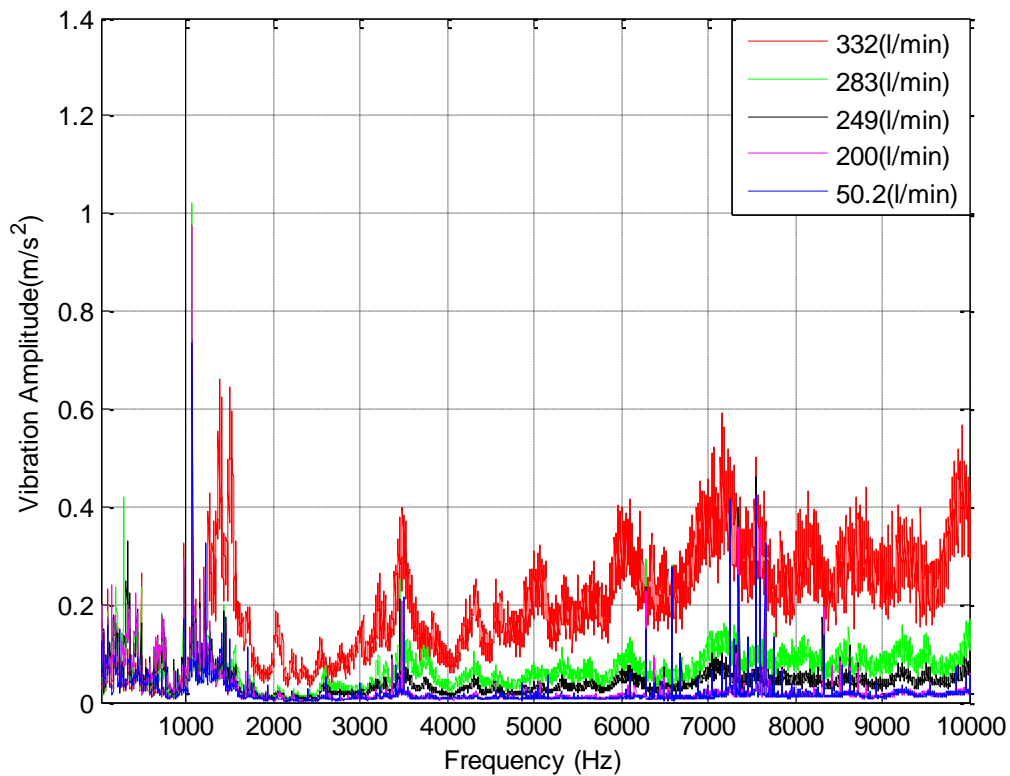


Figure 7-8 (a) Spectra of the vibration signal from the pump for different flow rates

In figure 7-8 (b) it can be seen that the vibration acceleration spectra for flow rates less than 283 l/min look show similar characteristics. It can also be seen that for established cavitation, there is a sharp increase in the level of vibration, particularly at the higher frequencies.

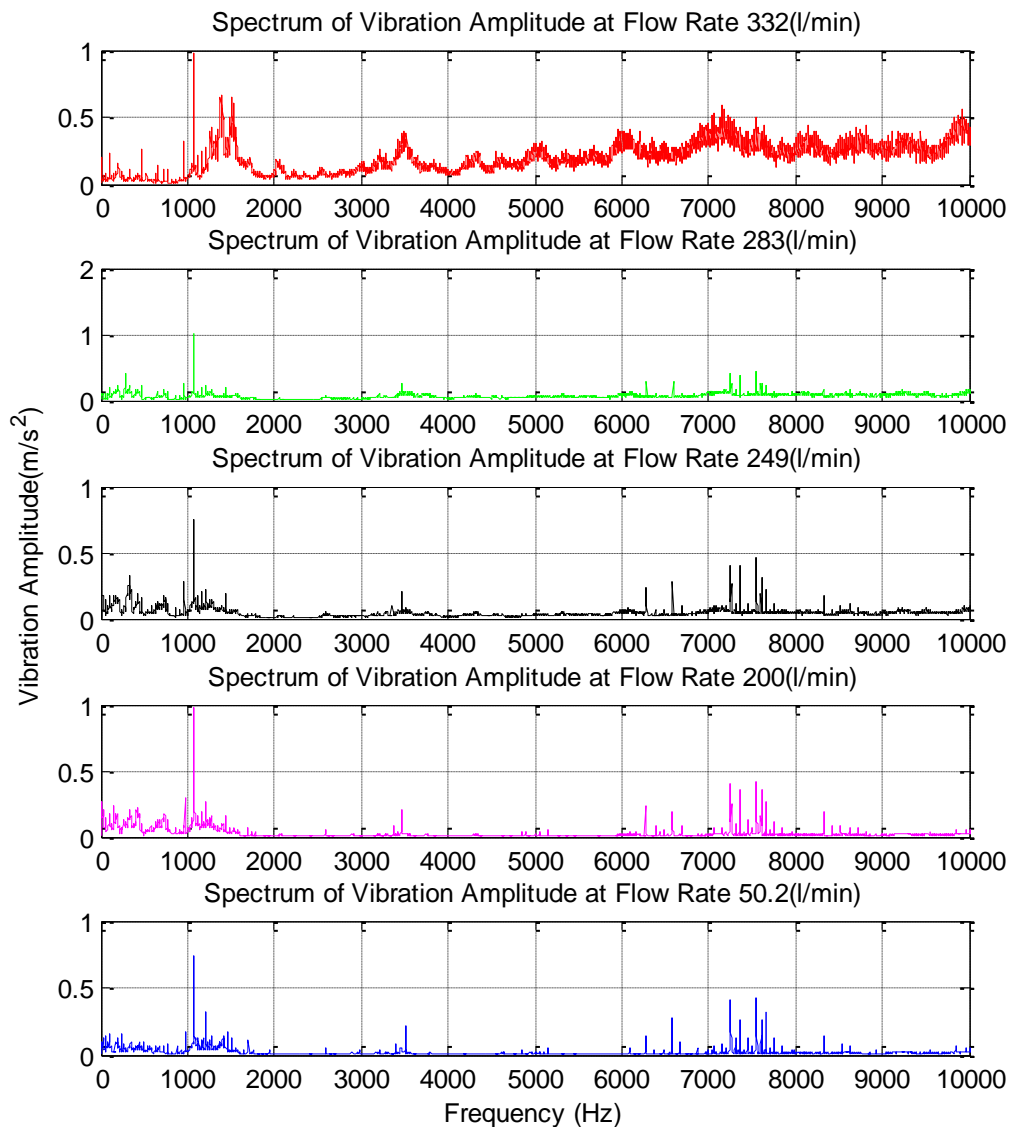


Figure 7-8 (b) Frequency spectra of the vibration signals at specified flow rates

7.4.1 Baseline spectral analysis

Because the turbulent noise at or near the BEP is at a minimum, the discrete components tend to dominate and the lower harmonics are more obvious and distinct (Dowling and Ffowcs-Williams, 1983). When operation is away from BEP the turbulent noise will increase and can even swamp the discrete components (Cudina, 2003; Cudina and Prezel, 2009). It is these characteristics that may allow the onset of pump cavitation to be diagnosed at different stages of its development by analysis of the vibration spectrum.

For convenience of presentation the vibration spectrum has been divided into three parts: 20Hz to 1kHz; 1kHz to 2kHz; and 2kHz to 10kHz, see Figures 7-9, 7-10 and 7-11 respectively, all of which are for a flow rate of 249 l/min. These figures show the discrete component characteristics present within the overall spectrum are due mainly to the periodicities in the flow due to the discrete nature of the pump's rotor blades and the interaction of the rotor blades with nearby stationary objects such as the volute tongue. These two mechanisms generate discrete components at the rotational frequency (RF=48.33 Hz) and its harmonics, see multiples of the RF at 48, 97, 145, 193, 290, 338, 435, 483, 677, 725 and 967 Hz. The blade passage frequency (BPF) for the five bladed impeller is 241.65 Hz, and corresponding harmonic peaks in the spectrum can be seen at 483, 725 and 967 Hz as can be seen in Figure 7-9 that there. There will be also peaks due to the driving motor at even multiples of 50Hz, these are somewhat overshadowed by the RF harmonics but can be discerned at 100, 200 and 300 Hz.. The frequency of the cooling fan was 581.5 Hz which is close to the twelfth harmonic of the RF (580 Hz).

The baseline spectrum is taken to be that measured at 249 l/min as this was the flow rate at which cavitation is first definitely present. At this flow rate and in the frequency range from 20 Hz to 1 kHz, the discrete components have much higher amplitudes than the broadband and are due to shaft rotation frequency and pump blade passing frequencies. Figure 7-9 shows that a large number of individual peaks have amplitudes which stand out above the background.

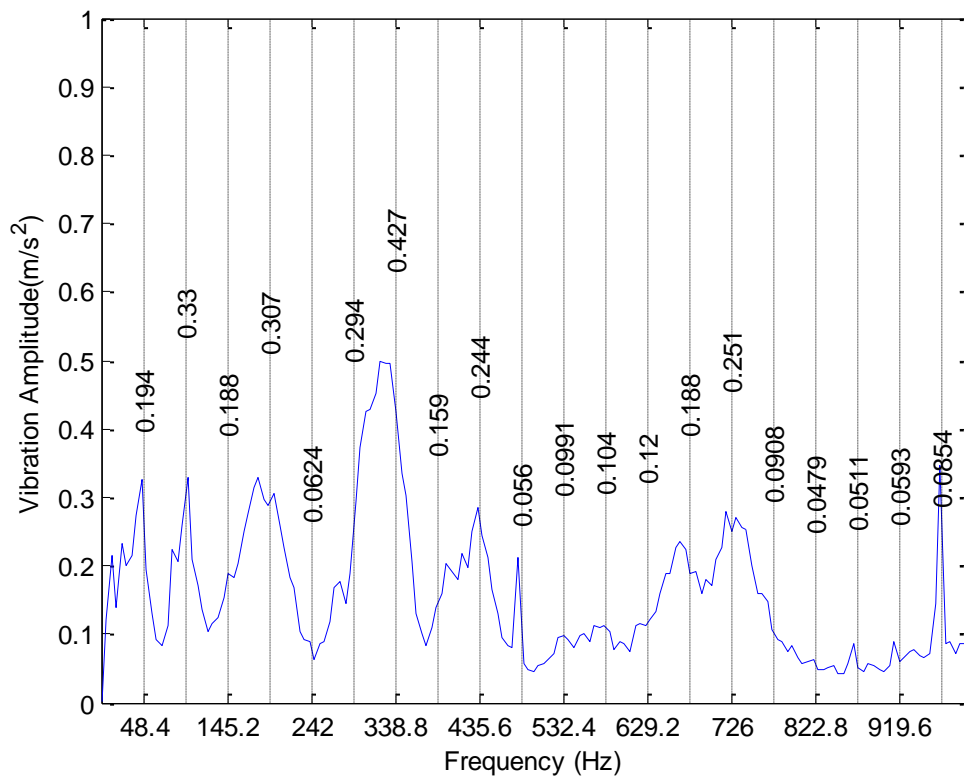


Figure 7-9 Baseline vibration spectrum 20 Hz - 1 kHz for flow rate 249 l/min

Figure 7-10 shows that in the frequency range 1kHz to 2kHz, there are some discrete components which stand out above the background, particularly the peak at 1066Hz. This frequency is a multiple (22) of the RF and thus a small peak would be expected. However, it is believed that this peak is due to structural resonances and – given that the speed of sound in water at 20⁰C is about 1490 m/s – this resonance corresponds to a pipe length of about 1.40 metres. This seems reasonable, but no detailed analysis was performed to determine the resonances in the water circuit.

Figure 7-11 is the baseline spectrum for the range 2kHz to 10kHz. Discrete components due to blade passing frequencies and structural resonances are present. Surprisingly, even though 249 l/min is the flow rate at which cavitation is becoming noticeable, the background level is still way below the individual peaks.

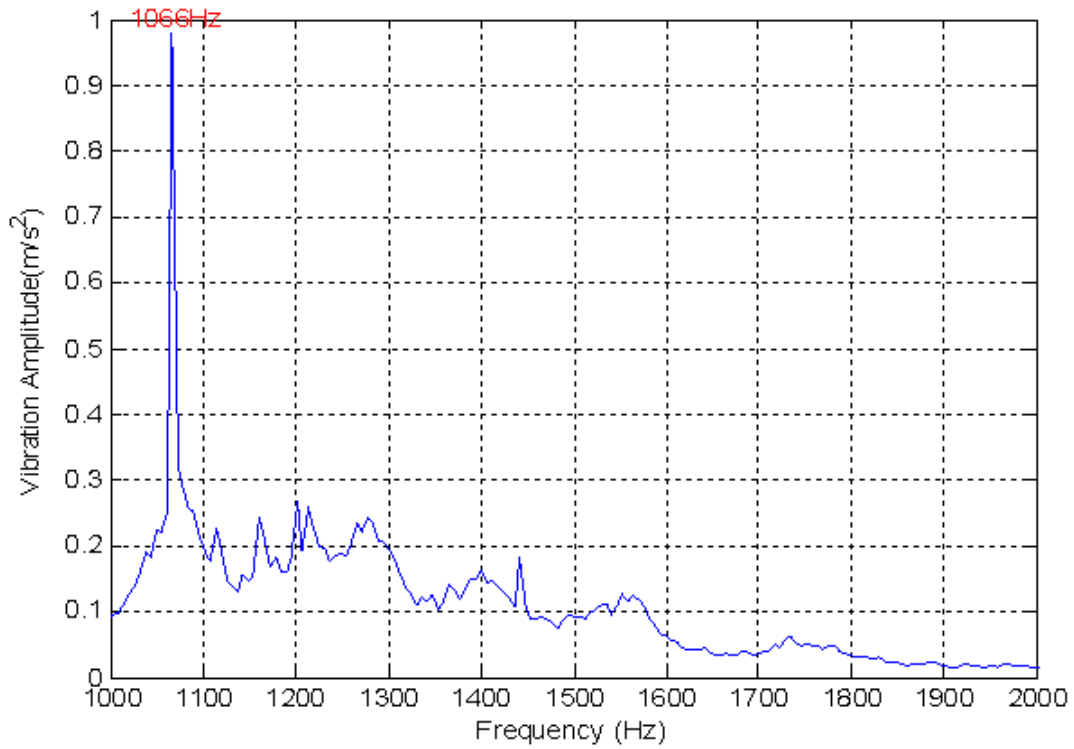


Figure 7-10 Baseline vibration spectrum for 1 kHz - 2 kHz for flow rate 249 l/min

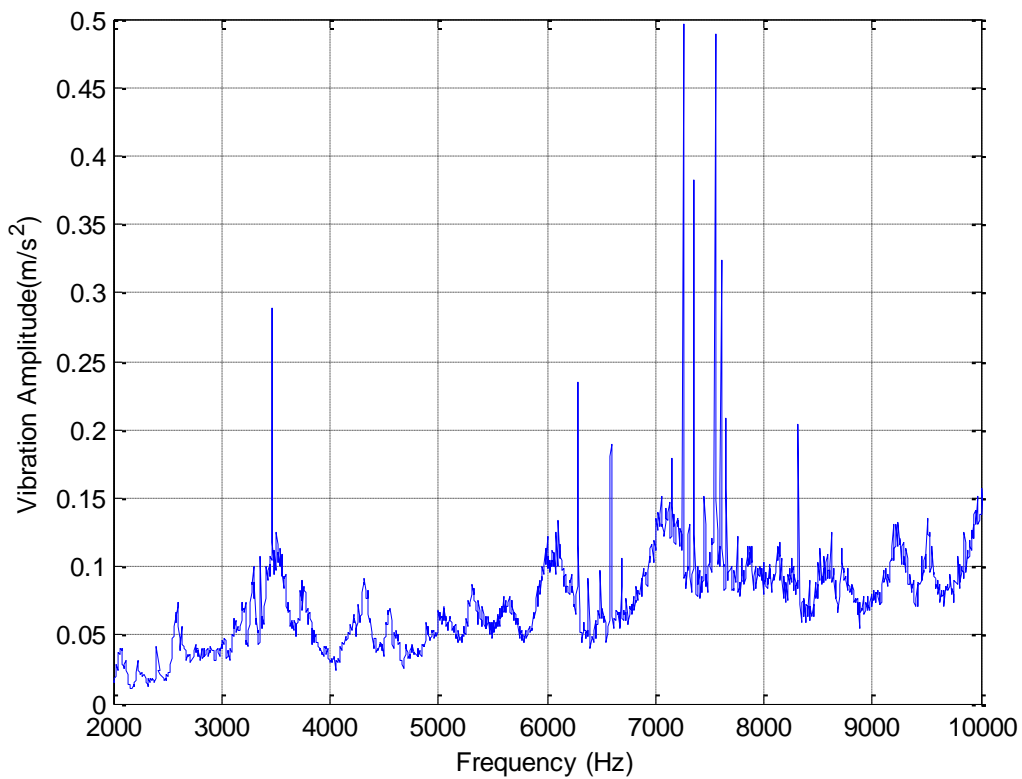


Figure 7-11 Baseline vibration spectrum for 2 kHz-10 kHz for flow rate 249 l/min

7.4.2 Spectral amplitude characteristics

Frequency range 20Hz - 1kHz

Figure 7-12 shows the “waterfall” for the vibration spectrum in the frequency range 20 Hz to 1 kHz for the flow range from about 10 l/min to about 370 l/min. At flow rates below about 120 l/min the vibration of the pump appears more or less constant. There is a gradual increase in the spectrum level when the flow rate approaches 200 l/min, then the vibration of the pump increases sharply and a clear and substantial peak can be observed at about 338 Hz, this is a harmonic of the rotational frequency ($7 \times \text{RF}$). While this peak dies away with further increase in the flow rate it appears a very good indicator of incipient cavitation. This particular frequency might be specific to this pump, but the principle that an individual component of the frequency might be a suitable indicator has already been proposed by Cudina (2003). A subsidiary peak at 435 Hz ($9 \times \text{RF}$) makes an appearance at about 150 l/min and becomes more distinct with the onset of cavitation. This peak is a possible alternative indicator for the onset of cavitation.

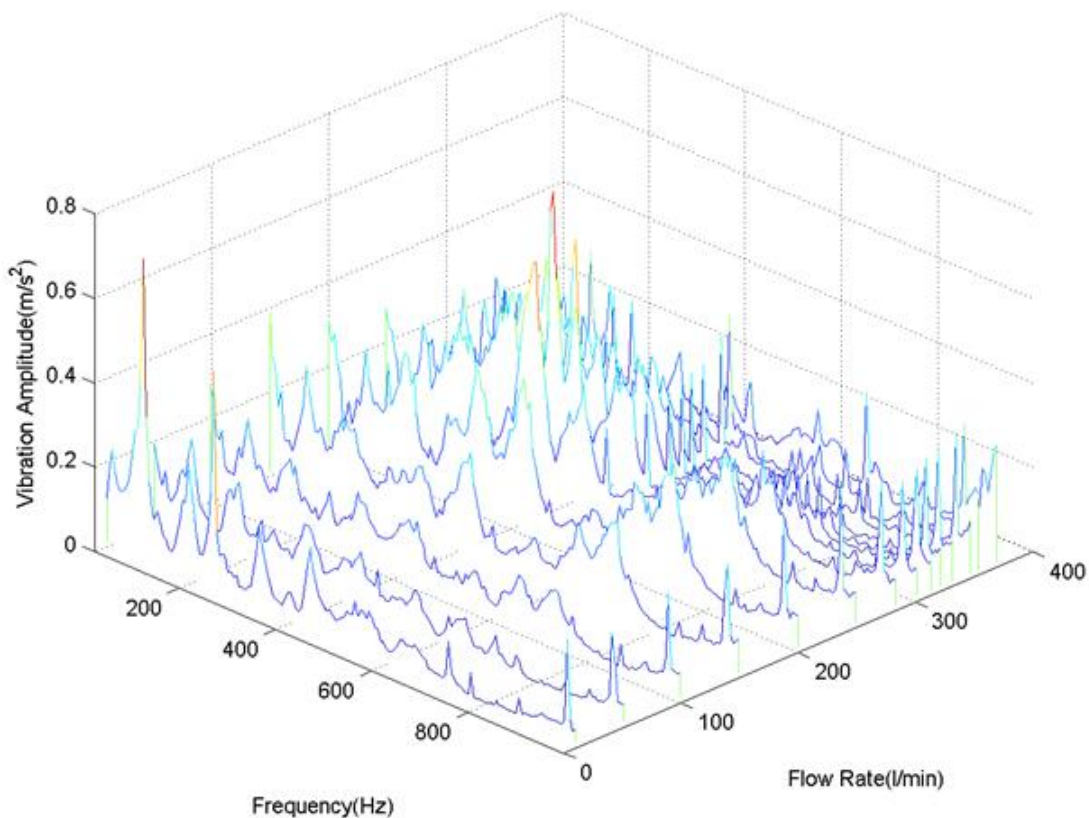


Figure 7-12 Waterfall for time-averaged Peak amplitude of vibration signal 20 Hz – 1 kHz

Frequency range 1kHz - 2kHz

Figure 7-13 shows the waterfall for the vibration spectrum in the frequency range 1 kHz to 2 kHz. Surprisingly, the vibration level of the pump remains more or less constant until the flow rate reaches approximately 300 l/min. However, as the flow rate increases above 300 l/min the broadband vibration of the pump steadily increases. There are some further changes in the vibration pattern with increase in flow, but these occur after the onset of cavitation.

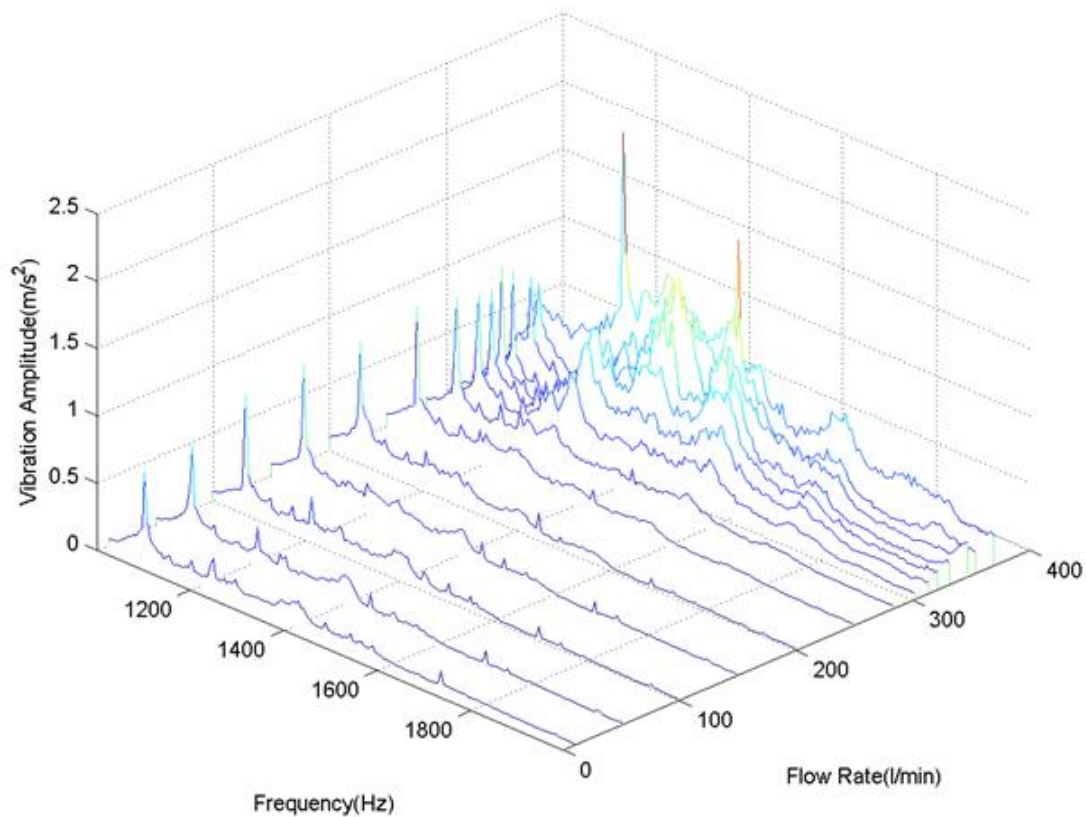


Figure 7-13 Waterfall for time-averaged Peak amplitude of vibration signal 1 kHz – 2 kHz

Frequency range 2kHz-10kHz

Figure 7-14 shows the waterfall of the vibration spectrum for the frequency range 2 kHz– 10 kHz. At these higher frequencies the vibration pattern remains approximately constant with a small increase in levels showing at a flow rate of approximately 250 l/min. At flow rates above 250 l/min, and particularly above about 300 l/min, the broadband vibration level of the pump increases substantially with the presence of large, broad peaks. Unfortunately, these peaks do not appear until after cavitation has been established.

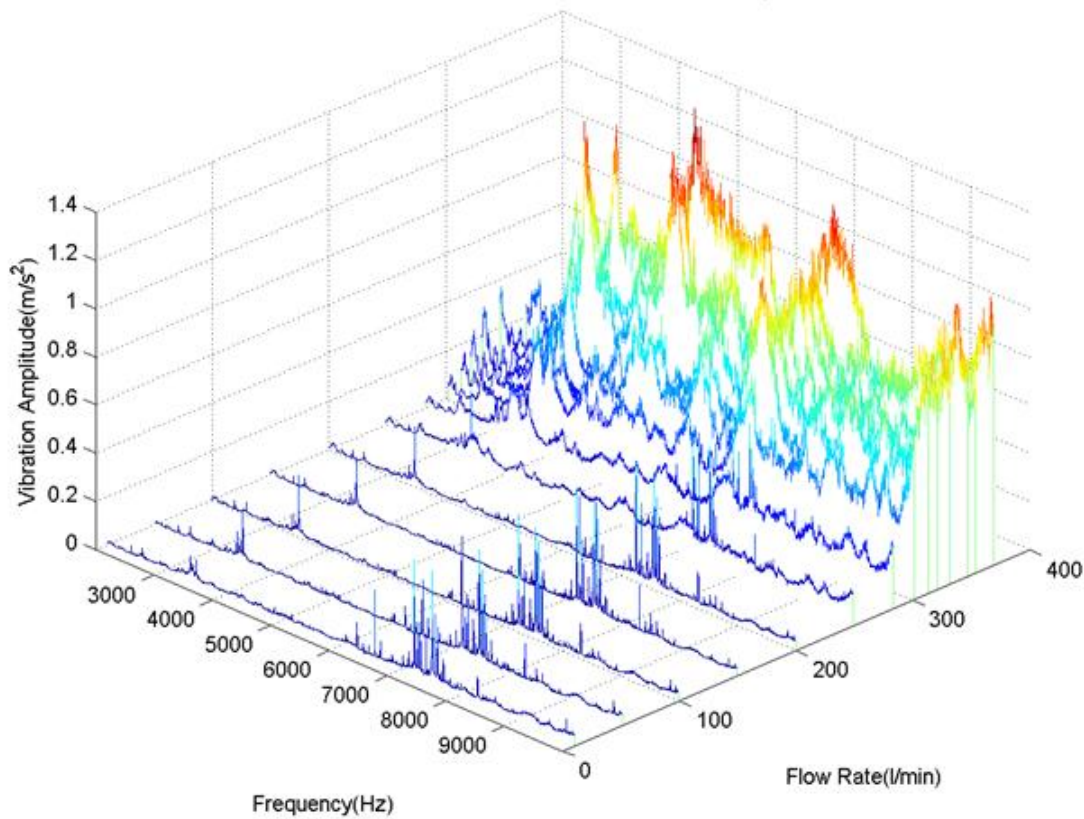


Figure 7-14 Waterfall for time averaged Peak amplitude of vibration signal 2 kHz – 10 kHz

7.5 Statistical measures from the frequency domain

To characterize changes in the spectra occurring with changes in flow rate as a means to identifying the onset of cavitation the Crest factor and Kurtosis were calculated for individual spectra. That is, for each flow rate the vibration spectrum was plotted and for this spectrum the Crest factor (peak value of the spectrum divided by the RMS value of the spectrum) and Kurtosis were determined.

7.5.1 Spectral crest factor

Figure 7-15 shows the Crest factor for the vibration spectra with increase in flow rate. It can be seen that the Crest factor exhibits a relatively smooth downward trend over the flow range 10 l/min to about 350 l/min. There is no significant change in the trend with the onset of cavitation so it is unlikely that the spectral Crest factor can be used to diagnose incipient cavitation. However, the leveling off of the Crest factor as about 300 l/min might be used to confirm that cavitation has been established.

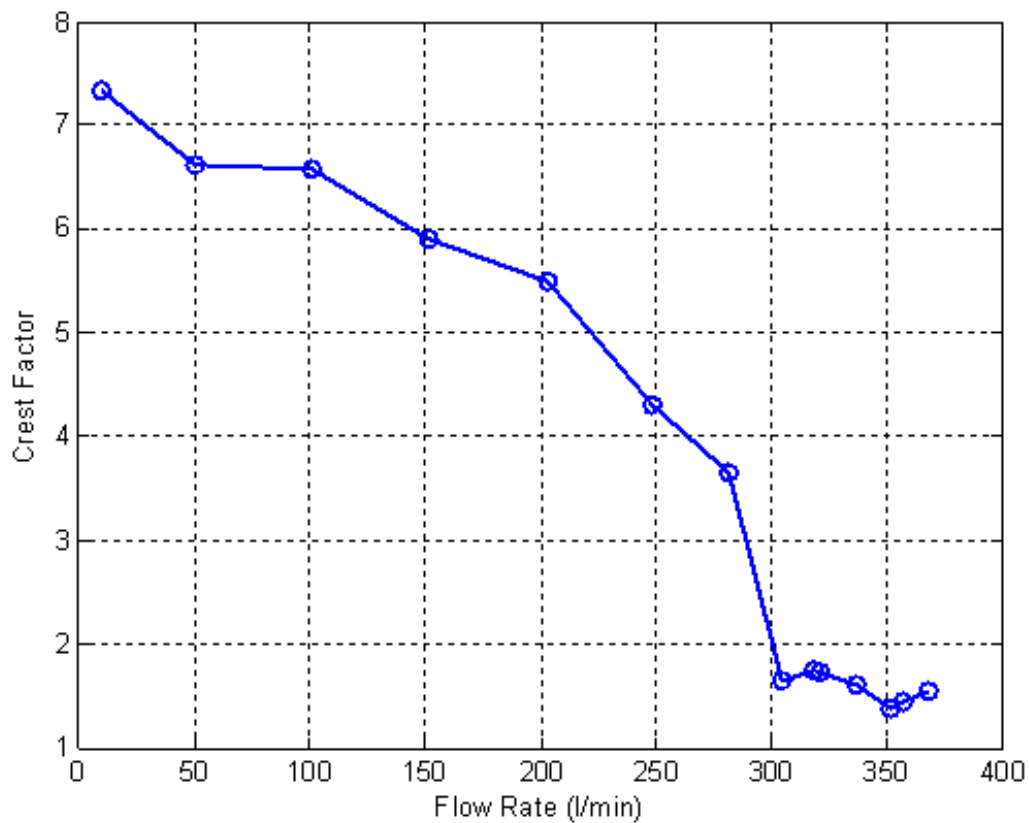


Figure 7-15 Crest factor of vibration spectra (10 Hz to 10 kHz) for different flow rates

7.5.2 Spectral kurtosis

Figure 7-16 shows the Kurtosis obtained from the individual vibration spectra as a function of flow rate. Because Kurtosis is a measure of how peaky the spectrum is. Here there appears to be a gradual decline in the value of the Kurtosis over the flow range from 10 l/min to 249 l/min, after which there is a sharp drop. The rapid drop is a clear indication of the presence of cavitation before established cavitation appears with a plateau at 300 l/min and above. The change in gradient of the curve at a flow of around 250 l/min is useful and could be used for the early detection of cavitation but, strictly speaking, it is not the onset of cavitation.

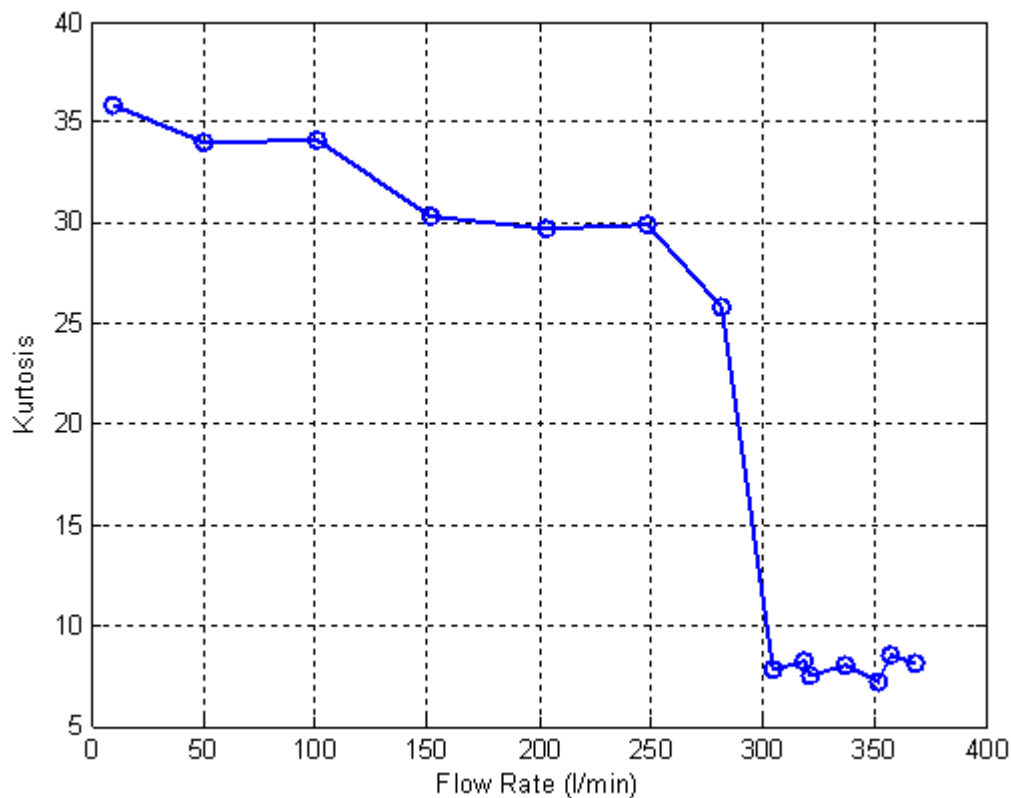


Figure 7-16 Kurtosis of vibration spectra (10 Hz to 10 kHz) for different flow rates

7.5.3 Spectral entropy

Figure 7-17 shows the spectral entropy obtained from the individual spectra as a function of flow rate. As explained in Section 3.7.3, spectral entropy would be expected to have a relatively low value at lower flow rates where the harmonic peaks due to the blade passing and rotational frequencies stand out above the background. The spectral entropy will then increase with increase in flow rate as background noise increased relative to the peaks, and would reach a maximum value as the signal increasingly resembles broad band noise, see Figures 7-12, 7-13 and 7-14.

The results obtained conform to this general analysis and indicates that spectral entropy could be used for monitoring for the onset of cavitation. Essentially, the increase in the spectral entropy gradient could be taken as the beginning of the increase in broadband noise, and an indication of incipient cavitation.

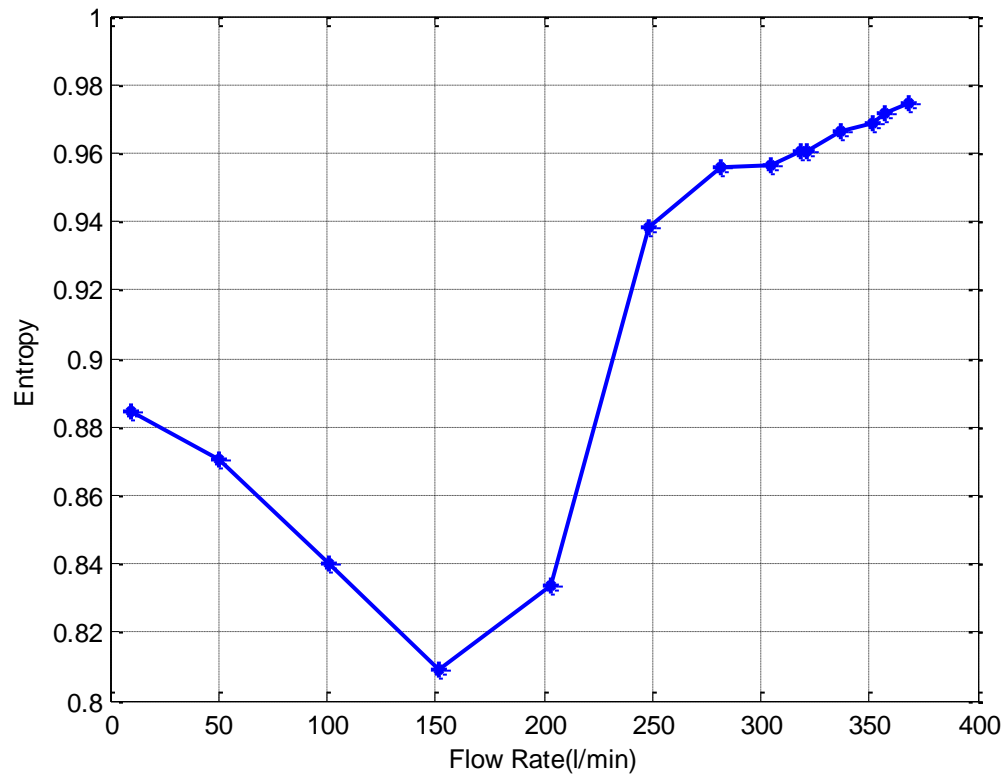


Figure 7-17 Spectral entropy of vibration spectra (10 Hz to 10 kHz) for different flow rates

The next chapter presents the results obtained from the measurement of the sound radiated from the pump. The structure of Chapter 8 will be the same as Chapter 7 for ease of comparison.

CHAPTER EIGHT

8. AIRBORNE ACOUSTIC SIGNAL ANALYSIS FOR DETECTION OF CAVITATION

This chapter describes the analysis of the experimental airborne acoustic signal obtained from the test pump for detection of incipient cavitation. A number of statistical parameters are examined as possible indicators of the onset of cavitation. For ease of cross-referencing, this chapter deliberately follows the structure of Chapter Seven.

8.1 Advantages and disadvantages of using airborne sound

The main advantage of acoustic signals is that they are airborne. Hence a microphone is enough to capture the signal. Microphones have the advantage that they are relatively easy and quick to replace and can be remotely installed, unlike accelerometers, pressure sensors and the shaft encoder. Time domain and frequency domain analysis of the airborne signal are shown to give information on the severity of cavitation in centrifugal pumps and can be used in cavitation detection

However, microphones tend to be expensive compared with accelerometers and hydrophones. In a normal industrial environment acoustic signals are likely to be contaminated by environmental and intrusive background noise. In practical, industrial situations it is likely that environmental noise control measures required by health and safety regulations - such as enclosing noisy centrifugal pumps - will interfere with the measurement procedure.

8.2 Time domain analysis

Figures 8-1 and 8-2, shows the time domain of the raw airborne acoustics signals for the pump operating at 249 l/min, and other flow rates, these flow rates are samples from the total number of flow rates shown in Table 7-1, and Appendix C. It can be seen that the signal changes with change in flow rate, and, once again, the question is whether there is sufficient change over the flow range of interest to confidently detect the onset of cavitation.

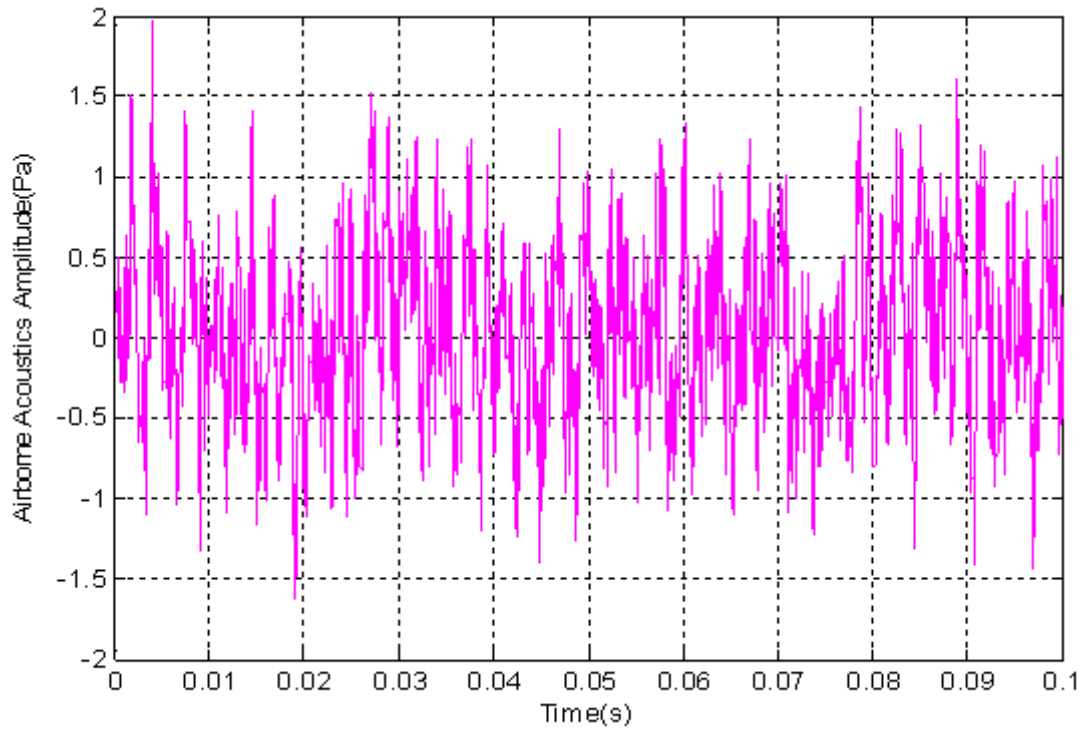


Figure 8-1 Raw time domain airborne acoustic signal for flow rate 249 l/min

As with the vibration measurements PDF, peak and RMS values, Crest factor and Kurtosis were used to analyse the time-domain vibration signals to determine whether they could be used as features to identify trends in the vibration signal. The spectral analysis used Kurtosis, Crest factor and Spectral Entropy.

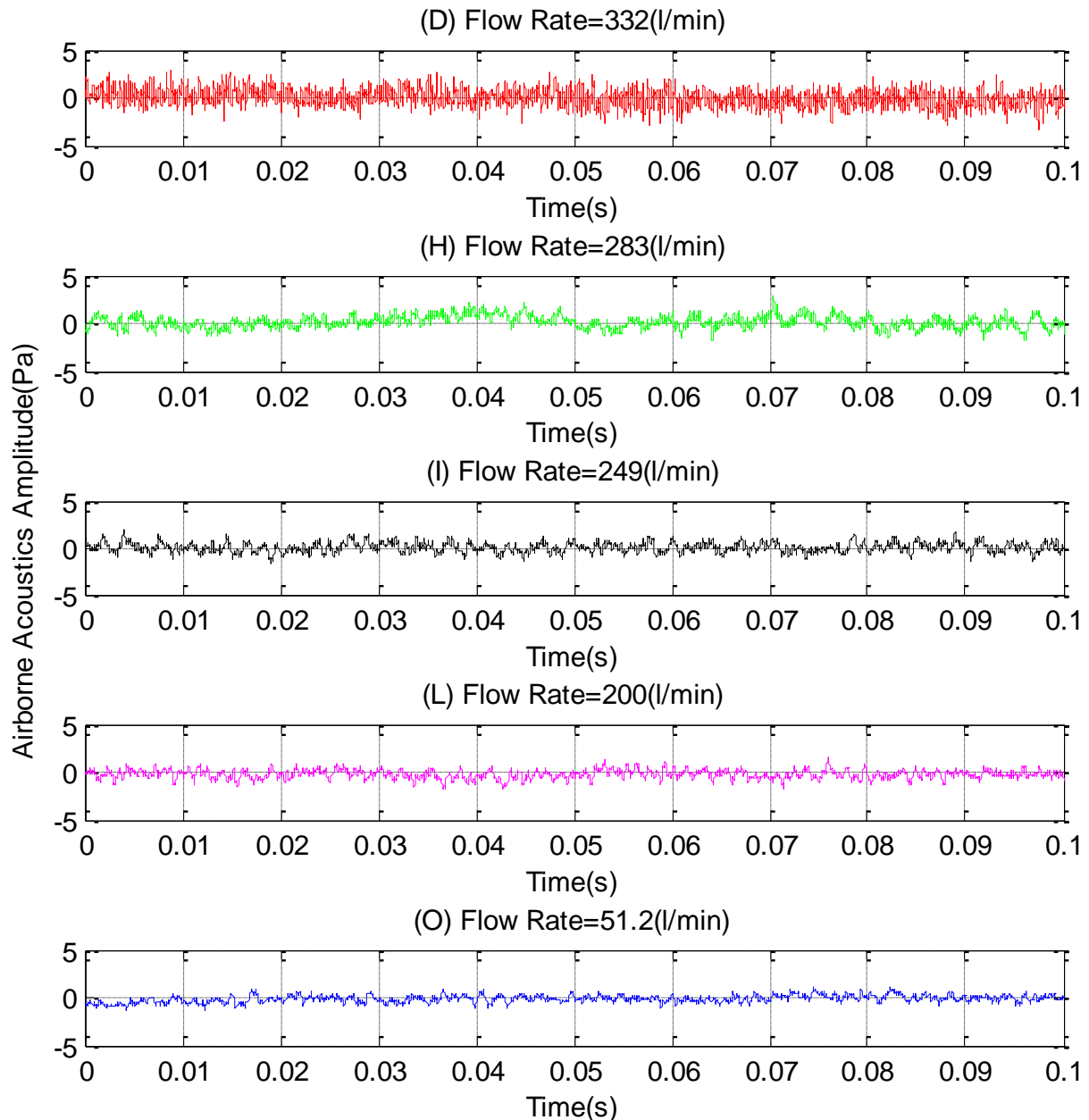


Figure 8-2 Raw time domain airborne acoustic signals at different flow rates

8.3 Conventional statistical measures from the time domain

8.3.1 Probability density function

Figure 8-3 (a) shows the PDFs of the acoustic signal for different flow rates. The airborne acoustic signals undergo a clear change in amplitude and frequency content as the pump flow increases, with the consequence that the PDF broadens and the peak amplitude gets smaller. Figure 8-3 (b) shows the amplitude of the PDF peak with flow rate and strongly suggests that the rate of change in the PDF is likely to be too gradual for the PDF of the airborne sound signal to be a good indicator of the onset of cavitation.

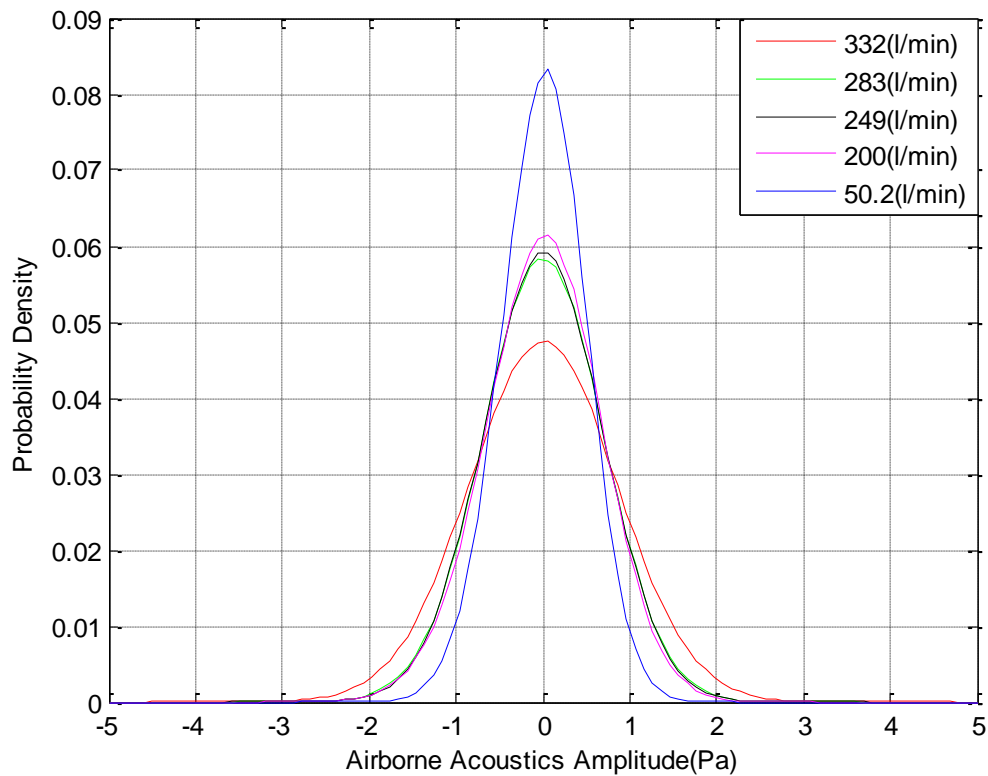


Figure 8-3 (a) PDF of time domain of airborne acoustics signal for different flow rates

Table 8-1 The values of the variances for the five curves shown in Figure 8-3(a) are:

PDF (Flow rate, l/min)	50.2	200	249	283	332
Variance	195.5	334	385	352	471
Standard Deviation (Pa)	4.47	18.3	19.6	18.8	21.7

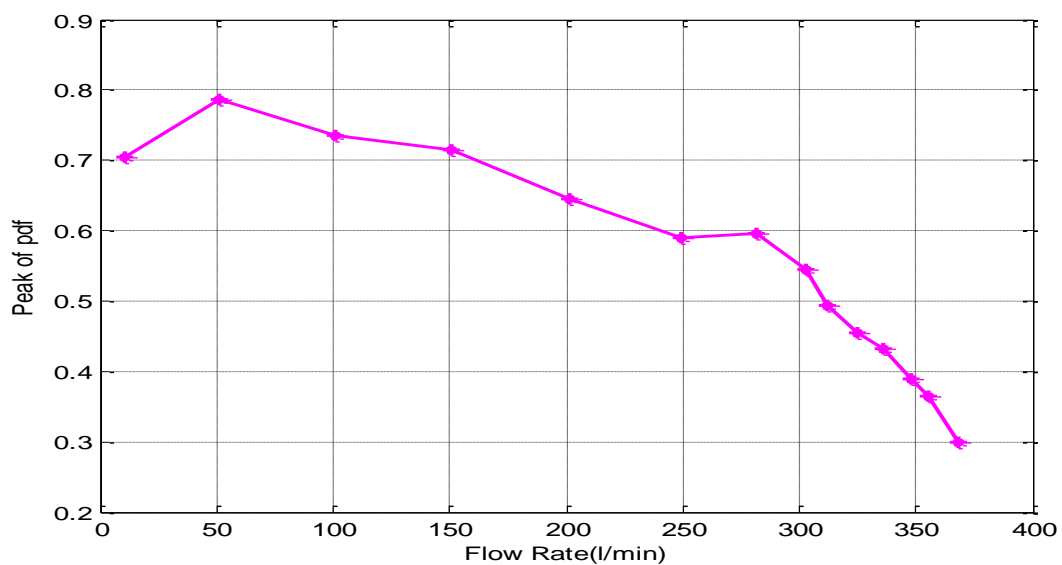


Figure 8-3 (b) Amplitude of PDF curve for airborne acoustic signal against flow rates

Figure 8-3 (b) clearly shows that there is a broad maximum value of the PDF centred at a flow rate of about 50 l/min. After this maximum there is a definite gradual decline in the PDF value which accelerates as the flow approaches 249 l/min. The change in gradient is not great but if it a general phenomenon then the turning point could be taken as an indication that cavitation has begun.

8.3.2 Peak value, RMS and Crest factor

Figures 8-4, 8-5 and 8-6 show the three statistical parameters: Peak value, RMS and Crest factor, respectively, for the different flow rates. It can be seen from Figures 8-4 and 8-5 that the trend followed by the Peak and RMS values is very similar. There is a gradual increase in magnitude with increase in flow rate below about 250 l/min, and a sharp rate of increase with the onset of established cavitation between 250 and above 300 l/min. The initial gradual increase in peak value followed by a slight leveling-off of the curve between about 250 l/min and 280 l/min and then a sharp increase in the rate of change of slope of the curve suggests the presence of a phenomenon which might be used to confirm established cavitation rather than incipient cavitation.

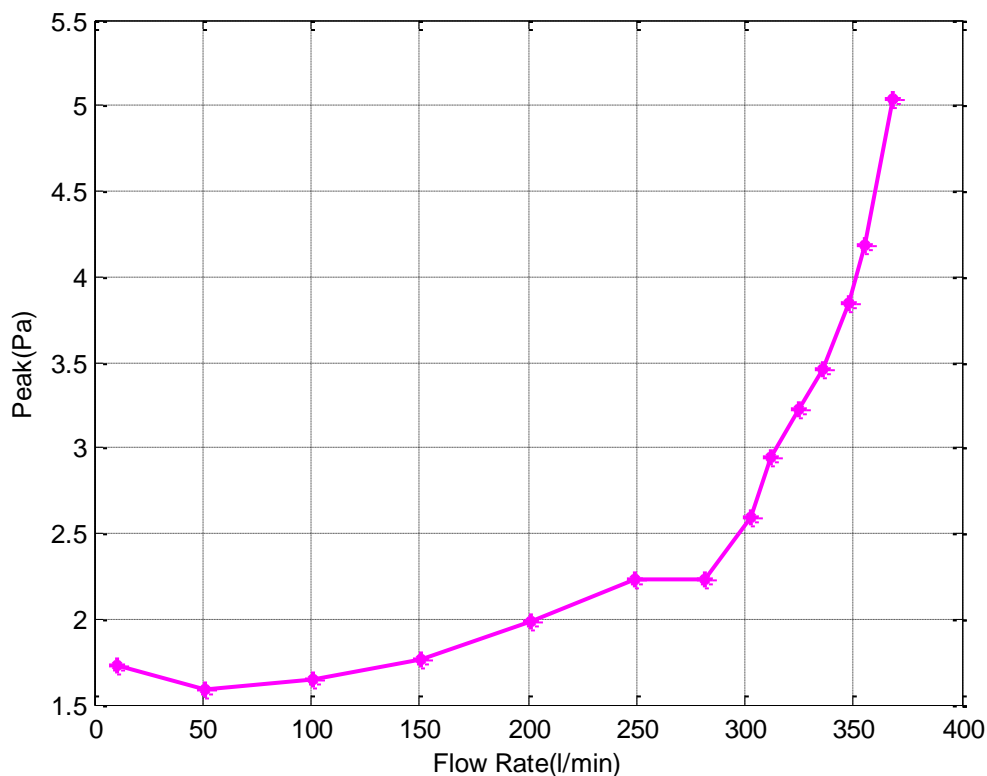


Figure 8-4 Peak value of time domain airborne acoustic signal with flow rate

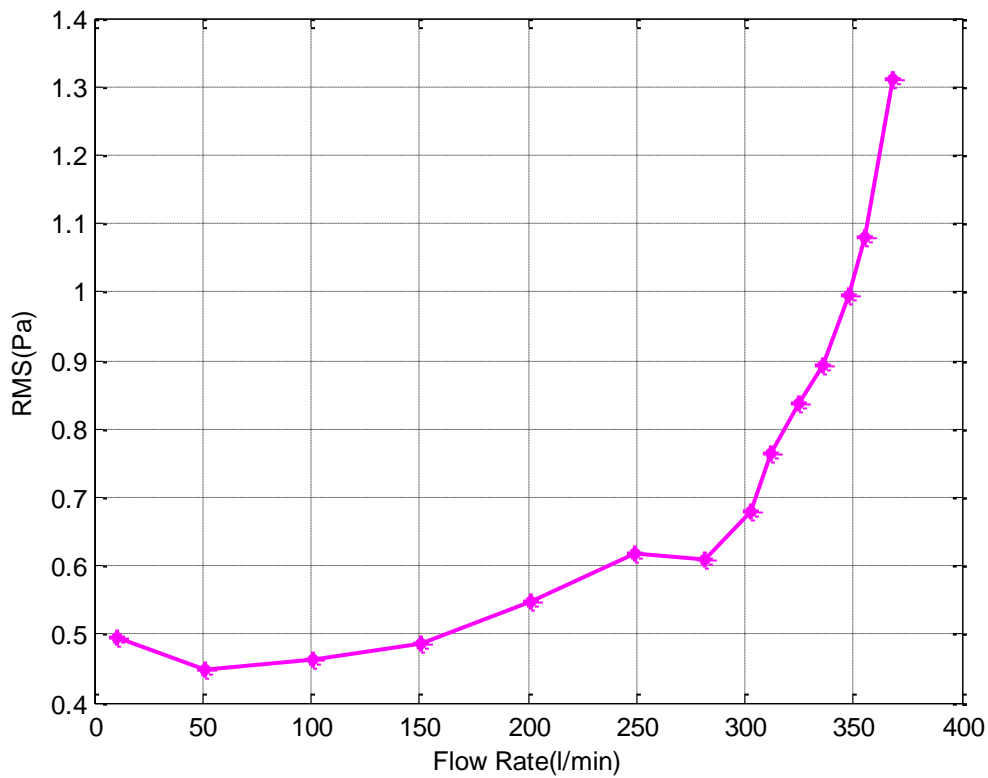


Figure 8-5 RMS of time domain airborne acoustic signal with flow rate

The Crest factor, Figure 8-6, shows the same general trend as Peak and RMS values, as of course it must, but interestingly the levelling off of the curve appears more pronounced, and might be a good indication of the onset of cavitation. However, because of the spread of the experimental results is quite wide, further research needs to be undertaken to confirm this.

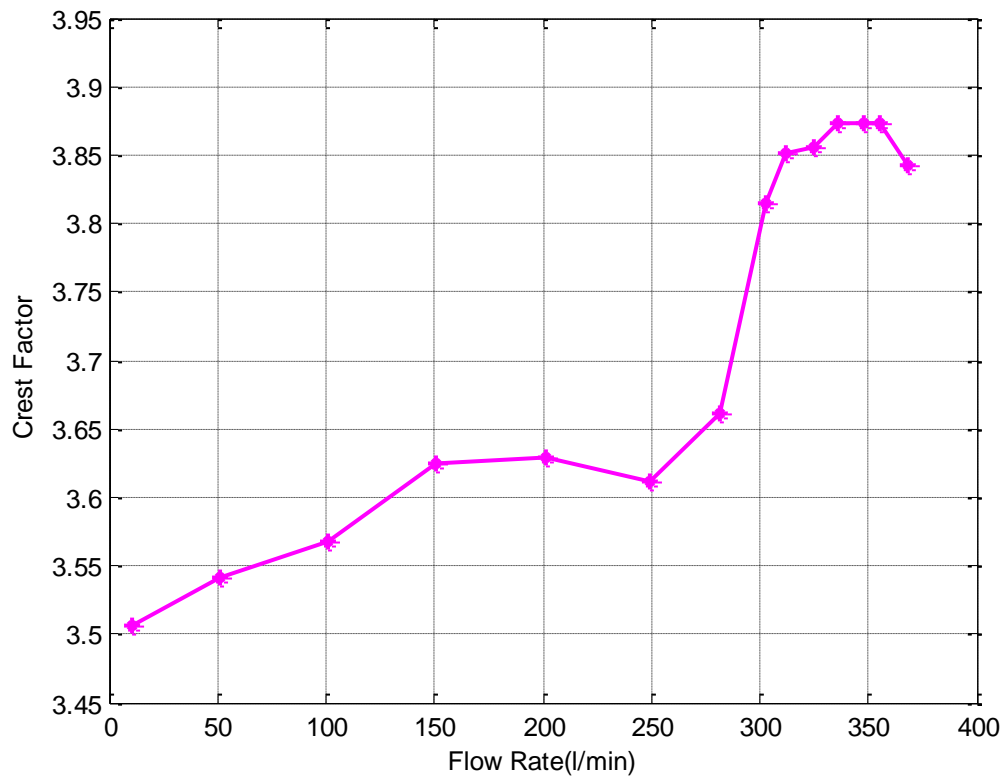


Figure 8-6 Crest factor of time domain airborne acoustic signal with flow rate

8.3.3 Kurtosis

Looking at Figure 8-7 there is a small peak in the kurtosis for the flow rates 150 l/min and 200 l/min, and there is a clear peak with established cavitation. However, the values of the Kurtosis are low, close to zero so the distribution of the peaks in the acoustic spectrum is close to Gaussian for the entire flow range.

Nevertheless, the observed dip in kurtosis at a flow rate of about 250 l/min is very interesting. The dip is clear and needs to be further evaluated for different pumps and systems, because if it is repeatable it would be a good indicator of incipient cavitation. However, the wide spread in observed readings means this phenomenon needs to be confirmed.

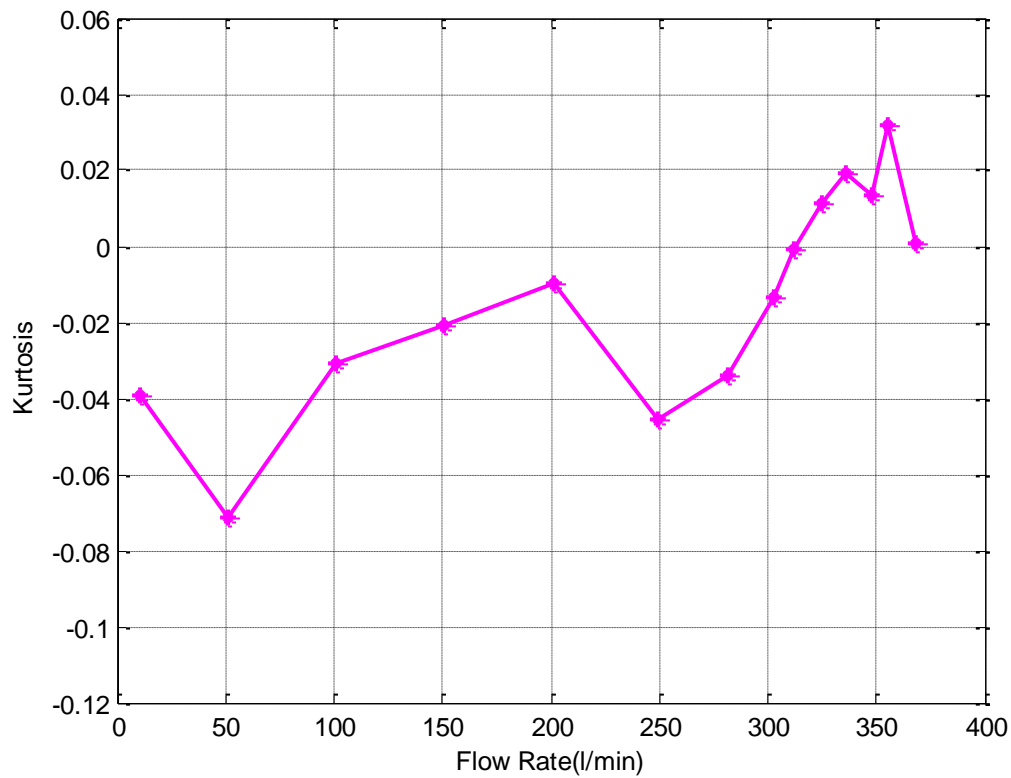


Figure 8-7 Kurtosis of time domain airborne acoustic signal with flow rate

8.4 Spectrum analysis

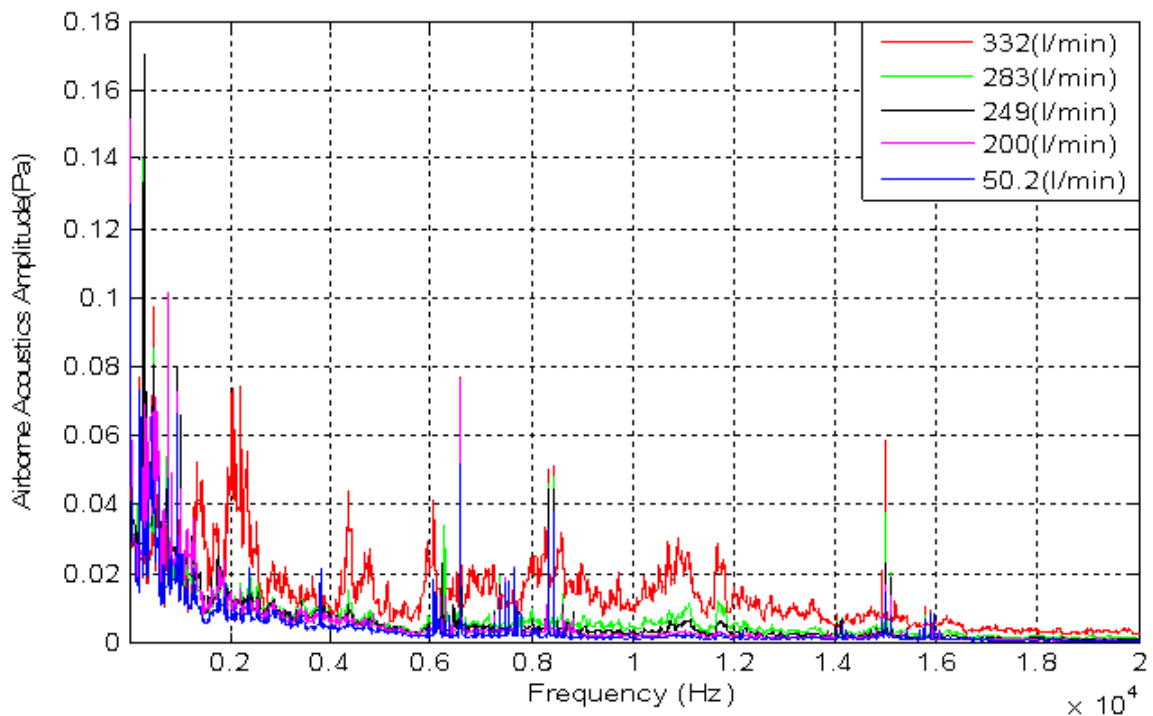


Figure 8-8 (a) Spectrum of the airborne acoustic signal from the pump for different flow rates

Figure 8-8, shows the spectrum of the airborne acoustic signal from the pump for a flow rate of 249 l/min and then for a number of flow rates. The spectra consist of two distinctive elements: discrete components and broadband noise.

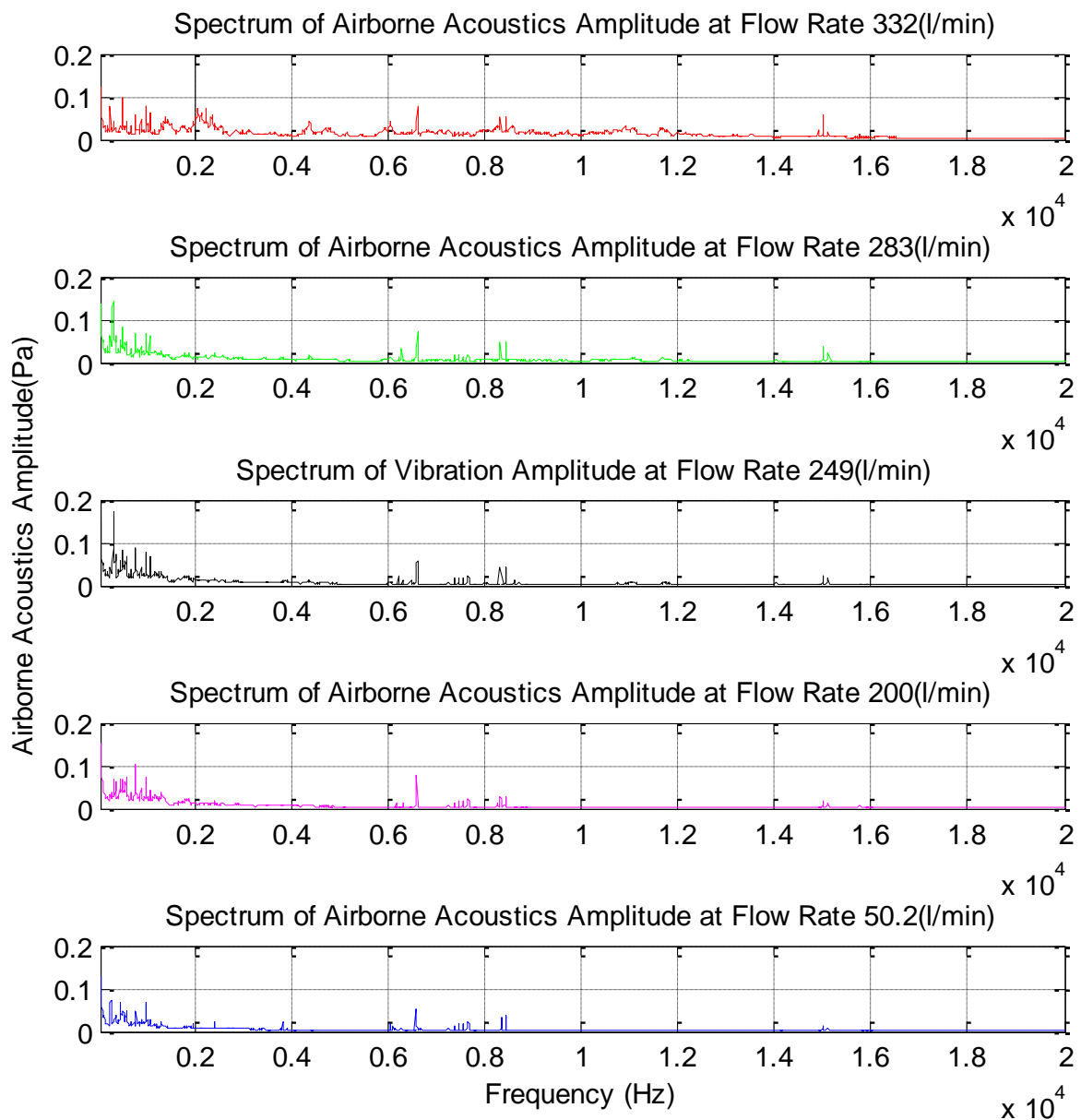


Figure 8-8 (b) Frequency spectra of acoustic signals at specified flow rates

8.4.1 Baseline spectral analysis

Again, and simply for convenience the acoustic spectrum has been divided into three parts: 20 Hz to 1 kHz; 1 kHz to 2 kHz; and 2 kHz to 20 kHz, see Figures 8-9, 8-10 and 8-11 respectively, all of which are for a flow rate of 249 l/min. As with the vibration measurements shown in Chapter 7, these figures show the discrete component characteristics

present within the overall spectrum are due mainly to the interaction of moving parts with nearby stationary objects, and periodicities in the flow due to the discrete nature of the pump's rotor blades. In the frequency range from 20 Hz to 1 kHz, the discrete components have much higher amplitudes than the broadband, see Figure 8-9.

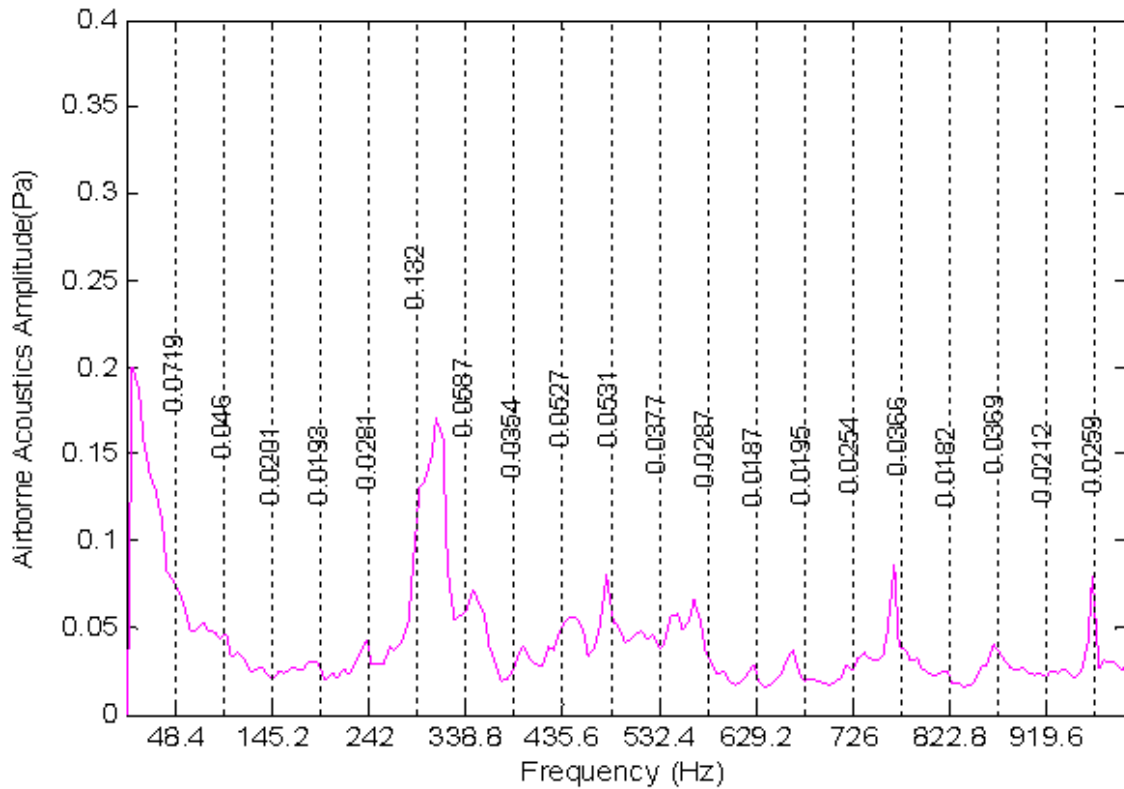


Figure 8-9 Baseline airborne acoustic spectrum 20 Hz - 1 kHz for flow rate 249 l/min

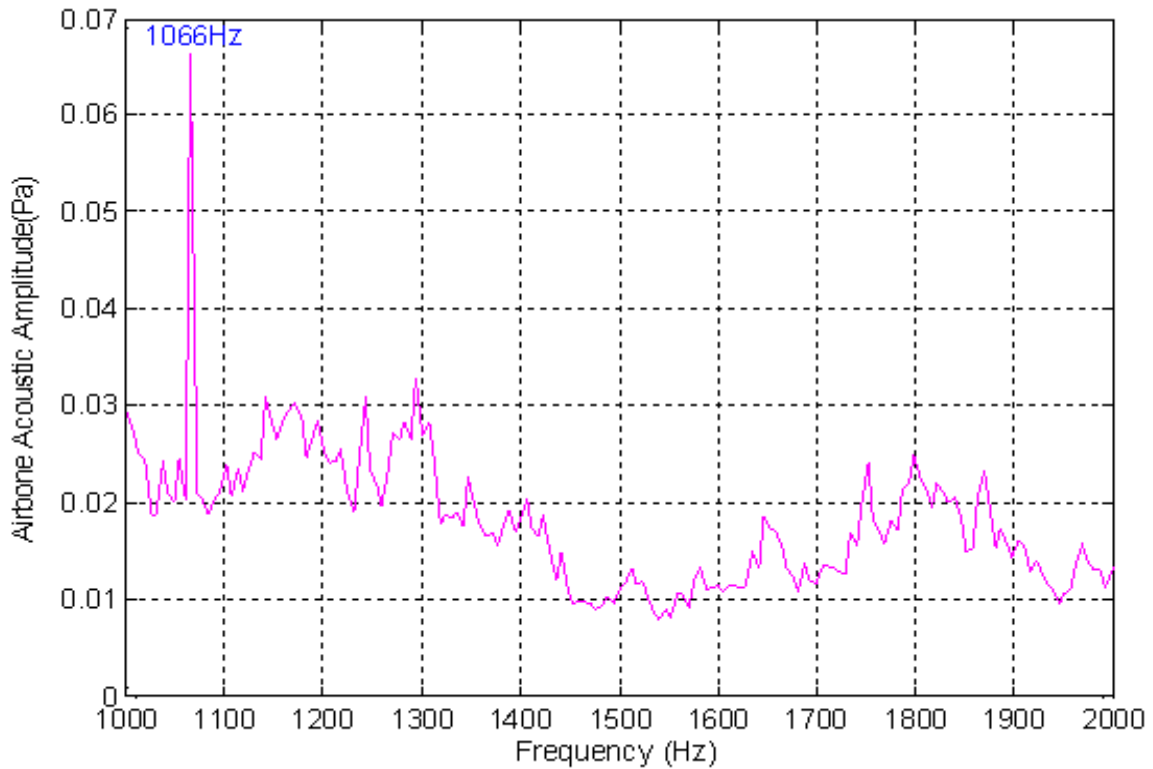


Figure 8-10 Baseline airborne acoustic spectrum 1 kHz-2 kHz for flow rate 249 l/min

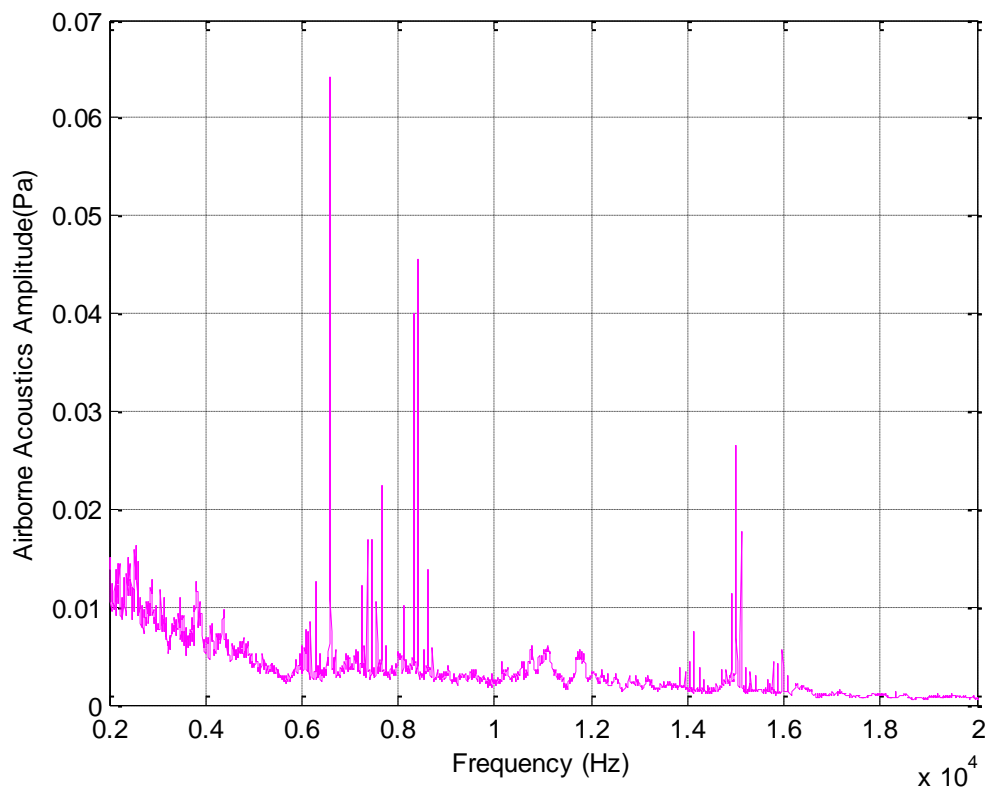


Figure 8-11 Baseline airborne acoustic spectrum for 2 kHz-20 kHz for flow rate 249 l/min

Figure 8-9 is dominated by a number of peaks and there is obviously a close correlation with the frequencies of the peaks in the corresponding vibration spectrum though, of course, the relative amplitudes will differ considerably.

Figure 8-10 shows that in the frequency range 1 kHz to 2 kHz, the dominant peak is at 1066Hz which is a harmonic of the RF. However as explained in Section 7.4.1, referring to Figure 7-10, this peak is probably due to a structural resonance.

Figure 8-11 is the baseline spectrum for the range 2 kHz to 10 kHz. Discrete components are present and these are probably due to structural resonances. The lengths corresponding to the two peaks 6.69 kHz and 8.42 kHz are 23 cm and 18 cm respectively. There are many such lengths of piping on the test rig but, as explained, previously no analysis was made of corresponding acoustic or vibration resonances. This is a good point for further work.

Surprisingly, even though 249 l/min is the flow rate at which cavitation is becoming noticeable, the background level is still way below the individual peaks.

8.4.2 Spectral amplitude characteristics

Frequency range 20Hz-1kHz

Figure 8-12 shows the “waterfall” for the airborne acoustics spectrum in the frequency range 20 Hz to 1 kHz for the flow range from about 10 l/min to about 370 l/min. At flow rates below about 200 l/min the airborne acoustic signal of the pump appears more or less consistent although there is a gradual increase in the peak at around 340Hz. At about 249 l/min there is a significant increase in the amplitude of the airborne acoustic signal and a clear and substantial peak can be observed at about 340Hz, this is a harmonic of the rotational frequency. This peak remains present with further increase in the flow rate to above 320 l/min and could be a very good indicator of the onset of cavitation. As mentioned in the previous chapter, this particular frequency might be specific to this pump, but the principle that an individual component of the frequency might be a suitable indicator has already been proposed.

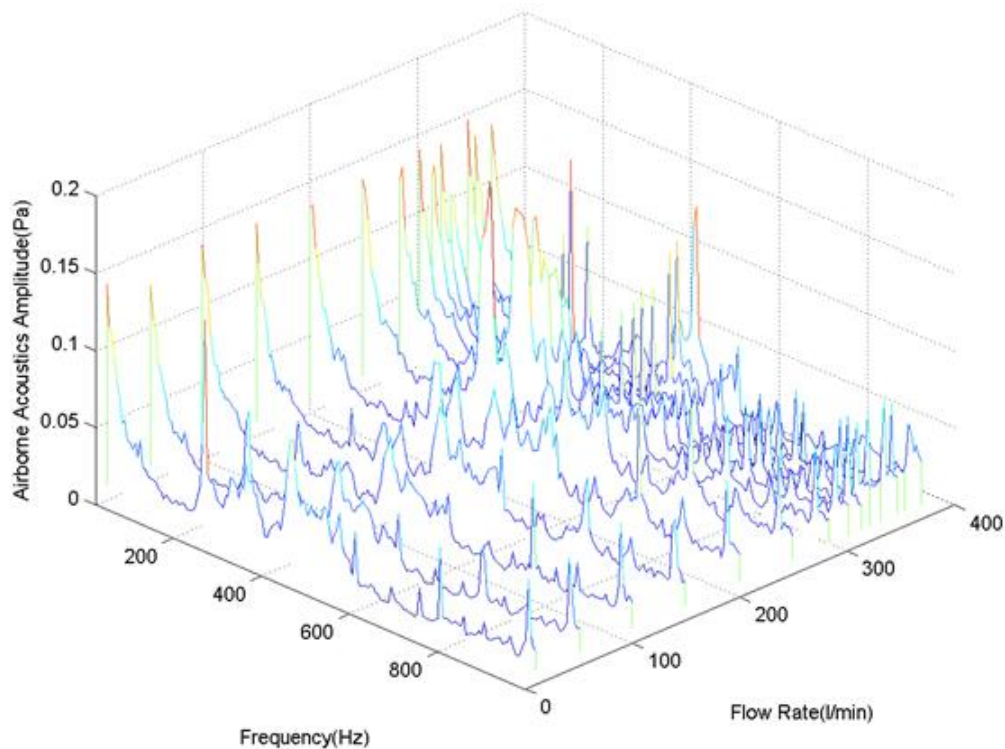


Figure 8-12 Waterfall time-averaged Peak amplitude of airborne acoustic signal 20 Hz- 1kHz

Frequency range 1kHz-2kHz

Figure 8-13 show the waterfall of the airborne acoustics spectrum for the frequency range 1 kHz to 2 kHz, the amplitude of the airborne signal remains more or less constant with small increases in a flow rate until approximately 250 l/min. For flow rates above 300 l/min broadband airborne noise from the pump can be seen in the frequency range 1200 Hz to 1500 Hz. This appears to occur too late to be useful in identifying the onset of cavitation. There is a very substantial increase in acoustic signal in the frequency range 1800 Hz to 2 kHz due to the increase in cavitation that occurs at flow rates above about 300 l/min, see Figures 8-8 (b) and 7-8 (a).

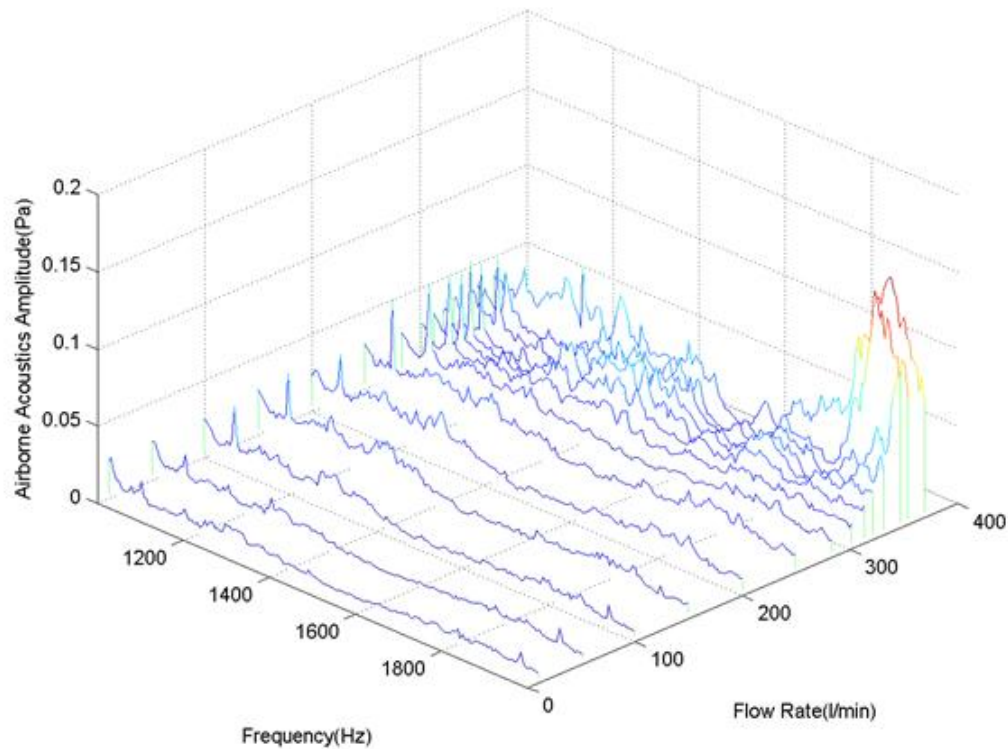


Figure 8-13 Waterfall of time-averaged Peak amplitude of airborne acoustics signal 1 kHz-2 kHz

Frequency range 2kHz-20kHz

Figure 8-14 show the waterfall for the airborne acoustic spectrum in the frequency range 2 kHz – 20 kHz. The airborne acoustic pattern appears to remain approximately more constant until the flow rate reaches more than 300 l/min. As the flow rate becomes greater than 300 l/min it appears that the single most noticeable event is the increase in amplitude of the peak at about 6.5 kHz. There are some further changes in the airborne acoustic pattern with increase in flow, but these occur after the onset of cavitation.

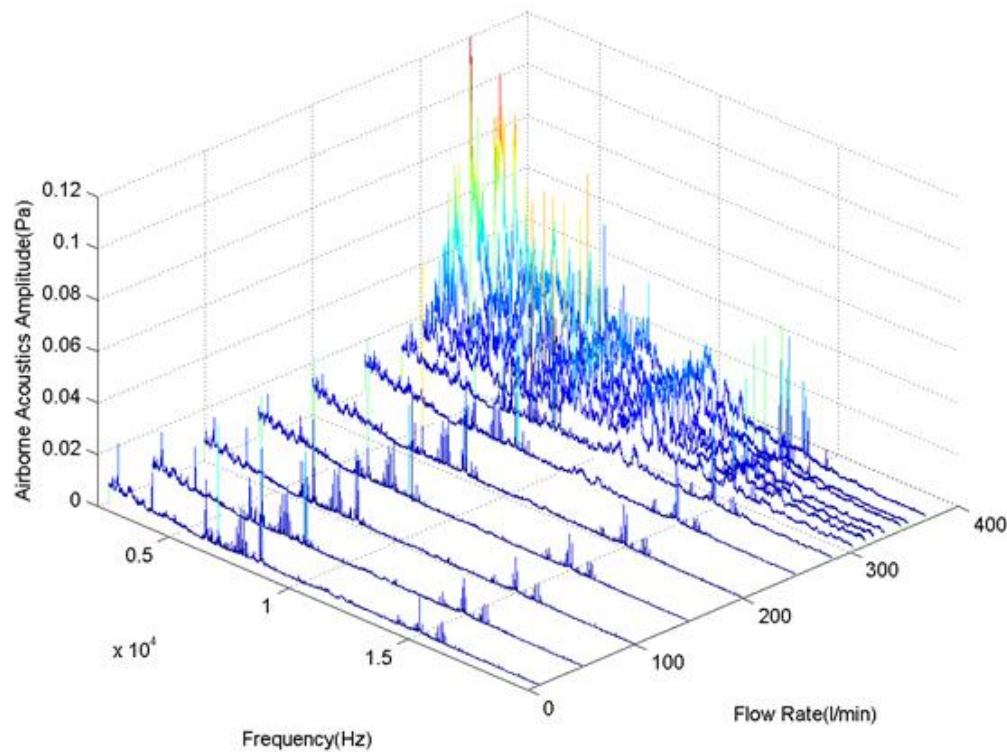


Figure 8-14 Waterfall of time averaged Peak amplitude of airborne acoustics signal 2 kHz-20 kHz

8.5 Statistical measures from the frequency domain

Figure 8-15 presents the change in value of the Crest factor for the airborne acoustic spectra with increase in flow rate. It can be seen that the Crest factor exhibits a relatively smooth downward trend over the flow range 100 l/min to about 350 l/min. The now familiar “knee” appears yet again at the flow rates where cavitation is known to begin. Further work is required to determine whether this “knee” is system specific or whether it is a general phenomenon associated with the onset of cavitation. If the latter, accurate identification of it would be a useful measure to determine the onset of cavitation

8.5.1 Spectral crest factor

Comparison of Crest factors for the time and frequency domains, Figures 8-6 and 8-15 respectively, show curves which move in opposite directions with increase in flow rate. This is because the two curves relate to very different physical measurements. As can be seen from Figures 7-8 (a) and 8-8 (b) the time domain signals for both measured acceleration and airborne sound increase only slowly until about 300 l/min, after which the cavitating flow

causes a sudden and dramatic increase in peak amplitude with respect to the RMS value. This is shown in the curve for the corresponding Crest factor as a slight increase with flow rate up to about 280 l/min after which there is a sudden increase.

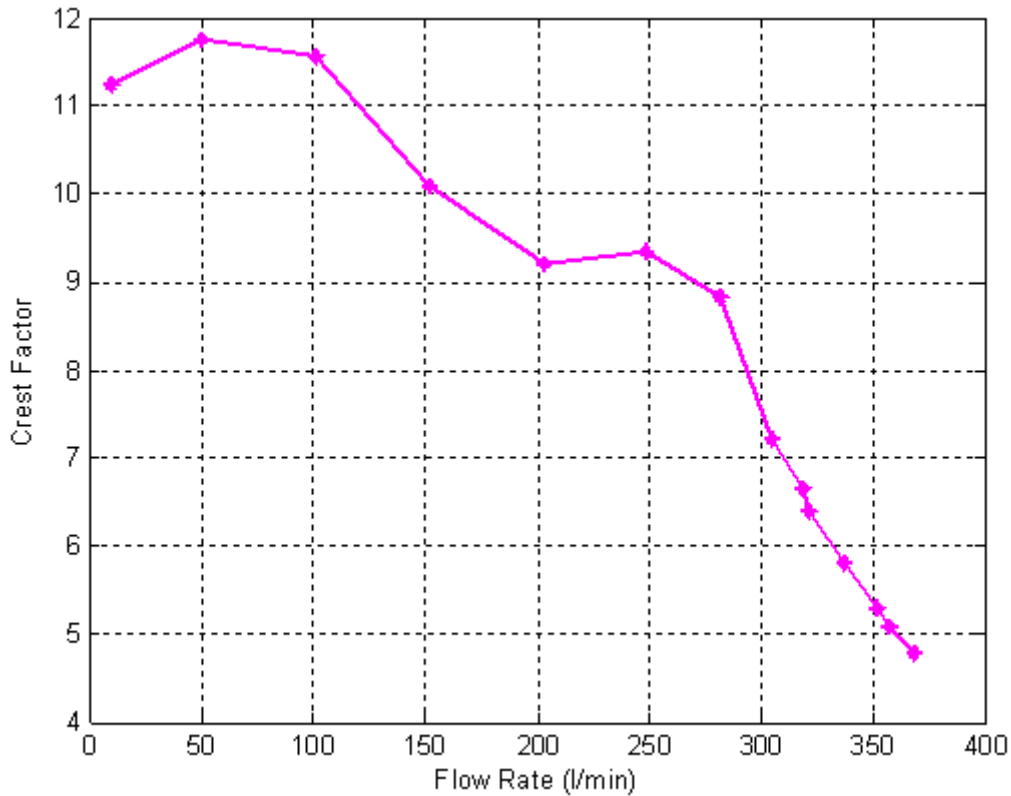


Figure 8-15 Crest factor of airborne acoustic spectra for different flow rates: 20 Hz to 20 kHz

With spectral analysis the Crest factor refers to the distribution of energy across the spectrum. As cavitation increases the spectrum moves away from a series of individual peaks towards more broadband noise and thus the Crest factor decreases in magnitude.

8.5.2 Spectral kurtosis

Figure 8-16 shows the values of Kurtosis obtained from the individual spectra as a function of flow rate. As with the vibration spectra, Kurtosis would be expected to initially increase as the peaks due to the blade passing and rotational frequencies and their harmonics increased, but then would fall away as number of peaks increased. The minimum in the Kurtosis is followed by a maximum at the onset of cavitation, and then by a rapid and clear reduction in Kurtosis value. This “knee” is promising as a mechanism to detect the onset of cavitation as it

is seen to start here at about 200 l/min. Of course it must be shown that this is not a system specific phenomenon.

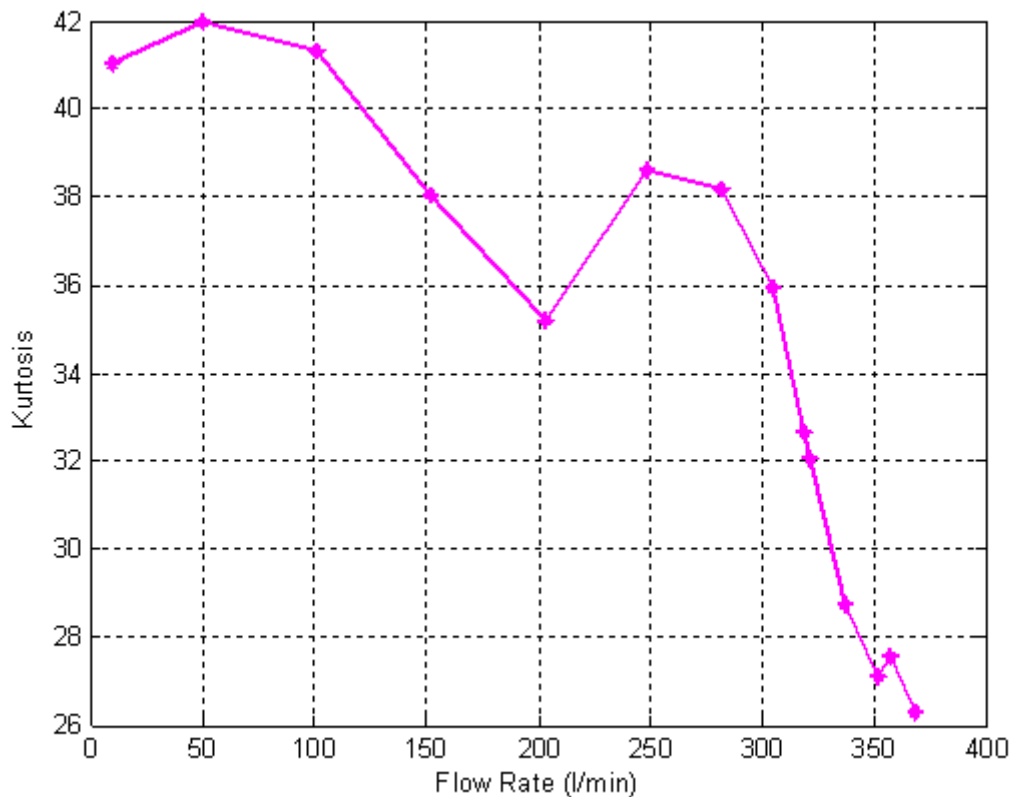


Figure 8-16 Kurtosis of airborne acoustics spectra for different flow rates: 20 Hz to 20 kHz

8.5.3 Spectral entropy

Figure 8-17 shows the values of spectral entropy obtained from the individual spectra as a function of flow rate. The results obtained indicate that spectral entropy of the airborne noise from the pump increases gradually with flow rate to about 200 l/min, where there is a clear dip in the value measured. This dip occurs close to the onset of cavitation, after which there is a sharp and rapid increase in the value of the spectral entropy. The local minimum at about 250 l/min is promising as a factor for the determining of the onset of cavitation but, once again, further work is required to determine whether it is system specific.

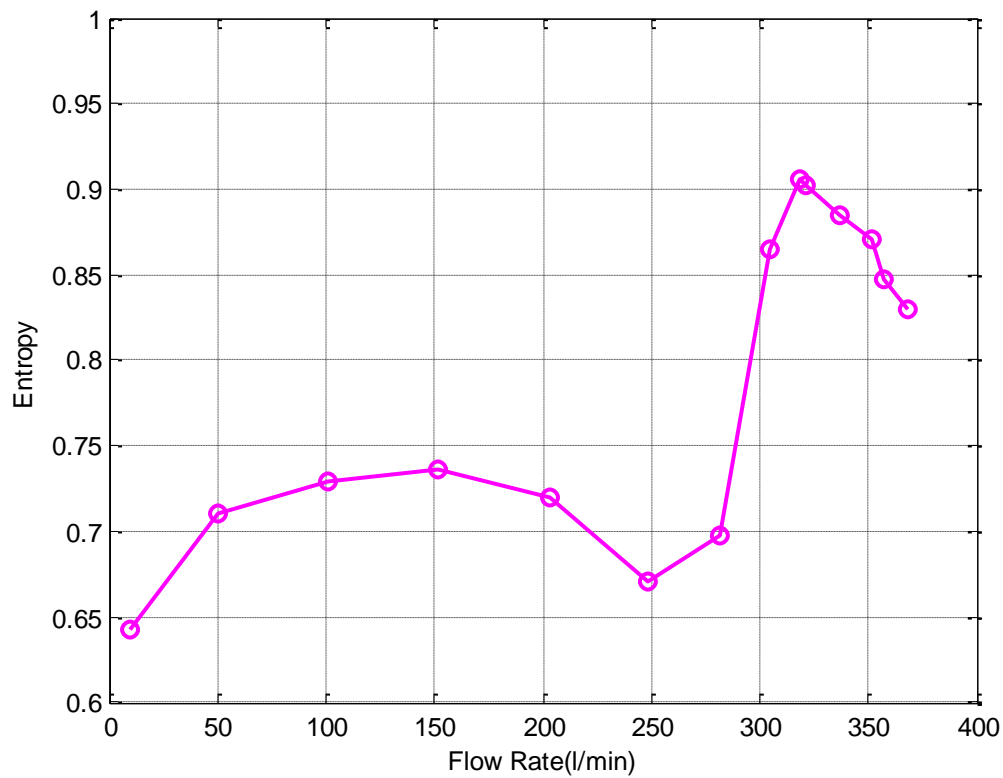


Figure 8-17 Spectral entropy of airborne acoustics spectrum with flow rate: 20 Hz to 20 kHz

The next chapter prediction of the onset of cavitation using the results obtained for the hydrophone measurements is presented. Comparison of the various methods will be presented in Chapter 10. In particular the relative performance of acoustic and capacitive methods will be given there.

CHAPTER NINE**9. HYDROACOUSTIC SIGNAL ANALYSIS FOR DETECTION OF CAVITATION**

This chapter describes the analysis of the experimental hydrophone signal obtained from the test pump for detection of incipient cavitation. A number of statistical parameters are examined as possible indicators of the onset of cavitation. For ease of cross-referencing, this chapter deliberately follows the structure of Chapters Seven and Eight.

9.1 Advantages and disadvantages of using hydrophone methods

Hydroacoustic transducers are, if care is taken with the initial placement, quick and easy to replace. Time domain and frequency domain analysis provides good information about severity of cavitation and can be used in fault detection and diagnosis.

However, hydroacoustic transducers tend to be expensive compared with accelerometers. The hydroacoustic signal will be the sum of all the sound waves arriving at the transducer from all the many surfaces of the pump and pipe work and this intrusive background noise may contaminate the signal and make cavitation diagnosis more difficult, hence the need for statistical analysis. It is therefore necessary to place the transducer as close as possible to the source of interest and this may not always be possible.

Time domain and frequency domain analyses, as will be shown are potentially very useful in detecting the early stages of cavitation.

9.2 Time domain analysis

Figures 9-1 and 9-2 show the raw hydroacoustic signal for the pump operating at 249 l/min and at different flow rates, see Table 7-1 and Appendix C. It can be seen that the amplitude of the raw signal changes with flow rate and, again, the question is whether there is sufficient measureable change to confidently detect the onset of cavitation. As explained in Chapter 4, both time and frequency-domain analyses are used to look for features which will indicate incipient cavitation.

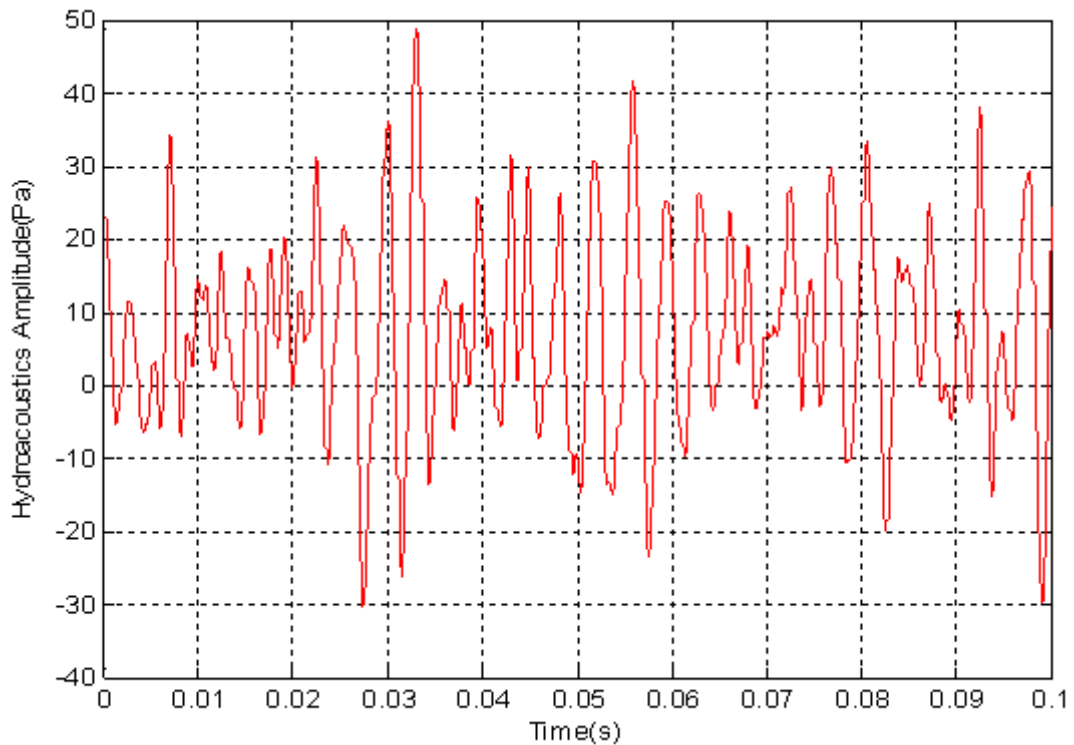


Figure 9-1 Time domain of raw hydroacoustic signal for flow rate 249 l/min

The common statistical parameters PDF, Peak and RMS values, Crest factor and Kurtosis were used to analyse the time domain vibration signals to determine whether they could be used to identify trends in the hydroacoustic signal. The spectral analysis used Kurtosis, Crest factor and Spectral Entropy.

Figure 9-2 shows a clear change in the time-domain of the hydroacoustic signal as the flow increased, with significant changes close to 249 l/min. However, the change in signal is nowhere near as marked as it was with either the vibration or airborne acoustic signals.

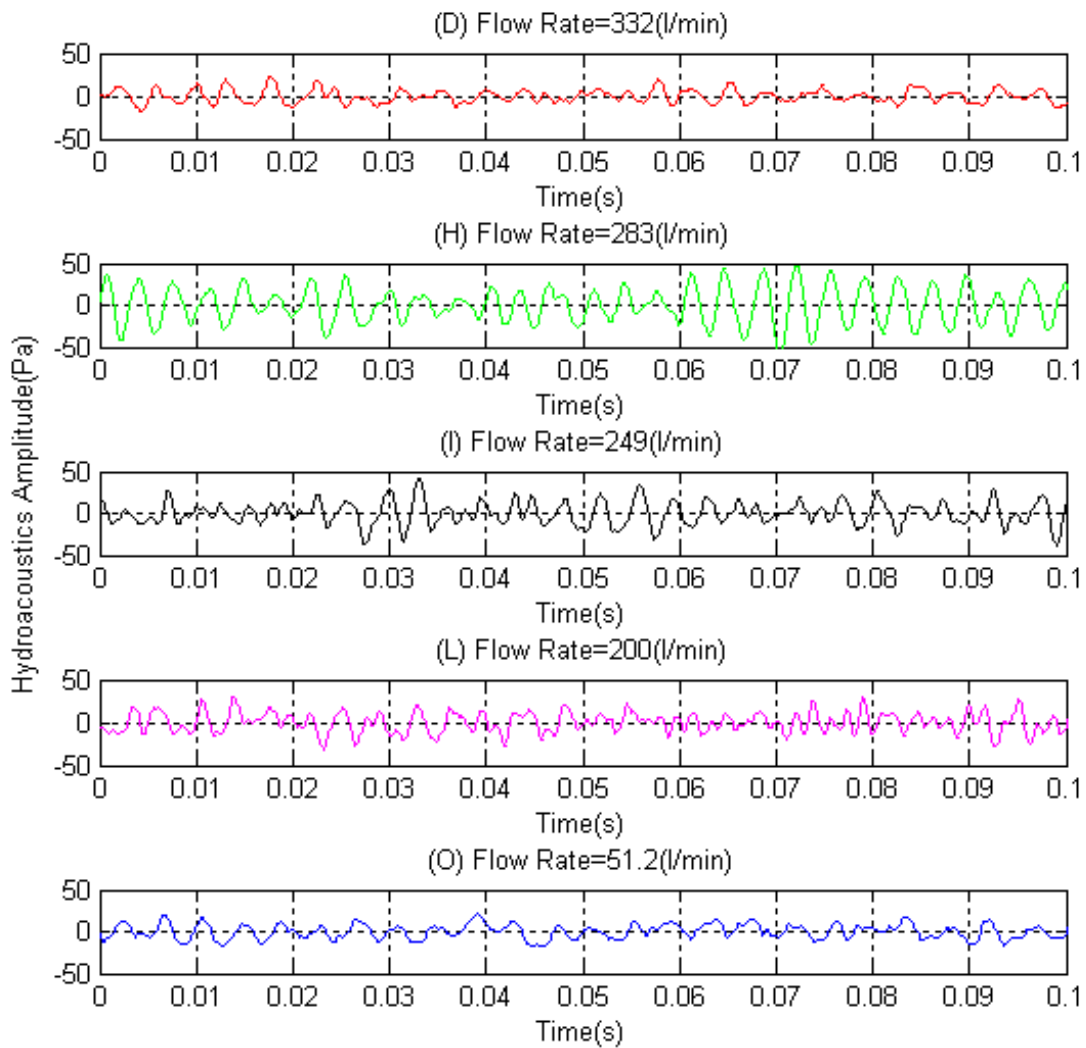


Figure 9-2 Time domain of raw hydroacoustic signals at specified flow rates

9.3 Conventional statistical measures from the time domain

9.3.1 Probability density function

Figure 9-3 (a) shows the PDF of the time domain of the hydroacoustic signal for the flow rates listed in Table 7-1. A clear change in the PDF can be seen as the flow increased, but with the hydroacoustic signal the peak occurs very definitely with fully established cavitation. Figure 9-3 (b) clearly shows that the amplitude of the PDF rises to a broad maximum quite early at a flow rate of about 100 l/min, after which it drops away and reaches a minimum value at about 280 to 300 l/min before rising sharply. The clear and distinct minimum occurs after the first clear signs of cavitation but before cavitation is fully

established. It is possible that this minimum could be used as an indicator that cavitation is occurring but is not yet at dangerous levels.

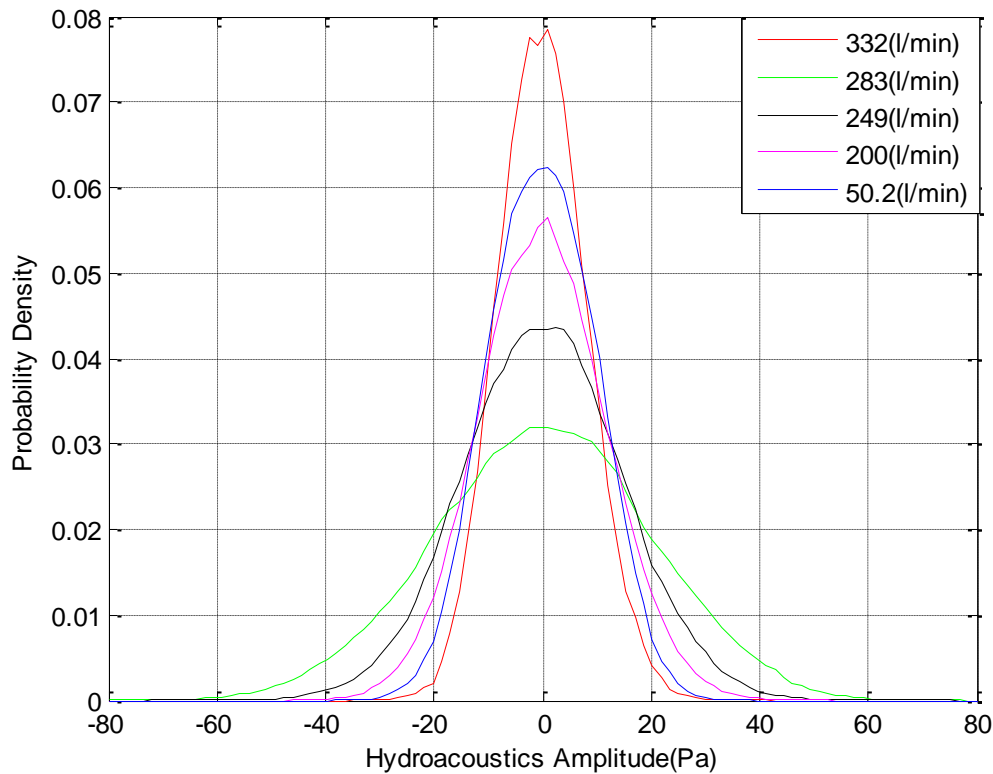


Figure 9-3 (a) PDFs of hydroacoustic signal for different flow rates

Table 9-1 The values of the variances for the five curves shown in Figure 9-3(a) are:

PDF (Flow rate, l/min)	50.2	200	249	283	332
Variance	217	292	356	508	142
Standard Deviation (Pa)	14.7	17.1	18.9	22.5	11.9

It can be seen when comparing the figures for the amplitude of the PDF curve against flow rate that there is a significant difference between those for the vibration and acoustic measurements (Figures 7-3 (b) and 8-3 (b), respectively) and Figure 9-3 (b) above. The curves representing the vibration and acoustic measurements both show an initial maximum and then decrease smoothly as the flow rate increases. This is different behaviour to the PDF curves for the hydrostatic signal above 300 l/min, which begin to increase quite rapidly at flow rates where cavitation is well established. This is attributed to the fact that the hydrophone transducer is in the flow and therefore subject directly to increased flow turbulence with cavitation.

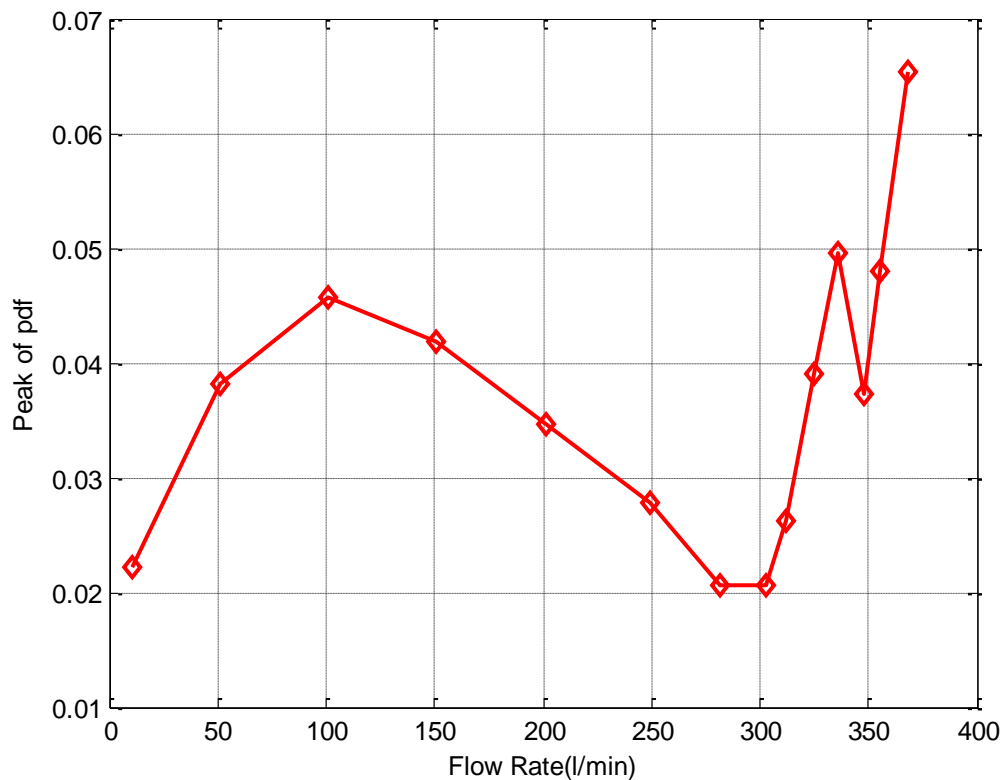


Figure 9-3 (b) Amplitude of PDF curve of hydroacoustic signal against flow rate

9.3.2 Peak value, RMS and Crest factor

Figures 9-4, 9-5 and 9-6 show the Peak and RMS values and Crest factor for the time-averaged time-domain hydroacoustic signals for different flow rates between 10.5 l/min and 370 l/min.

As with the vibration and airborne acoustic signals the trends seen in the Peak and RMS curves follow each other closely, see Figures 9-4 and 9-5. Both show a minimum at about 100 l/min, then a consistent rise to a peak occurring at a flow rate of about 280 l/min, after which there is a very rapid fall in both Peak and RMS values. The increase in Peak and RMS values between 100 and 280 l/min is consistent and this trend could be taken as a warning of the possible onset of cavitation. The peak at about 280 l/min and the rapid drop in values after that acts as a very definite confirmation of cavitation is occurring but not yet fully established.

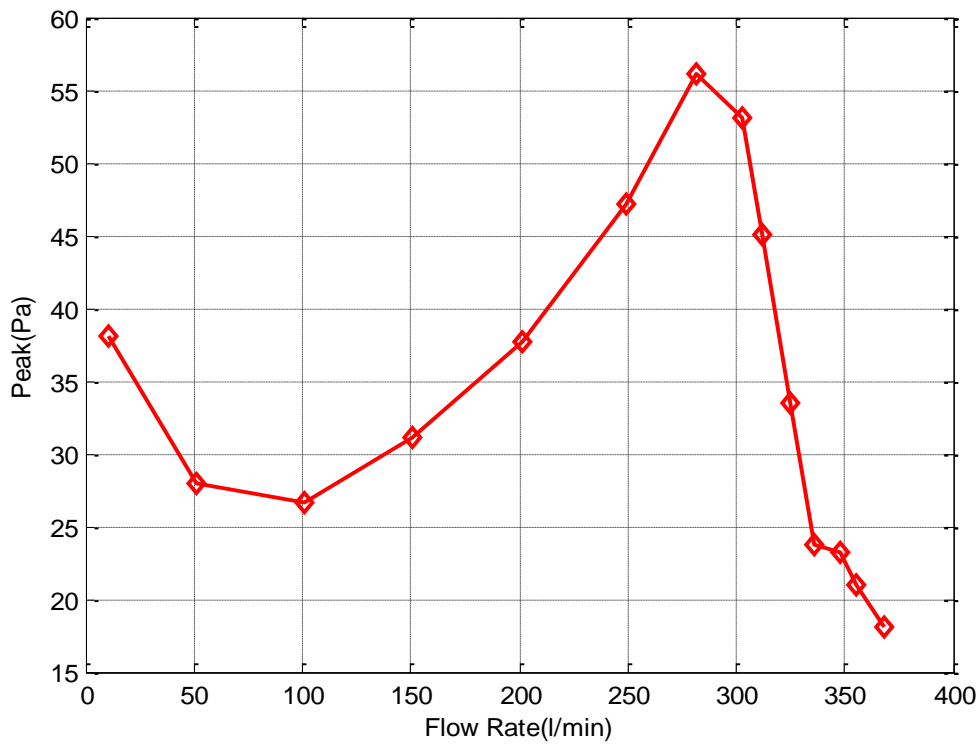


Figure 9-4 Peak value of time domain of hydroacoustic signal with flow rate

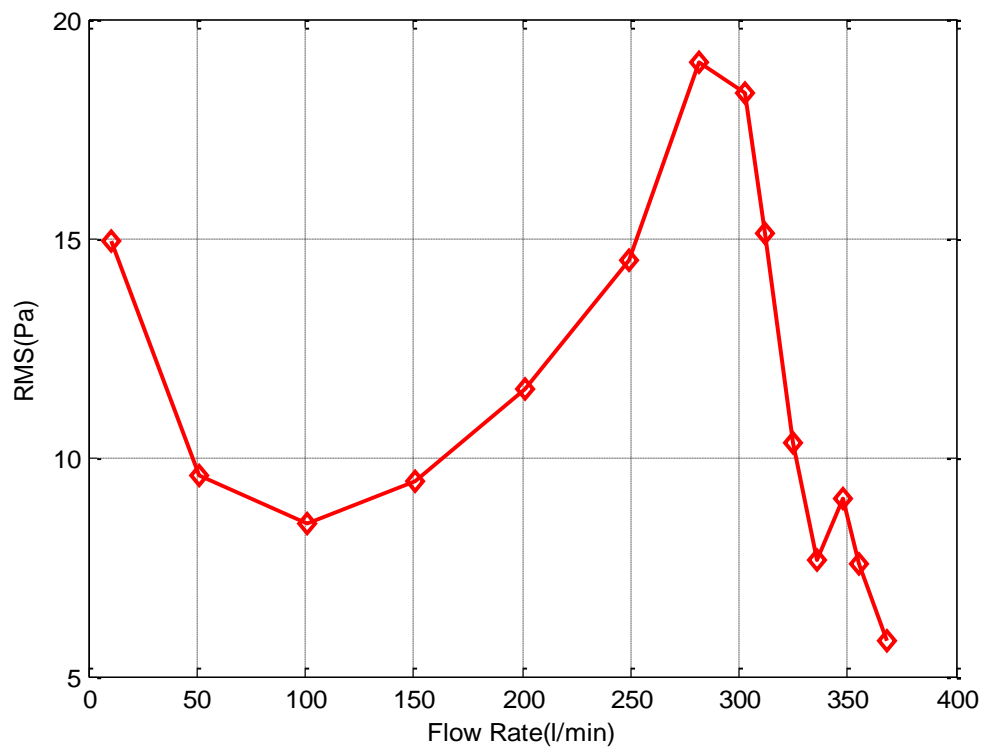


Figure 9-5 RMS value of time domain of hydroacoustic signal with flow rate

The plot of Crest factor against flow rate, Figure 9-6, shows an increase in value with flow rate and a broad peak between about 150 to 250 l/min. Once the maximum has occurred and been identified any subsequent significant decrease in value could – for this system at least – be taken as an indication the onset of cavitation. The Crest factor is the ratio of Peak to RMS, and its shape this depends on the curves shown in Figures 9-4 and 9-5. Despite the relative smoothness and similarities of the RMS and Peak values (except at 350 l/min for the RMS value) the curve representing the Crest factor shows some interesting features. A clear and gradual peak that reaches its maximum with the onset of cavitation, followed by a sudden trough with fully developed cavitation. This feature needs to be tested and confirmed on other systems.

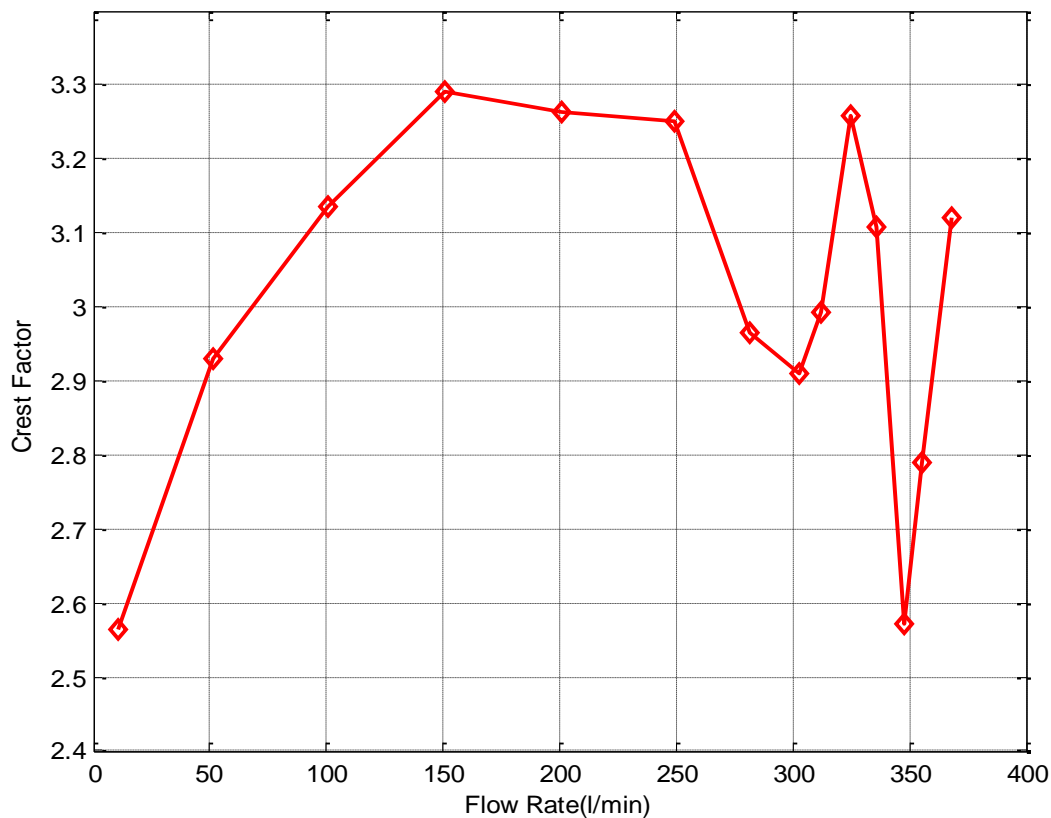


Figure 9-6 Crest factor of time domain of hydroacoustic signal with flow rate

9.2.3 Kurtosis

Figure 9-7 shows that the general shape of the curve for Kurtosis against flow rate is of a broad peak or hump, which starts to fall away with the onset of cavitation at about 250 l/min. The shape of the curve is very similar to that of the Crest factor shown above and the same

observations apply. The trough could be a good indication of the onset of cavitation but further work needs to be done to determine if it is specific to this system or more general.

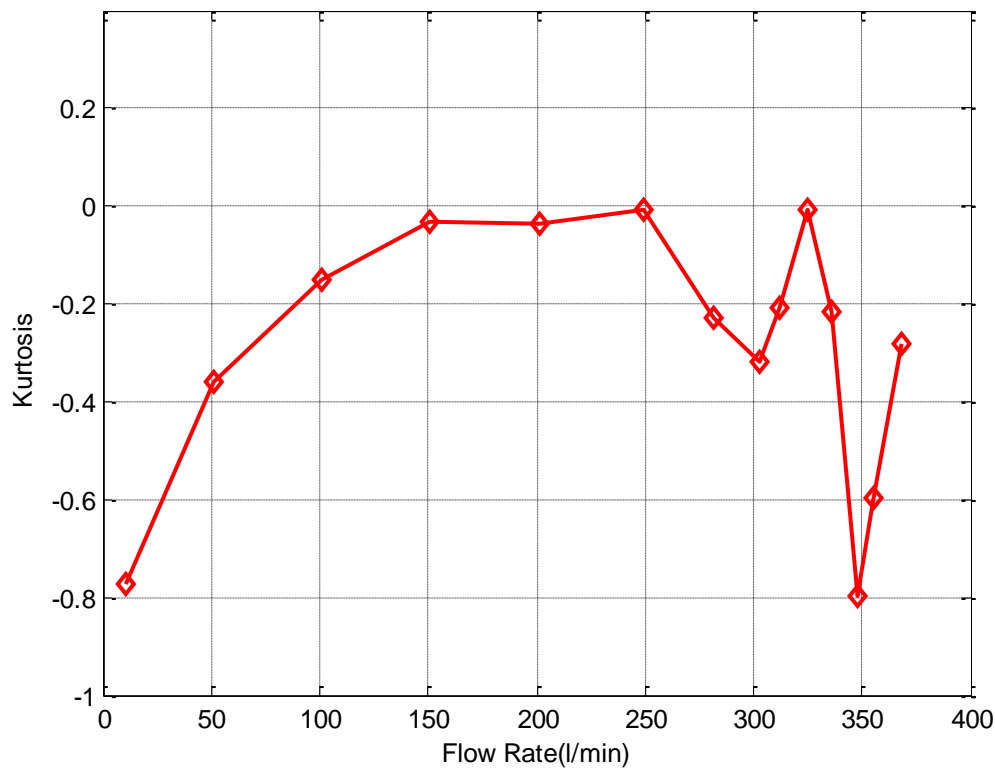


Figure 9-7 Kurtosis of time domain of the hydroacoustic signal with flow rate

As remarked in Section 7.3.3. The value of the Kurtosis is close to zero – few or no sudden peaks in the time domain signal – until after the 250 l/min when the value of the kurtosis begins to increase sharply. It is suggested that the explanation for this is that at 250 l/min cavitation is becoming established and sudden impulsive peaks can be expected in the signal.

9.4 Spectrum analysis

The time domain hydroacoustic signals were converted to the frequency domain using a FFT method. Figure 9-8, shows the hydroacoustic spectrum of the pump flow. It is clear from Figure 9-8 that the hydrophone signal contains very little information above about 1kHz.

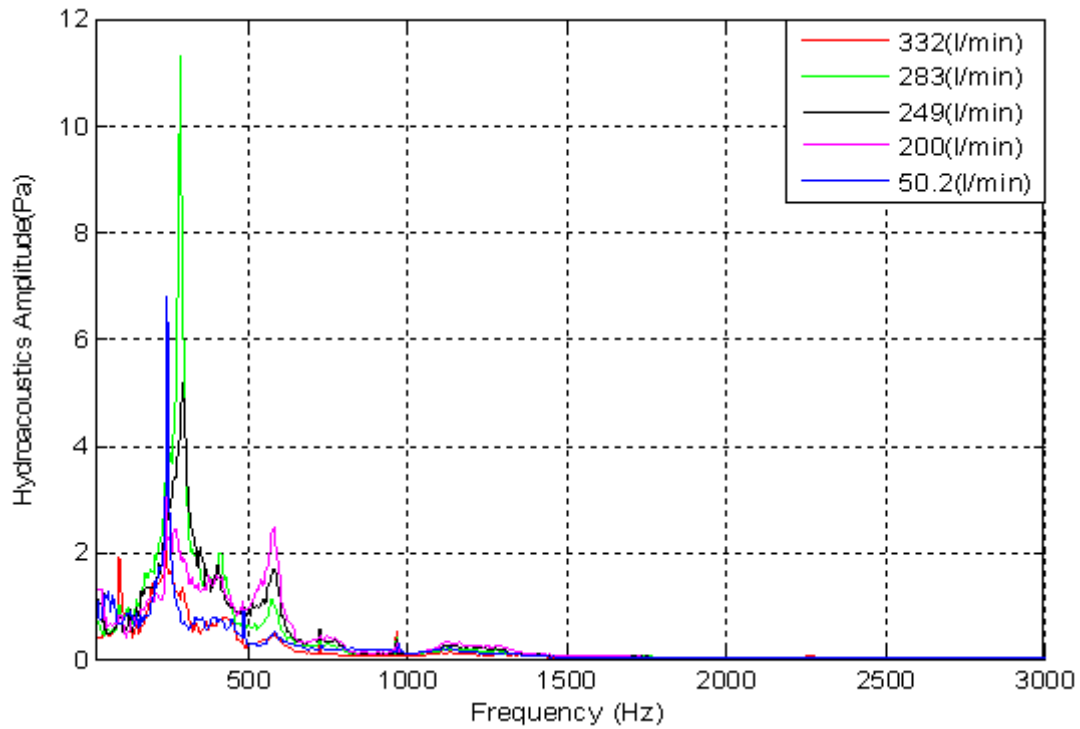


Figure 9-8 (a) Spectra (20 Hz – 3 kHz) of the hydroacoustic signal from pump for different flow rates

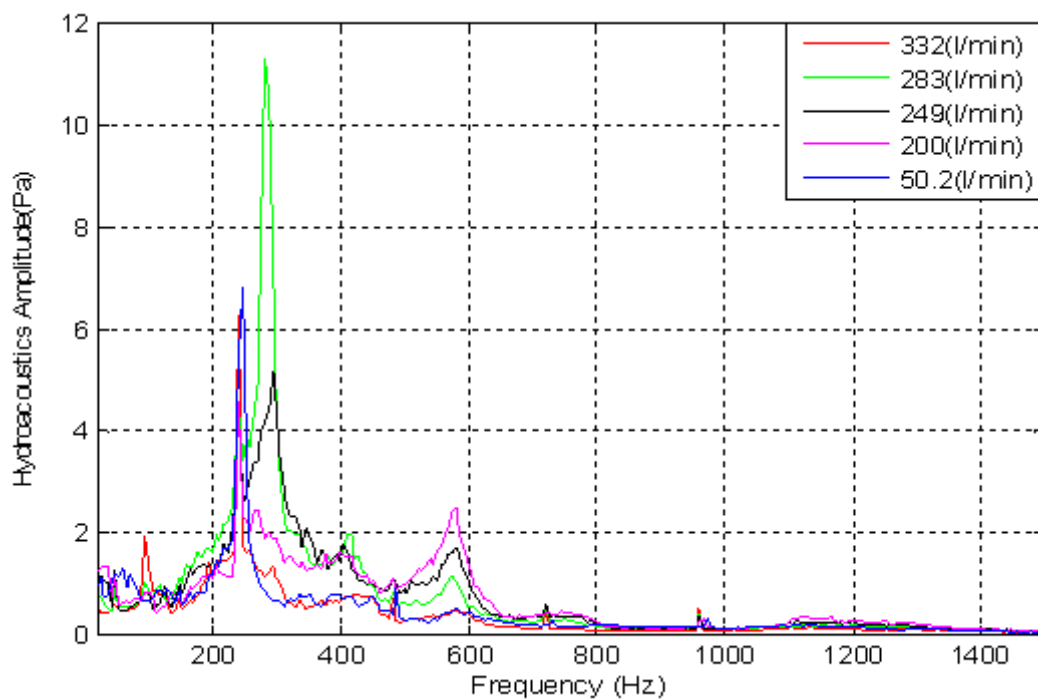


Figure 9-8 (b) Spectra (20 Hz – 1.5 kHz) of the hydroacoustic signal from the pump for different flow rates

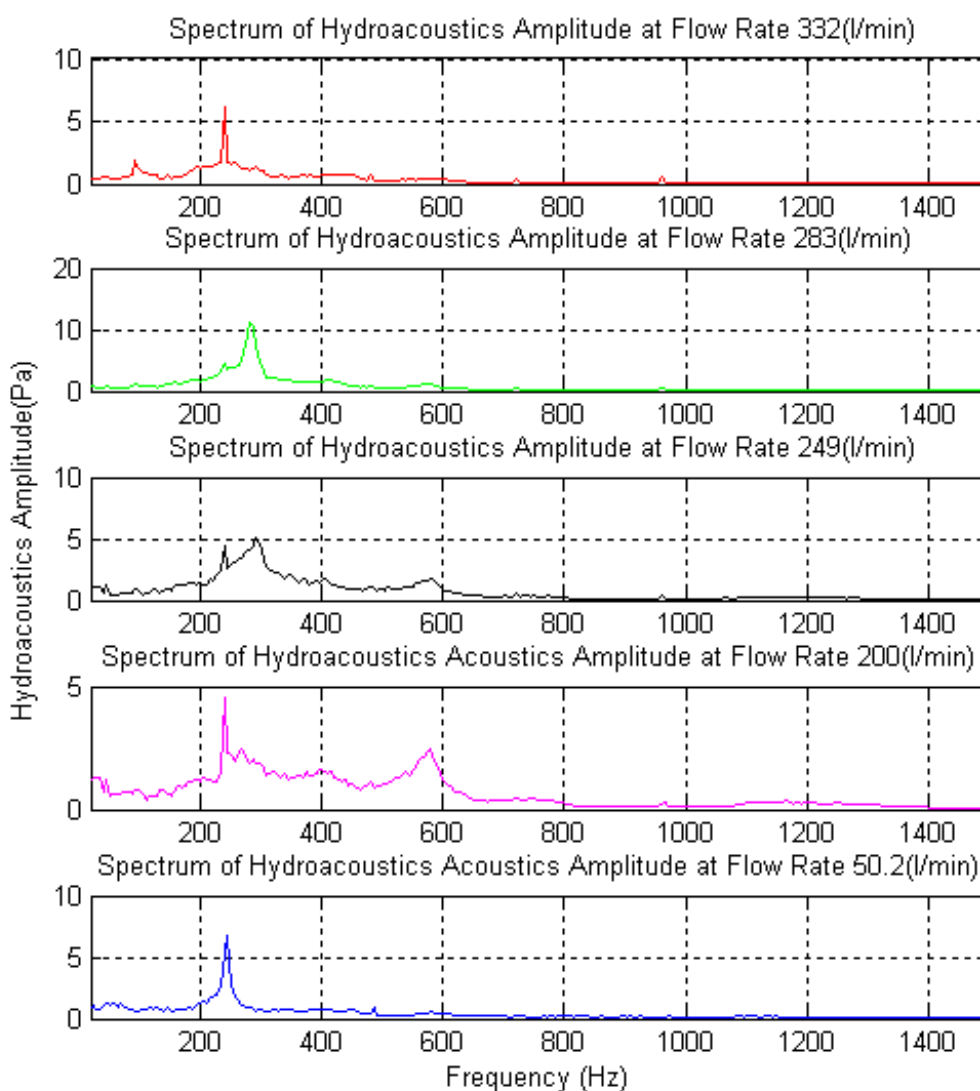


Figure 9-8 (c) Frequency spectra of the hydroacoustic signal at specific flow rates

9.4.1 Baseline spectrum analysis

Once again, for convenience, the spectrum has been divided into three parts: 20 Hz to 1 kHz, 1 kHz to 1.5 kHz and 1.5 kHz to 3 kHz, see Figures 9-10, 9-11 and 9-12 respectively, all of which are for the base line flow rate of 249 l/min. These again confirm the presence of discrete component characteristics due to the interaction of the rotor blades with nearby stationary objects and periodicities in the flow generated by the pump's rotor blades. Figure 9-9 again shows that these discrete components have much higher amplitudes than the background noise. Clearly the major peaks in the spectrum occur below 1 kHz, in particular

at 242 Hz (blade passing frequency and fifth harmonic of the RF) and 290 Hz (sixth harmonics of the RF).

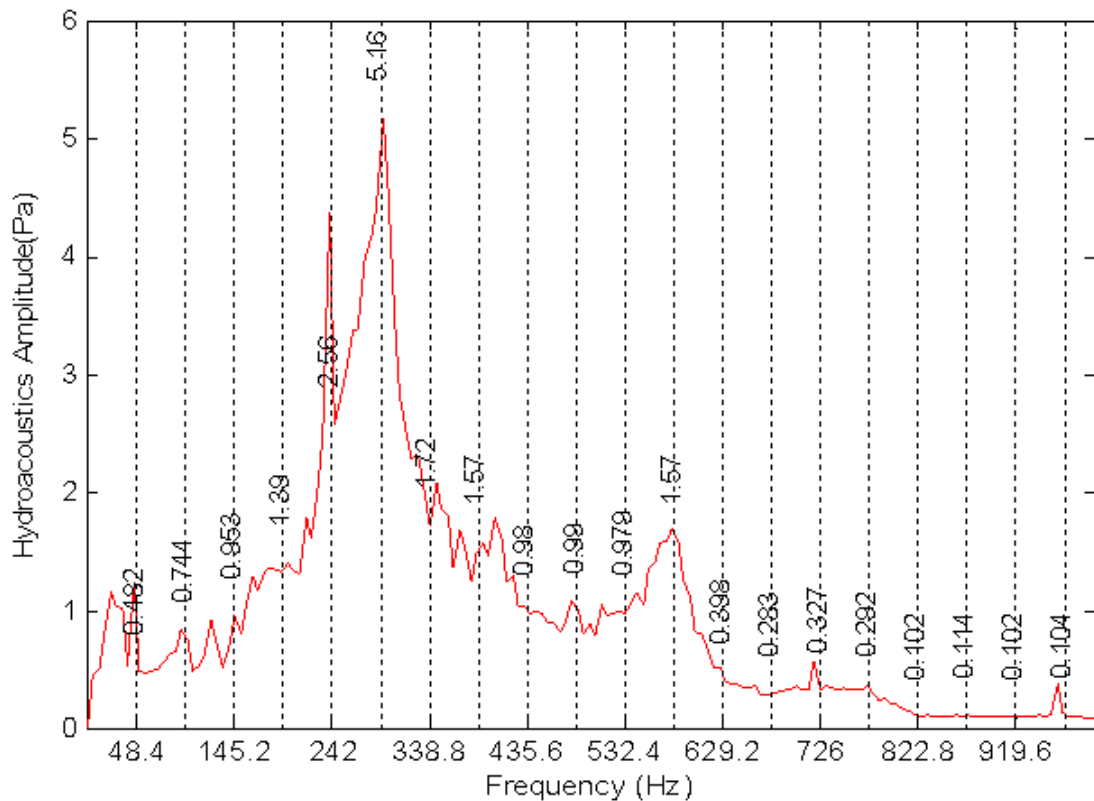


Figure 9-9 Baseline hydroacoustic spectrum (20 Hz-1 kHz) for flow rate 249 l/min)

Figure 9-10 shows that in the frequency range 1 kHz to 1.5 kHz, there are discrete components due to structural resonance at 1113 and 1201 Hz, which stand out well above the broad peak which exists between about 1050 and 1300 Hz. However these peaks are only one twentieth the magnitude of the peak at 290 Hz. Figure 9-11 is the baseline spectrum for the range 1.5 kHz to 2 kHz. Structural resonances are present but are not obvious being only a few percent of the magnitude of the peak at 290 Hz.

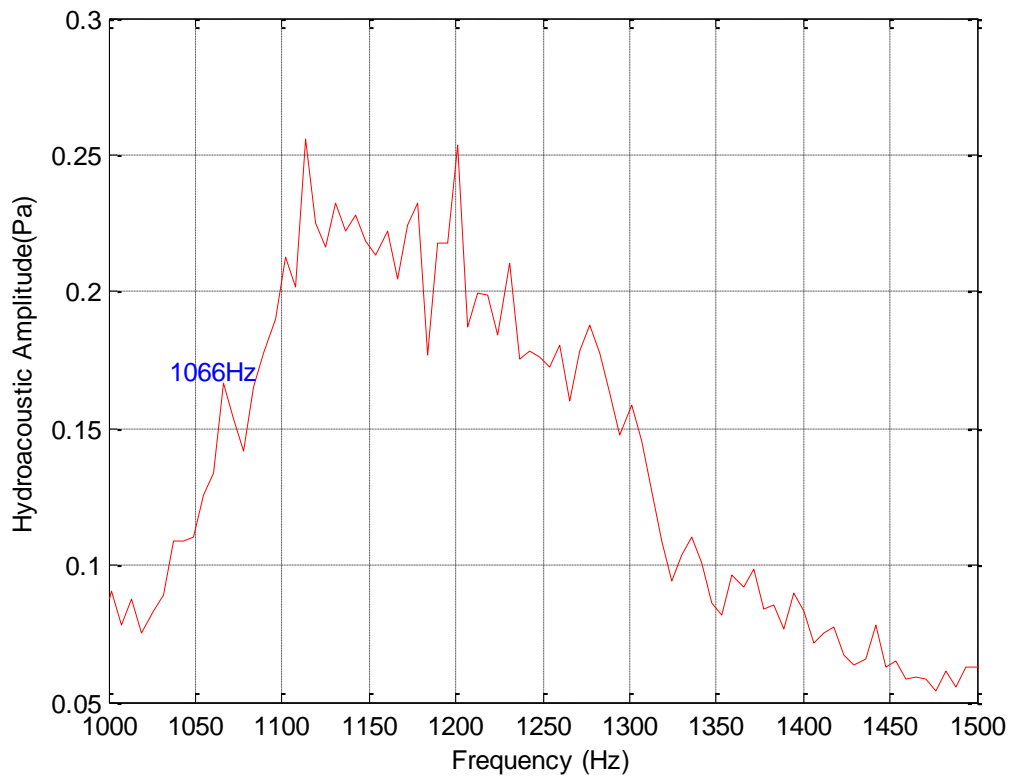


Figure 9-10 Baseline spectrum of hydroacoustic signal (1 kHz-1.5 kHz) for flow rate 249 l/min

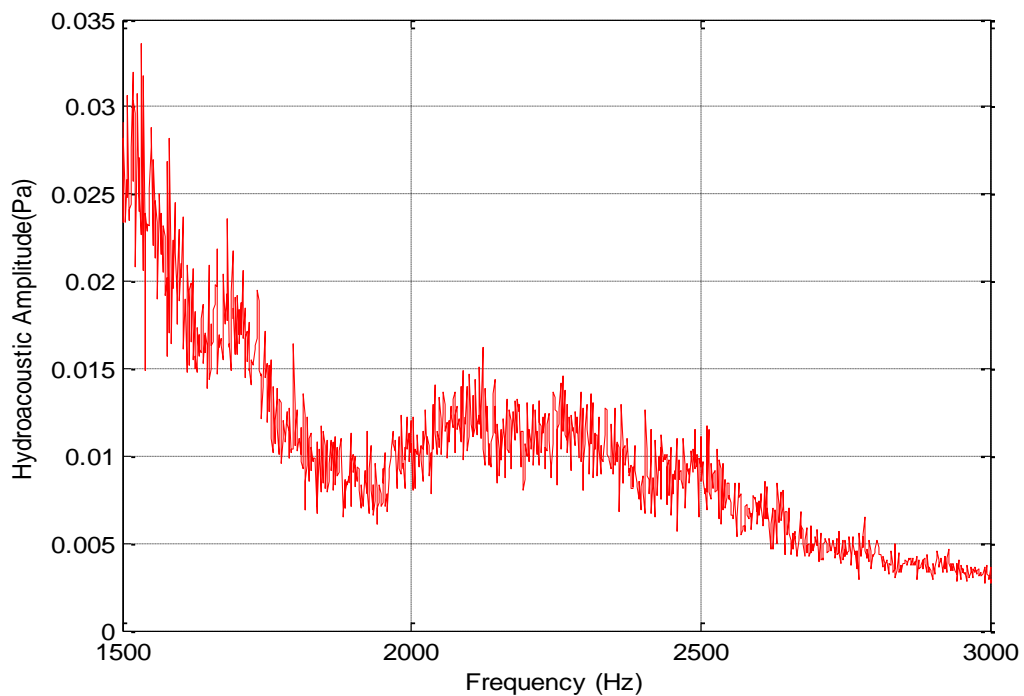


Figure 9-11 Baseline spectrum of hydroacoustic signal (1.5 kHz-3 kHz) for flow rate 249 l/min

9.4.2 Spectral amplitude characteristics

Each of the three hydroacoustic spectra was used to produce a waterfall of the signal for different flow rates, see Figures 9-12, 9-13 and 9-14.

Frequency range 20 Hz-1 kHz

Figure 9-12 shows the waterfall for the hydroacoustic spectrum for flow rates from 10 l/min to about 370 l/min. Apart from the peak at 242 Hz, the spectrum is pretty flat and remains like that until the flow rate reaches approximately 250 l/min when there is an increase in the 6th RF harmonic around 290Hz which rapidly grows into a peak that dominates the spectrum. The emergence of this peak is indicative of the onset of cavitation but further work is needed to determine its rate of growth and just how limited its application will be, because it is clearly system specific.

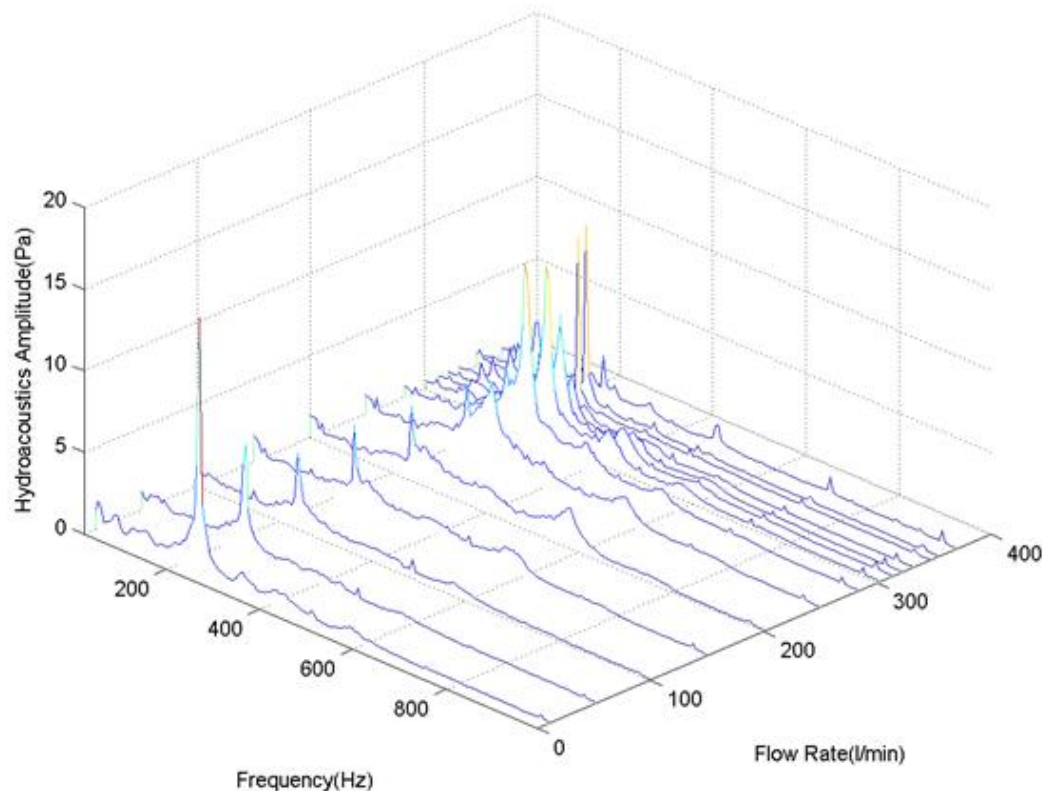


Figure 9-12 Waterfall for time-averaged Peak amplitude of hydroacoustic signal 20 Hz – 1 kHz

Frequency range 1kHz-1.5kHz

Figure 9-13 shows the waterfall for the hydroacoustic spectrum in the frequency range 1 kHz to 1.5 kHz. A broad peak begins to appear between about 1000 Hz and 1200 Hz which increases in amplitude and widens as the flow increases. It may well be that if the energy of this peak – measured using RMS or Peak value or area under the curve - exceeds a certain set

level that could be taken as an indication of the onset of cavitation, but such an indicator would, of course, be pump specific.

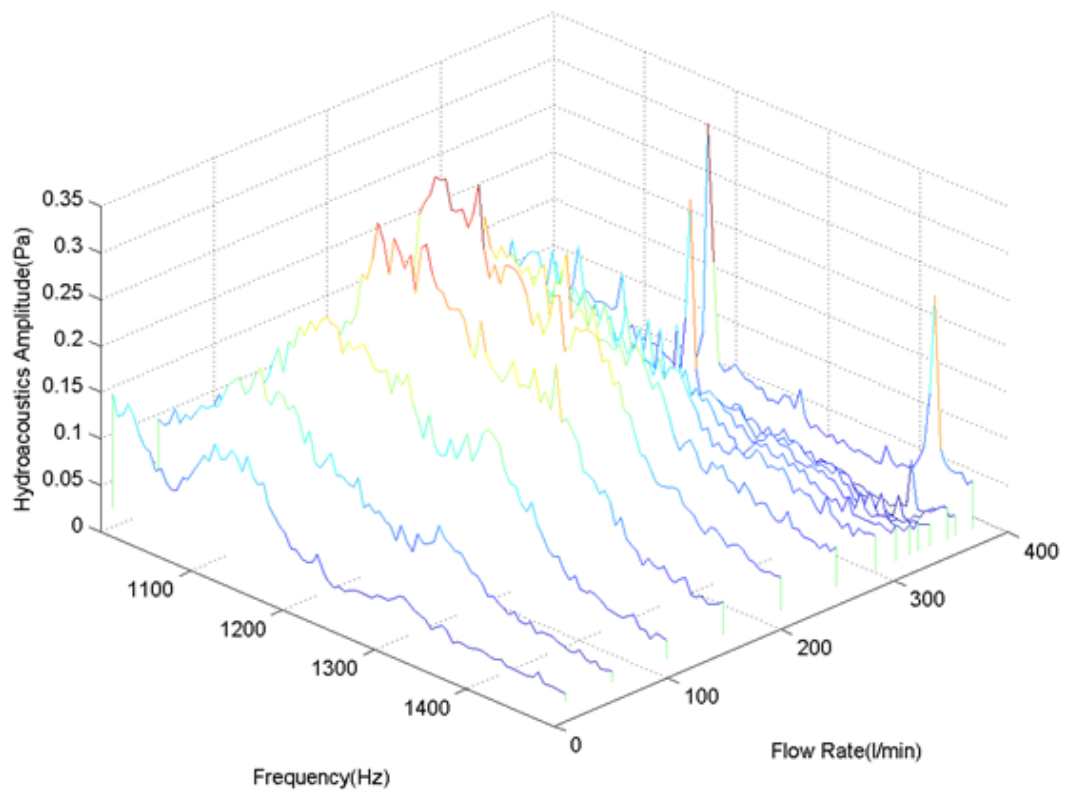


Figure 9-13 Waterfall for time-averaged Peak amplitude of hydroacoustic signal 1 kHz – 1.5 kHz

Frequency range 1.5 kHz-3 kHz

Figure 9-14 show the waterfall of the fluid acoustic spectrum for the frequency range 1.5kHz – 3kHz. It is clear that, compared to the two waterfalls shown above in Figures 9-12 and 9-13, there is a little to indicate the onset of cavitation. The small peaks that do appear at about 2.2 kHz are indicators of established cavitation and not incipient cavitation.

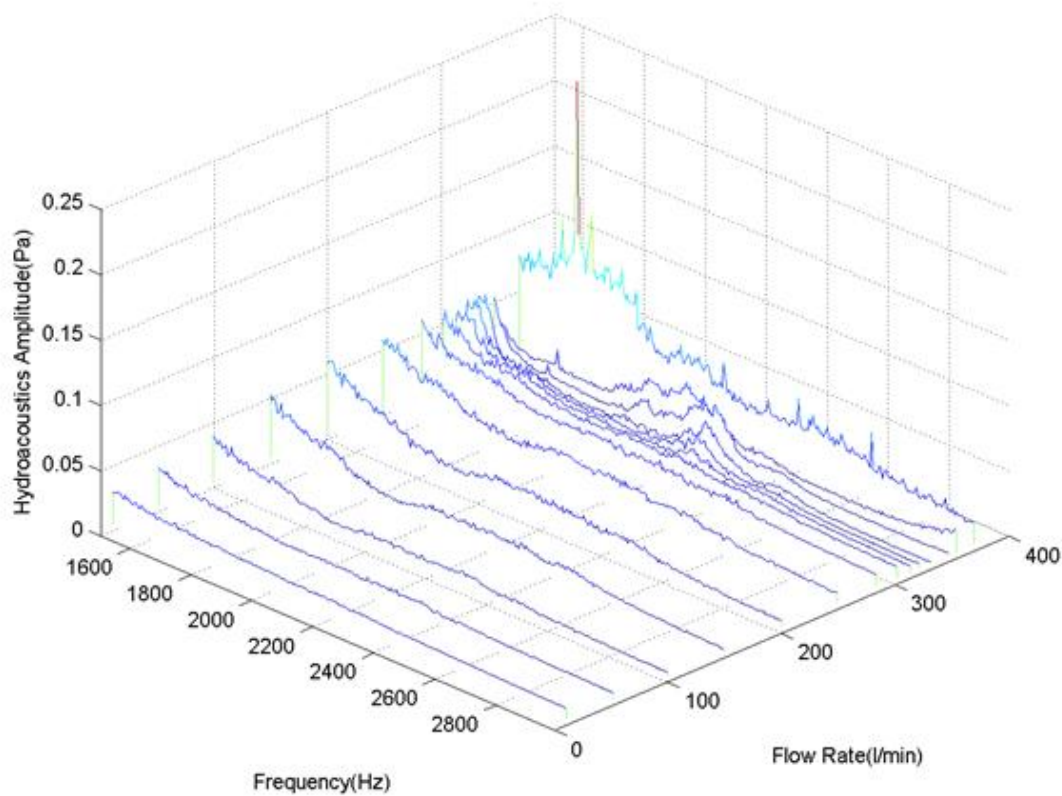


Figure 9-14 Waterfall for time-averaged Peak amplitude of hydroacoustic signal 1.5 kHz – 3 kHz

9.5 Statistical measures from the frequency domain

9.5.1 Spectral crest factor

Figure 9-15 shows the values of Crest factor for the hydroacoustic spectrum. It can be seen that the Crest factor is a clear minimum just before the onset of cavitation. The increase in the value of the Crest factor after this minimum should be useful in determining the onset of cavitation, and is one of the clearest indicators found in this investigation. This needs further investigation to determine whether the phenomenon is system specific.

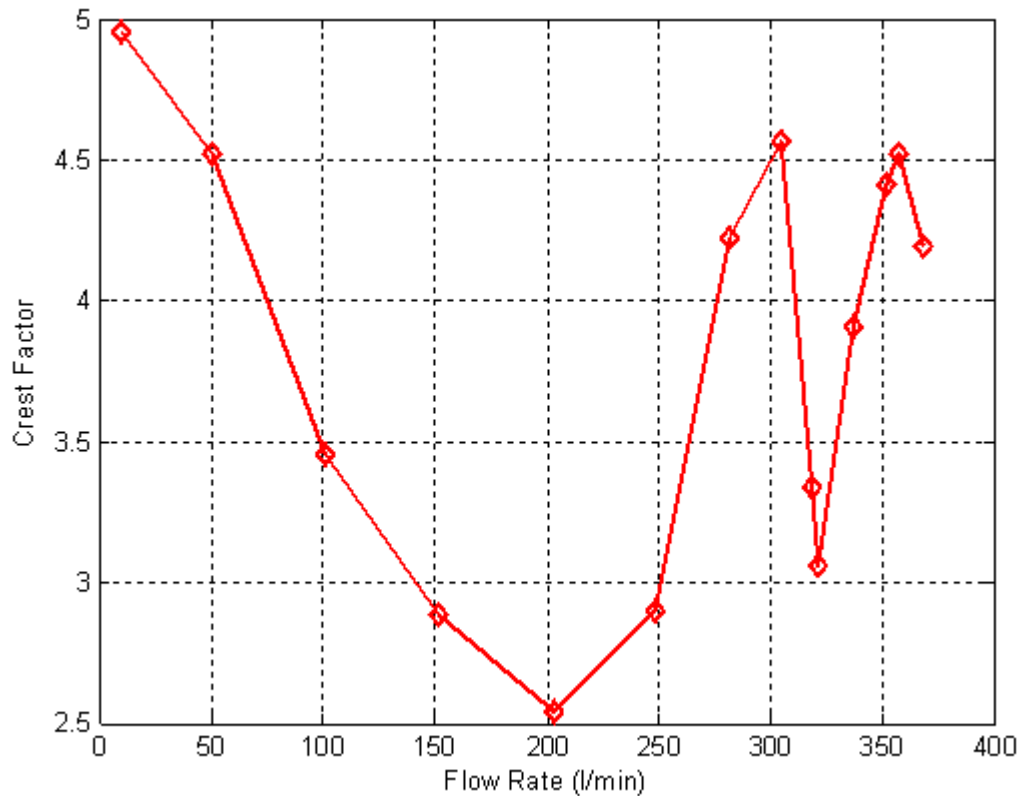


Figure 9-15 Crest factor of hydroacoustic spectra (20 Hz to 1.5 kHz) for different flow rates

9.5.2 Spectral kurtosis

Figure 9-16 shows the values of Kurtosis obtained from the individual spectra as a function of flow rate. The curve is a very similar in shape to that for the Crest factor, with a definite minimum in the flow region 200-250 l/min. Thus detection of this minimum would be a good method for determining the onset of cavitation. The precise position of the minimum needs to be confirmed by further work in other systems to ensure it does occur generally with the onset of cavitation.

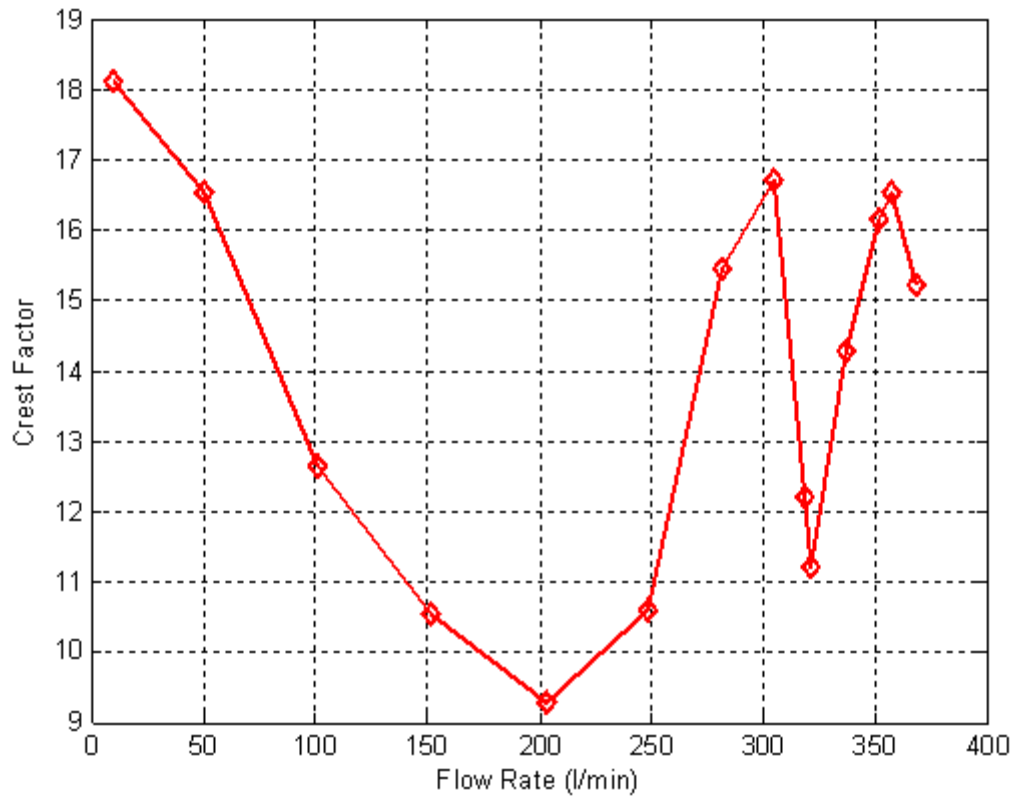


Figure 9-16 Kurtosis of hydroacoustic spectra (20 Hz to 1.5 kHz) for different flow rates

9.5.3 Spectral entropy

Figure 9-17 shows the spectral entropy as a function of flow rate. The spectrum appears to reach a peak at about 200 l/min, after which it first falls slowly and then falls more rapidly. The detection of this peak would be a method for detecting the onset of cavitation but, of course, needs to be confirmed for other systems. The oscillation in value of the spectral entropy at higher flow rates also needs to be confirmed.

.

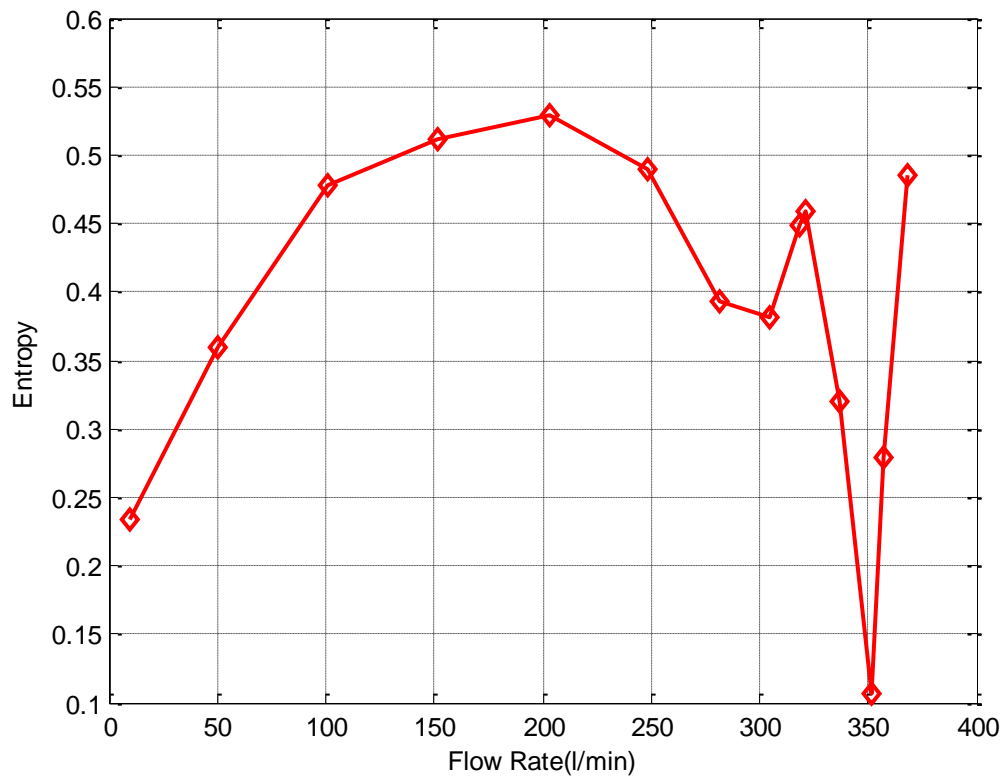


Figure 9-17 Spectral entropy of hydroacoustic spectra (20 Hz to 1.5 kHz) for different flow rates

The next chapter, Chapter 10 is the conclusions and suggestions for future work. It compares and evaluates the different techniques and statistical parameters used in this thesis for the detection and diagnosis of the onset of cavitation in a centrifugal pump. In particular the relative performance of hydroacoustic and capacitive methods will be given there.

CHAPTER TEN

10. Conclusions and suggestions for further work

The chapter compares and evaluates the different techniques used in this thesis for the detection and diagnosis of the onset of cavitation in a centrifugal pump. The efficacy of the different statistical parameters used to analyse the vibration, airborne acoustic, and hydroacoustic signals and conclusions are drawn on which are the most useful. Conclusions are also drawn on the progress made developing a capacitive sensor. The contributions to knowledge made by the researcher are presented as are suggestions for possible future work.

10.1 Review of aims and objectives

This section reviews the objectives and achievements of the research, by comparing them one by one to the objectives for this study presented in Chapter 1.

The main objectives and achievements of this research were:

Objective one: To describe the dynamics of centrifugal pumps, and the processes by which cavitation is generated

Achievement one: The construction and dynamics of centrifugal pumps is dealt with extensively in Section 1.2 and the first part of Section 2.2 the processes by which cavitation is generated and the types of cavitation are described in Section 2.4 (including cavitation as a system problem) and consequent damage to the system is presented in Section 2.5.

Objective two: To present and discuss the applications of machine health monitoring.

Achievement two: The general benefits of CM of machine health are presented as part of Section 1.3, Research motivation in Section 1.4, the review of the literature showed that this concept is well understood and universally accepted, thus it was not considered necessary to repeat the arguments again in this thesis.

Objective three: To review conventional methods of monitoring pumps and detecting cavitation.

Achievement three: Presents a review of the most common of the CM methods for the detection of cavitation: visual, in Section 3.1 vibration measurement, in Section 3.3 airborne sound, waterborne sound (hydrophone) in Section 3.2 and acoustic emission in Section 3.4. Statistical analysis of the signals from the latter four methods is becoming increasingly common in an effort to find a feature that defines cavitation. The more common statistical parameters (features) are defined and their possible application discussed in Section 3.5.3 and 3.7.2.

Objective four: To produce a new method for the detection of vapour bubbles in the flow that can be used alongside conventional methods. This novel sensing approach will be based on advances of sensor and material technologies and should be more sensitive and convenient than current methods.

Achievement four: The novel idea that capacitance measurement could be used to detect cavitation is first suggested in Section 3.3. It was then developed as a concept in Sections 5.2, 5.3 and 5.4 which describe how the idea came to this author and the principles of its use. Sections 6.1, 6.2, 6.3 and 6.4 describe the successful experimental testing of the capacitance sensor assembly.

Objective five: To design and build a test-rig that will allow the controlled onset of cavitation in a centrifugal pump, and allow the study of different pump parameters that may be used for cavitation detection and diagnosis. These parameters will include the signals obtained from pump vibration, pump airborne and waterborne noise and the signal from any new method developed.

Achievement five: The test rig facility and data acquisition system was developed as reported in Chapter 4. The system is re-circulatory, see Figure 4-4, driven by a Pedrollo F32/200HA general purpose centrifugal pump with speed control. Table 4-1 shows the component parts used in the construction of the system, and Section 4.3 lists the instrumentation attached to the system: paddle wheel meter for water flow, general purpose industrial pressure transducers for pipe pressure, precision accelerometers for vibration measurement, a precision microphone for airborne sound, a type one inch precision hydrophone for waterborne noise, and a miniature encoder for pump shaft speed. The data acquisition system was a Sinocera YE6230B combined with a CED 1401-Plus. The position of the capacitance sensor in the system is shown in Figure 5-7.

Objective six: To evaluate the pump system experimentally in terms of operational fault induction capability.

Achievement six: Cavitation was introduced into the system by progressively closing the valve in the discharge line with the valve in the supply line fully open, Figure 4-4. This is equivalent to increasing the value of the friction head (H_f) in Equation 2.4 and so reducing the value of the NPSHA. Cavitation was clearly present at flow rate of 249 l/min, and established cavitation was occurring at about 339 l/min (when the head is 6.7m). However, this is only an average value, inside the working pump there will be areas of higher and lower pressures, so we would expect the onset of cavitation to occur before 249 l/min. Cavitation was simulated with the capacitive sensor by including an air inlet valve in the pump supply

line. Because the pressure on the suction side of the pump is lower than ambient, air is “drawn into” the system, see Figure 6-3.

Objective seven: To process and analyse the data outputs from the accelerometers, microphone, hydrophone and any newly developed vapour bubble sensor. The analysis of data will be performed in time and frequency.

Achievement seven: The principles of the data collection and analysis are as shown schematically in Figures 4-29 and 4-30. The output from the sensor (e.g. from microphone or accelerometer pre-amplifier or from spectrum analyser for the capacitance device) is fed into the DAQ where it was sampled at 96 kHz for 10 seconds. The data was fed to the computer where Matlab performed statistical analyses both in the time, and frequency domains produced frequency waterfalls against flow rate and stored the data.

Objective eight: To perform a relative evaluation of the different methods and statistical techniques to ascertain which are most promising for the detection of the onset of cavitation in the given system.

Achievement eight: The four methods are discussed in Sections 10.3 and 10.4 with their relative advantages and disadvantages, as are the statistical features examined.

10.2 Conclusions on merits of the detection techniques

Cavitation is a phenomenon that is marked by high noise and vibration levels and so determination of established cavitation is not a problem. However, the determination of the onset of cavitation is quite something else. Here, it is necessary to confidently determine a small signal in high background noise.

Four separate techniques for the detection and diagnosis of cavitation in a centrifugal pump have been investigated; measurement of the vibration, airborne acoustic and hydroacoustic signals, and determination of the change in resonant frequency of a circuit containing a capacitance across the outlet pipe of the pump, see Chapters 6, 7, 8 and 9, respectively. Measurements were carried out using time, frequency, and frequency waterfalls against flow rate analyses of the signals from the sensors attached to the pump system. This chapter reviews the results obtained and draws conclusions on the relative merits of the four systems.

First the results obtained from the traditional methods are presented, followed by those from the capacitive system suggested and developed by the author.

Because the different methods are being compared it is better if their relative merits are presented and discussed according to the feature used to identify the presence of cavitation. Thus this chapter begins by examining the results obtained in the time domain, then frequency domain and finally frequency waterfalls against flow rate domain for vibration, airborne acoustic and hydroacoustic signals. Those best suited to detect the onset of cavitation are identified, and later possible further work for their improvement is suggested.

A capacitive sensor has been built and tested. The device has been shown to detect the presence of air bubbles in water flow but, unfortunately, at this stage of its development it does not match in sensitivity any of the other three methods tested, see suggestions for future work.

A flow rate of 249 l/min was found to be a flow rate at which cavitation was first definitely detected, while at a flow rate of 345 l/min cavitation was well established. Thus if a detection system responded at about 249 l/min it detected the early stages of cavitation, if clearly responded between 250 l/min and 350 l/min it was detecting developing cavitation and if responded above about 350 l/min it was detecting established cavitation. To detect the *onset* of cavitation a measuring system needs to respond unambiguously at or before 250 l/min.

10.3 Conclusions regarding time domain features

In this section the term “normalised” means simply that the actual values were divided by the corresponding maximum values so that vibration, airborne and waterborne signals all had the same maximum value of 1.

10.3.1 Probability density function

Figure 10-1 presents the PDF data for each the three traditional methods normalised to the maximum reading obtained for that set of data. Figure 10-1 shows a clear change in the time domain of the signal as the flow increased for all three signals; there is an initial broad peak followed by a decrease in amplitude. The vibration signal shows most clearly a relatively steeper drop in amplitude as the flow approaches 249 l/min. From Figure 10-1 it can be concluded that the PDF of the vibration signal for an accelerometer on the pump is the best of the three methods and could be a good indicator of the early stages of cavitation though, as will be suggested later a fusion of waterborne and vibration PDF data could give an earlier

and more confident diagnosis. These results need to be confirmed as a general phenomenon and not system specific.

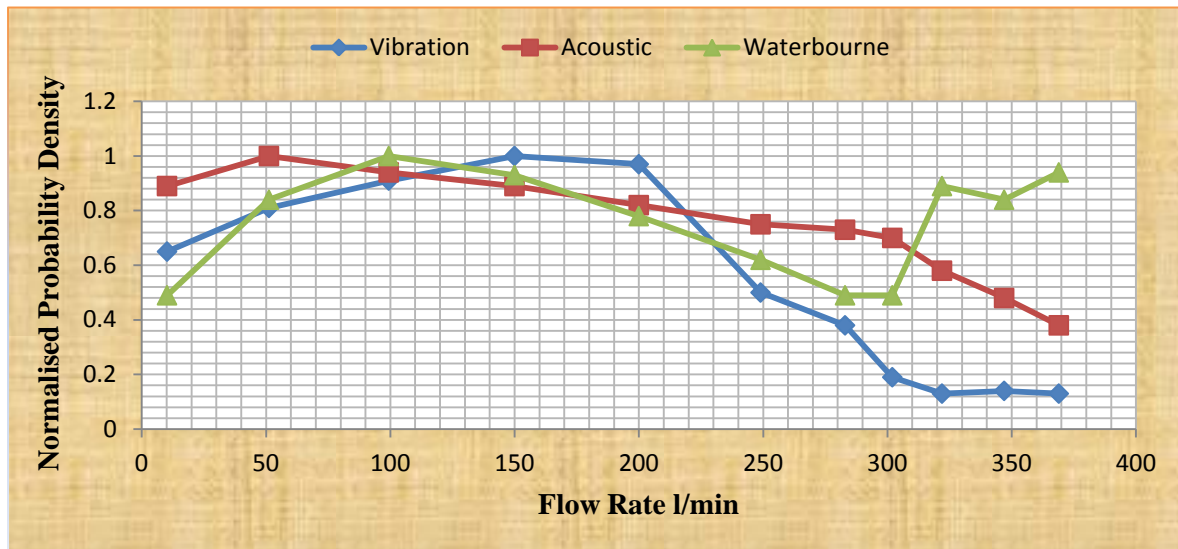


Figure 10-1 Normalised Probability Density for vibration, airborne acoustic and hydroacoustic time domain signals against flow rates in the range 10.5 l/min to 369 l/min

10.3.2 Peak value

Figure 10-2 presents the time averaged Peak values of the signal for each the three traditional methods normalised to the maximum reading obtained for that set of data. Figure 10-2 shows a clear change in the Peak values of the time domain of the signal as the flow increased for all three signals; there is an initial trough followed by an increase in amplitude. The hydrophone signal shows a minimum value at about 100 l/min after which the peak value increases and the maximum value obtained from the hydrophone occurs at about 300 l/min which is before cavitation is fully established. The vibration signal has a minimum at about 150 l/min and its steepest increase once the flow has passed 249 l/min. It is again concluded that a fusion of signals could prove a useful indicator that cavitation is present in a system but not yet fully established.

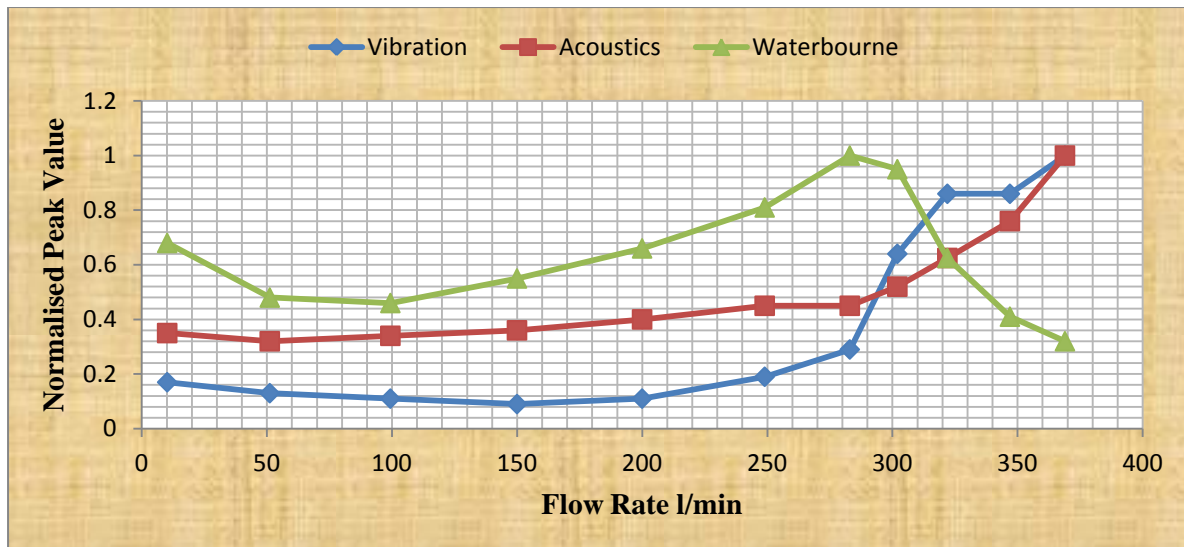


Figure 10-2 Normalised Peak values for vibration, airborne acoustic and hydroacoustic signals against flow rates in the range 10.5 l/min to 369 l/min

10.3.3 RMS value

Figure 10-3 presents the RMS values of the signal for each of the three traditional methods normalised to the maximum reading obtained for that set of data. Figure 10-3 shows the same general trends as Figure 10-2; there is an initial trough followed by an increase in amplitude. The hydrophone signal shows a minimum value at about 100 l/min after which the peak value increases and the maximum value obtained from the hydrophone occurs at about 280 – 300 l/min which is before cavitation is fully established. The vibration signal has the steepest rise in amplitude once the flow has passed 200 l/min. Once again the conclusion is that a combination of waterborne noise and vibration signals could prove a useful indicator that cavitation is present in a system but not yet fully established.

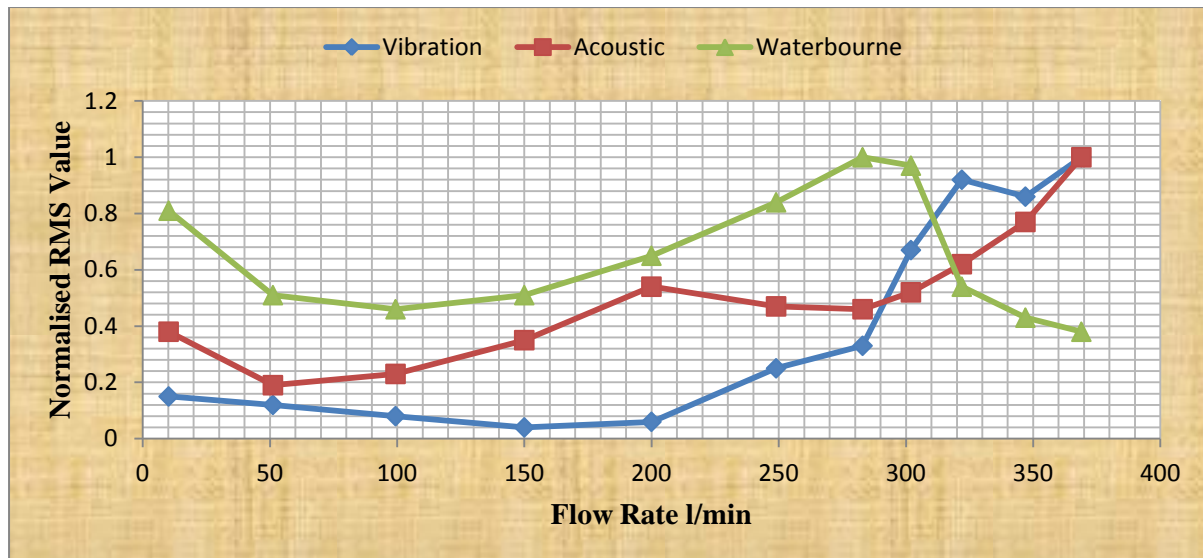


Figure 10-3 Normalised RMS values for vibration, airborne acoustic and hydroacoustic signals against flow rates in the range 10.5 l/min to 369 l/min

Since Peak and RMS values for a signal are related (in the case of a sine wave, of course, $V_P = V_{RMS}\sqrt{2}$) it is not surprising that the two parameters give similar results. But as we are dealing with relatively complex signals it is to be expected that the two quantities will differ in their details. Crest factor is not included in this chapter as it is the peak value divided by the corresponding RMS value and added nothing qualitatively new to the discussion.

The conclusions regarding the effectiveness of kurtosis of the time domain signal as a measure of incipient cavitation was that at flow rates below about 250 l/min the value of the kurtosis was close to zero. That as cavitation developed and became established, impulsive peaks occurred in the time domain which increased the value of the kurtosis, but this fact meant that kurtosis was a good marker for established cavitation but not for incipient cavitation.

10.4 Conclusions regarding frequency domain features

10.4.1 Spectral crest factor

Figure 10-4 presents the spectral Crest factor (SCF) of the spectrum of the signal for each the three traditional methods normalised to the maximum reading. The SCF for the vibration and acoustic signals are very similar with a broad peak at low flow rates followed by a more or less gradual decrease. The SCF for the vibration signal drops away more quickly and thus might be said to be a better measure of existing cavitation. However, the SCF of the hydrophone signal shows a clear minimum just before the onset of noticeable cavitation,

followed by an increase in the SCF value which is quite different from the other two signals. The conclusion is that this minimum and subsequent increase in the SCF for the hydrophone signal is very promising as an indicator of incipient cavitation.

It should be noted that the frequency ranges for the three signals were not the same because the signal from the hydrophone contained virtually no information above about 1500 Hz so only the frequencies below 1500 Hz were included here.

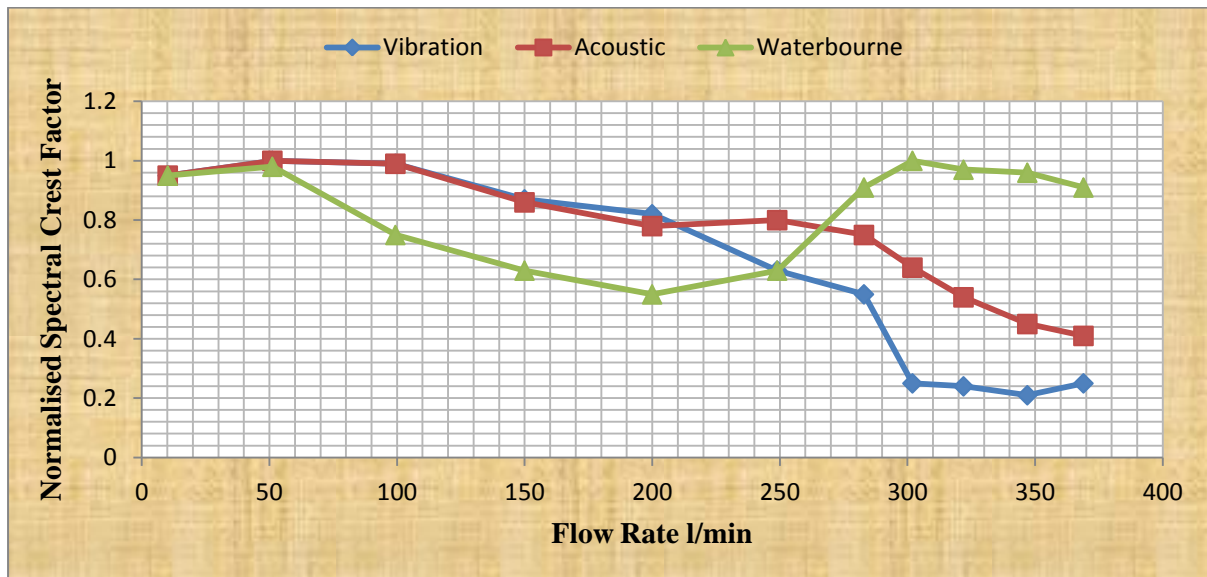


Figure 10-4 Normalised spectral Crest factor for vibration, airborne acoustic and hydroacoustic signals against flow rates in the range 10.5 l/min to 369 l/min

10.4.2 Spectral kurtosis

Figure 10-5 presents the Kurtosis of the spectrum of the signal for each of the three traditional methods normalised to the maximum reading. The Kurtosis for the vibration and acoustic signals show a very similar broad peak up to a flow rate of about 250 l/min, after which the vibration signal falls away quite rapidly. The Kurtosis is the better measure for existing cavitation. However, the trend for the Kurtosis of the hydrophone signal is to decrease gradually to about 250 l/min, after which there is a clear increase in the value of the Kurtosis which is quite different from the other two signals. It is concluded that for kurtosis the change in gradient from negative to positive is very promising as a possible indicator of the early stages of cavitation.

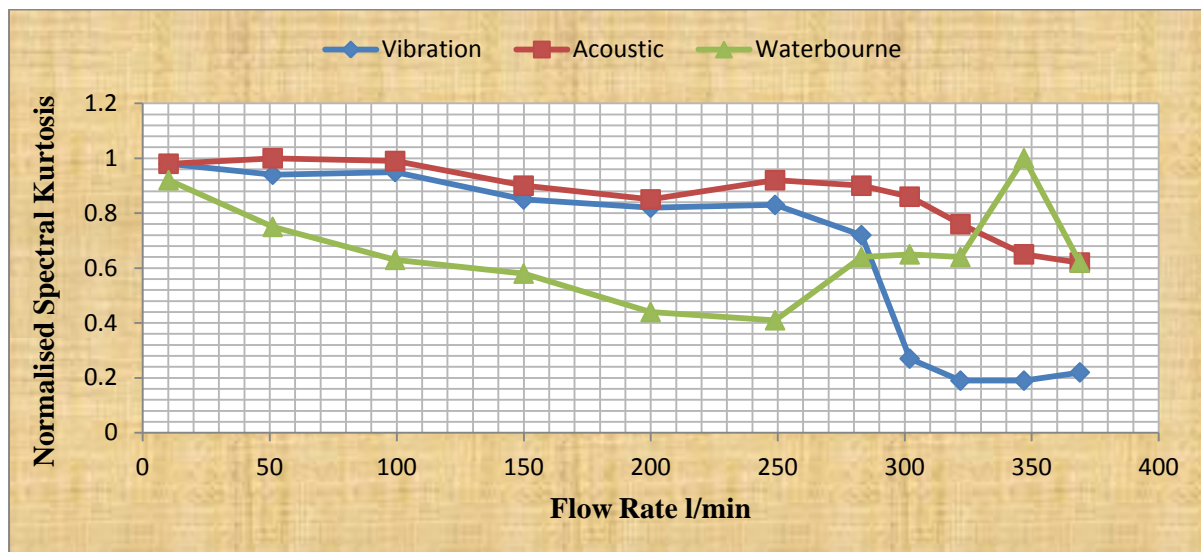


Figure 10-5 Normalised Spectral Kurtosis for vibration, airborne acoustic and hydroacoustic signals against flow rates in the range 10.5 l/min to 369 l/min

10.4.3 Spectral entropy

Figure 10-6 presents the results for Spectral Entropy of the spectrum of the signal for each of the three traditional methods normalised to the maximum reading. While the three curves may look similar, there are important differences. The general conclusion reached was that each of them, in its own way might be used to indicate the early stages of cavitation.

The vibration signal shows a broad minimum centred on about 150 l/min, after which it increases to a maximum value at about 300 l/min. The change of gradient from negative to positive could be an indication of the very beginning of cavitation. The levelling out of the trend would be an indication of the presence of established cavitation.

The Spectral Entropy of the signal from the microphone shows a maximum at about 150 l/min, followed by a minimum at about 250 l/min rising to a maximum at about 325 l/min.

The Spectral Entropy of the signal from the hydrophone rises to a clear maximum at about 200 l/min, and falls to a minimum at about 300 l/min. The maximum at 200 l/min could be an indication of incipient cavitation and the change in gradient from negative to positive at about 280 – 300 l/min would be an indicator of the early stages of cavitation.

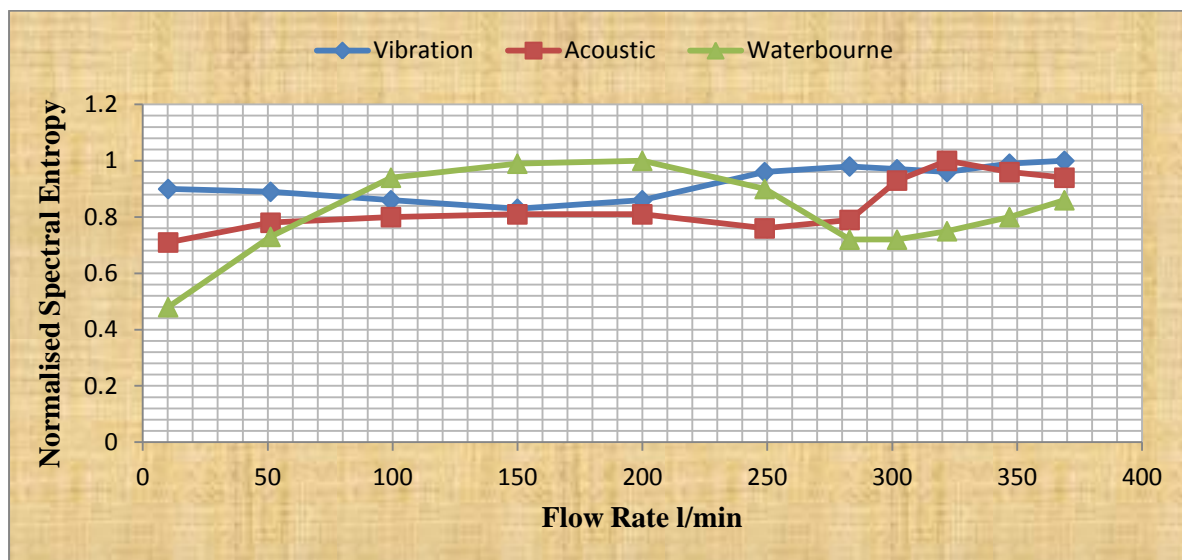


Figure 10-6 Normalised spectral entropy for vibration, airborne acoustic and hydroacoustic signals against flow rates in the range 10.5 l/min to 369 l/min

10.5 Spectral amplitude characteristics

Figures 7-12, 8-12 and 9-12 show the frequency domain “waterfalls” for the vibration, airborne and waterborne signals. Each of these three figures is for the lowest frequency range 20Hz to 1kHz examined as this appears (to the eye) to contain the most useful information. For the vibration signal there is a gradual increase in the spectrum level when the flow rate approaches 200 l/min, with the appearance of a clear peak at about 340Hz which could be a good indicator of incipient cavitation. The same peak appears in the airborne acoustic signal and is distinct at 249 l/min.

This particular frequency might be specific to this pump, but the principle that an individual component of the frequency might be a suitable indicator has already been proposed by Cudina (2003). In the vibration spectrum a subsidiary peak at 435 Hz appears at about 150 l/min and becomes more distinct with the onset of cavitation. This peak is a possible complementary indicator for incipient cavitation.

The hydrophone signal shows only one significant peak at 242 Hz for flow rates from 10 l/min to about 250 l/min, after which there is an increase in the 6th RF harmonic around

290Hz which rapidly grows into a peak that dominates the spectrum. For this system the emergence of this peak is indicative of the onset of cavitation. However, further work is needed to determine its rate of growth and just how wide its application could be.

Without considerable training and experience it is unlikely that human observation of the “waterfalls” will produce a useful method of detecting the onset of cavitation, see below in suggestions for future work.

10.6 Progress with capacitive sensor

The statistical methods extract useful information from the signal using mathematical techniques. In that sense they are an indirect measurement of the onset of cavitation. In contrast, the capacitance method is direct. The signal itself, the resonant frequency, is the measure of whether cavitation is present. This is a big advantage for this method.

It has been demonstrated that a void fraction sensor based on the change in value of the average dielectric constant between the plates of a capacitor is possible, see Figures 6-7, 6-8 and 6-9. It can be seen in Figure 10-7, reproduced below, that the presence of cavitation vapour bubbles in the flow is detected. The curve shown in Figure 10-7, for the 534 MHz resonant frequency demonstrate a small but definite change in the resonant frequency by the time flow rate has reached 249 l/min, and an obvious change after about 300 l/min. We know that small vapour bubbles are present in the flow below 249 l/min, but that there are not many of them (otherwise they would be visible). The capacitance method appears sensitive to the presence of these bubbles as can be seen by the slight positive gradient of the curve between about 150 l/min and 280 l/min. This is the region of incipient cavitation leading up to readily observable cavitation. Above about 300 l/min the gradient of the curve increases sharply as the cavitation becomes fully established. We can say definitely that measurement of the resonant frequency of the LCR circuit is confirmed as a method of detecting cavitation in a pipe system, and that it is a promising method for the detection of the onset of cavitation.

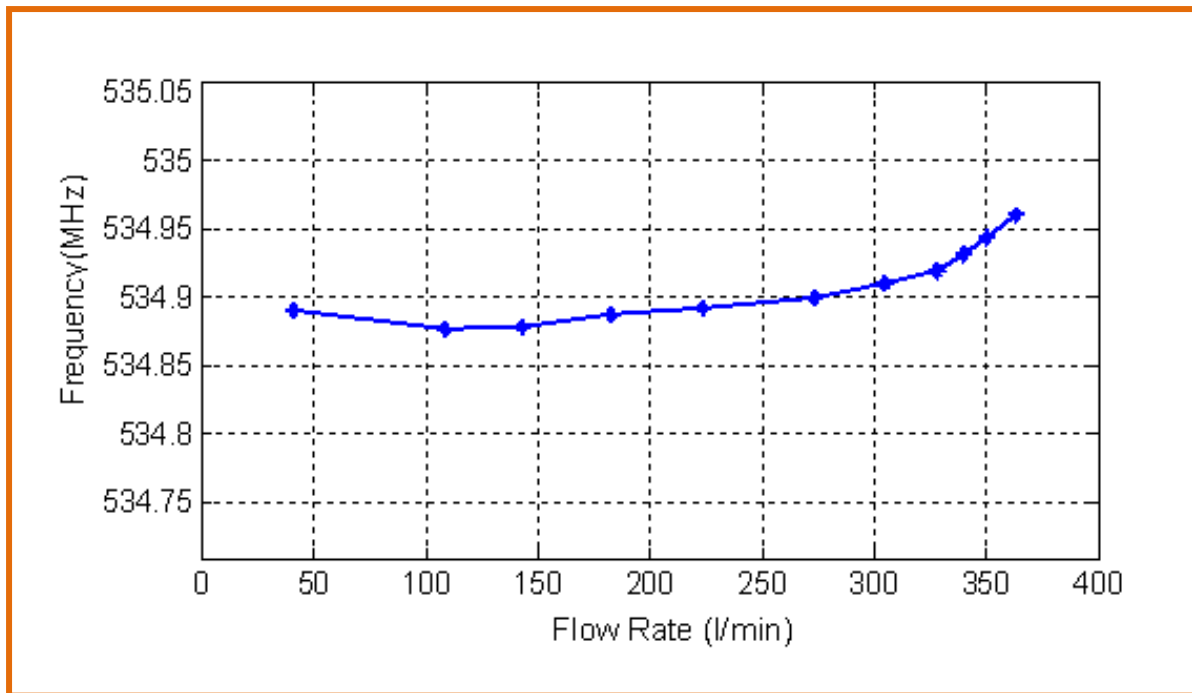


Figure 10-7 Resonant frequency of signal against flow rate

However, the design used however suffered from a number of drawbacks and was unable to clearly and definitively detect the onset of cavitation in the given system. With the experience gained it can be said immediately (i) the ratio of plate area to plate separation needs to be maximised (this would have the added benefit of reducing edge effects) and alternative plate designs considered e.g. concentric tubular plates, or multi-plates (ii) the shielding needs to be reconsidered, the present system was developed piecemeal as it became clear just how important stray effects were for this sensor (stray capacitances, resistance and inductance in the circuit need to be better identified and controlled), (iii) the pipe wall has considerable effect on C_T and a more suitable material should be found ($\epsilon_r = \epsilon_w$ for best matching) that would enable the change in C_e with void fraction to have greatest overall effect. Of course there are other considerations that could be addressed, see under further work.

10.7 Contributions to knowledge

First contribution: A systematic study has been carried out comparing the effectiveness of performance of certain statistical measures of vibration, airborne sound and waterborne sound in the detection of the early stages of cavitation in a centrifugal pump see Chapters 7, 8 and 9. This study will assist future researchers to determine the relative merits (strengths and

weaknesses) of each system of measurement and the statistical parameters used for particular applications to the monitoring of centrifugal pumps.

Second contribution: The author has suggested an entirely new method for the detection of the onset of cavitation see Chapter 5, and 6 .An underpinning theory has been developed for a capacitive device and a prototype constructed and tested. This is the first documented study that has investigated the use of the capacitive technique for detection of cavitation in a centrifugal pump (Sections 6.2, 6.3 and 6.4) as no reports in the literature have been found of using this technique for such a purpose.

Third Contribution: The author believes that the use of spectral entropy techniques for the analysis of the vibration, airborne sound and waterborne signal in the detection of the early stages of cavitation in a centrifugal pump (Sections 7.5.3, 8.5.3 and 9.5.3) is novel as no reports in the literature have been found of using spectral entropy for this purpose.

10.8 Suggestions for future work

The first suggestion: would be for minor changes to the test rig, e.g. a transparent casing for the pump to give a better view of the sites where cavitation begins.

The second suggestion: To insert light sources and photodiodes, or stroboscopes and computer aided a high speed camera in the pump casing to give visual observation of the onset of cavitation. This may record the construction of a transparent pump casing to provide the necessary level of lamentation.

The third suggestion: Repeating the measurements using a range of similar centrifugal pumps or using pumps with different design of impellers, using different fittings (elbows, tees, etc.,) to deliberately generate turbulence in the system and observe the effects on the onset of cavitation. Also necessary is to test which of the findings in this research are system/pump specific.

The fourth suggestion: To introduce cavitation into the system use different ways; such as increasing the liquid temperature by installing a heater in the tank, injecting gas into the

system inlet, reducing the total liquid pressure by using a vacuum pump in the piping system inlet or by changing the pump flow rate using either throttling valves or a speed controller.

The fifth suggestion: would be to change the piping of the test rig from plastic to steel pipe, and to investigate both the effect of this on the onset of cavitation and the use of the capacitive technique.

The sixth suggestion: to take certain promising features such as the spectral entropy for the accelerometer, microphone and hydrophone signals and attempt a fusion of these through an appropriate algorithm to maximise the accuracy of prediction of the onset of cavitation.

The seventh suggestion: to directly extend this work and use intelligent algorithms to examine combinations of factors already found to be the most promising, e.g. frequency domain spectral Crest factor for vibration and waterborne signals could be combined using an artificial neural network (ANN) to optimise recognition of the onset of cavitation. The fusion could also be of the PDF value/trend for one measure with, say, the RMS of another.

The eighth suggestion: to extend the use of ANNs to a general investigation as to what features might be used; these could include direct observations of individual peaks in the FFT derived spectrum (e.g. the peak at 340 Hz in the vibration spectrum) which appear to behave in a manner which could make it a good indicator of the early stages of cavitation. Of course the ANN could combine any number of these peaks. If ANN are used then as these can be “self taught”, having a spectrum peak which is pump specific would pose no serious problem to the identification of the onset of cavitation as the ANN would automatically adapt to the given pump system.

The ninth suggestion: to develop and refine the capacitive technique for detection of the presence of cavitation in flows. In particular this will require a more detailed modelling and analysis of the capacitor sensing device and enhancement of its sensitivity. Precise suggestions which have already been made include: maximising plate area to plate separation, finding a material for the wall such that $\epsilon_r = \epsilon_w$, reconsider the electrical circuit and better shielding.

The tenth suggestion: to investigate the amplitudes of system and structural resonances as a mechanism for the early detection of cavitation. The large peaks obtained in the spectrum of

the vibration signal suggest that this natural phenomenon could be an indication of the onset of cavitation.

APPENDIXS

Appendix A

❖ CENTRIFUGAL PUMP DIMENSIONS AND SPECIFICATIONS

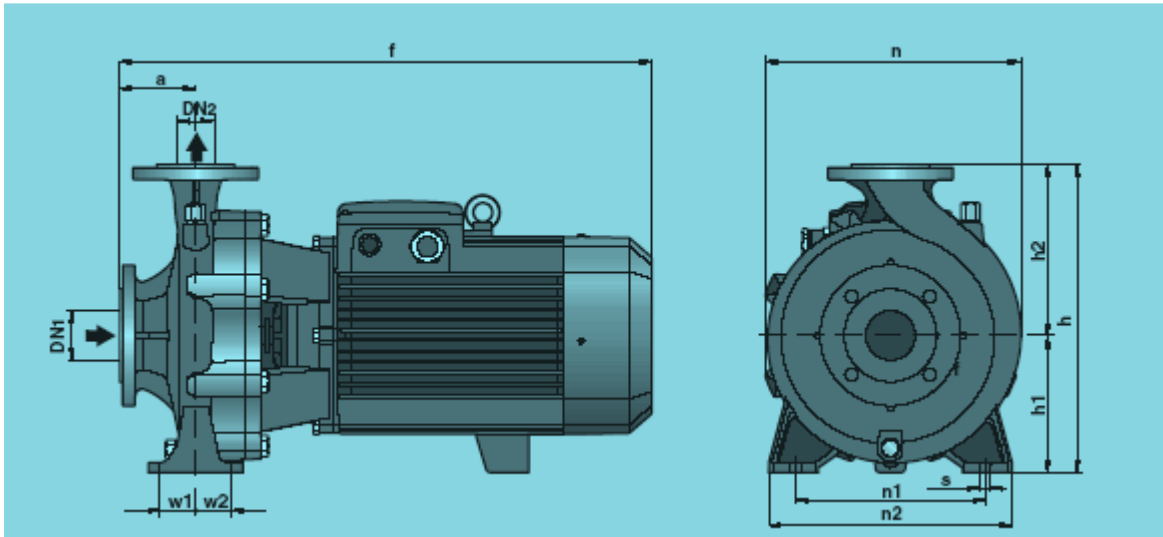


Figure A.1 Centrifugal pump Pedrollo F32 / 200AH

Inlets		Dimensions mm											Kg
Dn1	Dn2	a	f	h	h1	h2	n	n1	n2	w1	w2	s	(3~)
50	32	80	469	340	160	180	270	190	240	35	35	14	52.8
POWER		Q m ³ /h l/min	0	6	9	12	15	18					
			0	100	150	200	250	300					
KW	HP	Head (m)	59	55	52	49	44	38					
4	5.5												

❖ CURVES AND PERFORMANCE DATA AT N=2900 l/min

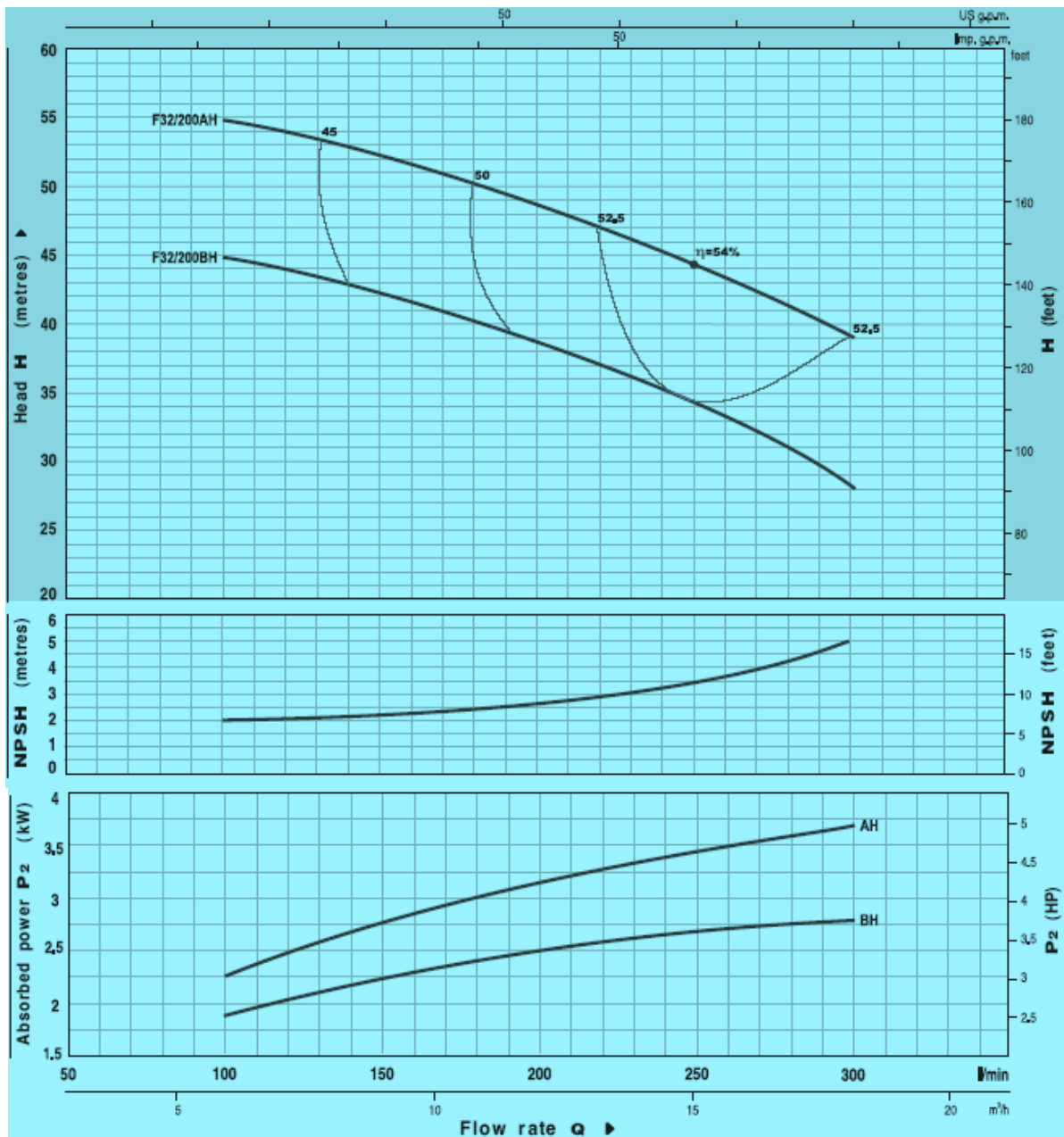
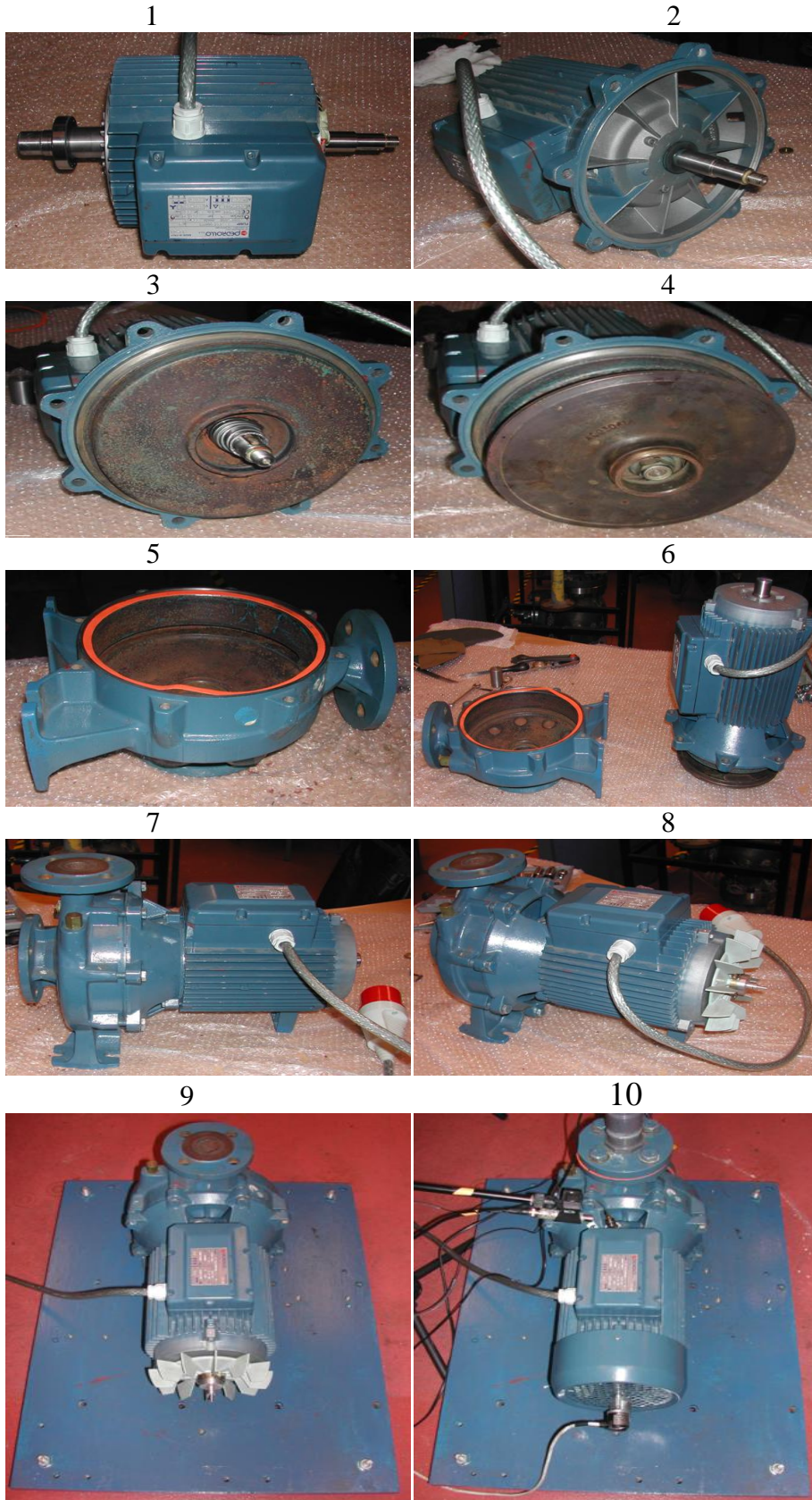


Figure A.2 Manufacturer's data

❖ COMPONENTS OF A CENTRIFUGAL PUMP



Appendix B

Pump bearing and pump mechanical seal dimensions BT/FN 24mm

Deep groove ball bearings, single row
 Product information

Tolerances , see also text
 Radial internal clearance , see also
 Recommended fits
 Shaft and housing tolerances

Principal dimensions			Basic load ratings		Fatigue load limit P_u	Speed ratings		Mass	Designation
d	D	B	dynamic	static C_0		Reference speed	Limiting speed		
mm			kN		kN	r/min		kg	-
30	62	16	20,3	11,2	0,475	24000	15000	0,20	6206-Z*

Calculation factors
 k_r 0,025
 f_0 14

Every care has been taken to ensure the accuracy of this calculation but no liability can be accepted for any loss or damage whether direct, indirect or consequential arising out of the use of the calculation.

Bearing: **6206-Z**

d [mm]:

D [mm]:

n_i [r/min]:

n_e [r/min]:

Bearing data of own choice

P [mm]:

D_w [mm]:

z:

α [degrees]:

n_i [r/min]:

n_e [r/min]:

f_i [Hz]:

f_e [Hz]:

f_c [Hz]:

f_r [Hz]:

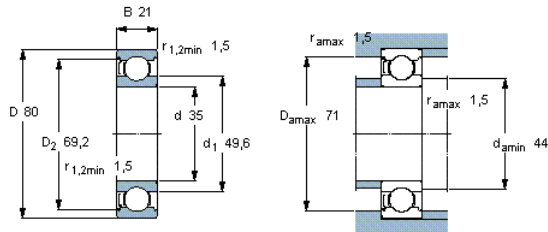
Frequencies from potential damages

f_{ip} [Hz]:

f_{ep} [Hz]:

f_{rp} [Hz]:

Deep groove ball bearings, single row						Tolerances, see also text Radial internal clearance, see also text Recommended fits Shaft and housing tolerances			
Principal dimensions			Basic load ratings		Fatigue load limit P_u	Speed ratings		Mass	Designation
d	D	B	dynamic	static		Reference speed	Limiting speed		
mm			kN		kN	r/min		kg	-
35	80	21	35,1	19	0,815	19000	12000	0,46	6307-Z*



Calculation factors
 k_f 0,03
 f_0 13

Every care has been taken to ensure the accuracy of this calculation but no liability can be accepted for any loss or damage whether direct, indirect or consequential arising out of the use of the calculation.

Bearing **6307-Z**

d [mm]

D [mm]

n_i [r/min]

n_e [r/min]

Bearing data of own choice

P [mm]

D_w [mm]

z

α [degrees]

n_i [r/min]

n_e [r/min]

f_i [Hz]

f_e [Hz]

f_c [Hz]

f_r [Hz]

Frequencies from potential damages

f_{ip} [Hz]

f_{ep} [Hz]

f_{rp} [Hz]

f_i [Hz]

f_e [Hz]

f_c [Hz]

f_r [Hz]

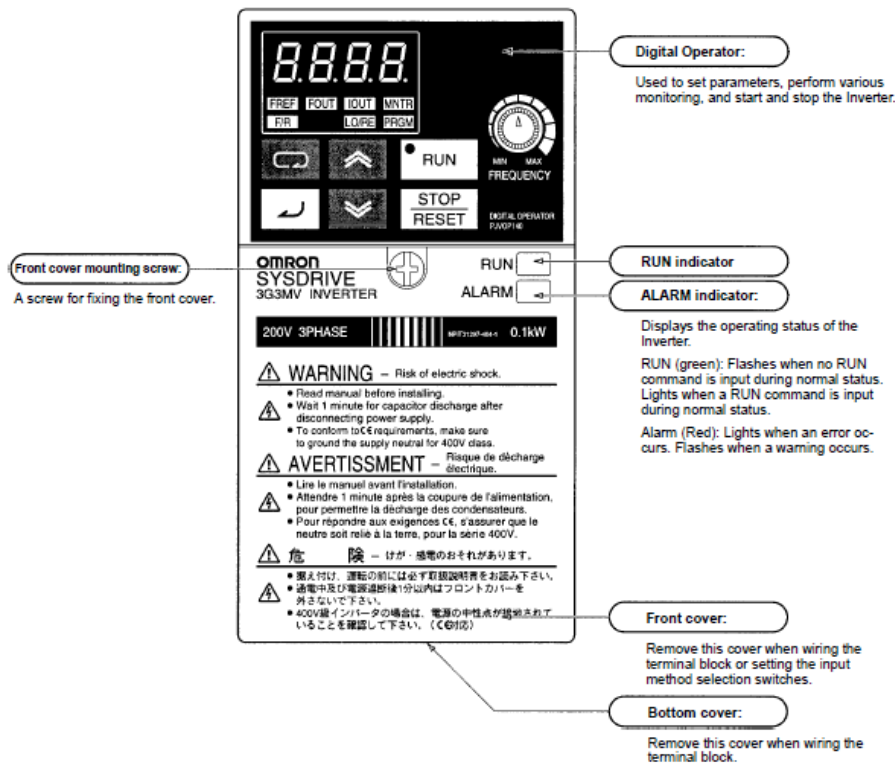
f_{ip} [Hz]

f_{ep} [Hz]

f_{rp} [Hz]

SPEED CONTROLLER

■ Panel



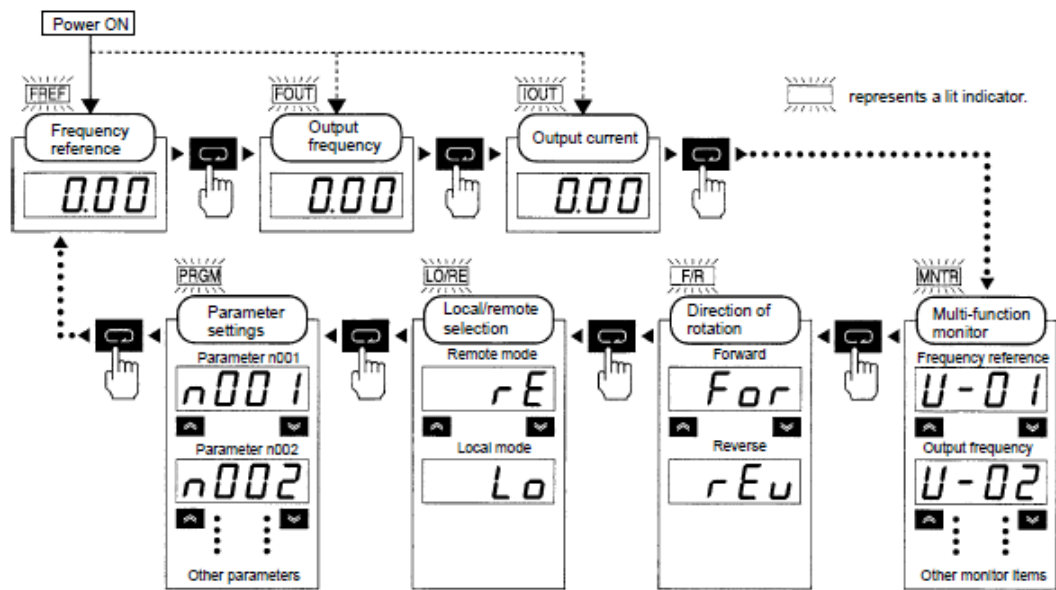
■ Digital Operator



Appearance	Name	Function
	Data display	Displays relevant data items, such as frequency reference, output frequency, and parameter set values.
	Frequency adjuster	Sets the frequency reference within a range between 0 Hz and the maximum frequency.
	Frequency reference indicator	The frequency reference can be monitored or set while this indicator is lit.
	Output frequency indicator	The output frequency of the Inverter can be monitored while this indicator is lit.
	Output current indicator	The output current of the Inverter can be monitored while this indicator is lit.
	Multi-function monitor indicator	The values set in U01 through U10 are monitored while this indicator is lit.
	Forward/Reverse selection indicator	The direction of rotation can be selected while this indicator is lit when operating the Inverter with the RUN Key.
	Local/Remote selection indicator	The operation of the Inverter through the Digital Operator or according to the set parameters is selectable while this indicator is lit. (See note 1.)
	Parameter setting indicator	The parameters in n001 through n179 can be set or monitored while this indicator is lit. (See note 2.)
	Mode Key	Switches the simplified-LED (setting and monitor) item indicators in sequence. Parameter being set will be canceled if this key is pressed before entering the setting.
	Increment Key	Increases multi-function monitor numbers, parameter numbers, and parameter set values.
	Decrement Key	Decreases multi-function monitor numbers, parameter numbers, and parameter set values.
	Enter Key	Enters multi-function monitor numbers, parameter numbers, and internal data values after they are set or changed.
	RUN Key	Starts the Inverter running when the 3G3MV is in operation with the Digital Operator.
	STOP/RESET Key	Stops the Inverter unless parameter n007 is set to disable the STOP Key. Used to reset the Inverter when an error occurs. (See note 3.)

- Note:**
1. the status of the local/remote selection indicator can be only monitored while the Inverter is in operation. Any RUN command Input is ignored while this indicator is lit.
 2. While the Inverter is in operation, the parameters can be only monitored and only some parameters can be changed. Any RUN command input is ignored while the parameter setting indicator is lit.
 3. For safety reasons, the reset function cannot be used while an operation instruction (forward/reverse) is being input. Turn the operation instruction OFF before using this function.

■ Selecting Indicators



Note: If the power is turned OFF with the FOUT or IOUT indicator lit, the same indicator will light when the power is turned ON again. In other cases, the FREF indicator will light when the power is turned ON.

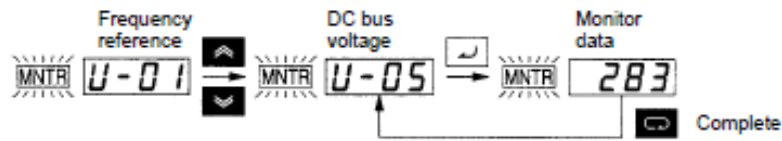
Frequency Reference Settings



Key sequence	Indicator	Display example	Explanation
	FREF	6.00	Power ON Note If the FREF indicator has not been lit, press the Mode Key repeatedly until the FREF indicator is lit.
↑ ↓	FREF	6000	Use the Increment or Decrement Key to set the frequency reference. The data display will flash while the frequency reference is set. (see note)
↵	FREF	6000	Press the Enter Key so that the set value will be entered and the data display will be lit. (see note)

Note: The Enter Key need not be pressed when performing the setting for n08. The frequency reference will change when the set value is changed with the Increment or Decrement Key while the data display is continuously lit.

Multi-function Display

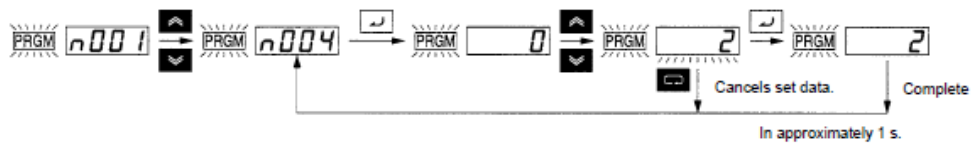


Key sequence	Indicator	Display	Explanation
	FREF	6.00	Power ON
	MNTR	U-01	Press the Mode Key repeatedly until the MNTR indicator is lit. U01 will be displayed.
	MNTR	U-05	Use the Increment or Decrement Key to select the monitor item to be displayed.
	MNTR	283	Press the Enter Key so that the data of the selected monitor item will be displayed.
	MNTR	U-05	The monitor number display will appear again by pressing the Mode Key.

Status Monitor

Item	Display	Display unit	Function
U-01	Frequency reference	Hz (see note 1)	Monitors the frequency reference. (Same as FREF)
U-02	Output frequency	Hz (see note 1)	Monitors the output frequency. (Same as FOUT)
U-03	Output current	A	Monitors the output current. (Same as IOUT)
U-04	Output voltage	V	Monitors the internal output voltage reference value of the Inverter.
U-05	DC bus voltage	V	Monitors the DC voltage of the internal main circuit of the Inverter.
U-06	Input terminal status	---	Shows the ON/OFF status of inputs. Terminal S1: Multi-function input 1 Terminal S2: Multi-function input 2 Terminal S3: Multi-function input 3 Terminal S4: Multi-function input 4 Terminal S5: Multi-function input 5 Terminal S6: Multi-function input 6 Terminal S7: Multi-function input 7
U-07	Output terminal status	---	Shows the ON/OFF status of outputs. Terminal MA: Multi-function contact output Terminal P1: Multi-function photo-coupler output 1 Terminal P2: Multi-function photo-coupler output 2
U-08	Torque monitor	%	Displays the torque being currently output as a percentage of the rated motor torque. This display can only be made in vector control mode.

Parameter Settings



Key sequence	Indicator	Display example	Explanation
	FREE	000	Power ON
[Mode Key]	PRGM	n001	Press the Mode Key repeatedly until the PRGM indicator is lit.
[Up] [Down]	PRGM	n004	Use the Increment or Decrement Key to set the parameter number.
[Enter]	PRGM	0	Press the Enter Key. The data of the selected parameter number will be displayed.
[Up] [Down]	PRGM	2	Use the Increment or Decrement Key to set the data. At that time the display will flash.
[Enter]	PRGM	2	Press the Enter Key so that the set value will be entered and the data display will be lit. (see note 1)
In approximately 1 s.	PRGM	n004	The parameter number will be displayed.

Note: 1. To cancel the set value, press the Mode Key instead. The parameter number will be displayed.
 2. There are parameters that cannot be changed while the Inverter is in operation. Refer to the list of parameters. When attempting to change such parameters, the data display will not change by pressing the Increment or Decrement Key.

Appendix C

The baseline spectrum of the acquired signal contains many important features. Table C.3, 4 and 5 summarises the spectrum analysis of the acquired vibration, acoustic and hydrophone data.

Table C.3 Features in the vibration spectrum at flow rate 249 l/min

Component RF = Rotational Frequency = 48.34Hz BPF = Blade Passing Frequency = 241.7Hz CF = Cooling Fan = 581.5Hz	Frequency Hz	Peak amplitude (m/s ²) at 249 l/min
1xRF	48.34	0.079
2xRF	96.68	0.210
3xRF	145.0	0.084
4xRF	193.4	0.16
1xBPF	241.4	0.035
2xBPF and 10xRF	483.4	0.002
1 x CF and 12xRF	581.5	0.060
3xBPF and 15 x RF	725.1	0.005
4xBPF and 20 x RF	966.8	0.059
22 x RF	1066	0.744
(2kHz-10kHz)	3.463	0.257
(2kHz-10kHz)	6.287	0.253
(2kHz-10kHz)	7.254	0.474
(2kHz-10kHz)	7.354	0.333
(2kHz-10kHz)	7.553	0.479
(2kHz-10kHz)	7.554	0.462
(2kHz-10kHz)	7.607	0.317

Table C.4 Features in the airborne acoustic spectrum at flow rate 249 l/min

Component RF = Rotational Frequency = 48.34Hz BPF = Blade Passing Frequency =241.7Hz CF = Cooling Fan = 581.5Hz	Frequency of acoustic peak (Hz)	Peak amplitude (m/s ²) at 248 l/min
RF	48.34	0.045
BPF	241.4	0.108
6 x RF	290.0	0.044
7 x RF	338.4	0.070
9 x RF	435.1	0.032
2 x BPF	486.4	0.007
CF	580.1	0.008
3 x BPF	725.1	0.011


4 x BPF	966.8	0.036
(1kHz-2kHz)	1066	0.024
(2kHz-10kHz)	6.592	0.064
(2kHz-10kHz)	8.420	0.045

Table C.5 Features in the hydroacoustic spectrum at flow rate 249 l/min

Component RF = Rotational Frequency = 48.34Hz BPF = Blade Passing Frequency = 241.7Hz CF = Cooling Fan = 581.5Hz	Frequency Hz	Peak amplitude (m/s ²) at 248 l/min
RF	48.34	1.21
2 x RF	96.68	0.710
3 x RF	145.0	0.719
4 x RF	193.4	0.616
BPF and 5 x RF	241.7	1.425
6 x RF	290.0	5.16
7 x RF	338.4	0.071
8 x RF	386.7	0.758
9 x RF	435.1	0.597
2 x BPF and 10 x RF	483.4	0.454
CF and 12 x RF	581.5	1.57
3 x BPF and 15 x RF	725.1	0.171
4 x BPF and 20 x RF	966.8	0.104
22 x RF(1kHz-1.5kHz)	1066	0.100
(1 kHz-1.5kHz)	1113	0.256
(1kHz-1.5kHz)	1188	0.105
(1kHz-1.5kHz)	1201	0.188
(1.5kHz-3kHz)	1500	0.062
(1.5kHz-3kHz)	1553	0.059

Appendix D

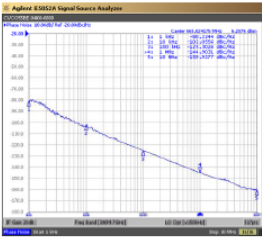
CRYSTEK - CVCO55B Voltage Controlled Oscillator



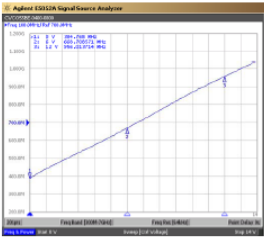
Voltage Controlled Oscillator-VCO
CVCO55BE-0400-0800

PERFORMANCE SPECIFICATION	MIN	TYP	MAX	UNITS
Lower Frequency:	800		400	MHz
Upper Frequency:				MHz
Tuning Voltage:	0		12	VDC
Supply Voltage:	4.75	5.0	5.25	VDC
Output Power:	+2.0	+7.0	+12.0	dBm
Supply Current:		17		mA
Harmonic Suppression (2 nd Harmonic):		-6		dBc
Pushing:			5.0	MHz/V
Pulling, all Phases:			3.0	MHz/p-pV
Tuning Sensitivity:		47		MHz/V
Phase Noise @ 10kHz offset:		-105		dBc/Hz
Phase Noise @ 100kHz offset:		-129		dBc/Hz
Load Impedance:		50		Ω
Input Capacitance:			200	pF
Operating Temperature Range:	-10		+70	°C
Storage Temperature Range:	-45		+90	°C

Phase Noise (1 Hz BW, Typical)




Tuning Curve (Typical)



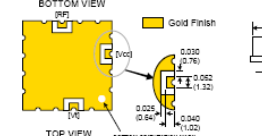
Page 1 of 2

12730 COMMONWEALTH DRIVE • FORT MYERS, FLORIDA 33913
 PHONE: 239-561-3311 • 800-237-3361
 FAX: 239-561-1025 • www.crystek.com

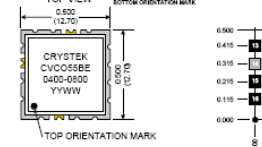


Voltage Controlled Oscillator-VCO
CVCO55BE-0400-0800


BOTTOM VIEW



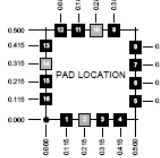
TOP VIEW



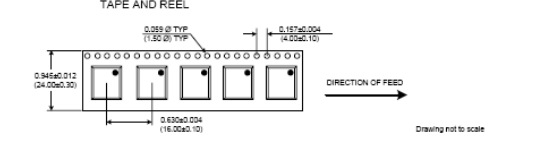
SIDE VIEW



PAD LOCATION



TAPE AND REEL





Product Control:


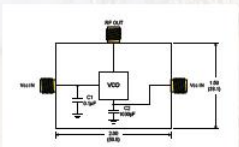
Crystal Part Number: CVCO55BE-0400-0800	Release Date: 28-March-08	Specification is subject to change without notice
Revision Level: E	Responsible: C. Vies	Page 2 of 2

12730 COMMONWEALTH DRIVE • FORT MYERS, FLORIDA 33913
 PHONE: 239-561-3311 • 800-237-3361
 FAX: 239-561-1025 • www.crystek.com

VCC Evaluation Boards


CRYSTEK MICROWAVE
A DIVISION OF CRYSTEK CORPORATION

VCO EVALUATION BOARDS






Model CEVAL-055 Shown


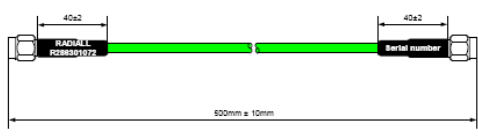
Features:
Connectors: Gold Plated SMA Female Connectors
Frequency Range: DC to 6GHz
PCB: 0.062" FR4
Operating Temperature: -40°C to +85°C

Crystek's VCO Evaluation boards are a turn key solution to easy stand alone testing. Evaluation boards are constructed using rigid 0.062" FR4 PCB material. Solder down connection method insures that the VCO will receive proper grounding for best testing results. Evaluation boards are available for 0.3" x 0.3" and 0.5" x 0.5" Industrial Standard VCO foot prints. Crystek also produces a line of RF Cables that can be purchased seperately to make connection to equipment an effortless task.

Part Number	Description
CEVAL-033	0.3" x 0.3" VCO CVCO33 Model
CEVAL-055	0.5" x 0.5" VCO CVCO55 Model


12730 COMMONWEALTH DRIVE • FORT MYERS, FL 33913
 PHONE: 239-561-3311 • 800-237-3061
 FAX: 239-561-1025 • WWW.CRYSTEK.COM

CABLE ASSEMBLY HF SMA M M 0.25M

 <small>Connect to the future</small> Service cordons BP 30 Rue Viepeau 37110 Châteaurenault	TECHNICAL DATA SHEET <small>Fiche technique</small> CABLE ASSEMBLY <small>cordon</small>	PART NUMBER : R286301072 Référence ISSUE : 07/32 Edition DATE : 08/08/2007 Date																					
CUSTOMER : SPECIFICATION : - ISSUE : - DATE : 19/05/2007 <small>Client Spécification Issue Date</small>																							
<small>All dimensions are in mm / Toutes les dimensions sont indiquées en mm</small>																							
																							
<table style="width: 100%; border: none;"> <tr> <td style="width: 33%; border: none;"> Connectors designation: <small>Designation connecteurs</small> </td> <td style="width: 33%; border: none;"> Connector 1: R125055002 <small>Connecteur 1</small> SMA straight plug Stainless steel passivated Torque wrench : 110 N.cm <small>Couple de serrage</small> </td> <td style="width: 33%; border: none;"> Connector 2: R125055002 <small>Connecteur 2</small> SMA straight plug Stainless steel passivated Torque wrench : 110 N.cm <small>Couple de serrage</small> </td> </tr> </table>			Connectors designation: <small>Designation connecteurs</small>	Connector 1: R125055002 <small>Connecteur 1</small> SMA straight plug Stainless steel passivated Torque wrench : 110 N.cm <small>Couple de serrage</small>	Connector 2: R125055002 <small>Connecteur 2</small> SMA straight plug Stainless steel passivated Torque wrench : 110 N.cm <small>Couple de serrage</small>																		
Connectors designation: <small>Designation connecteurs</small>	Connector 1: R125055002 <small>Connecteur 1</small> SMA straight plug Stainless steel passivated Torque wrench : 110 N.cm <small>Couple de serrage</small>	Connector 2: R125055002 <small>Connecteur 2</small> SMA straight plug Stainless steel passivated Torque wrench : 110 N.cm <small>Couple de serrage</small>																					
Cable designation / Designation câble: F1703-134 - SHF4.2M Protective Jacket / Gaine de protection: - <small>Outer diameter / Diamètre extérieur :</small> 4.20 mm max Marking / Marquage: White marking on black heatshrink sleeves																							
ELECTRICAL CHARACTERISTICS / Caractéristiques électriques <table style="width: 100%; border: none;"> <tr> <td style="width: 33%;"><small>Characteristic impedance</small></td> <td style="width: 33%;">50 ±1 Ohms</td> <td style="width: 33%;"></td> </tr> <tr> <td><small>Impedance characteristic</small></td> <td></td> <td></td> </tr> <tr> <td><small>Frequency band :</small></td> <td>DC - 18 GHz</td> <td></td> </tr> <tr> <td><small>Range of frequency</small></td> <td></td> <td></td> </tr> <tr> <td><small>Insertion loss max</small></td> <td>1.10 dB</td> <td>at 18GHz at 20°C</td> </tr> <tr> <td><small>Max return loss :</small></td> <td>1.30 ±1</td> <td>(17,63dB) in the Frequency band : DC - 18GHz</td> </tr> <tr> <td><small>ROS max</small></td> <td></td> <td></td> </tr> </table>			<small>Characteristic impedance</small>	50 ±1 Ohms		<small>Impedance characteristic</small>			<small>Frequency band :</small>	DC - 18 GHz		<small>Range of frequency</small>			<small>Insertion loss max</small>	1.10 dB	at 18GHz at 20°C	<small>Max return loss :</small>	1.30 ±1	(17,63dB) in the Frequency band : DC - 18GHz	<small>ROS max</small>		
<small>Characteristic impedance</small>	50 ±1 Ohms																						
<small>Impedance characteristic</small>																							
<small>Frequency band :</small>	DC - 18 GHz																						
<small>Range of frequency</small>																							
<small>Insertion loss max</small>	1.10 dB	at 18GHz at 20°C																					
<small>Max return loss :</small>	1.30 ±1	(17,63dB) in the Frequency band : DC - 18GHz																					
<small>ROS max</small>																							
MECHANICAL CHARACTERISTICS / Caractéristiques mécaniques <table style="width: 100%; border: none;"> <tr> <td style="width: 33%;"><small>Static bending radius :</small></td> <td style="width: 33%;">25 mm</td> <td style="width: 33%;"></td> </tr> <tr> <td><small>Rayon de courbure statique</small></td> <td></td> <td></td> </tr> <tr> <td><small>Dynamic bending radius :</small></td> <td>40 mm</td> <td></td> </tr> <tr> <td><small>Rayon de courbure dynamique</small></td> <td></td> <td></td> </tr> <tr> <td><small>Life (Connectors) :</small></td> <td>500 Cycles</td> <td></td> </tr> <tr> <td><small>Vie de manipulateur connecteurs</small></td> <td></td> <td></td> </tr> </table> <div style="border: 1px solid black; padding: 5px; width: fit-content; margin-left: auto; margin-top: 10px;"> CUSTOMER'S APPROVAL Service or Company's stamp Name Date </div>			<small>Static bending radius :</small>	25 mm		<small>Rayon de courbure statique</small>			<small>Dynamic bending radius :</small>	40 mm		<small>Rayon de courbure dynamique</small>			<small>Life (Connectors) :</small>	500 Cycles		<small>Vie de manipulateur connecteurs</small>					
<small>Static bending radius :</small>	25 mm																						
<small>Rayon de courbure statique</small>																							
<small>Dynamic bending radius :</small>	40 mm																						
<small>Rayon de courbure dynamique</small>																							
<small>Life (Connectors) :</small>	500 Cycles																						
<small>Vie de manipulateur connecteurs</small>																							
ENVIRONMENTAL CHARACTERISTICS / Caractéristiques environnementales : Temperature range : -55 to +105°C <small>Gamme de température</small>																							
<table style="width: 100%; border: none;"> <tr> <td style="width: 25%;"><small>C. BAR</small></td> <td style="width: 25%;">07/32</td> <td style="width: 25%;">08/08/2007</td> <td style="width: 25%;">Update of the temperature range</td> <td style="width: 20%;"><small>C. DAVENEL</small></td> </tr> <tr> <td><small>C. BAR</small></td> <td>07/28</td> <td>10/07/2007</td> <td>first issue</td> <td><small>J. SENOAT</small></td> </tr> <tr> <td><small>Name / nom</small></td> <td><small>Issue / Edition</small></td> <td><small>Date</small></td> <td><small>Modification</small></td> <td><small>Checked by</small></td> </tr> </table>			<small>C. BAR</small>	07/32	08/08/2007	Update of the temperature range	<small>C. DAVENEL</small>	<small>C. BAR</small>	07/28	10/07/2007	first issue	<small>J. SENOAT</small>	<small>Name / nom</small>	<small>Issue / Edition</small>	<small>Date</small>	<small>Modification</small>	<small>Checked by</small>						
<small>C. BAR</small>	07/32	08/08/2007	Update of the temperature range	<small>C. DAVENEL</small>																			
<small>C. BAR</small>	07/28	10/07/2007	first issue	<small>J. SENOAT</small>																			
<small>Name / nom</small>	<small>Issue / Edition</small>	<small>Date</small>	<small>Modification</small>	<small>Checked by</small>																			

REFERENCES

- Abouelwafa, M. and Kendall, E.** 1980. The use of capacitance sensors for phase percentage determination in multiphase pipelines, *IEEE Trans. Instrum. Meas.* Vol. 29, Issue 1 pp.24–27
- Adams, M.** 2000. *Rotating machinery vibration from analysis to troubleshooting.* Taylor & Francis, New York
- Adams, V. Erickson, B. Needelman, B. and Smith, M.** 1996. Field investigation of bearing housing oil cleanliness. *Proc. 13th Int. Pump User's Symposium*, Texas A&M University, Houston .USA
- Albarbar, A. Elhaj, M. Gu, F. and Ball, A.** 2004. Independent component analysis for enhancing diesel engine air-borne acoustics signal to noise ratio. *Proc.9th Conference on Mechatronics*,Turkey, pp.345-355
- Alfayez, L. Mba, D. and Dyson, G.** 2005. The application of acoustic emission for detecting incipient cavitation and the best efficiency point of a 60KW centrifugal pump; case study *NDT & E International*, Vol 38, Issue 5, pp .354-358
- Alhashmi, S.** 2005. *Detection and diagnosis of cavitation in centrifugal pumps.* PhD Thesis, University of Manchester
- Al Kazzaz, S., Ahmed, S. and Singh, G.** 2002. *Experimental investigations on induction machine condition monitoring and fault diagnosis using digital signal processing techniques.* Elsevier Science: U.K
- Al Thobiani, F. Gu, Fengshou and Ball, A.,** 2010. The monitoring of cavitation in centrifugal pumps using Spectral Entropy of vibro-acoustic measurements. *CM 2010 and MFPT 2010: Seventh International Conference on Condition Monitoring and Machinery Failure Prevention Technologies*, 22-24 June 2010, Stratford-upon-Avon, UK
- Al Thobiani, F., Gu, F., and Ball, A.,** 2011. Monitoring of cavitation in centrifugal pumps using a non-invasive capacitance sensor. *Proc. 24th Int. Congress on Condition Monitoring and Diagnostics Engineering Management*, Stavanger, Norway
- Arnold, K., and Stewart, M.** 1999. *Surface Production Operation, Design of Oil-Handling System and Facilities*, GULF Publishing Company. USA
- Arthur, N. and Penman, J.** 2000. Induction machine condition monitoring with higher order spectra. *IEEE Trans. Ind. Elec.*, Vol. 47, No. 5, pp. 1031 – 1041
- Ashok, K. Sunghal, M. Li, H. and Jiang, Y.** 2002. Mathematical basis and validation of the full cavitation model. *J. Fluids Eng.* Vol 124, No3, pp. 617-625
- Ball, A.D.,** 1991. *Machine Condition Assessment and Fault Diagnosis*, PhD thesis, University of Manchester

- Ball, J. and Tullis, J.** 1973. Cavitation in butterfly valves. *ASCE Journal. Hydraulics Div.*, Vol 93, pp .1303-1318
- Beebe, R.** 2004. *Predictive maintenance of pumps using condition monitoring*. Elsevier, U.K
- Bies, D. and Hansen, C.** 2003. *Engineering Noise Control.*, pp.501. Taylor and Francis: U.K.
- Brennen, C.** 1995. *Cavitation and Bubble Dynamics*. Oxford University Press: U.K
- Bachus, L. and Custodio, A.** 2003. *Know and Understand Centrifugal Pumps*. Elsevier, U.K
- Barnard, P.** 1991. *The Way Forward*, Meeting of British Institute of Mechanical Engineers
- Baydar, N.** 2000. *The Vibro-Acoustic Monitoring of Gearboxes*, PhD thesis, University of Manchester
- Bloch, H.** 1998. *Improving Machinery Reliability*, Gulf, USA
- Bloch, H. and Budris, A.** 2004. *Pump User's Handbook: Life Extension*, Fairmont Press: USA
- Bloch, H. and Roddis, A.** 2007. Pump bearing distress and seal failure, new statistics on the value of bearing housing protection. *Uptime Magazine*, November issue, USA
- Bloch, H. and Budris, A.** 2006. *Pump User's Handbook: Life Extension*. Fairmont Publishing Company, USA
- Bloch, P.** 2008. *Pump condition monitoring*, [Accessed 15th March 2009] Available from <http://www.peopleflo.com>
- Bolton, W.** 2000 *Instrumentation and Measurement Pocket Book*, USA
- Braun, S.** 1975. The extraction of periodic waveforms by time averaging, *Acustica*, Vol.32.pp.69-77
- Brennan, C.** 2005. *Hydrodynamic of Pumps*. Cambridge University Press, UK
- Brennan, C.** 2005. *The Fundamentals of Multiphase Flow*. Cambridge University Press, UK
- Budris, A.** 2009. Effect-of-cavitation-on-centrifugal-pump-performance. [Accessed 28th May 2009] Available from <http://news.lubipumps-na.com/blog/>
- Casada, D.** 1999. Energy and reliability considerations for adjustable speed driven pumps, *Industrial Energy Technology Conference*, pp. 53-62, Houston, USA
- Cernetic, J.** 2009. The use of noise and vibration signals for detecting cavitation in kinetic pumps. *Proc. IMechE* Vol. 223 Part C: Jnl. Mech. Eng. Science pp.1645-1655
- Chapman, S.** 1991. *Electric Machinery Fundamentals*, McGraw-Hill, New York

Choi, J. 2006 *Model Based Diagnostics of Motors and Pumps*, PhD thesis, University of Texas at Austin, USA

Chartered Institution of Building Services Engineers Guide, 2007. Section C: Reference Data, Part 4 Flow of Fluids in Pipes and Ducts. CIBSE, U.K

Chaurette, J. 2004. Centrifugal pump specific speed primer and the affinity laws. Online: http://www.pumpfundamentals.com/download-free/spec_speed_pr-extract.pdf Accessed January 2010

Chu, S. Dong, R. and Katz, J. 1995. Relationship between unsteady flow, pressure fluctuations and noise in a centrifugal pump - Part B: Effects of blade-tongue interactions. *ASME, Jnl. Fluids Engineering*, Vol. 117, pp. 30-35

Collins, J. 1993. *Failure of Materials in Mechanical Design; Analysis, Prediction, Prevention*. John Wiley and Sons Ltd, U.K

Courbiere, P. 1984. An acoustical method for characterizing the onset of cavitation in nozzles and pumps. *2nd Int. Symp. on Cavitation Inception*, ASME Winter Meeting New Orleans

Cudina, M. 1998. Noise as an indicator of cavitation instability in centrifugal pumps, *Journal of Mechanical Engineering*, Vol. 45

Cudina, M. 2003. Noise as an indicator of cavitation in a centrifugal pump. *Acoustical Physics*, Vol.49 Issue 4, pp. 1335-1347

Cudina, M. and Prezelj, J. 2003. Detection of cavitation phenomenon in a centrifugal pump using audible sound, *Mechanical Systems and Signal Processing*, Vol.17 (6), pp. 1335-1347

Cudina, M. and Prezelj, J. 2009. Detection of cavitation in the operation of kinetic pumps: use of discrete frequency tone in audible pump spectra using audible sound, *Applied Acoustics* Vol.70, Issue 4, pp 540-564

D'Agostino, L. and Salvetti M. 2007. Fluid dynamics of cavitation and cavitating turbopumps, *CISM Courses and Lectures*, Vol 496, Springer Wein: USA

de Silva, C. 2005. *Shock and Vibration Handbook*, Taylor and Francis: USA pp.17-25

de Silva, C. 2006. *Vibration Fundamentals and Practice*, Taylor & Francis, USA

Decker, H. 2003. Spiral bevel pinion crack detection in a helicopter gearbox. *Proc. American Helicopter Society*, 59th Annual forum, pp.1222-1232, Phoenix, AZ

Decoursey, W. 2003. *Statistics and probability for engineering applications with Microsoft® Excel*, College of Engineering, University of Saskatchewan Saskatoon, Newnes, USA

Devi, S. Siva, K. Shanker, N. and Prabakaran, K. 2010. A Comparative study between vibration and acoustic signals in HTC cooling pump and chilling pump. *IACSIT International Journal of Engineering and Technology*, Vol.2, No.3, pp. 1793-8236

Dister, C. 2003. On-line health assessment of integrated pumps, *Aerospace Conference*, No.7, pp. 3289 – 3294

Djebala, A. Ouelaa, N. Hamzaoui, N. and Chaabi, L. 2006. Detecting mechanical failures inducing periodical shocks by wavelet multi-resolution analysis. Application to rolling bearings fault diagnosis. *Mechanika*, No.2, Vol.58, pp.1392-1207

Doguer, T. and Strackeljan, J. 2009. Vibration analysis using time methods for the detection of small roller bearing defects. *Int. Conf. on Vibrations in Rotating Machines*, Vienna, Austria

Dowling, A. and Ffowcs-Williams, J. 1983. *Sound and Sources of Sound*, John Wiley & Sons

Dron, J. 2004. Improvement of the sensitivity of the scalar indicators (crest factor, kurtosis) using a de-noising method by spectral subtraction: application to the detection of defects in ball bearing. *Journal of Sound and Vibration*, Vol.270, Issues.1-2, pp. 61-73

Ebersbach S. Peng Z. and Kessissoglou N. 2006. The investigation of the condition and faults of a spur gearbox using vibration and wear debris analysis techniques, *Wear* Vol. 260, Issues 1-2, pp.16-24

Elhaj, M. Gu, F. and Ball, A. 2003. A study of instantaneous angular speed of a compressor for condition monitoring, *COMADEM*, Vaxjo Sweden; pp. 271-279

Entek, I. 1993. Vibration acceleration severity chart for general horizontal rotating machinery. *Technical Associates of Charlotte*, pp. 2-9

Escaler, X. Egusquiza, E. Farhat, M. Avellan, F. and Coussirat, M. 2006. Detection of cavitation in hydraulic turbines. *Mechanical System and Signal Processing*, Vol 20 pp.984-1007

Farhat, M., Guennoum, F. and Avellan, F. 2002, Leading edge cavitation dynamics, Proc. ASME Fedsm, Montreal. Part 1: Instrumentation, Proceedings of the 21st IAHR Symposium Joint ASME - *European Fluids Engineering Summer Conference, Montreal*, Canada, June 14-18, Available from lmh.epfl.ch/component/option,com_infoscience/

Flood, S. 2007. Mechanical seal reliability - What realistically can be achieved, *IMEchE Mechanical Sealing Technology Seminar*, London, UK

GEMS Sensors and Controls 2011 Plainville, CT 06062, USA

Girdhar, P. 2004. *Practical Machinery Vibration Analysis and Predictive Maintenance*. Newnes, UK

- Girdhar, P.** 2005. *Practical Centrifugal Pumps: Design, Operation and Maintenance*, Elsevier: U.K
- Gladston, J. and Bevirt, W.** 1996. *HVAC Testing, Adjusting, and Balancing Field Manual*, 3rd edition, McGraw-Hill Education, Europe
- Sinocera**, 2009 Product Systlebook-2009, No 1, Yuqi Street, Yangzhou City, P.R. China
- Global sensor technology**, [Accessed 23rd November 2008] Available from <http://www.globalsensortech.com/resources.php>
http://www.gemssensors.com/uploadedFiles/Literature/Spec_Sheets/RFO.pdf
- Gorla, R. and Khan, A.** 2003. *Turbomachinery: Design and Theory*. Marcel Dekker Inc., USA
- Grist, E.** 1999. *Cavitation and the Centrifugal Pump, A Guide for Pump Users*, Taylor and Francis, U.K
- Gulich, J.,** 2007. *Centrifugal Pumps*, Springer, USA
- Harris, T.** 2001. *Rolling Bearing Analysis*. John Wiley and Sons Inc., New York, pp.993-1000
- Herbich, J.,** 2000. *Handbook Of Dredging Engineering*, McGraw Hill: USA
- Hengstler.,** 2011. Encoders UK Ltd., Sutton Coldfield, Birmingham, B75 7BU
- Hrivnak, S.** 2003. *Centrifugal pump vibrations the causes*, Tennessee Eastman, Eastman chemical company. (www.vibration.org) [Accessed 12th January 2009]
- Huang, S. Stott, A. Green, R. and Beck, M.** 1988. Electronic transducers for industrial measurement of low value capacitances, *Journal of Physics E: Scientific Instruments*, Vol 21. Number 3 pp.242–250
- Huang, S. Green, R. Plaskowski, A. and Beck, M.** 1988. A high frequency stray-immune capacitance transducer based on the charge transfer principle, *IEEE Trans. Instrum. Meas* 37, pp.368–373
- Jaworek, A. Krupa, A. and Trela, M.** 2004. Capacitance sensor for void fraction measurement. *Water/steam Flows, Flow Measurement and Instrumentation*, Vol.15, No.5-6, pp.317-324
- Jaworek, A. and Krupa, A.** 2004. Gas/liquid ratio measurements by rf resonance capacitance sensor, *Sensors and Actuators A* 113 pp. 133–139
- Jaworek, A. Krupa, A. and Trela, M.** 2010. Phase-shift detection for capacitance sensor measuring void fraction in two-phase flow, *Sensors and Actuators A* 160 (2010) pp.78–86
- Kaiser, G.** 1994 *A Friendly Guide to Wavelets*, Birkhauser, Boston, 1994.

- Karassik, L. Messina, J. Cooper, P. and Heald, C.** 2007. *Pump Handbook*, McGraw-Hill, New York
- Khin Cho Thin.** 2008. Design and performance analysis of centrifugal pumps, *Proc World Academy of Science, Engineering and Technology*, Vol 36 Dec 2008 issn 2070-3740.
- Knapp, R. Daily, J. and Hammitt, F.** 1970. *Cavitation*. Engineering Society Monograph, McGraw Hill: USA
- Körner, T. W.** (1996) *Fourier Analysis*, Cambridge University Press, UK
- Koivula, T.** 2000. *On Cavitation in Fluid Power*. Tampere University of Technology, Finland [Accessed 14th June 2009] Available from www.ewp.rpi.edu/hartford/~ernesto/F2006/EP/Aids/Papers/.../Koivula.pdf
- Lebold, M. McClintic, J. Campbell, R. Byington, C. and Maynard, K.** 2000. Review of vibration analysis methods for gearbox diagnostics and prognostics. *Proc. 54th Meeting of the Society for Machinery Failure Prevention Technology*, Virginia Beach, pp.623-634. May 1-4, 2000, pp. 623-634 [Accessed 20th June 2009] Available from ieeexplore.ieee.org/iel5/5028855/5069167/05069182.pdf?tp.
- Legarth, B. and Tvergaard, V.** 2010. 3D analyses of cavitation instabilities accounting for plastic anisotropy. *Journal of Applied Mathematics and Mechanics*, Vol 90, Issue9 pp.701-709
- Li, C. and Pickering, C.** 1992. Robustness and sensitivity of non-dimensional amplitude parameters for diagnosis of fatigue spalling, *Condition Monitoring and Diagnostic Technology*, Vol.2, No.3, pp.81-84
- Li, W.** 2000. *A Study of Diesel Engine Acoustic Characteristics*, PhD Thesis, University of Manchester
- Liu, H. Lin, J. and Liangsheng, Q.** 1997. FFT Spectral Entropy and its application in fault diagnosis. *China Mech. Eng.*, 4 (E6.10), pp.157–159
- Löfsten, H.** 1999. Management of industrial maintenance – economic evaluation of maintenance policies, *Int. Jnl. of Operations & Production Management* Vol.19 No.7, pp.716-737
- Loser, T. Wajman, R. and Mewes, D.** 2001. Electrical capacitance tomography: image reconstruction along electrical field lines, *Measurement Science and Technology* Volume 12, Number 8 pp.1083–1091
- Lucifredi, A. and Silvestri, P.** 2008. Virtual experimental modal analysis: an application of simulation models to diagnostics, *The Fifth Int. Conf. on Condition Monitoring and Machinery Failure Prevention Technologies*, Scotland, UK
- Liu, H., Lin, J., and Liangsheng, Q.** FFT spectral entropy and its application in fault diagnosis. *China Mech. Eng.*, 1997, 4(E6.10), 157–159.
- Mackay, R.,** 2004. *The Practical Pumping Handbook*, Elsevier, Canada

McMillan, R. 2004. *Rotating Machinery: Practical Solutions to Unbalance and Misalignment*, Marcel Dekker: USA

McNally Institute. 2009. *Pumps, Centrifugal Pumps, PD Pumps, Seals and Mechanical Seals Data*, Florida, USA, [Accessed 25th January 2009] Available from mcnally@mcnallyinstitute.com

McNulty, P. and Pearsall, I. 1982. Cavitation inception in pumps. *ASME J. Fluids Eng*, Vol 104, pp. 99-104

Mathew, J. 1989. Monitoring the vibration of rotating machine elements - An overview. *The Bulletin of the Center of Machine Condition Monitoring*, Monash University, Vol.1, no.1, pp.2.1-2.13

Naid, A., Gu, F., and Ball, A 2009. Fault Detection and Diagnosis of Reciprocating Compressors Using Motor Current Signature Analysis, PhD thesis, University of Huddersfield

Naid, A., Gu, F., Shao, Y., Al-Arbi, and Ball, A. 2009. Bispectrum analysis of motor current signals for fault diagnosis of reciprocating compressors, *Key Engineering Materials (Volumes 413 - 414) Volume Damage Assessment of Structures VIII*. Eds Chu, F., Ouyang, H., Silberschmidt, V., Garibaldi, L., Surace, C., Ostachowicz, W.M. and Jiang D, pp. 505-511 DOI 10.4028/www.scientific.net/KEM.413-414.505 Online since June, 2009

Neill, G. Reuben, R. Sandford, P. Brown, E. and Steel, J. 1977. Detection of incipient cavitation in pumps using Acoustic Emission, *Proc. IMech*, Vol 211 Part E, pp.267-277

Neumaier, R. 1997. *Hermetic Pumps: The Latest Innovations and Industrial Applications of Sealless Pumps*. Elsevier, UK

Norton, M. and Karczub, D. 2003. *Fundamentals of Noise and Vibration Analysis For Engineers*. CUP, UK

Omron, 2009 Omron Europe, 2132 JD Hoofddorp, Netherlands

Ozdemir, S. 2007. Measures of uncertainty in power split systems. *Mechanism and Machine Theory*, Vol 42, issue 2, pp.159–167

Pan, Y. Chen, J. and Li, X. 2008. Spectral Entropy: a complementary index for rolling element bearing performance degradation assessment. *Mechanical Engineering Science*, pp.1223-1231, Vol.233, China

Pedrollo, 2008 Pedrollo Distribution Ltd., 9 Cavendish Lichfield Rd Industrial Estate, Tamworth, B79 7XH

Piersol, A. and Paez, T. 2010. *Shock and Vibration Handbook*, 6th Ed. McGraw-Hill,

Peng Z. and Kessissoglou N. 2003 An integrated approach to fault diagnosis of machinery using wear debris and vibration analysis, Elsevier, *Wear*, Volume 255, Issues 7-12, pp. 1221-1232

- Peng Z. Kessissoglou N. and Cox M.** 2005. A study of the effect of contaminant particles in lubricants using wear debris and vibration condition monitoring techniques, *Wear* Volume 258, Issues 11-12, pp.1651–1662
- Planning, I.T.C.a.B.,** 2004. *Draft Business Plan of ISO/TC 115-Pumps*, pp.4
- Qiu, H., Lee, J., Lin, J., and Yu, G.** Robust performance degradation assessment methods for enhanced rolling element bearing prognostics. *Adv. Eng. Inf.*, 2003, **17**(3–4), 127–140
- Ramroop, G. Liu, K. Gu, F. Payne, B. and Ball, A.,** 2001 Airborne acoustic condition monitoring of a gearbox system, in: *Electronic Proceedings of the 5th Annual Maintenance and Reliability Conference*, Gatlinburg, Tennessee, USA
- Rao, K.** 2002. Companion Guide. ASME BPVC: Criteria and commentary select aspects *ASME Boiler, Press Vessel & Piping Codes*
- Reeves, T.** 2007. Prevent pump damage through automatic detection of cavitation. *Machinery Health*, [Accessed 10th Apr 2009] Available from http://www.emersonprocess.com/home/library/articles/pumps-systems/pumps-systems0705_reeves.pdf
- Reimche, W.** 2003. *Basic Vibration Monitoring for Fault Detection and Process Control*, University of Hannover, Germany
- Rose, P.** 2007. *Detecting NPSH Available and Cavitation in Pumps Through High Frequency Pressure Measurement*. MSc Cranfield University
- Sachse, W.** 1991. *Acoustic Emission*. American Society for Testing and Materials, Baltimore, USA
- Sadettin Orhan, Nizami Akturk, Veli Celik, 2006. Vibration monitoring for defect diagnosis of rolling element bearings as predictive maintenance tool, comprehensive case studies Elsevier, *NDT&E International* Vol.39, Issue 4, pp. 293–298
- Sahdev, M.** 1987. Centrifugal pumps: basics concepts of operation, maintenance, and troubleshooting, Part1. *Presented at the Chemical Engineers' Resource*, Texas, USA [Accessed 20th November 2007] Available from <https://oa.doria.fi/bitstream/handle/.../nbnfi-fe200805161399.pdf>
- Say, M.** 1982 *Alternating Current Machines*, Pitman: London.
- Scannell, K. and Colegrave, P.** 2001. *Noise Control in the Built Environment*, (Ed. Roberts J.P) Gower Technical, pp.37-38.U.K
- Scheffer, C.** 2008. Pump condition monitoring through vibration analysis. *Pump: Maintenance, Design, and Reliability Conference, Session 5*, IDC Technologies, Stellenbosch University
- Schöb, R.** 2002. Centrifugal pump without bearings or seals, *World Pumps*, July, pp.34-37

- Shah, Y. Pandit, A. and Moholkar, V.** 1999. *Cavitation Reaction Engineering*, Kluwer Academic, Springer Verlag, USA
- Shannon, C.** 1948. A mathematical theory of communication. *Bell System Technical Journal*, Vol.27, pp.379–423, 623-656
- Shreve, D.** 1995. *Signal Processing for Effective Vibration Analysis*, IRD Mechanalysis, Inc, Ohio
- Silverman, B.** 1986. *Density Estimation for Statistics and Data Analysis*, Chapman Hall, London
- Sinnott, R.** 2005. *Coulson and Richardson's Chemical Engineering*, Elsevier, U.K
- Smith, J.** 2007 *Mathematics of the Discrete Fourier Transform (DFT) with Audio Applications*, Second Edition, W3K Publishing,
- Söderholm, P.** 2005. *Maintenance and continuous improvement of complex systems – Linking stakeholder requirements to the use of built in test systems*. ISRN: LTU-DT –05/52—SE, Doctoral Thesis, Luleå University of Technology, Sweden. [Accessed 20 September 2010] Available from publ.luth.se/1402-1757/2007/18/LTU-LIC-0718-SE.pdf
- Spectra Quest Inc.** 2006. Air bubble and cavitation vibration signatures of a centrifugal pump, USA: Spectra Quest [Accessed 20th September 2009] Available from www.iwtc.info/2008_pdf/6-4.PDF
- Spellman, F.** 2003. *Handbook of Water and Wastewater Treatment Plant Operations*, Lewis, USA
- Spellman, F.** 2000. *Pumping Fundamentals*, Water and Wastewater Maintenance Operator Series, Technomic, USA
- Sreejith, B. Verma, A. and Srividya, J.** 2008. Fault diagnosis of rolling element bearing using time-domain features and neural networks. *IEEE Region 10 Colloquium and the Third ICIS*, Kharagpur, No. 409, India
- Stavale, A. Lorence, J. and Sabini, E.** 2000. *Development of a Smart Pumping System.*, ITT Industries, Fluid Technology Corp.-Industrial Pump Group, ITT Industries: pp 1-22. New York. [Accessed 20th October 2008] Available from ww.gouldspumps.com/download.../smart_pumping_system.pdf
- Sticlaru, C. and Davidescu, A.** 2004. Studies by finite element method applied on face seals. *Mechanical Engineering* Vol.2, No.1, pp.59-68, University of Timișoara, Romania
- Tandon, N. and Choudhury, A.** 1999. A review of vibration and acoustic measurement for the detection of defects in rolling element bearings, *Tribology International*, Vol.32 Issue 8, pp.469-480

- Teotrakool, K.** 2007 *Adjustable Speed Driver Bearing Fault Detection Via Support Vector Machine Incorporating Feature Selection Using Genetic Algorithm*. PhD thesis, Faculty of the Graduate School at the University of Missouri-Columbia
- Tollefsen, J. and Hammer, E.** 1998. Capacitance sensor design for reducing errors in phase concentration measurements, *Flow Measurement and Instrumentation* Volume 9, Issue 1, pp. 25-32
- Tropea, C.** 2007. *Springer Handbook on Experimental Fluid Dynamics*, Springer Science, NY USA
- Tuzson, J.** 2000. *Centrifugal Pump Design*. John Wiley & Sons: U.K.
- Tyldesley, A.** 2003. Mechanical seals on process plant, [Accessed 30th March 2009] Available from www.hse.gov.uk/foi/internalops/hid/din/521.pdf
- UNEP.** 2004. Bureau of Energy Efficiency, Pumps and Pumping Systems, Chapter 6 in Energy Efficiency Guide for Industry in Asia, *India, Ministry of Power* [online] [Accessed 20 September 2010] Available from www.energyefficiencyasia.org
- Vachtsvanos, G.** 2006. *Intelligent Fault Diagnosis and Prognosis for Engineering Systems*. John Wiley & Sons. New Jersey, USA
- Van der Meulen, J.** 1972. Incipient and desinent cavitation on hemispherical nosed bodies, *Marine Engineering*, Vol 19 No 209
- Volk, M.** 2005. *Pump Characteristics and Applications*, Second Edition, Michael Volk, Volk & Associates Inc., USA. Available from www.crcpress.com
- Wahren, U.** 1997. *Practical Introduction to Pumping Technology*, GULF Publishing Company: USA
- Watson, M.** 2007. A comprehensive high frequency vibration monitoring system for incipient fault detection and isolation of gears, bearing and shafts/couplings in turbine engines and accessories, *American Society of Mechanical Engineers*, Montreal, Canada
- Webb, D.** 1976. *Noise Control in Mechanical Services*. Sound Research Laboratories, U.K
- White, R.** 2002. Using electrical capacitance tomography to monitor gas voids in a packed bed of solids, *Meas. Sci. Technol.* Volume 13, Issue 12, pp.1842–1847
- Williams, J., Davies, A. and Drake, P.** 1994. *Condition-Based Maintenance and Machine Diagnostics*, Chapman and Hall: U.K
- Wowk, V.** 1991. *Machinery Vibration Measurement and Analysis*, U.K: McGraw-Hill Professional, pp.4-6

Wu, R. Chiang, C. and Tasi, J. 2006. The real-time optimal spectrum analysis system based on personal computer. *Proceedings of 15th IASTED International Conference on Applied Simulation and Modelling*, Greece